Available online at www.sciencedirect.com
SCIENCE DIRECT®
Physics Reports 417 (2005) 211–342
PHYSICS REPORTS
www.elsevier.com/locate/physrep

# Random network models and quantum phase transitions in two dimensions

B. Kramer[a,*,1], T. Ohtsuki[b], S. Kettemann[a]

[a] *I. Institut für Physik, Universität Hamburg, Jungiusstraße 9, 20355 Hamburg, Germany*
[b] *Department of Physics, Sophia University, Kioi-cho 7-1, Chiyoda-ku, Tokyo, Japan*

Accepted 18 June 2005

editor: C.W.J. Beenakker

Dedicated to Klaus von Klitzing on the occasion of the 25th anniversary of the Quantum Hall Effect

**Abstract**

An overview of the random network model invented by Chalker and Coddington, and its generalizations, is provided. After a short introduction into the physics of the Integer Quantum Hall Effect, which historically has been the motivation for introducing the network model, the percolation model for electrons in spatial dimension 2 in a strong perpendicular magnetic field and a spatially correlated random potential is described. Based on this, the network model is established, using the concepts of percolating probability amplitude and tunneling. Its localization properties and its behavior at the critical point are discussed including a short survey on the statistics of energy levels and wave function amplitudes. Magneto-transport is reviewed with emphasis on some new results on conductance distributions. Generalizations are performed by establishing equivalent Hamiltonians. In particular, the significance of mappings to the Dirac model and the two-dimensional Ising model is discussed. A description of renormalization group treatments is given. The classification of two-dimensional random systems according to their symmetries is outlined. This provides access to the complete set of quantum phase transitions like the thermal Hall transition and the spin quantum Hall transition in two dimensions.

* Corresponding author.
*E-mail address:* kramer@physnet.uni-hamburg.de (B. Kramer).
[1] Permanent address: International University Bremen, Campusring 1, 28759 Bremen, Germany.

0370-1573/$ - see front matter © 2005 Published by Elsevier B.V.
doi:10.1016/j.physrep.2005.07.001

The supersymmetric effective field theory for the critical properties of network models is formulated. The network model is extended to higher dimensions including remarks on the chiral metal phase at the surface of a multi-layer quantum Hall system.


*PACS:* 72.15.Rn; 71.23.An; 73.43.−f; 73.43.Nq

*Keywords:* Quantum Hall effect; Random network model; Localization; Quantum phase transition; Multi-fractal; Conformal invariance; Dirac Hamiltonian; Ising model; Supersymmetry; Symmetry class; Superspin chain; Spin quantum Hall effect; Thermal quantum Hall effect; Chiral metal; Layered system

---

**Contents**

## 1. Introduction

At the end of the seventies of the past century, many thought that solid state physics had matured to such a degree that practically everything important had been discovered. Superconductivity seemed to be well understood with the transition temperatures ceasing to increase further. Semiconductor physics had developed almost into an engineering discipline. No significant further progress of the field of solid state physics was predicted for the foreseeable future. It was widely believed in the community that the development more or less had come to an end. In this situation, a completely new and by no one foreseen phenomenon was discovered in the magneto-transport properties of a commercial electronic device, the Silicon MOSFET. The *Integer Quantum Hall Effect* was found.

This experimental discovery, together with several others that came roughly at the same time, opened a completely new area of solid state research and during the forthcoming years initiated a truly novel view on the field of condensed matter. This concerns the quantum mechanical properties of disordered and interacting electronic solid state systems on mesoscopic scales of which the Quantum Hall Effect is only one example, though a very prominent one. Until today, researchers in the field of the Quantum Hall Effect continue to produce new surprises, perhaps not on daily, but certainly on monthly time scales. In many cases, these concern only at first glance the smaller area of the quantum Hall phenomenon. Often, as in the case of the fractional Quantum Hall Effect, the discovered phenomena later turn out to be of much wider importance than foreseen at the time of their discovery.

In this review article[2] we want to describe one example of such a development, namely the discovery and further development of a theoretical model which originally was designed to describe a special aspect

[2] In contrast to the short overview that has been published earlier [B. Kramer, S. Kettemann, T. Ohtsuki, Physica E 20 172 (2003); cond-mat/0309115], the present article is supposed to provide a much more self-contained—as much as it is possible—overview of the derivation of the network model and its quantum mechanical properties, amended by some recent results. Much emphasis is on generalizations of the model and many connections to other models and descriptions of quantum phase transitions, especially in two dimensions.

of the integer Quantum Hall Effect, namely the localization–delocalization quantum phase transition in a Landau band in the limit of long-range randomness. Later, the model—although at first glance very specialized and restricted—has been shown to be able to account for many phenomena in a much wider class of systems, namely the disorder-induced quantum phase transitions in seemingly *all* of the different presently considered disordered systems. The model, invented by Chalker and Coddington in 1988, describes a *random network* of currents.

In the following sections of this introductory section, we first provide shortly some insight into, and understanding of the integer Quantum Hall Effect as it has been originally detected. Our considerations will be based on the so-called localization model. This is used for describing some fundamental physical aspects of the Integer Quantum Hall Effect, the interplay between a high—so-called *quantizing*—magnetic field, and the disorder in the system due to impurities. This interplay can lead to a localization–delocalization transition in a two-dimensional electronic system. To the best of our present knowledge, this appears to be a paradigm of a genuine *quantum phase transition*. Together with the gauge argument first proposed by Laughlin, this can explain not only the very existence of plateaus in the Hall conductivity as a function of the electron density, and the simultaneous vanishing of the magneto-conductivity, but also the quantization in integer units of $e^2/h$. The Chalker–Coddington network model is now widely accepted as one possibility for describing the fundamental physics behind the quantum Hall phase transition. While the latter is nevertheless still waiting for a complete and quantitative theoretical description with predictive power, especially including the precision aspect, the network model of Chalker and Coddington seems to have acquired more fundamental importance also in other fields of solid state physics like superconductivity and magnetism, as will be seen below.

### *1.1. The discovery of the Quantum Hall Effect*

The Quantum Hall Effect has been discovered by Klaus von Klitzing in 1980 when working as a guest researcher at the *High Magnetic Field Laboratory* of the Max-Planck-Gesellschaft in Grenoble [1] (Fig. 1). He was investigating the electronic transport in a Silicon MOSFET subject to a high magnetic field of about 18 T flux density at temperatures near 1 K. To his great surprise, he found that the Hall resistance $R_H$—the ratio between the Hall voltage across the two-dimensional electron inversion layer in the transistor, and the source–drain current, ($I = 1\,\mu$A)—shows extremely well-defined plateaus when changing the gate voltage $U_g$. In the gate voltage regions of these Hall plateaus, he found the longitudinal magneto-resistance to be vanishingly small. Most strikingly, he was able to identify the values of the Hall resistances of the plateaus as integer fractions of $h/e^2$

$$R_H = \frac{1}{j}\frac{h}{e^2} \quad (j = 1, 2, 3, \ldots)\ . \tag{1}$$

Here, $h$ is the Planck constant and $e$ the elementary charge.

Klaus von Klitzing found that the relative uncertainty of the plateau values was much better than $10^{-5}$ in the very first experiments. Thus, as a surprise, despite of the presence of strong disorder and electron interactions in the MOSFET, the effect appeared to be very promising for measuring the *Sommerfeld constant* $\alpha = (\mu_0 c_0/2)(e^2/h)$ ($c_0 = 299\,792\,458\,\mathrm{ms}^{-1}$ speed of light in vacuum, $\mu_0 = 4\pi \times 10^{-7}\,\mathrm{NA}^{-2}$ permeability of vacuum) independently from optics. Also, von Klitzing immediately realized the importance of his finding for metrological applications, i.e. the realization, dissemination and

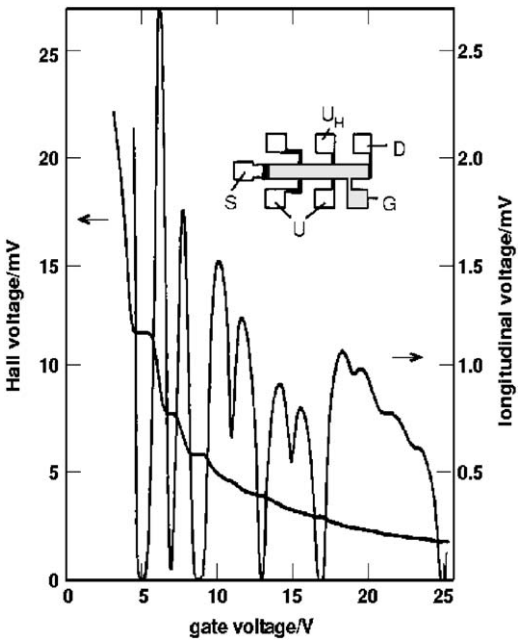


Fig. 1. The Integer Quantum Hall Effect [1]. The Hall voltage $U_H$ (left axis) shows plateaus in regions of the gate voltage $U_g$ where the source drain voltage $U$ (right axis) is vanishingly small. The experiment was done on a Si-MOSFET of length 400 μm and width 50 μm at $B = 18\,\mathrm{T}$ and at a temperature $T = 1.5\,\mathrm{K}$.

maintenance of the "Ohm", the unit of the electrical resistance. Eventually, this led to the re-definition of the "Ohm" in terms of the *von Klitzing constant* $R_K = 25\,812.8085\,\Omega$ in 1990. Meanwhile, the experimental reproducibility of the quantized values of the Hall resistance has been improved to values better than $10^{-9}$. This is of special importance in view of the metrological applications [2]. Some excellent reviews about the Integer Quantum Hall Effect can be found in the literature [3–6].

The discovery of the von Klitzing effect stimulated intense experimental and theoretical research in many international laboratories. A particularly important discovery was made only 2 years later by the group of Tsui, Stormer and Gossard at Bell Laboratories [7]. In this experiment, a GaAs/AlGaAs-heterostructure which contained the dopant impurities only far from the electron inversion layer was used. As a consequence, these samples had a very high electron mobility in the inversion layer at the interface of a few hundred thousand $\mathrm{cm}^2/\mathrm{Vs}$. The researchers detected quantization of the Hall conductivity at fractional multiples of $e^2/h$ at temperatures of a few 0.1 K.

By improving the sample fabrication technology, more and more such additional fractional features were uncovered. Hitherto, electron mobilities of more than $10,000,000\,\mathrm{cm}^2/\mathrm{Vs}$ have been achieved and several dozens of the fractionally quantized features in the Hall resistance (and their counterparts in the magneto-resistance) are known now [8]. They have been associated with hierarchies of novel correlated electron states induced by the electron–electron interaction [9–11]. The existence of these states goes far beyond the traditional phenomenological Fermi liquid picture for electrons in metallic systems. Thus, the *Fractional Quantum Hall Effect* has opened a new field in the physics of *correlated* electrons, but is not the subject of this review article.

### 1.2. The localization model

According to the theory of the classical Hall effect the Hall resistivity of independent particles with the charge $e$ is a monotonic function of the magnetic flux density $B$ and the number density $n_e$ of the charges. This can be easily seen by using the Drude friction model for diffusion of charges in external crossed electric and magnetic fields [12]. It yields for the components of the conductivity tensor

$$\sigma_{xx} = \frac{\sigma_0}{1 + (\omega_B \tau)^2}, \quad \sigma_{yx} = \omega_B \tau \sigma_{xx} \ . \tag{2}$$

Here, $\sigma_0 = e^2 n_e \tau / m^*$ is the Drude conductivity. The mean free time $\tau$ of the particles due to scattering is assumed to contain all microscopic processes. The effective mass $m^*$ contains the effect of the lattice of atoms and interactions. The quantity $\omega_B = eB/m^*$ is the cyclotron frequency. The resistance components are obtained by inverting the conductivity tensor

$$\rho_{xx} = \frac{\sigma_{xx}}{\sigma_{xx}^2 + \sigma_{yx}^2}, \quad \rho_{xy} = \frac{\sigma_{yx}}{\sigma_{xx}^2 + \sigma_{yx}^2} \ . \tag{3}$$

For strong magnetic field ($B \to \infty$) $\sigma_{xx} \propto B^{-2}\tau^{-1} \to 0$. Correspondingly, since $\sigma_{yx} \neq 0$, the magnetoresistivity $\rho_{xx} \propto \sigma_{xx} \to 0$. The Hall resistivity is

$$\rho_{xy} := \rho_{\mathrm{H}} = \frac{1}{\sigma_{yx}} = \frac{B}{en_e} \ . \tag{4}$$

As the von Klitzing experiment contradicts this result, it is clear that the quantum nature of the two-dimensional electron system in the MOSFET subject to the high magnetic field must be the reason for the quantization of the Hall resistivity at sufficiently low temperatures.

For the Landau model for a single spinless electron in two dimensions in a perpendicular homogeneous magnetic field $\boldsymbol{B} = \nabla \times \boldsymbol{A}$, the vector potential given in the Landau gauge $\boldsymbol{A} = (0, Bx, 0)$, the Schrödinger equation is

$$H_0 \psi_{nk}(x, y) := \frac{1}{2m^*} \left( \frac{\hbar}{\mathrm{i}} \nabla + e\boldsymbol{A} \right)^2 \psi_{nk}(x, y) = E_{nk} \psi_{nk}(x, y) \ . \tag{5}$$

It is solved by the Landau states

$$\langle x, y | nk \rangle := \psi_{nk}(x, y) = \frac{1}{L^{1/2}} \, \mathrm{e}^{\mathrm{i}ky} \phi_n(x - X_k) \ , \tag{6}$$

where $X_k = -k\ell_B^2$ and $\ell_B := \sqrt{\hbar/eB}$ the magnetic length. The eigenvalues are the Landau levels

$$E_{nk} = \hbar\omega_B \left( n + \frac{1}{2} \right) \ . \tag{7}$$

They are associated with the normalized eigenfunctions

$$\phi_n(x) = \frac{1}{\sqrt{\pi^{1/2} \ell_B n!}} \exp\left( \frac{-x^2}{2\ell_B^2} \right) H_n\left( \frac{x}{\ell_B} \right) \tag{8}$$

with the Hermite polynomials $H_n$ ($n = 0, 1, 2, 3, \ldots$). The Landau states are degenerate with respect to the wave number $k$ with a degree per unit area of

$$n_B = \frac{eB}{h} = \frac{B}{\Phi_0} , \tag{9}$$

the density of flux quanta, $\Phi_0 = h/e$, in the system. This degeneracy can be easily understood by considering the maximum possible number of Landau wave functions (Eq. (6)) that can be contained in a system of the size $L^2$ [12],

$$X_k^{\max} = \frac{2\pi\ell_B^2}{L} n_B = L . \tag{10}$$

An important quantity is the *filling factor* which is defined by the ratio of the electron number density and the density of flux quanta,

$$\nu_B = \frac{n_e}{n_B} . \tag{11}$$

Integer filling factors $\nu_B = j$ correspond then to $j$ completely filled Landau levels. At the corresponding electron densities, the Hall resistance is an integer fraction of $h/e^2$ (cf. Eq. (4)).

However, this does *not* explain the existence of the wide plateaus in $\rho_{xy}(n_e)$ since upon increasing $n_e$ the Fermi level jumps between the Landau levels. In order to generate the observed wide plateaus, it is necessary to keep the Fermi level continuously varying *between* the Landau levels when changing $n_e$, but *without* changing the resistivity values of the plateaus.

A mechanism that can account for this pinning without affecting transport is localization of the wave functions due to disorder induced by the presence of the impurities in the system [13–15]. By introducing randomness into the Landau model of Eq. (5),

$$H = H_0 + V(\boldsymbol{r}) \tag{12}$$

the degeneracy of the Landau levels is removed. Here, $V(\boldsymbol{r})$ is a randomly varying potential which is usually defined via its statistical properties. The Landau levels are broadened into Landau bands by the disorder, with localized eigenstates occurring in the band tails. These localized states can pin the Fermi level at the corresponding eigenenergies. A qualitative picture of the density of states of such a model Hamiltonian is shown in Fig. 2.

Localized states correspond to random wave functions with envelopes that are exponentially decaying at large distances from some localization center [16,17]. This implies exponentially decaying correlation functions which indicates that the localized states cannot contribute to dc-transport at zero temperature. This means that the magneto-conductivity, and correspondingly the magneto-resistivity, vanish for filling factors corresponding to the energy regions of the localized states, while the Hall conductivity, and correspondingly the Hall resistivity, stay at a constant value.

On the other hand, non-localized—extended—states near the band centers, which do not decay exponentially and are spread randomly across the entire system, can account for electron transport. For filling factors close to half integer numbers, which correspond to the energy regions near the centers of the Landau bands, one expects peaks in the magneto-resistivity with widths that reflect the widths of the energy regions of the extended states. Simultaneously, the Hall resistivity is expected to change from one plateau value to the next. Often, these spectral regions are denoted as *compressible* since the

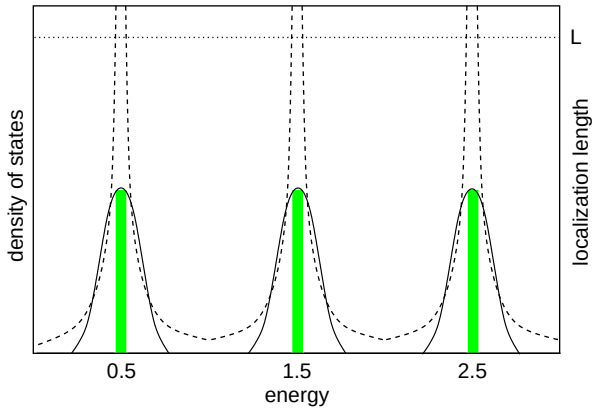


Fig. 2. Schematic picture of the density of states (full line, arb. units) and the localization lengths (dashed line, arb. units) as a function of the energy (in units of the cyclotron energy) in the localization model. When introducing a static random potential into the Landau model, Landau levels are broadened into bands consisting of "incompressible" spectral regions that correspond to localized states in the band tails, and "compressible" regions of effectively delocalized states (shaded) near the band centers. In the latter regions, the localization length exceeds the system size $L$. At finite temperature, the system size is replaced by the temperature-dependent phase coherence length $L_\phi$.

Fermi energy hardly changes with increasing electron number while the localized states are associated with *incompressible spectral regions* where the Fermi level strongly changes when varying the electron number [18].

As long as the Fermi level stays within the region of localized states, the zero temperature conductivity components are not changed. Assuming that the extended states provide the correctly quantized values of the Hall conductivity, and simultaneously a vanishing magneto-conductivity, one obtains the experimentally observed behavior of the conductivity. However, *that* the Hall conductance remains correctly quantized *exactly* at integer multiples of $e^2/h$ in the regions of localization, needs closer consideration. Laughlin's gauge argument, which we will shortly discuss below, is supposed to provide an explanation.

All of the analytical and numerical results obtained until recently are consistent with the picture that at the absolute zero of temperature the localization length diverges only at specific energies close to the centers of the Landau bands with a universal exponent $\nu$ which is independent of the specific form of the randomness and the band index [19,20],

$$\xi(E - E_n) = \frac{\xi_n}{|E - E_n|^\nu} , \tag{13}$$

where the constant $\xi_n$ depends on microscopic details of the randomness and on the Landau band index $n$. It will be one of the main tasks of the following sections to explain this critical behavior in some detail.

Table 1 contains a representative selection of the exponents determined numerically. If the exponent were universal the quantum Hall effect could be considered as a paradigm of a genuine universal quantum phase transition.

An important issue is how to detect this critical exponent in an experiment. As in an experiment the size of the two-dimensional electron system is finite, it is intuitively clear that the singularities of the localization length near the band centers cannot be resolved. Furthermore, at non-zero temperature, inelastic processes will lead to phase breaking scatterings between different eigenstates [16,17]. The latter

Table 1
Critical exponents $\nu$ of the quantum Hall phase transition in the lowest Landau band obtained by various theoretical methods

| $\nu$ | Model | Method | Reference |
|---|---|---|---|
| $\infty$ | Short-range impurities | Self-consistent perturbation | [21] |
| $\approx 2$ | Peierls tight binding | Transfer matrix scaling | [22] |
| $\approx 2.0$ | Short-range impurities | Recursive Green function | [23,24] |
| 2.35(3) | Random Landau matrix | Recursive Green function | [19,20] |
| 2.3(1) | Random Landau matrix | Recursive Green function | [25] |
| 2.4(2) | Random Landau matrix | Recursive Green function | [26] |
| 2.4(1) | Finite range impurities | Chern number scaling | [27] |
| $\approx 2.3$ | Spin–orbit scattering | Thouless number scaling | [28] |
| $\approx 2$ | Double layer system | Thouless number scaling | [29] |
| $\approx 2$ | Random matrix model | Scaling of level statistics | [30] |
| 2.5(5) | Chalker–Coddington | Transfer matrix scaling | [31] |
| 2.4(2) | Random saddle points | Transfer matrix scaling | [32] |
| 2.5(5) | Chalker–Coddington type | Real space renormalization | [33] |
| 2.39(1) | Chalker–Coddington type | Real space renormalization | [34–36] |
| 2.5(4) | Super spin chain | Density matrix renormalization | Obtained from [37] |
| 2.33(3) | Counter-propagating chiral Fermions | Monte Carlo | [38] |

Numbers in parentheses denote the uncertainty in the last digit of the exponent.

can be described by a mean, temperature-dependent phase breaking time $\tau_\phi(T)$ which can be assumed to increase with decreasing temperature according to

$$\tau_\phi(T) \propto \frac{1}{T^p} \tag{14}$$

with an exponent $p$ of order 1. During the time interval $\tau_\phi$, the electron can be considered as moving diffusively under the influence of the impurity scattering. This suggests to define a phase coherence length

$$L_\phi(T) = \sqrt{D\tau_\phi(T)} \tag{15}$$

with a disorder-induced diffusion constant $D$ that is related to the dc-conductivity via the Einstein relation $\sigma = e^2 D(E_\mathrm{F})\rho(E_\mathrm{F})$ where $\rho(E_\mathrm{F})$ is the density of states at the Fermi level.

In order to connect the singular behavior of the localization length with the results of a transport experiment it is important to note that a localized state appears extended if its localization length does exceed the system size $L$ or, at non-zero temperature, the above phase coherence length $L_\phi$ (Fig. 2). This implies that the widths of the peaks in the magneto-conductivity at the centers of the Landau bands are given by the condition $\xi(\Delta E) = \min\{L, L_\phi(T)\}$. The resulting characteristic temperature behaviors [19,20] have been found to be consistent with experimental data [39–44].

One still needs an argument as to why the Hall conductance is exactly quantized at integer multiples of $e^2/h$ in spite of the presence of the impurity potential. Such an argument has been pioneered by Laughlin [45]. The idea is to relate the current in an ideally metallic cylinder, subject to a homogeneous magnetic field perpendicular to the cylinder's surface, to the change of the total electronic energy $E(\Phi)$ when adiabatically changing a magnetic flux piercing the cylinder along its axis (Fig. 3),

$$I = \frac{\Delta E}{\Delta \Phi} \ . \tag{16}$$

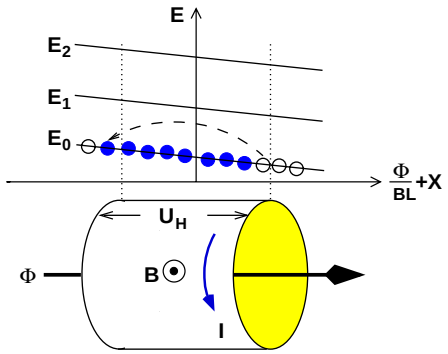


Fig. 3. Illustrating Laughlin's gauge argument: introducing a magnetic flux $\Phi$ along the axis of the cylinder corresponds to a shift of the wave number in azimuthal direction by $e\Phi/\hbar L$. A change of the gauge flux by $\Delta\Phi = \Phi_0$ corresponds to a shift of exactly $2\pi/L$. This leads to a corresponding shift in $X_k$ that is equivalent to transferring one electron per Landau band from one edge of the cylinder to the other that corresponds to a change in energy of $eU_{\mathrm{H}}$.

Introducing a gauge flux $\Phi$ along the axis of the cylinder corresponds to a shift of the wave number in azimuthal direction by $e\Phi/\hbar L$. This can also be considered as a change in the boundary condition.

A change of the flux by $\Delta\Phi = \Phi_0$ corresponds to a shift of exactly $2\pi/L$ and leads to a corresponding shift in $X_k$ (cf. Eq. (6)) that is equivalent to transferring one electron per Landau band from one edge of the cylinder to the other.[3] When occupying $j$ Landau bands, a transfer of $j$ electrons is associated with one flux quantum. Due to the presence of a Hall voltage $U_{\mathrm{H}}$ across the cylinder, the Landau levels are no longer degenerate, but on a straight line with a slope given by the Hall electric field $U_{\mathrm{H}}/L$ (Fig. 4). The energy change caused by the flux change is then $\Delta E = jeU_{\mathrm{H}}$, and the Hall current

$$I = j\,\frac{e^2}{h}U_{\mathrm{H}}\ , \tag{17}$$

consistent with integer quantization of the Hall conductance.

As presented, the argument seems to hold only for the ideal Landau Hamiltonian applied to a system of finite width. However, it can also be used in the presence of disorder [22]. To understand this, one has to have in mind that on the one hand, by definition, localized states are insensitive to changes in the boundary conditions or, equivalently, flux changes. On the other hand, the flux sensitivity of the extended states is enhanced, in order to compensate for the localized states [3–5,47–50]. This compensation is assured to be exact such that the final result for the current is the same as in Eq. (17).

Despite there exist several experimental features apparently related to electron interaction [51–59], it seems that the integer quantization of the Hall conductance can be understood within the localization model without taking into account the correlations between the electrons [5].

On the other hand, for explaining the fractionally quantized Hall effect, interaction and correlation effects are generally accepted to constitute the necessary ingredients for generating the *excitation gaps*

[3] Strictly speaking, for a two-dimensional system with periodic boundary conditions in one direction and fixed boundary conditions in the perpendicular direction, one finds a non-degenerate energy spectrum that differs from the Landau spectrum by the presence of edge states [12,46]. However, for the present qualitative argument, this is not important.

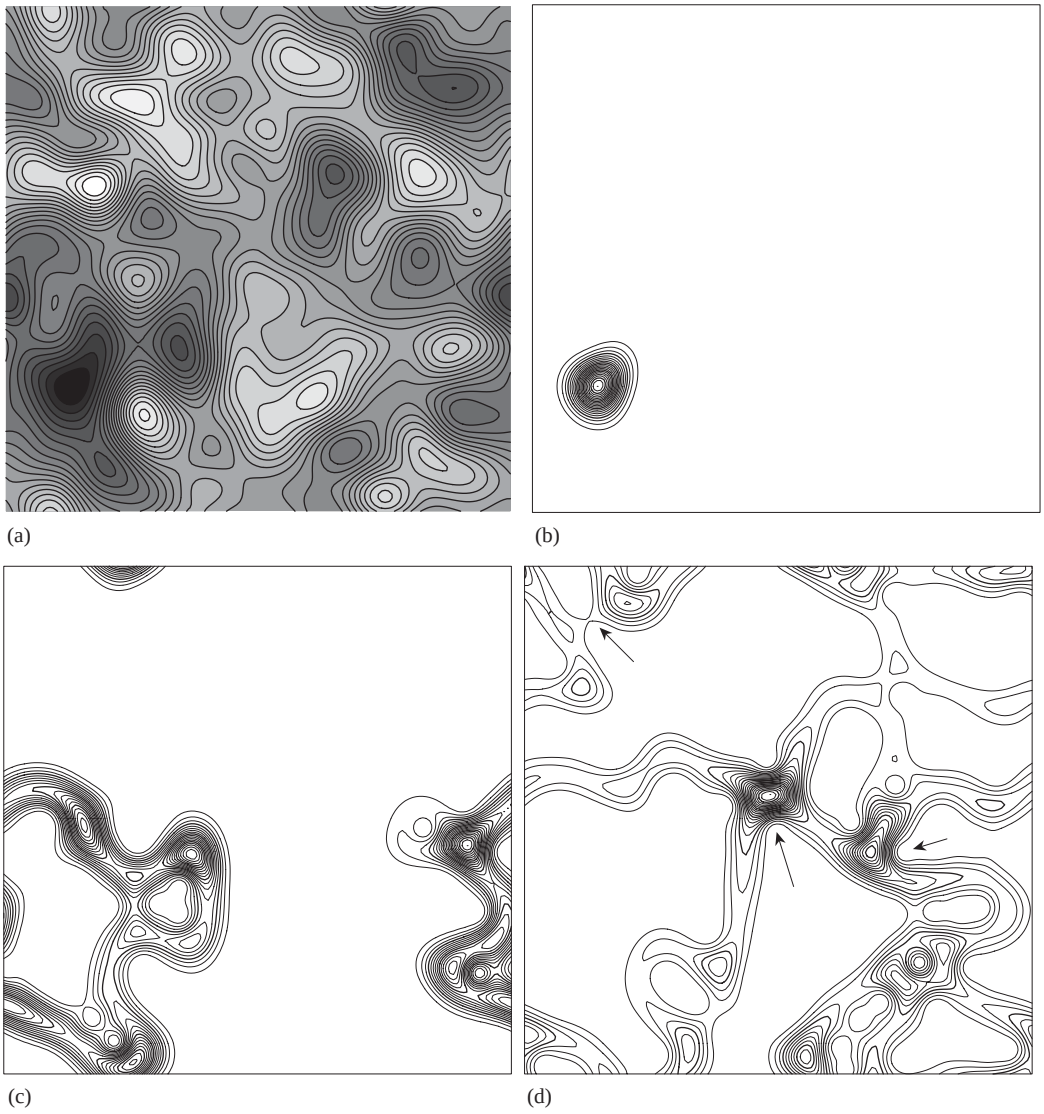


Fig. 4. Long-range correlated random potential obtained as superposition of randomly placed Gaussian potentials with a width $\ell_c = 2\ell_B$ and some examples of eigenfunctions. (a) gray scale plot of the potential landscape with equipotential lines indicated; white: high potential, black: low potential; (b)–(d) the moduli of a selection of characteristic wave functions corresponding to (b) a low energy in the tail of a Landau Band, localized in a deep potential valley; (c) an intermediate energy in the Landau band, still localized and following mainly an equipotential line; (d) an energy near the center of the Landau band, extending essentially along equipotential lines, occasionally inter-connected via tunneling near the saddle points of the potential (indicated by arrows).

between the many-electron ground states associated with rational filling factors. Nevertheless, in order to generate the fractional *plateaus* in the Hall conductivity, disorder is believed to be essential in pinning the chemical potential, in close analogy to the Integer Quantum Hall Effect.

### *1.3. Plan of the article*

In summary, the Quantum Hall Effect—consistent with all of the presently available experiments—seems to be an exact and very fundamental phenomenon. One needs for its physical understanding, and in particular for a theory with predictive power, not only interactions and correlations in a two-dimensional many-body system but in particular, and somewhat counter-intuitively—in view of the precision aspect—the presence of a certain amount of disorder. It is one of the main purposes of this article to review our present understanding, why, in spite of and due to the disorder, the Quantum Hall Effect is the most exact phenomenon known in low-dimensional electron systems. We will restrict ourselves to the *Integer* Quantum Hall Effect, ignoring interactions completely.

Especially, we will discuss the localization concept by introducing the so-called random network model originally invented by Chalker and Coddington [31] in order to describe the localization of quantum states in a random potential with long-range spatial correlations in the presence of a strong, "quantizing" magnetic field. Later, we will discuss several generalizations of the network model which underline the general importance of the phenomenon.

We will proceed in the following sections by pursuing a strategy which we hope will enable non-specialists in the field to understand the main ideas in a self-contained way. We will always start from elementary accessible facts that form the background of more complicated relations before we eventually describe to some extent the issues that are more at the frontier of present research. As the field has been, and still is, extremely rapidly growing, we cannot guarantee that all of the available results have been included, especially the most recent ones. We have attempted our best to include at least references to all of the important results. We apologize in advance to all colleagues, whose research efforts might not be sufficiently highlighted according to their importance or even not be included at all.

The plan of the paper is as follows. In the next section, the so-called percolation model for an electron in a spatially slowly varying random potential landscape is introduced in some detail. It can be viewed as the backbone of the random network model. If it is supplemented by quantum effects, it can be considered as a precursor of the random network model of Chalker and Coddington for describing localization in the presence of a quantizing magnetic field.

The latter will be introduced in Section 3. In Section 4, the localization properties of the model will be discussed in some detail. Strangely enough, technical difficulties seem to have prevented a high-precision determination of the critical exponent up to now for the original Chalker–Coddington random network model. Section 5 contains some results for the transport properties, especially near the quantum critical point.

In Section 6, we investigate the renormalization group approach for describing the critical properties in some detail. Especially, we will emphasize here that one can use this as a starting point for the definition of a truncated Chalker–Coddington model which can be treated numerically exactly and allows for determining the critical exponent with high precision.

Sections 7, 8, 9 and 10 contain extensions to a number of equivalent Hamiltonians, to systems with other symmetries, and to an equivalent field theoretical formulation of the random network model of Chalker and Coddington, respectively. In these sections, we have attempted to provide some flavor of the power and importance of the model in fields other than the quantum Hall phase transition. While we will review much numerical and experimental evidences for the universality of the quantum Hall transition, any attempts to classify it, like other two-dimensional phase transitions, based on the conformal invariance at the critical point have failed so far.

In Section 10 we review a very recent suggestion, namely that the quantum Hall critical point may belong to a new class of critical points being described by a supersymmetric conformal field theory [60,61]. This is based on the fact that an anisotropic version of the Chalker–Coddington model as well as the random Landau model at the critical point can both be mapped on the Hamiltonian of a chain of antiferromagnetic superspin chains. We review its derivation, and the progress which has been achieved towards the characterization of the quantum Hall transition that way, although an analytical calculation of its critical exponents is still missing.

Generalizations to several layers and higher dimensions are briefly discussed in Section 11 before we conclude by summarizing the status of the field and comment on possible future developments.

## 2. The percolation model

We start by describing the physics of the so-called percolation model for the Quantum Hall Effect. In this model, which is valid in the limit of a *very high magnetic field*, the quantum mechanical wave functions are assumed to percolate along the equipotential lines of a slowly varying random potential landscape, in analogy to a classical percolating fluid in a random system [62]. Using this picture of a percolating wave function, one can understand why localized wave functions may exist, and, in particular, why there may be isolated critical points in the energy spectrum of the Hamiltonian where the localization length diverges. This high-field limit is often denoted as the classical percolation limit, although what is percolating is probability amplitude and not a classical fluid. In the quantum mechanical version of the model, tunneling of probability amplitude between the equipotential lines is taken into account whenever they get close to each other in space. In this version, the necessary competing ingredients—quantum tunneling and interference—are included such that a generic universal quantum mechanical localization–delocalization transition can be described.

The percolation model provides the physical background of the Chalker–Coddington network model—a generic model which is assumed to describe the *universal* quantum mechanical properties of non-interacting electrons in two dimensions in the presence of a random potential subject to a strong perpendicular magnetic field.

### 2.1. Wave functions in a spatially correlated random potential in a strong magnetic field

The origin of the random potential in the plane of the inversion layer $V(x, y)$ of the electrons in a GaAs/AlGaAs heterostructure or a MOSFET transistor is the impurities in the semiconductor material, especially as a consequence of the doping. These impurities are distributed randomly at some distance from the inversion layer. Thus, only the Coulomb tails of their potentials do influence the dynamics of the charges. This implies that the distribution of the potential energy $V(x, y)$ is long-range correlated in space. For convenience, we assume in the following that the spatial average of the random potential vanishes. This can always be achieved by a suitable choice of the zero of energy. For the correlator we assume

$$\overline{V(x', y')V(x, y)} := W^2 C(x' - x, y' - y) \ , \tag{18}$$

with the correlation function $C(x, y)$ having an exponential or Gaussian decay length $\ell_c$ much longer than the magnetic length $\ell_B$. It is also assumed that the probability distribution of the potential, $P[V(x, y)]$ is symmetric and homogeneous, i.e. independent of the origin of coordinate system.

Fig. 4 shows an example of such a long-range correlated random potential, together with several examples of the corresponding wave functions. They were obtained by solving numerically the Schrödinger equation

$$[H_0 + V(x, y)]\psi_\nu(x, y) = E_\nu\psi_\nu(x, y) \tag{19}$$

in the basis of the Landau states. An important characteristic feature to be kept in mind is that the wave function amplitudes are essentially non-zero only along equipotential lines of the potential. In addition, when two equipotential lines get close to each other near a saddle point of the potential, the amplitude becomes high *across* the saddle point. This can be taken as an indication of quantum tunneling as indicated in Fig. 4 by arrows.

The qualitative features of the wave functions in Fig. 4 may be taken as the motivation for introducing the concept of a percolating probability amplitude which we will now describe. The resulting model is important because it allows for qualitative understanding of localization in two-dimensional electron systems in the presence of a strong magnetic field. It allows also to understand why, within each Landau band, there must be an energy where the localization length diverges. This energy corresponds to the percolation critical point at which the wave function can percolate throughout the entire system. The basic physical ingredients of the percolation model may then be used to establish as an idealized version the random quantum network which allows for systematically dealing with certain universal localization and transport phenomena, especially in the quantum Hall critical regime.

In order to introduce the essential idea, we consider the Schrödinger equation (19) in the limit $\ell_c \gg \ell_B$ that can always be achieved for very large magnetic field, $B \to \infty$ [63]. In this limit, we will eventually also fulfill the condition $\hbar\omega_B \gg W$ such that the disorder-induced mixing of the Landau bands can be neglected.

It is of advantage to introduce new coordinates [5,63,64]

$$X = -k\ell_B^2, \quad Y = -\mathrm{i}\ell_B^2\frac{\mathrm{d}}{\mathrm{d}X} := \frac{\ell_B^2}{\hbar}P \ . \tag{20}$$

They are called center-of-motion coordinates. This is reasonable since $X$ is the center of the Gaussian wave packet in the $x$-direction of the Landau states (Eq. (6)). Furthermore, one observes that $(\mathrm{i}\mathrm{d}/\mathrm{d}k)^p$ plays the role of $\langle y^p\rangle$ by calculating the matrix elements of $y^p$ in the Landau states ($p$ integer). At finite magnetic field, the electrons can be viewed as describing cyclotron orbits with radius $\ell_B$ around the center of motion. For $\ell_B \ll \ell_c$ the diameter of the cyclotron orbit becomes vanishingly small such that $(x, y)$ can be replaced by center of motion $(X, Y)$.[4] The center-of-motion coordinates fulfill commutation relations similar to position and momentum operators,

$$[X, Y] = \mathrm{i}\ell_B^2 \ . \tag{21}$$

[4] Note that this limit has to be taken only after the thermodynamic limit $L \to \infty$ has been performed which is necessary to make $X$ a continuous variable.

We start by writing the solutions of the Schrödinger equation for the system of the size $L$ in the representation of the Landau states

$$\Psi(x, y) = \sum_{nk} C_n(-\ell_B^2 k)\psi_{nk}(x, y) := \sum_{nX} \langle xy|nX\rangle\, C_n(X) \ . \tag{22}$$

This gives

$$\sum_{X'} (E_n \delta_{X,X'} + \langle nX|V|nX'\rangle) C_n(X') = EC_n(X) \tag{23}$$

with inter-Landau band couplings neglected as a consequence of the high-field limit, index $k$ on the energy $E_n$ of the Landau level omitted due to degeneracy, and the Kronecker delta $\delta_{X,X'}$. The potential matrix elements are

$$\langle nX|V|nX'\rangle = \frac{1}{L}\int \mathrm{d}x\, \mathrm{d}y \phi_n(x - X)V(x, y)\phi_n(x - X')\mathrm{e}^{\mathrm{i}y(X-X')/\ell_B^2} \ . \tag{24}$$

Since the potential is slowly varying on the scale of $\ell_B$ it may be expanded into a power series near some arbitrary $y_0(x)$ in Eq. (24). With this, one easily verifies that

$$\int \mathrm{d}y V(x, y)\mathrm{e}^{\mathrm{i}y(X-X')/\ell_B^2} = V\left(x, -\mathrm{i}\ell_B^2 \frac{\mathrm{d}}{\mathrm{d}X'}\right)\frac{1}{L}\int \mathrm{d}y \mathrm{e}^{-\mathrm{i}y(X-X')/\ell_B^2} \ . \tag{25}$$

Finally, the integration with respect to $x$ may be approximated by assuming $x \approx X$ in the potential since at high magnetic field $|\phi_n(x - X)|^2$ can be assumed to be very well localized near $X$ within a distance $\ell_B$. Now Eq. (23) becomes

$$V(X, Y(X'))C(X')|_{X=X'} \approx EC(X) \ . \tag{26}$$

Here, $E$ is the energy corresponding to the equipotential line, and the index $n$ has been suppressed. Furthermore, $E_n$ has been assumed to be the zero of the energy. This is justified since the distance between the Landau bands increases $\propto B$ and the disorder broadening of the bands is only $\propto \sqrt{B}$ such that at high field the couplings between the bands due to disorder can be neglected.

The random Schrödinger equation (26) can approximately be solved by using the semi-classical WKB (Wentzel–Kramers–Brillouin) Ansatz

$$C(E, X) \propto \exp\left[-\mathrm{i}\int^X \mathrm{d}X' k(E, X')\right] \ , \tag{27}$$

neglecting the derivatives of the local wave number $k(E, X)$ with respect to $X$. This is possible for sufficiently smooth randomness such that second order, and higher-order derivatives in the expansion may be omitted. Under these assumptions, the dispersion $k(E, X)$ fulfills

$$E = V[X, \ell_B^2 k(E, X)] \ . \tag{28}$$

This establishes a most remarkable result, namely that the eigenfunctions can be considered as the superpositions of the Landau states that are associated with the equipotential line associated with the energy $E$.

### 2.2. The form of the semiclassical wave functions

The general form of these wave functions which propagate on the equipotential lines may be conjectured by considering the elementary example of a two-dimensional harmonic potential $V(x, y) = V_0(x^2 + y^2)$. This represents approximately the situation far from the Landau band center near a local minimum or maximum of the potential. Of course, this model can be solved exactly. However, it is instructive to look at it using the above percolation viewpoint.

The equipotential lines are the circles $X^2 + \ell_B^4 k^2(E, X) = E/V_0 := \epsilon$. By applying Eq. (26) and calculating $C(X)$ from Eq. (27) one obtains

$$C(X) \propto \exp\left[-\frac{\mathrm{i}\epsilon_m}{2\ell_B^2}\arccos\left(\frac{X}{\sqrt{\epsilon_m}}\right) \mp \frac{\mathrm{i}X}{2\ell_B^2}\sqrt{\epsilon_m - X^2}\right] . \tag{29}$$

The energy is given by the condition that $C(X)$ must be a periodic function of $X$. This implies for the closed integral over the equipotential circle

$$\oint \mathrm{d}X'\, k(E, X') = \frac{\pi\epsilon_m}{\ell_B^2} := 2\pi m \quad (m \text{ integer}) . \tag{30}$$

This is consistent with the result one obtains for the lowest Landau level in the symmetric gauge with the definition $V_0 := e^2B_0^2/8m^*$, and $m$ being the angular momentum quantum number [65].

By inserting the result equation (29) into the expression for the wave function equation (22) one gets for $\ell_B^2 \ll \hbar\omega_B/V_0$, i.e. neglecting the inter-Landau level coupling, an expression for the wave function which is a reasonable approximation for $X/\sqrt{\epsilon_m} < 1$,

$$\psi(x, y) \propto \int_{-\sqrt{\epsilon_m}}^{\sqrt{\epsilon_m}} \mathrm{d}X\, \exp\left[-\frac{\mathrm{i}X}{2\ell_B^2}\left(2y \pm \sqrt{\epsilon_m - X^2}\right)\right] \exp\left[-\frac{(x-X)^2}{2\ell_B^2}\right] \times \exp\left[-\frac{\mathrm{i}\epsilon_m}{2\ell_B^2}\varphi_m(X)\right] \tag{31}$$

with $\varphi_m(X) = \arccos(X/\sqrt{\epsilon_m})$. Approximate evaluation of the integral gives

$$\psi(x, y) \propto \exp\left[-\frac{\mathrm{i}xy}{2\ell_B^2}\right] \exp\left[-\frac{1}{8\ell_B^2}\left(y \pm \sqrt{\epsilon_m - x^2}\right)^2\right] \mathrm{e}^{-\mathrm{i}k_m u} . \tag{32}$$

The wave number corresponds to $k_m := m/\sqrt{\epsilon_m}$ and $u = \varphi\sqrt{\epsilon_m}$ is the azimuthal coordinate on the circle with the radius $\sqrt{\epsilon_m}$. The phase factor mediates a gauge transformation to the symmetric gauge. The Gaussian factor localizes the wave function along the circle within an interval of the width $\approx 2\sqrt{2}\ell_B$.

This suggests that in general the wave functions corresponding to the equipotential lines can be written in the form [66,67]

$$\psi(x, y) \propto f(v)\mathrm{e}^{\mathrm{i}\kappa(u,v)u} \tag{33}$$

with a local wave number $\kappa(u, v)$ that depends on coordinates $u$ and $v$ which parameterize the distance along and perpendicular to the equipotential line $V(x, y) = E$, respectively. The function $f(v)$ is

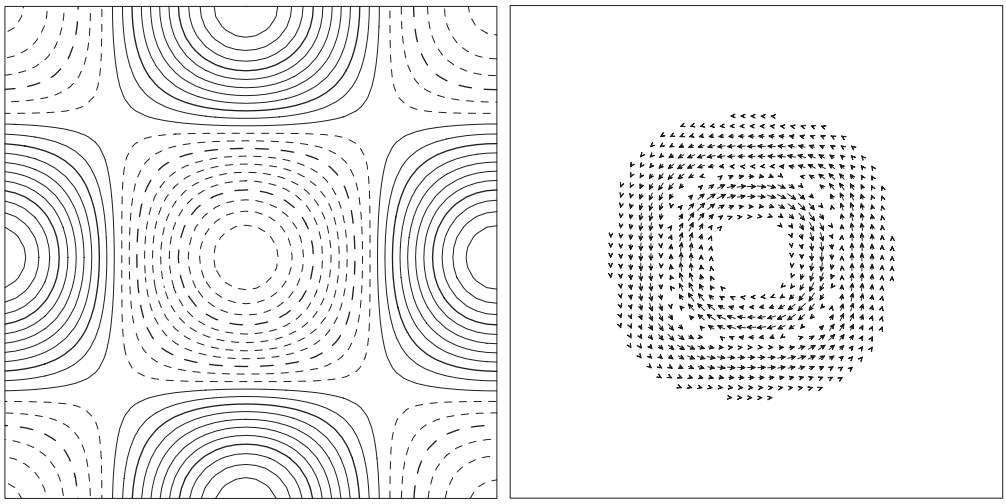


Fig. 5. (a) Scheme of a potential profile near the local potential minimum, and (b) the current density of a state localized along an equipotential line. The current density circles within a region of diameter $2\ell_B$ around the equipotential line. Only the net current flows along the equipotential line.

non-vanishing only within a region of the approximate width $\ell_B$ along this line. Locally, the wave function has the form of a wave propagating along the equipotential line. This is associated with an equilibrium current density

$$\boldsymbol{j} \propto \frac{1}{m^*}\boldsymbol{e}_u |f(v)|^2 \hbar\kappa(u, v) \tag{34}$$

that yields a net current along the equipotential line

$$\boldsymbol{j} \propto \frac{\hbar\kappa(u, v)}{m^*}\,\boldsymbol{e}_u \ . \tag{35}$$

Perpendicular to the direction of $u$, the current density obviously must vanish (Fig. 5). Classically, the net current is produced by the cyclotron motion of the electron which drifts along the equipotential line in the strong magnetic field and the local electric field of the potential that is directed perpendicular to the equipotential line (Fig. 5). This visualizes that only superpositions of those Landau states can contribute to the eigenstates which are located near the equipotential line at the corresponding eigenenergy.

The quantum mechanical problem of solving the Schrödinger equation of a particle in a high magnetic field and a random potential has thus been replaced by the task of finding the equipotential lines in the random potential landscape. This corresponds to a classical percolation problem [68]. Recently, another connection between quantum Hall plateau transitions and percolation, based on the classical limit of quantum kinetic equations, has been discussed [69,70].

### 2.3. Localization in the percolation limit

The localization properties in this limit of a very strong magnetic field may now be easily discussed [66,71]. Consider the smoothly varying landscape of the random potential (Fig. 4). When the energy is very low (or very high), the corresponding equipotential lines are closed trajectories captured within the minima (or maxima) of the potential (Fig. 4b). When the energy increases, these closed trajectories begin to meander around several of the minima (or maxima) (Fig. 4c).

The wave functions that correspond to these equipotential lines are necessarily localized superpositions of Landau states. They are localized exponentially as has been shown in [72]. Only at a certain critical energy, say $E_c$, close to the center of a Landau band, an equipotential line can percolate through the whole system. Only at this energy the wave function can propagate throughout the entire system in the limit of infinite system size (Fig. 4d). The energy $E_c$ corresponds to the percolation threshold of the classical percolation problem. For symmetric distribution of the potential, $P(V) = P(-V)$, the critical energy is at the center of the Landau band, $E_c = 0$.

Thus, the percolation picture allows immediately for a very important conclusion: since the percolating equipotential lines are closed for all energies except the critical energy of the percolation threshold, all of the wave functions must be localized except for the one associated with the critical energy.

Let us define the localization length $\xi_p(E)$ as the correlation length of a percolating equipotential line. Then, percolation theory says that $\xi_p(|E - E_c|)$ must increase according to a power law as $|E - E_c|$ decreases,

$$\xi_p(E - E_c) \propto \frac{1}{|E - E_c|^{\nu_p}} , \tag{36}$$

with a universal exponent $\nu_p = 4/3$ that has been calculated exactly [73].

### 2.4. Tunneling correction to the percolating wave functions

When two equipotential lines get close to each other near a saddle point of the potential, tunneling processes will occur. In order to determine the localization length, these have to be taken into account [74]. For a symmetric distribution of the potential, the tunneling, however, will not change the position of the critical energy.

A general definition of the localization length in terms of the Green function is [17]

$$\gamma(E) := \frac{1}{\xi(E)} = -\lim_{|\boldsymbol{r}-\boldsymbol{r}'|\to\infty} \frac{\langle \ln |G(\boldsymbol{r}, \boldsymbol{r}'; E)| \rangle}{|\boldsymbol{r} - \boldsymbol{r}'|} \tag{37}$$

with $\langle \ldots \rangle$ denoting the ensemble average with the above probability distribution of the potential, $P$. It is well known [75–79], that in weakly disordered systems, defined by $k_F l \gg 1$, where $l$ is the disorder induced mean free path and $k_F$ the Fermi wave number, the disorder averaged electron wave function amplitude $\langle \psi(\mathbf{x}, t) \rangle$ decays on length scales of the order of $l$, since the random phase shifts associated with the scattering at the impurities are averaged out. This destroys the information on multiple scattering, and thus on localization. In order to describe localization, it is therefore necessary to average over disorder functions containing higher moments of the propagator $G$, like the expression used in Eq. (37). Furthermore, it is

well established that this quantity is self-averaging, namely its ensemble average coincides with its most probable value [17] in the thermodynamic limit. Therefore, one can calculate instead of the ensemble average the spatial average for a given realization of the random potential. We will now use this definition of the localization length for estimating the correction to the critical exponent, $\nu_{\mathrm{p}}$, of the percolation model due to tunneling at the saddle points of the potential.

Using the above implicit dispersion relation, Eq. (28), we first determine the Green function in the mixed representation $(X, k(E_0, X))$ where $E_0$ denotes the energy of an equipotential line,

$$G(X, k(E_0, X); E) = \frac{1}{E - E_0(k, X) - \mathrm{i}\eta} , \tag{38}$$

with $\eta$ a positive infinitesimal real number. By Fourier transforming with respect to $k$ one can determine the behavior of the Green function along the $y$-axis which is sufficient for estimating the asymptotic behavior at $|y| \to \infty$,

$$G(X, y; E) = \frac{1}{2\pi} \int \mathrm{d}k \mathrm{e}^{-\mathrm{i}ky} G(X, k; E) , \tag{39}$$

one obtains

$$G(X, y; E) \propto \sum_j \mathrm{e}^{-\mathrm{i}k_j(E,X)y} = \sum_j \mathrm{e}^{-\mathrm{i}\,\mathrm{Re}\,k_j y} \mathrm{e}^{-\mathrm{Im}\,k_j(E,X)|y|} , \tag{40}$$

where $k_j(E, X)$ are the complex roots of Eq. (28) for given $X$ and $E = E_0$. The asymptotic exponential decay of the Green function for $|y| \to \infty$ is given by the spatial average of the smallest $\mathrm{Im}\,k_j(E, X) > 0$,

$$\gamma(E) = \left\langle \min_j \mathrm{Im}\,k_j(E, X) \right\rangle_P . \tag{41}$$

As described above (compare Fig. 4), we need to consider saddle point regions of the random potential near $E_{\mathrm{c}}$, since predominantly it will be here where the wave functions are connected between different equipotential lines via tunneling, and for the critical behavior, energies close to $E_{\mathrm{c}}$ are important. Near a saddle point $(X_0, k_0)$, the potential can be expanded (Fig. 6),

$$V(X, \ell_B^2 k) = E_{\mathrm{c}} - a^2(X - X_0)^2 + b^2 \ell_B^2 (k - k_0)^2 . \tag{42}$$

From $E = V(X, \ell_B^2 k)$ one obtains the solution

$$k - k_0 = \pm \frac{1}{b\ell_B} \sqrt{E - E_{\mathrm{c}} + a^2(X - X_0)^2} . \tag{43}$$

Due to symmetry, it is sufficient to consider, say, $E < E_{\mathrm{c}}$. Then, $\mathrm{Im}\,k \neq 0$ only for $E_{\mathrm{c}} - E > a^2(X - X_0)^2$

$$\mathrm{Im}\,k(E, X) = \frac{1}{b\ell_B} \sqrt{E_{\mathrm{c}} - E - a^2(X - X_0)^2} . \tag{44}$$

Averaging this with respect to $X$ yields

$$\gamma(E) \propto \int_{X_-}^{X_+} \mathrm{d}X \sqrt{E_{\mathrm{c}} - E - a^2(X - X_0)^2} \propto E_{\mathrm{c}} - E \tag{45}$$

with $X_\pm = X_0 \pm \sqrt{E_{\mathrm{c}} - E}/a$.

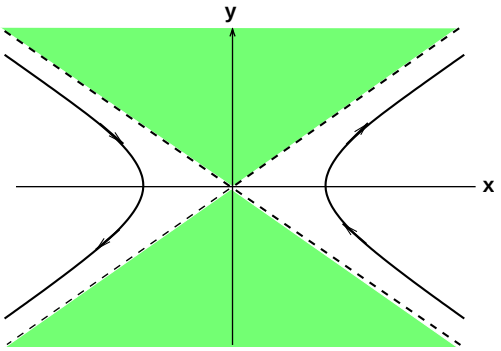


Fig. 6. Equipotential trajectories of a saddle point potential for an energy below the saddle point potential. Dashed lines: equipotential lines exactly at the energy of the saddle point; shaded: region with potential energy higher than the saddle point energy $E_c$ (after [80]).

The asymptotic exponential decay for energies near $E_c$ can be estimated by using the following heuristic argument. The equipotential lines representing the wave functions form percolation clusters with an energy dependent correlation length $\xi_P(E) \sim |E - E_c|^{-4/3}$. Delocalization of the wave functions associated with these clusters can occur via tunneling through the saddle points that connect different equipotential clusters. The number of saddle points will be proportional to the size of the clusters at energy $E$, namely $\propto \xi_P(E)$. Thus, the probability of finding the saddle point with the smallest $\gamma$ at energy $E$ connecting two adjacent clusters will be $\ell_B/\xi_P(E)$. The saddle point with the *smallest* $\gamma$ will dominate the asymptotic behavior of the wave functions. All of the contributions of the other saddle points will be exponentially suppressed with the diameter of the clusters. Therefore, we finally can write for the average inverse localization length the power law

$$\gamma(E) \propto \frac{1}{\xi_P(E)}|E - E_c| \propto |E - E_c|^{4/3+1} \ . \tag{46}$$

According to this qualitative argument, the critical exponent of the localization length in a quantum Hall system including the effect of quantum tunneling should be $\nu = 7/3$, without interactions.

It has taken considerable theoretical [19,20,23,81–83] and experimental [39–42] efforts to determine quantitatively this exponent for two-dimensional disordered Landau system without interaction. The most accurate numerical values obtained so far are $\nu = 2.35 \pm 0.03$ by using a random Landau matrix model [20], $\nu = 2.33 \pm 0.03$ from a Monte Carlo calculation for chiral fermions [38], and a renormalization group approach based on a random network model $\nu = 2.39 \pm 0.01$ [34–36] (cf. Table 1). Numerical investigations were done for a variety of completely different models, including white noise [19,23] as well as long-range correlated [31,82] randomness and including also higher Landau bands [20,83]. All of the results are consistent with these values within error bars. This strongly suggests that the critical exponent of the quantum phase transition associated with the Quantum Hall Effect is indeed universal, and does not depend on the microscopic details of the model used.[5] Although the near coincidence of

[5] For very long range correlated randomness there recently seems to be evidence that $\nu$ changes [84].

this exponent with the value 7/3, as obtained from the simple heuristic argument outlined above, seems compelling we caution that an analytical derivation of the critical exponents at the quantum Hall transition is still lacking. Recent progress towards achieving this goal is reviewed in Section 10.

## 3. The random network model

The results obtained in the above discussed high-magnetic field limit may be used not only for estimating the critical behavior but also as a starting point for constructing a model that contains all of the necessary physical ingredients—backscattering and tunneling—for describing the quantum critical points near the centers of the Landau levels and the corresponding transport quantities. If the critical behavior could be shown to be universal such a model should be of great importance. This would be especially true, if one could use the model as a starting point for more rigorous theoretical formulations.

As argued above, percolation of probability amplitude along equipotential lines as well as tunneling of amplitude between equipotential lines near the saddle points of the potential have to be taken into account on an equal footing when determining critical properties. This suggests to construct a model consisting of a regular lattice of saddle points that are connected via links along which probability amplitude can propagate.

### *3.1. The scattering wave functions associated with a saddle point*

Before doing so, it is instructive to consider saddle point tunneling more formally from the scattering point of view, and establish an exact expression for the transmission probability. As a side remark, we note that this is yet another illuminating example of a quantum wave function that can be treated exactly in the high magnetic field limit [80].

The most simple saddle point is defined by the quadratic potential considered in the previous section with equal coefficients $a^2 = b^2 \equiv U$ [80]

$$V_{\mathrm{sp}}(x, y) = E_{\mathrm{c}} + U(y^2 - x^2) \ . \tag{47}$$

The classical trajectories in such a potential for energies below $E_{\mathrm{c}}$ are shown in Fig. 6. For the corresponding quantum mechanical wave functions the considerations of the previous sections apply when neglecting tunneling between the trajectories. This can be justified for energies well below (or well above) $E_{\mathrm{c}}$. However, when $E \approx E_{\mathrm{c}}$ this is no longer the case.

The total Hamiltonian including the saddle point

$$H = H_0 + V_{\mathrm{sp}}(x, y) = \frac{1}{2m^*}\left(\frac{\hbar}{\mathrm{i}}\nabla + e\boldsymbol{A}\right)^2 + V_{\mathrm{sp}}(x, y) \tag{48}$$

is quadratic in the variables. It can be diagonalized in analogy with in the case of the two-dimensional harmonic oscillator.

However, here we follow the very illuminating method used in [80]. For the vector potential, we assume the symmetric gauge, $\boldsymbol{A} = (B/2)(-y, x)$. We perform first a unitary transformation that brings the Hamiltonian into a separable form.

By introducing the new variables

$$a_x = \frac{x}{2\ell_B} + \ell_B \frac{\partial}{\partial x} \ , \tag{49}$$

$$a_y = \frac{y}{2\ell_B} + \ell_B \frac{\partial}{\partial y} \ , \tag{50}$$

that fulfill the commutation relations

$$[a_x, a_x^\dagger] = [a_y, a_y^\dagger] = 1 \ , \tag{51}$$

$$[a_x, a_y] = [a_x^\dagger, a_y^\dagger] = 0 \ , \tag{52}$$

the Hamiltonian becomes

$$\begin{aligned} H = {} & \frac{\hbar\omega_B}{2}(a_x^\dagger a_x + a_y^\dagger a_y + 1) + \frac{\hbar\omega_B}{2\mathrm{i}}(a_x^\dagger a_y - a_y^\dagger a_x) \\ & + \gamma[(a_y + a_y^\dagger)^2 - (a_x + a_x^\dagger)^2] + E_\mathrm{c} \ , \end{aligned} \tag{53}$$

where $\gamma = U\ell_B^2$. The unitary transformation

$$\begin{pmatrix} a_x \\ a_y \end{pmatrix} = \begin{pmatrix} \mathrm{i}\cos\phi & \sin\phi \\ -\sin\phi & -\mathrm{i}\cos\phi \end{pmatrix} \begin{pmatrix} b_1 \\ b_2 \end{pmatrix} \ , \tag{54}$$

with $\tan(2\phi) = -\hbar\omega_B/4\gamma$, transforms the Hamiltonian into a sum of two independent terms, $H_1(b_1, b_1^\dagger)$ and $H_2(b_2,\ b_2^\dagger)$,

$$H_1 = (b_1^\dagger \quad b_1) \begin{pmatrix} \frac{\hbar\omega_B}{4} - \hbar\Omega & \gamma \\ \gamma & \frac{\hbar\omega_B}{4} - \hbar\Omega \end{pmatrix} \begin{pmatrix} b_1 \\ b_1^\dagger \end{pmatrix} \ , \tag{55}$$

$$H_2 = (b_2^\dagger \quad b_2) \begin{pmatrix} \frac{\hbar\omega_B}{4} + \hbar\Omega & -\gamma \\ -\gamma & \frac{\hbar\omega_B}{4} + \hbar\Omega \end{pmatrix} \begin{pmatrix} b_2 \\ b_2^\dagger \end{pmatrix} \ , \tag{56}$$

where $\hbar\Omega = \sqrt{\gamma^2 + (\hbar\omega_B/4)^2}$, and

$$[b_1, b_1^\dagger] = [b_2, b_2^\dagger] = 1 \ , \tag{57}$$

$$[b_1, b_2] = [b_1, b_2^\dagger] = 0 \ . \tag{58}$$

These can be diagonalized by a Bogoliubov transformation,

$$\begin{pmatrix} b_i \\ b_i^\dagger \end{pmatrix} = \begin{pmatrix} \cosh\theta_i & \sinh\theta_i \\ \sinh\theta_i & \cosh\theta_i \end{pmatrix} \begin{pmatrix} c_i \\ c_i^\dagger \end{pmatrix} \ , \tag{59}$$

with $\tanh(2\theta_1)=\gamma^{-1}(-\hbar\omega_B/4+\hbar\Omega)$, and $\tanh(2\theta_2)=\gamma(\hbar\omega_B/4+\hbar\Omega)^{-1}$, which gives for the Hamiltonian

$$H = E_1\left(c_1^2 + c_1^{\dagger 2}\right) + E_2\left(c_2^\dagger c_2 + \tfrac{1}{2}\right) + E_\mathrm{c}\ , \tag{60}$$

with

$$[c_1, c_1^\dagger] = [c_2, c_2^\dagger] = 1\ , \tag{61}$$

$$[c_1, c_2] = [c_1, c_2^\dagger] = 0 \tag{62}$$

and the energy eigenvalues

$$E_1 = \sqrt{\gamma^2 - \left(\frac{\hbar\omega_B}{4} - \hbar\Omega\right)^2}\ , \tag{63}$$

$$E_2 = 2\sqrt{\left(\frac{\hbar\omega_B}{4} + \hbar\Omega\right)^2 - \gamma^2}\ . \tag{64}$$

Finally, we introduce variables

$$\begin{aligned} X &= \frac{1}{\sqrt{2}\mathrm{i}}(c_1^\dagger - c_1), \quad s = \frac{1}{\sqrt{2}}(c_2^\dagger + c_2)\ , \\ P &= \frac{1}{\sqrt{2}}(c_1^\dagger + c_1), \quad p = \frac{1}{\sqrt{2}\mathrm{i}}(c_2 - c_2^\dagger) \end{aligned} \tag{65}$$

and obtain

$$H = H_1 + H_2 = E_1(P^2 - X^2) + \tfrac{1}{2}E_2(p^2 + s^2) + E_\mathrm{c}\ , \tag{66}$$

with the commutation relations

$$[X, P] = [s, p] = \mathrm{i}\ , \tag{67}$$

$$[s, X] = [s, P] = [p, X] = [p, P] = 0\ . \tag{68}$$

Thus, apart from the factor $\ell_B^2/\hbar$ in Eq. (20), $H_1$ corresponds to the center-of-motion part of the total Hamiltonian, and $H_2$ is a one-dimensional harmonic oscillator which implies that the wave function is harmonically confined in the direction of $s$.

The eigenfunctions of the Hamiltonian can now be factorized

$$\Psi(X, s) = \phi(X)\psi_n(s)\ , \tag{69}$$

where $\psi_n$ corresponds to the $n$th harmonic oscillator level.

In order to arrive at a scattering solution of the Schrödinger equation, we prepare a initial wave packet at $\langle X^2\rangle \approx \langle P^2\rangle \gg 1$. Since

$$\frac{x}{\ell_B} = \sqrt{2}(\alpha_1 X - \beta_2 s), \quad \frac{y}{\ell_B} = \sqrt{2}(\beta_1 P + \alpha_2 p) \tag{70}$$

with

$$\alpha_i = \cos\phi\, \mathrm{e}^{-\theta_i}, \quad \beta_i = -\sin\phi\, \mathrm{e}^{\theta_i} \quad (i = 1, 2)\ , \tag{71}$$

we have asymptotically

$$\frac{\langle x\rangle}{\alpha_1} \approx \frac{\langle y\rangle}{\beta_1}\ . \tag{72}$$

Since $\hbar\omega_B \gg \gamma$, $\beta_1/\alpha_1 \approx -1$, and the wave packet is centered near an asymptote of the equipotential line of $V_{\mathrm{sp}}$ in the upper left quadrant of the $(x, y)$-plane (Fig. 6).

In order to find the transmission probability, we need now to construct a scattering wave function. The eigenfunction $\phi$ satisfies

$$H_1\phi(X) = E_1(P^2 - X^2)\phi(X) = [E - (n + \tfrac{1}{2})E_2 - E_{\mathrm{c}}]\phi(X)\ , \tag{73}$$

or equivalently

$$\left(\frac{\mathrm{d}^2}{\mathrm{d}X^2} + X^2 + \epsilon\right)\phi(X) = 0 \tag{74}$$

with the energy parameter

$$\epsilon = \frac{E - (n + 1/2)E_2 - E_{\mathrm{c}}}{E_1}\ . \tag{75}$$

In the limit of high magnetic field, $E_2 = \hbar\omega_B$ and $E_1 = \gamma$. Therefore, $\epsilon$ measures the energy deviation from the saddle point energy $E_{\mathrm{c}}$ in a Landau band normalized by a typical potential strength.

This Schrödinger equation is discussed in detail in [85]. The eigenfunctions even and odd in $X$ are

$$\begin{aligned}
\Phi_+ &= \mathrm{e}^{-\mathrm{i}X^2/2} F\left(\frac{1 + \mathrm{i}\epsilon}{4}\left|\frac{1}{2}\right|\mathrm{i}X^2\right)\ ,\\
\Phi_- &= X\mathrm{e}^{-\mathrm{i}X^2/2} F\left(\frac{3 + \mathrm{i}\epsilon}{4}\left|\frac{3}{2}\right|\mathrm{i}X^2\right)\ ,
\end{aligned} \tag{76}$$

where $F$ is a confluent hypergeometric function. For large $|X|$ they can be written in the form

$$\begin{aligned}
\Phi_+(X) &= \frac{\Gamma(1/2)}{\Gamma(Z_+)}\mathrm{e}^{-\mathrm{i}(\pi/2)Z_+^*} f(Z_+^*; X)\mathrm{e}^{\mathrm{i}X^2/2} + \text{c.c.}\ ,\\
\Phi_-(X) &= \frac{\Gamma(3/2)}{\Gamma(Z_-)}\mathrm{e}^{-\mathrm{i}(\pi/2)Z_-^*} f(Z_-^*; X)X\mathrm{e}^{\mathrm{i}X^2/2} + \text{c.c}\ .
\end{aligned} \tag{77}$$

with the definitions $f(z; X) = |X|^{-2z}$, $Z_- = (3 + \mathrm{i}\epsilon)/4$, $Z_+ = (1 + \mathrm{i}\epsilon)/4$.

The currents in these states are related to the derivatives

$$\frac{\partial}{\mathrm{i}\partial X}\mathrm{e}^{\pm\mathrm{i}X^2/2} = \pm X\mathrm{e}^{\pm\mathrm{i}X^2/2}\ . \tag{78}$$

Therefore, each first term in Eqs. (77) corresponds to a currents in the positive $x$-direction. The conjugate complex term represents a current in the negative $x$-direction.

These solutions are linearly superposed, $\phi_t = A\Phi_+ + B\Phi_-$, to form the scattering wave functions which must fulfill boundary conditions such that for $X > 0$ only a transmitted wave function exists with the current flowing away from the origin. This leads to the relation

$$A\frac{\Gamma(1/2)}{\Gamma(Z_+^*)}e^{i\pi/8} + B\frac{\Gamma(3/2)}{\Gamma(Z_-^*)}e^{i3\pi/8} = 0\ . \tag{79}$$

One finds after some algebra for the transmitted wave for large values of $X < 0$

$$\phi_t(X) = f(Z_+; X)e^{-\pi\epsilon/8}e^{iX^2/2}\left[A\frac{\Gamma(1/2)}{\Gamma(Z_+)}e^{-i\pi/8} + B\frac{\Gamma(3/2)}{\Gamma(Z_-)}e^{-i3\pi/8}\right] \tag{80}$$

and for the incoming wave

$$\phi_i(X) = f(Z_+; X)e^{-\pi\epsilon/8}e^{-iX^2/2}\left[A\frac{\Gamma(1/2)}{\Gamma(Z_+^*)}e^{i\pi/8} - B\frac{\Gamma(3/2)}{\Gamma(Z_-^*)}e^{i3\pi/8}\right]\ . \tag{81}$$

This guarantees that for $X > 0$ no incoming wave exists. The transmission probability is defined by

$$T(\epsilon) = \lim_{X\to\infty}\frac{|\phi_t(X)|^2}{|\phi_i(-X)|^2}\ . \tag{82}$$

One gets from the above equations by using the relations for the $\Gamma$-functions

$$\Gamma(z)^* = \Gamma(z^*), \quad \Gamma\left(\frac{1}{4} + iy\right)\Gamma\left(\frac{3}{4} - iy\right) = \frac{\sqrt{2}\pi}{\cosh\,\pi y + i\sinh\pi y}\ , \tag{83}$$

the final result

$$T(\epsilon) = \frac{1}{1 + \exp(-\pi\epsilon)}\ . \tag{84}$$

For $\epsilon \to -\infty$, well below the saddle point energy, the transmission probability vanishes. The incoming wave is completely reflected. For $\epsilon \to +\infty$, the transmission probability approaches unity. Exactly at the saddle point energy, $\epsilon = 0$, one has $T(0) = 1/2$. For energies near the saddle point, one can expand

$$T(\epsilon) \approx \frac{1}{2} + \frac{\pi}{4}\epsilon + \cdots\ . \tag{85}$$

### *3.2. Parameterizing the scattering at a saddle point*

As we have seen, the percolating wave functions of the electron carry an equilibrium current density. Near the points where percolating wave functions approach each other closely, quantum tunneling takes place.

A natural model for the description of the percolating quantum states can then be obtained by considering a network of current loops, occasionally inter-connected via tunneling near the saddle points of the

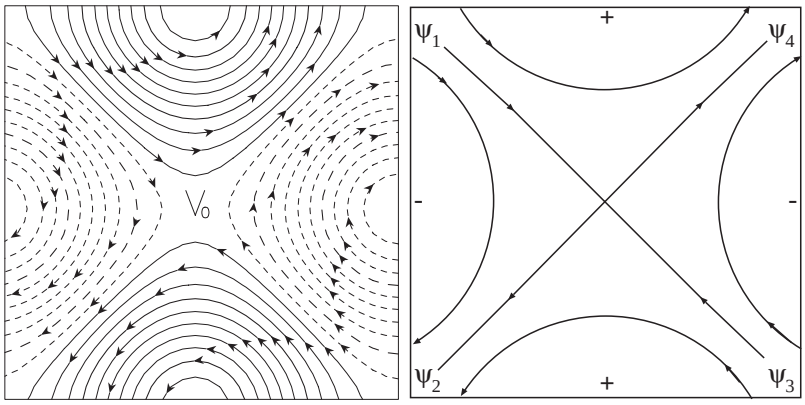


Fig. 7. (a) Potential landscape near a saddle point with adjacent maxima (full equipotential lines) and minima (dashed equipotential lines). (b) The corresponding idealized potential landscape with incoming ($\psi_1$ and $\psi_3$) and outgoing ($\psi_2$ and $\psi_4$) current amplitudes flowing along equipotential lines. Note that the saddle point energy is denoted here by $V_0$.

potential (Fig. 4). The simplest choice is a regular network. Disorder can be introduced either by randomizing the relative phases of the current loops and/or the heights of the saddle points. The distribution of the wave function amplitude is then closely related to that of the corresponding quantum currents and the asymptotic behavior is essentially determined by the coherent interplay of the quantum transmission and scattering near the saddle points.

Let us consider the region close to a specific saddle point, say $E_c$. The potential landscape can be modeled by two neighboring adjacent potential maxima and minima (Fig. 7). We assume that the directions of the currents along the equipotential lines in the potential minima and maxima are clockwise and counter clockwise, respectively. Let us consider energies close $E_c$. There are four equipotential lines that enter the region of the saddle point. The total current entering and leaving the saddle point region must be conserved (Fig. 7).

The effect of the saddle point potential can be considered as a quantum transmission problem as described above [31]. In more simplified terms, we assume that the amplitudes which correspond to the currents on the boundary of the saddle point region are $\psi_1 \ldots \psi_4$ with the amplitudes of incoming and outgoing currents $\psi_1$, $\psi_3$ and $\psi_2$, $\psi_4$, respectively. The formal relationship between them can be described by a scattering matrix $\mathbf{S}$,

$$\begin{pmatrix} \psi_2 \\ \psi_4 \end{pmatrix} = \mathbf{S} \begin{pmatrix} \psi_1 \\ \psi_3 \end{pmatrix} . \tag{86}$$

In general, the $\mathbf{S}$ matrix can be written as [86,87]

$$\mathbf{S} = \begin{pmatrix} e^{-i\varphi_2} & 0 \\ 0 & e^{i\varphi_4} \end{pmatrix} \begin{pmatrix} -r & t \\ t & r \end{pmatrix} \begin{pmatrix} e^{i\varphi_1} & 0 \\ 0 & e^{-i\varphi_3} \end{pmatrix} , \tag{87}$$

where $0 \leqslant r \leqslant 1$, $0 \leqslant t \leqslant 1$, $r^2 + t^2 = 1$, and $r^2$ and $t^2$ are the probabilities of the current $\psi_1$ to be reflected to $\psi_2$ and to be transmitted to $\psi_4$, respectively. Note that the current conservation relation implies

$$|\psi_1|^2 + |\psi_3|^2 = |\psi_2|^2 + |\psi_4|^2 \tag{88}$$

which is always valid due to the unitarity of the scattering matrix **S**.

For iterative numerical calculations, it is useful to introduce the transfer matrix **T** that is equivalent to **S**. It relates the amplitudes on the left, $(\psi_1, \psi_2)^{\mathrm{T}}$, to those on the right-hand side of the saddle point, $(\psi_4, \psi_3)^{\mathrm{T}}$ (T denotes the transposed).

$$\begin{pmatrix} \psi_4 \\ \psi_3 \end{pmatrix} = \mathbf{T} \begin{pmatrix} \psi_1 \\ \psi_2 \end{pmatrix} . \tag{89}$$

Using Eqs. (86) and (87) one finds the result

$$\mathbf{T} = \begin{pmatrix} \mathrm{e}^{\mathrm{i}\varphi_4} & 0 \\ 0 & \mathrm{e}^{\mathrm{i}\varphi_3} \end{pmatrix} \begin{pmatrix} 1/t & r/t \\ r/t & 1/t \end{pmatrix} \begin{pmatrix} \mathrm{e}^{\mathrm{i}\varphi_1} & 0 \\ 0 & \mathrm{e}^{\mathrm{i}\varphi_2} \end{pmatrix} . \tag{90}$$

For completeness, we only mention here, that due to the current conservation, the $2 \times 2$-matrix **T** must fulfill the symmetry condition (cf. Section 9)

$$\mathbf{J} = \mathbf{T}^{\dagger}\mathbf{J}\mathbf{T} \quad \text{with} \quad \mathbf{J} = \begin{pmatrix} 1 & 0 \\ 0 & -1 \end{pmatrix} . \tag{91}$$

It is useful to relate the present description to the microscopic saddle point model introduced above. By using Eq. (91), and imposing the correct asymptotic behavior from the scattering geometry in Fig. 7, one can write the reflection and transmission amplitudes $r$ and $t$ in terms of a single parameter

$$r := \frac{1}{\cosh\, \Theta} \tag{92}$$

and by the current conservation relation $t = \sqrt{1 - r^2}$,

$$t = \tanh\, \Theta . \tag{93}$$

Eq. (90) can be written in terms of the variable $\Theta$,

$$\begin{aligned} \mathbf{T} &= \begin{pmatrix} \mathrm{e}^{\mathrm{i}\varphi_4} & 0 \\ 0 & \mathrm{e}^{\mathrm{i}\varphi_3} \end{pmatrix} \begin{pmatrix} \operatorname{cotanh} \Theta & \operatorname{cosech} \Theta \\ \operatorname{cosech} \Theta & \operatorname{cotanh} \Theta \end{pmatrix} \begin{pmatrix} \mathrm{e}^{\mathrm{i}\varphi_1} & 0 \\ 0 & \mathrm{e}^{\mathrm{i}\varphi_2} \end{pmatrix} \\ &= \begin{pmatrix} \mathrm{e}^{\mathrm{i}\varphi_4} & 0 \\ 0 & \mathrm{e}^{\mathrm{i}\varphi_3} \end{pmatrix} \begin{pmatrix} \cosh \Theta' & \sinh \Theta' \\ \sinh \Theta' & \cosh \Theta' \end{pmatrix} \begin{pmatrix} \mathrm{e}^{\mathrm{i}\varphi_1} & 0 \\ 0 & \mathrm{e}^{\mathrm{i}\varphi_2} \end{pmatrix} . \end{aligned} \tag{94}$$

$\Theta'$ and $\Theta$ being related via

$$\sinh\, \Theta \sinh\, \Theta' = 1 . \tag{95}$$

By comparing with Eq. (84) one finds that the dimensionless parameter $\Theta$ must depend monotonically on the energy of the equipotential line. It characterizes completely the transmission properties of the saddle

point. For $E \ll E_c$ and $E \gg E_c$, $\Theta \ll 1 (r \approx 1)$ and $\Theta \gg 1 (t \approx 1)$, respectively. This is because for $E \ll E_c$, $\psi_1 \approx \psi_2$ for almost all $\psi_3$ and $\psi_4$, and for $E \gg E_c$, $\psi_1 \approx \psi_4$. One can determine the energy dependence of $\Theta$ by comparing with the above microscopic result near $\epsilon = 0$ where $T(0) = 1/2 := |t|^2 = \tanh^2 \Theta_c$ and expanding for $\Theta \approx \Theta_c$ since the model is only suitable for the region near the saddle point energy, $E_c$. One finds (cf. Eq. (85))

$$\Theta(\epsilon) \approx \Theta_c + \frac{\pi\epsilon}{2\sqrt{2}} + \cdots \tag{96}$$

with the saddle point value $\Theta_c = \ln(1 + \sqrt{2})$.

The characteristic feature of this model for the transmission through a saddle point is that incident and transmitted channels are locally separated. The interplay between the saddle point potential and the high magnetic field introduces a spatial separation of the incoming and outgoing channels. This makes the model particularly suited for describing the critical localization features in the quantum Hall region.

### *3.3. Establishing the random network of saddle points*

Starting from the smooth random landscape of the potential, the network model could now be defined from a random system of circular, localized wave functions of the type Eq. (33), equivalent to circular equilibrium currents. These would correspond to states associated with randomly distributed sites. For technical convenience, however, it is preferable to assume the circular wave functions to have random phases and being associated with the sites of a regular lattice. In addition, it is reasonable to assume that nearest-neighbored wave functions are connected by tunneling contacts described by the above transfer matrices **T** (cf. Eq. (90)). This enables the particles to hop from one circular state to another. A delocalization mechanism for the total wave function is introduced in this way.

The model constructed is the analogue at high magnetic field of a two-dimensional Anderson model for a disordered system [17,88,89]. The site states of the latter are replaced by the circular currents of the former, and the hopping amplitudes by the unitary transfer matrices. As in the Anderson model, the network contains the necessary competing ingredients—localization within the circular current states and tunneling between them—for describing a localization–delocalization phase transition. In the case of the Anderson model, there is no phase transition in two dimensions. As we have already seen above, the present network model must show a singularity in the localization properties which represents a quantum phase transition point. This will be discussed in more detail in the next section.

But let us first complete the model by providing a more formal description, especially suitable for numerical work. We consider a two-dimensional rectangular geometry with $2M \times 2L$ current loops on a square lattice (Fig. 8). The structure of the current flow near the nodes described by $\mathbf{S}'$ is rotated by $\pi/2$ as compared with that of the nodes described by **S** (Fig. 8). We have

$$\begin{pmatrix} \psi_1 \\ \psi_3 \end{pmatrix} = \mathbf{S}' \begin{pmatrix} \psi_2 \\ \psi_4 \end{pmatrix} \tag{97}$$

with the $\pi/2$ rotated scattering matrix

$$\mathbf{S}' = \begin{pmatrix} e^{-i\varphi'_1} & 0 \\ 0 & e^{i\varphi'_3} \end{pmatrix} \begin{pmatrix} -t & r \\ r & t \end{pmatrix} \begin{pmatrix} e^{i\varphi'_2} & 0 \\ 0 & e^{-i\varphi'_4} \end{pmatrix}, \tag{98}$$

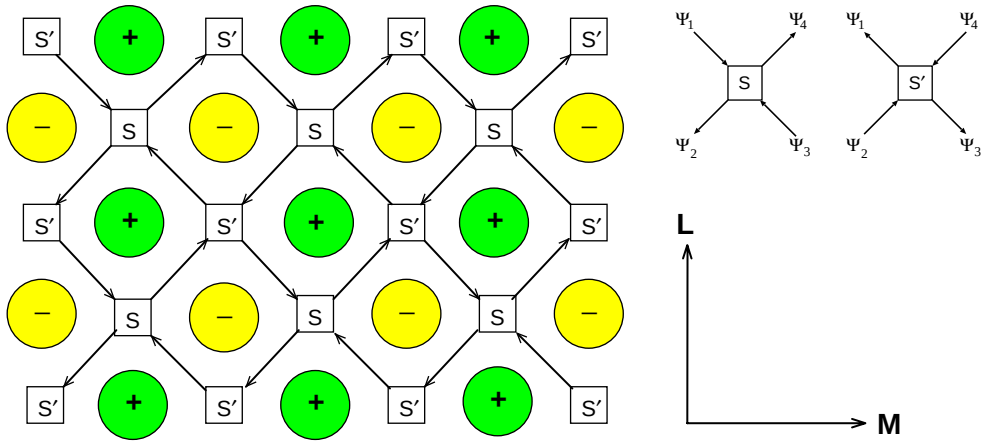


Fig. 8. Left: the network model in the quantum Hall regime: + and − indicate the hills and valleys of the potential, respectively. The scattering at the saddle points is characterized by **S** matrices, **S** and **S**′. The arrows indicate the directions of the guiding center motion. Right: the scattering described by **S**′ differs from that of **S** by $\pi/2$ rotation in the incoming and outgoing channels; $L$ width of the system, $M$ length of the system in the direction of the repeated application of the transfer matrix.

that results in a corresponding transfer matrix $\mathbf{T}'$ relating $(\psi_4, \psi_3)^t$ to $(\psi_1, \psi_2)^t$,

$$\mathbf{T}' = \begin{pmatrix} e^{i\varphi'_4} & 0 \\ 0 & e^{i\varphi'_3} \end{pmatrix} \begin{pmatrix} 1/r & t/r \\ t/r & 1/r \end{pmatrix} \begin{pmatrix} e^{i\varphi'_1} & 0 \\ 0 & e^{i\varphi'_2} \end{pmatrix}, \tag{99}$$

or in terms of $\Theta$,

$$\mathbf{T}' = \begin{pmatrix} e^{i\varphi'_4} & 0 \\ 0 & e^{i\varphi'_3} \end{pmatrix} \begin{pmatrix} \cosh\Theta & \sinh\Theta \\ \sinh\Theta & \cosh\Theta \end{pmatrix} \begin{pmatrix} e^{i\varphi'_1} & 0 \\ 0 & e^{i\varphi'_2} \end{pmatrix}. \tag{100}$$

The transfer matrix $\mathbf{T}_L^M$ that relates the amplitudes on the left of the sample $(\psi_{0,1}, \psi_{0,2}, \ldots, \psi_{0,2L})^{\mathrm{t}}$ to those on the right $(\psi_{M,1}, \psi_{M,2}, \ldots, \psi_{M,2L})^{\mathrm{t}}$ ($L$ integer) is then defined as follows. We divide the system along the direction of $M$ into slices, each containing $L$ of subsequent saddle point scatterers and the $2L$ corresponding channels (Fig. 8). The latter are assumed to have completely random phases. The amplitudes at the end of the system can then be written in terms of a transfer matrix[6]

$$\begin{pmatrix} \psi_{M,1} \\ \psi_{M,2} \\ \cdot \\ \cdot \\ \cdot \\ \psi_{M,2L} \end{pmatrix} = \mathbf{T}_L^M \begin{pmatrix} \psi_{0,1} \\ \psi_{0,2} \\ \cdot \\ \cdot \\ \cdot \\ \psi_{0,2L} \end{pmatrix} \tag{101}$$

[6] We use here the somewhat unconventional notation that $M$ and $L$ denote the length and width of the system, respectively. The reason is that when discussing the numerical scaling in the next section, we prefer to use $L$ for the length scaling instead of $M$.

with the product of the transfer matrices

$$\mathbf{T}_L^M = \mathbf{T}^{(M)}\mathbf{T}^{(M-1)}\cdots\mathbf{T}^{(2)}\mathbf{T}^{(1)} \ , \tag{102}$$

where

$$\mathbf{T}^{(k)} = \mathbf{V}_1^{(k)}\mathbf{V}_2\mathbf{V}_3^{(k)}\mathbf{V}_4 \ . \tag{103}$$

Here the matrix $\mathbf{V}_4$ is given by

$$(\mathbf{V}_4)_{i,j} = \begin{cases} \cosh\Theta' & i=j=n, \qquad\qquad n=1,\ldots,2L, \\ \sinh\Theta' & \begin{cases} i=j+1=2n, \\ i=j-1=2n-1, \end{cases} \quad n=1,2,\ldots,L, \\ 0 & \text{otherwise}, \end{cases} \tag{104}$$

and $\mathbf{V}_2$ by

$$(\mathbf{V}_2)_{i,j} = \begin{cases} \cosh\Theta & i=j=n, \qquad\qquad n=2,3,\ldots,2L-1, \\ \sinh\Theta & \begin{cases} i=j+1=2n+1, \\ i=j-1=2n, \end{cases} \quad n=1,2,\ldots,L-1 \ . \end{cases} \tag{105}$$

Assuming periodic boundary conditions in the transverse direction gives

$$\begin{aligned} (\mathbf{V}_2)_{1,1} &= (\mathbf{V}_2)_{2L,2L} = \cosh\Theta \ , \\ (\mathbf{V}_2)_{1,2L} &= (\mathbf{V}_2)_{2L,1} = \sinh\Theta \ , \end{aligned} \tag{106}$$

while for fixed boundary conditions one has to use

$$\begin{aligned} (\mathbf{V}_2)_{1,1} &= (\mathbf{V}_2)_{2L,2L} = 1 \ , \\ (\mathbf{V}_2)_{1,2L} &= (\mathbf{V}_2)_{2L,1} = 0 \ . \end{aligned} \tag{107}$$

All other matrix elements of $\mathbf{V}_2$ are 0.

When propagating from one node to the other, the probability amplitudes gain phase factors. This is contained in the matrix elements of $\mathbf{V}_1^{(k)}$ and $\mathbf{V}_3^{(k)}$,

$$(\mathbf{V}_l^{(k)})_{i,j} = \delta_{ij}\,\mathrm{e}^{\mathrm{i}\phi_i^{(k)}} \quad (l=1,3) \ . \tag{108}$$

Since the distance between the nodes is random, we assume that $\phi_i^{(k)}$ are independent and uniformly distributed between $[0, 2\pi)$. So far, this is the only source of randomness in the model. Note that the phases $\varphi$ and $\varphi'$ in Eqs. (90) and (99) can be included in the $\phi$'s in Eq. (108).

In this form, the transfer matrix method [17,88,89] has been applied to the model for estimating the critical behavior of the localization length in the quantum Hall regime [31] to be described in more detail in the following section.

Attempting some completeness, we mention at this point that some versions of the network, which essentially reproduce features of the underlying classical percolation problem, and with random saddle point potential values $E_c$ have been used to obtain detailed information about the longitudinal conductivity and several classical percolation properties [32,90–92]. A classical version of the regular network consisting of coupled metallic wires has been used to calculate the Hall conductance. Quantization in

integer (positive and negative) units of $e^2/h$ has been predicted consistent with earlier findings for the pure quantum Hall case without any disorder [93,94]. The model has been also used to study the localization problem in two dimensions in the presence of a random magnetic field [95,96]. As our emphasis will be on the universal features of the network model in the forthcoming sections, we will not go into the details of these works.

## 4. The localization–delocalization transition in the network model

In this section we will explore the localization properties of the original Chalker–Coddington network introduced in the previous Section 3. As this has been a key issue for establishing the model, this will be done in some detail. Necessarily, for obtaining quantitative information about the critical behavior, numerical methods will be used. We attempt to provide a complete overview of the statistical properties of the energy spectrum and the wave functions near the critical point, as far as it is presently available.

The model has been the subject of numerous numerical studies which are all similar in spirit but different in the details [32,97–100]. We provide here results obtained recently by the numerical scaling method [88,89] which have been undertaken in order to improve the treatment of corrections to scaling. For obtaining reliable and precise results for the critical exponent, the latter has been shown to be decisively important [83,101]. To our great disappointment, however, as we will show below, up to now it has not been achieved to remove corrections to scaling to such a degree that the precision of the exponent of the Chalker–Coddington network model can compete with the results obtained for other models in particular the random Landau model, see Table 1!

We will also discuss the critical properties of the wave functions as well as the eigenenergy statistics. Due to its simplicity, the network model enables us to investigate them in detail, and because of universality, they are supposed to be generally valid for two-dimensional electron systems in high perpendicular magnetic fields.

To study the localization–delocalization transition, we investigate the scaling properties of the localization length in a quasi-one-dimensional long strip for which the localization length is calculated by the transfer matrix method and apply the finite-size scaling method developed earlier for estimating the asymptotic value in the thermodynamic limit. The value of the critical exponent $\nu$ in the network model [31,32,102,103] is consistent with, though considerably less accurate than, earlier results obtained for several very different models such as the random Landau model with a white noise potential [23,24] and the random matrix model including spatial correlations of the randomness [19,20]. This supports strongly that the model of Chalker and Coddington belongs to the same universality class as the models considered previously, in spite of the intriguingly large corrections to scaling which defy the high accuracy in the estimate of the critical exponents.

### 4.1. Numerical scaling at the localization–delocalization transition

To determine the critical behavior quantitatively, we use the numerical finite size scaling approach. We define a quantity $F_L$ which is a function of a set of parameters $x_i$ characterizing the system, such as the Fermi energy, parameters characterizing the disorder, as the variance and the correlation length, the magnetic field, and the system size $L$ [104],

$$F_L = f(\{x_i\}, L) \ . \tag{109}$$

We assume the existence of a scaling law such that $F_L$ can be expressed as

$$F_L = F(\chi L^{1/\nu}, \phi_1 L^{y_1}, \phi_2 L^{y_2}, \ldots) \ , \tag{110}$$

with $\chi$ being the relevant scaling variable and $\phi_i$ denoting the irrelevant ones. The latter nevertheless can cause corrections to scaling as long as the system size is finite. Therefore, in a numerical calculation they must not be ignored. These variables characterize distances from the critical point, $\nu$ is the critical exponent and $y_i < 0$ are the exponents of the irrelevant scales. Eventually, in the limit of infinite system size, only the relevant scaling variable survives, and Eq. (110) becomes

$$f_L = F_1\left(\frac{L}{\xi}\right) \ , \tag{111}$$

with $\xi \sim \chi^{-\nu}$. The quantity $\chi$ as a function of some control parameter, say $x$, can be expanded near the critical point $x_c$

$$\chi = \chi_1(x - x_c) + \chi_2(x - x_c)^2 + \cdots \ . \tag{112}$$

Which quantity should be used as the scaling variable $F_L$? It should be a quantity that shows a singularity in the limit of infinite system size as one crosses the localization–delocalization critical point. Furthermore, it should be a quantity to be determined numerically easily, precisely and effectively. There are several such quantities, such as for instance the level spacing distribution [105] or the conductance (see below). Here, we consider the renormalized localization length in the *finite* system (MacKinnon–Kramer variable), $\Lambda$, introduced previously [88] which we will now define.

Consider a very long strip of width $L$. This is a quasi-one-dimensional system and all the states are expected to be localized. The localization length $\lambda(L; x_1, x_2, \ldots)$ is a function of the width of the strip, $L$. Now let us define

$$\Lambda(L; x_1, x_2, \ldots) = \frac{\lambda(L; x_1, x_2, \ldots)}{L} \ . \tag{113}$$

If the system parameters are such that $\lambda(L \to \infty; x_1, x_2, \ldots)$ remains finite, the system is in the localized regime and $\Lambda(L \to \infty; x_1, x_2, \ldots) \to 0$. The localization length is then given by $\xi = \lambda(L \to \infty; x_1, x_2, \ldots)$. On the other hand, if $\lambda(L \to \infty; x_1, x_2, \ldots)$ increases faster than $\propto L$, the system is in the delocalized state, and $\lambda(L \to \infty; x_1, x_2, \ldots)$, the correlation length in the metallic regime, corresponds to the inverse of the dc-conductivity [88,89]. The critical point is defined by the condition $\Lambda(L \to \infty; x_{1c}, x_{2c}, \ldots) = \text{const} = \Lambda_c$ (critical MacKinnon–Kramer variable).

The most efficient way to calculate $\lambda(L)$ is the transfer matrix method [17]. We define the product of the transfer matrices Eq. (102) and consider the limit

$$\Gamma = \lim_{M\to\infty} (\mathbf{T}_L^M \mathbf{T}_L^{M\dagger})^{1/2M} \ . \tag{114}$$

The theorem by Oseledec [106–109] guarantees that $\Gamma$ has always positive eigenvalues, which are denoted as $\exp(\pm\gamma_i)$ where $\gamma_i (> 0)$ can be interpreted as the exponential change of the wave function for a single slice. The smallest value of $\gamma_i$ is the inverse of the quasi-one-dimensional localization length [17],

$$\frac{1}{\lambda(L)} = \min\{\gamma_i\} \ . \tag{115}$$

This definition can be shown to be equivalent to the one in terms of the exponential decay of the Green function which could also be used to study $\lambda(L)$ [110]. If one is interested only in the localization length the transfer matrix method has been shown to be superior.

### 4.2. Numerical results near the quantum critical point

The two-dimensional electron systems in high magnetic fields are characterized by many control parameters such as Fermi energy, magnetic fields as well as parameters describing the properties of randomness. In the Chalker–Coddington model, however, all the informations are contained in a single parameter, the transmission at the saddle point. In the actual simulation, it is convenient to use as control parameter

$$x = -\ln \sinh \Theta \ , \tag{116}$$

With this choice of $x$, we obtain from Eq. (92)

$$t = \frac{1}{\sqrt{\mathrm{e}^{2x}+1}}, \quad r = \frac{1}{\sqrt{\mathrm{e}^{-2x}+1}} \ . \tag{117}$$

Due to the particle–hole symmetry ($r \leftrightarrow t$) the localization length is an even function of $x$. Comparing Eqs. (84) and (117) we note that $x$ can be interpreted as the energy measured from the center of the Landau band.

In the actual simulation, we need to simulate not too small systems so that only a single relevant scaling variable and at most one irrelevant variable are sufficient for fitting the data. In this case, the scaling form Eq. (110) reads

$$\Lambda(L) = F(\chi L^{1/\nu}, \phi L^{y}) \ , \tag{118}$$

where $\chi$ is related to $x$ via Eq. (112). We consider in the calculation the region $x \ll 1$ so that $\chi \sim x$ and $\phi = \text{const}$.

As noted above, due to particle–hole symmetry $\Lambda$ is an even analytic function of $x$ as long as $L$ is finite. By assuming $xL^{1/\nu}$ to be sufficiently small in order to truncate the expansion after the second order, Eq. (118) can be expressed as

$$\Lambda(L) = \Lambda_{\mathrm{c}} + a_1(xL^{1/\nu})^2 + a_2(xL^{1/\nu})^4 + b_0 L^{y} + c_0 L^{2y} + \cdots \ , \tag{119}$$

Previously, this non-linear fitting scheme has been working perfectly well for the three-dimensional Anderson transition [101,111–113] as well as in the case of two-dimensional systems with strong spin–orbit coupling [114,115].

High precision data are required for a precise determination of the exponent. As seen in Fig. 9, for such data the corrections to scaling are not negligible [102]. Unfortunately, a stable fit that takes into account these corrections has not yet been found [116,117]. As a result, there has not been any significant improvement of the precision of the estimate of $\nu$ over the original estimate of $\nu = 2.5 \pm 0.5$ by Chalker and Coddington [31].

Fluctuations of the transmission properties of the saddle points cause another type of randomness in addition to the phase randomness assigned to the wave function when traveling from one node to another. These fluctuations are equivalent to randomness in the mass of the Dirac Hamiltonian to be described later

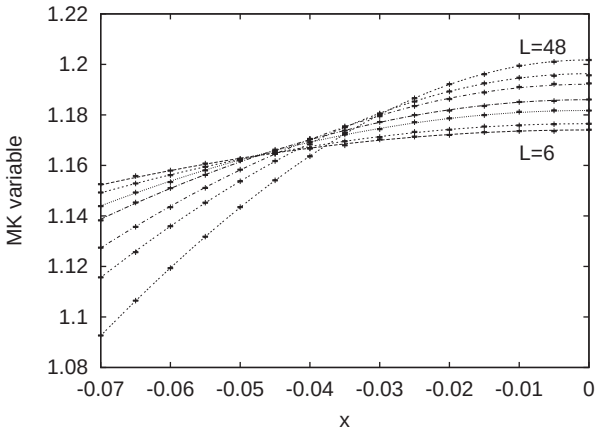


Fig. 9. MacKinnon–Kramer variable $\Lambda(L)=\lambda(L)/L$ as a function of $x$ for $L=6$, 8, 12, 16, 24, 32 and 48. The relative uncertainty of the data is 0.02%. The curves are results of the fitting according to Eq. (119) with $\Lambda_c = 1.23$, $\nu = 2.48$ and $y = -0.53$. The fitting, however, is unstable, so the curves should be regarded as guides to the eye.

in Section 7. It has been numerically demonstrated that this effect gives larger—but irrelevant—corrections to scaling [102].

### 4.3. The critical properties of the wave functions

Exactly at the critical point $t = r = 1/\sqrt{2}$ ($x = -\ln\sinh\Theta = 0$), the wave function is delocalized. It is now well established that due to the divergence of the length scale, the wave function at the critical point shows multi-fractal behavior [118–120]. This self-similar structure is in principle reflected in an anomalous temperature behavior of the diffusion constant, the energy level statistics, the conductance distribution, and many other properties.

Since the Chalker–Coddington model is characterized by the scattering matrices at saddle points rather than by the Hamiltonian, the wave function must be determined from the scattering matrices. Let the amplitude on the link $l$ be $\psi_l$. As explained above, the stationary states of the model must satisfy [121,122]

$$\psi_m = t_{mk}\psi_k + t_{ml}\psi_l \ , \tag{120}$$

where $t_{mk}$ and $t_{ml}$ relate the amplitudes $\psi_k$ and $\psi_l$ to $\psi_m$ (Fig. 10). This can be rewritten as

$$\mathbf{U}(E)\Psi = \Psi \ , \tag{121}$$

with $\mathbf{U}(E)\mathbf{e}_l = t_{ml}(E)\mathbf{e}_m + t_{nl}(E)\mathbf{e}_n$, $\mathbf{e}_i$ being the unit vector with the $i$th component unity, $|t_{mk}|^2 = T = 1 - |t_{ml}|^2 := 1/2$ at the critical point, and $\Psi$ the vector with the components $\psi_m$. Again, we assume for simplicity that randomness enters only via the phases of the amplitudes.

Eq. (121) has non-zero scattering solutions only for certain discrete energies $E_\nu$, which determine the eigenstates and eigenenergies of the system [123]. Solving Eq. (121), however, is in general very complicated for a disordered system. We will derive an alternative method by establishing equivalent Hamiltonians later in Section 7.

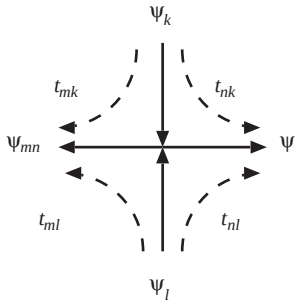


Fig. 10. The stationary wave function relation characterized by the scattering matrix amplitudes. Incoming waves and outgoing waves are $\psi_l, \psi_k$ and $\psi_m, \psi_n$, respectively.

For the moment, we proceed by calculating instead the return probability [124] from the equation of motion determined by Eq. (121). We start by introducing the time $t_0$ during which the incident wave packet passes the scatterer and measure time $t$ in units of $t_0$. We can then define the time evolution operator

$$\mathbf{U}(t) = \mathbf{U}^t(E) \ , \tag{122}$$

where $t$ is an integer.

The probability $P(t)$ of return within the period of time $t$ is determined by the probability density of the wave packet at time $t$ near a given scatterer, say located at the origin, which was previously located there at $t = 0$. This is defined by

$$P(t) = |\langle 0|\mathbf{U}(t)|0\rangle|^2 \ . \tag{123}$$

The return probability is related to the fractal dimension $D(2)$ defined by the second moment of the probability density, the inverse participation number $p_2(L)$

$$p_2(L) := \langle |\Psi(\boldsymbol{r})|^4 \rangle \propto \frac{1}{L^{2+D(2)}} \tag{124}$$

with $\langle \ldots \rangle$ denoting a configurational average. If we integrate $p_2(L)$ over the two-dimensional system and then take the inverse, we have $L^{D(2)}$ and we can interpret this quantity as the portion of space where the wave function amplitude is significant.

Let the wave packet spread to the radius $r(t)$ after time $t$, the number of sites occupied becomes $\sim r(t)^{D(2)}$. On the other hand, the conductivity at the quantum Hall transition is finite, and from the Einstein relation

$$\sigma = e^2 \rho D \tag{125}$$

($\rho$ the density of states per volume and $D$ the diffusion constant), we see that $D$ is finite, hence $r(t) \sim t^{1/2}$. One then finds [125–129]

$$P(t) \propto t^{-D(2)/2} \ . \tag{126}$$

In general dimension the diffusion radius $r$ is proportional to $t^{1/d}$[130], hence

$$P(t) \propto t^{-D(2)/d} \ . \tag{127}$$

For the spatial dimension $d = 2$, we can estimate $D(2) = 1.52 \pm 0.06$ from numerical simulations [124]. This is in agreement with the results in the continuum model [118,131] as well as in the tight-binding model [126].

A similar idea has been developed to calculate the local density of states [132] from which one can calculate the multi-fractal exponents $D(q)$ that are defined by the higher moments of the density,

$$p_q(L) := \langle |\Psi(\boldsymbol{r})|^{2q} \rangle \propto \frac{1}{L^{2+(q-1)D(q)}} \propto \frac{1}{L^{2+\tau(q)}} \ . \tag{128}$$

The moments of the density characterize the degree of localization of the wave function. For plane waves, $p_q(L) \propto L^{-2q} \to 0$ in the thermodynamic limit. For localized states $p_q(L) \propto L_0^{-2q} \to \text{const.} \neq 0$. Generally, the fractal dimensionalities $D(q)$ depend on $q$ and $\tau(q)$ is non-linear in $q$. This is the celebrated multi-fractal behavior [133]. It means that the complex structure of wave function at the critical point can not be described by single dimension $D(2)$ but infinite number of generalized dimensions are required to characterize it.

A convenient quantity to summarize the behavior of the multi-fractal exponents is to introduce a Legendre transformation on $\tau(q)$ by defining [134–136]

$$\alpha = \frac{\mathrm{d}\tau(q)}{\mathrm{d}q} \tag{129}$$

and the $f(\alpha)$-spectrum

$$f(\alpha) = \alpha q - \tau(q) \ . \tag{130}$$

The physical meaning of the quantity $f(\alpha)$ can be understood by relating it to the probability distribution of the random amplitudes of $\Psi$, $P_\Psi(|\Psi|^2)$. Starting point is the identity between the latter and the distribution, $P_\alpha(\alpha)$, of the random variable

$$\alpha := -\frac{\ln|\Psi|^2}{\ln L} \ , \tag{131}$$

$$P_\alpha(\alpha)\,\mathrm{d}\alpha = P_\Psi(|\Psi|^2)\mathrm{d}|\Psi|^2 \ . \tag{132}$$

The inverse participation numbers are obtained in terms of these distributions

$$p_q(L) = \int \mathrm{d}|\Psi|^2 |\Psi|^{2q} P_\Psi(|\Psi|^2) = \int \mathrm{d}\alpha \mathrm{e}^{-\alpha q \ \ln \ L} P_\alpha(\alpha) \ . \tag{133}$$

In order to obtain the correct dependence of $p_q(L)$ on the system size the distribution of $\alpha$ must be of the form

$$P_\alpha(\alpha) \propto \mathrm{e}^{[f(\alpha)-2]\ln \ L} \ . \tag{134}$$

For very large $L$, the average in Eq. (133) is dominated by the maximum of $f(\alpha)$ at $\alpha_0$. Thus, $\alpha_0$ is the exponent of the system size dependence of the *typical* value of the probability,

$$(|\Psi|^2)^{\mathrm{typ}}(L) := \mathrm{e}^{\langle \ln(|\Psi|^2)\rangle} \propto \frac{1}{L^{\alpha_0}} \ . \tag{135}$$

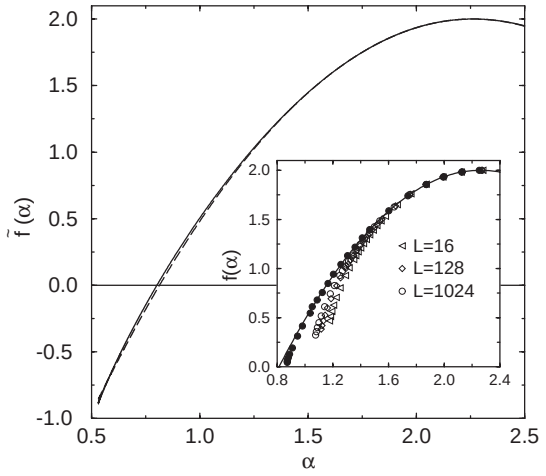


Fig. 11. The $f(\alpha)$-spectrum at the quantum Hall transition determined numerically (full line) and the result of an analytical conjecture (dashed line) with $\alpha_0 = 2.262$. Inset: spectra of typical eigenfunctions for different system sizes $L$ and extrapolated with $L \to \infty$ (from Ref. [137]).

Fig. 11 shows some numerical results for $f(\alpha)$ together with the result obtained from the Dirac model with random vector potential ([120], see Section 7.3 below) which is exactly parabolic

$$f(\alpha) = 2 - \frac{(\alpha - \alpha_0)^2}{4(\alpha_0 - 2)} \tag{136}$$

with $\alpha_0 = 2 + \Delta_A/\pi$ where $\Delta_A$ is the variance of the random vector potential which is in that case equivalent to the random phases associated with the links of the network.

Again, this is in agreement with the diagonalization analysis [131]. Together with the analytical results from the Dirac model, which will be described below, this provides strong evidence for the overall conjecture that the Integer Quantum Hall Effect is a quantum critical phenomenon. A graphical representation of a multi-fractal wave function at the critical point is shown in Fig. 12.

The fractal dimensionality of the wave function can be related to the MacKinnon–Kramer parameter $\Lambda_c$ by assuming conformal invariance [31,139–142]. The quantity $\alpha_0$, is related to $\Lambda_c$ by (see Section 5.3 for more details)

$$\alpha_0 = 2 + \frac{1}{\pi \Lambda_c} \ , \tag{137}$$

which is in excellent agreement with the numerical results [102,137,142,143].

### 4.4. Energy level statistics near the critical point

Random matrix theory is a very powerful tool to characterize the properties of complex systems [144,145]. It can also be applied to the localization–delocalization transition. In the metallic regime, the overlap of the wave functions is strong, which results in strong level repulsion. In the limit of large

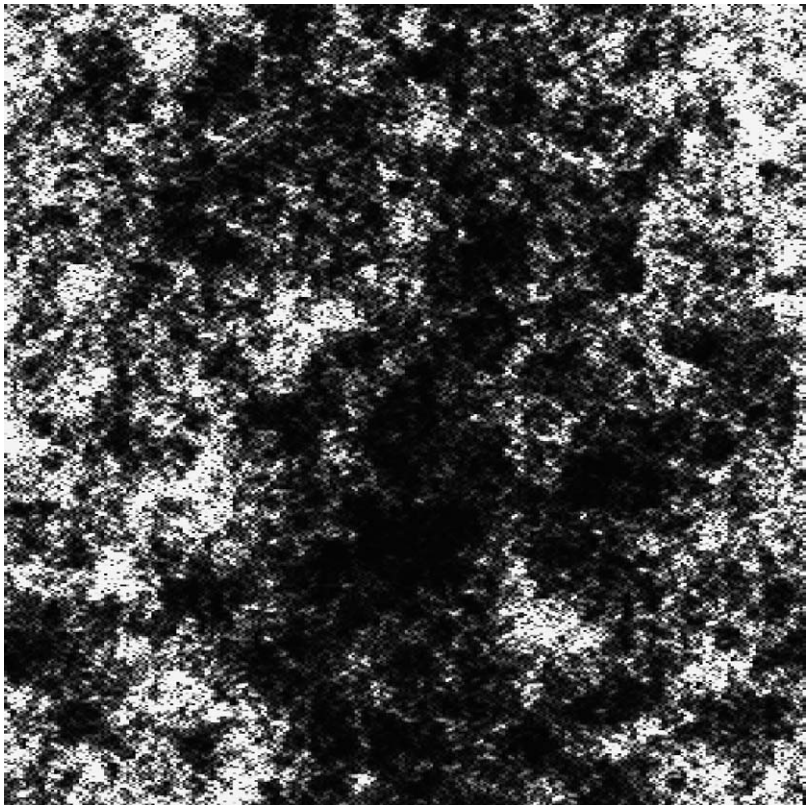

Fig. 12. Squared amplitude of a critical wave function in a Chalker–Coddington network of 256 × 256 saddle points. Darker areas denote lower square amplitude. No characteristic lengths scale can be identified (figure taken from [138]).

system size, the energy level spacing $s$ (in units of the mean level spacing) is given approximately by the distribution function

$$P(s) \propto s^{\beta} \mathrm{e}^{-A(\beta)s^2} \ . \tag{138}$$

This is often denoted as the Wigner surmise. The value of the parameter $\beta$ (=1, 2, 4) is determined by the symmetry of the system. The value of the constant $A$ depends on $\beta$. When the system has both time reversal and spin rotation symmetry, $\beta = 1$. This is called the *orthogonal* symmetry class. If the system has only time reversal symmetry but spin rotational symmetry is broken by spin–orbit interaction, $\beta = 4$. This characterizes the *symplectic* class where level repulsion is strongest. If $\beta = 2$, time reversal symmetry is broken, irrespectively of whether or not spin rotational symmetry is present. This is the *unitary* symmetry class. Symmetries classes are indeed very important ingredients for characterizing the universal properties of a quantum phase transitions. We will discuss this in more detail later in Section 9.

On the other hand, when the states are localized, the correlations between eigenenergies vanish in the limit of large system size. Then, the level spacing distribution $P(s)$ is Poissonian, $P(s) = \exp(-s)$. When the system size is finite, the correlations between energy values are still present and the spacing distribution deviates from the Poissonian. The deviation from the limit of infinite system size can be

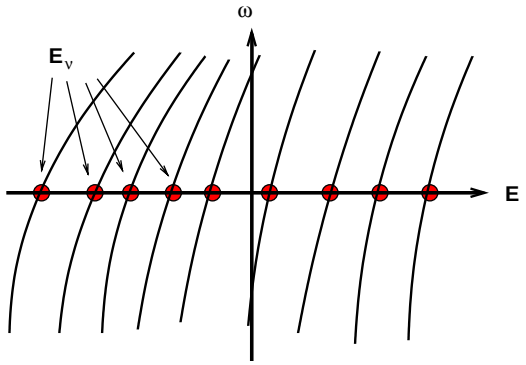


Fig. 13. Scheme of the quasi-energies $\omega_v$ as a function of $E$. The condition $\omega_v = 0$ gives the eigenenergies, $E_v$.

described by using a single parameter scaling assumption Eq. (111) [30,146–148,105]

$$P(s) = f\left(s, \frac{L}{\xi}\right) , \tag{139}$$

where $\xi$ is the localization length. For the ordinary metal–insulator transition, the above equation has two branches corresponding to metallic and insulating phases. In the Chalker–Coddington model, we do not have a true metallic phase. Therefore, we expect to find only a single branch.

Exactly at the critical point, $\xi$ diverges and $P(s)$ becomes size independent. It is neither a Poissonian nor it corresponds to the Wigner surmise, but has both characteristics. It grows as $s^\beta$ for $s \ll 1$ as in the case of the Wigner surmise and it decays according to $\exp(-As)$ for $s \gg 1$ like the Poisson distribution [105,149,150] (Fig. 13).

We now want to obtain the energy level statistics from Eq. (121). To achieve this, we need a method to extract information about energy eigenvalues from the transfer matrix approach. This requires the construction of an equivalent Hamiltonian which we will do below in great detail. For the present purposes it is sufficient to consider the following.

First we note that the eigenvalue equation of the unitary operator $\mathbf{U}(E)$ is

$$\mathbf{U}(E)\Psi_v = \mathrm{e}^{\mathrm{i}\omega_v}\Psi_v \ . \tag{140}$$

The eigenenergies $E_v$'s that correspond to the stationary states are obtained from the condition $\exp[\mathrm{i}\omega_v(E_v)] = 1$.

The statistics of the energy levels obtained from the condition $\omega(E) = 0$ is the same as that of levels obtained by $\omega = \Omega$, since the latter correspond to the solution for $U'(E) = \mathrm{e}^{-\mathrm{i}\Omega}U(E)$ which belongs to the same universality class. This together with the level repulsion leads to the conjecture that $\omega_v(0)$ obey the same statistics as $E_v$ [151]. The quantities $\omega_v(0)$ are often called quasi-energies. This assumption greatly simplifies the numerical calculation. The results, for example the form of $P(s)$ at the critical point, agree in fact very well with those obtained for the continuum model [152]. Due to the simplicity of the network model and the possibility of using the quasi-energy concept, the level statistics can be investigated in detail.

Another important quantity to characterize a random sequence of energy levels is the so-called number variance defined by [144]

$$\Sigma_2(N) = \langle (n - N)^2 \rangle = \langle n^2 \rangle - N^2 \ , \tag{141}$$

where $n$ is the number of levels in a randomly chosen interval $N\Delta$ ($\Delta$ average level spacing), $\langle \cdots \rangle$ denotes the configurational average, and $N = \langle n \rangle$. In the insulating region, $\Sigma_2(N) = N$. In the metallic region, it increases only logarithmically $\Sigma_2(N) \sim \ln N$ due to the level repulsion that makes the spectrum rigid. At the metal–insulator transition,

$$\lim_{N\to\infty} \frac{\Sigma_2(N)}{N} = \chi \ , \tag{142}$$

with $0 < \chi < 1$ [147].

The value $\chi = 1$ implies that the system is an insulator with no level repulsion, and $\chi = 0$ is equivalent to metallic behavior with maximal level repulsion. The fact that $0 < \chi$ means that the level repulsion is weakened as compared to the metallic limit. This is due to the fact that the wave function has a very sparse multi-fractal structure. Thus, $\chi$ reflects the multi-fractal behavior of the wave functions. In fact, the quantity $\chi$ and the fractal dimension $D(2)$ are related via [153]

$$\chi = \frac{d - D(2)}{2d} \ . \tag{143}$$

Inserting $D(2) = 1.52 \pm 0.06$ and $d = 2$ yields $\chi = 0.120 \pm 0.005$. Klesse and Metzler have estimated $\chi$ from the quasi-energies, $\chi = 0.124 \pm 0.006$, in agreement with Eq. (143) [151]. This agreement, however, is not exact since Eq. (143) holds only approximately as has been discussed in Refs. [154,155].

## 5. Linear electrical transport at zero-temperature

The linear electrical conductance of a quantum system at zero temperature is related to quantum mechanical transmission via the Landauer formula [156,157]. Thus, the network model is perfectly designed to provide quantitative information about the linear conductance. If the model describes the physics near the critical point, one can expect also that it is especially suitable for the critical conductance. The study of the linear conductance tells us the importance of the conductance distribution instead of the averaged conductance, which converges to a form independent of the system size. The qualitative behavior of the conductance distribution is expected to be valid even in different situations such as 4-terminal conductance measurement.

In this section we want to discuss the quantum conductance and its distribution function at the critical point at absolute zero of the temperature. For the conductance, we use a slightly modified random network model (Fig. 14 and [158]).

### 5.1. The transfer matrix and the conductance

The general wave function on the left-hand side of the system is a superposition of the incident and reflected amplitudes, $\{\psi^{\mathrm{L}}_{\mathrm{i},i}\}$ and $\{\psi^{\mathrm{L}}_{\mathrm{o},i}\}$, respectively. These are related to those on the right-hand side,

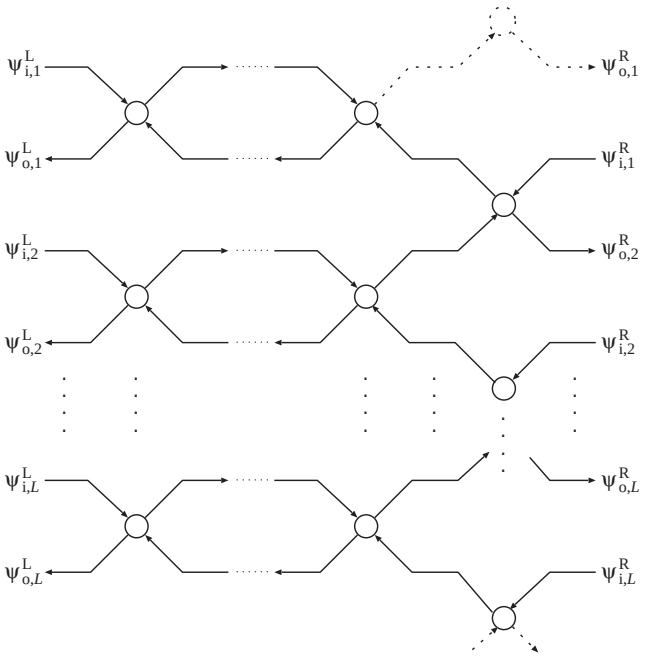


Fig. 14. The network model as modified for calculating the two terminal conductance. The amplitudes $\psi^{\mathrm{L}}_{\mathrm{i},i}$ and $\psi^{\mathrm{L}}_{\mathrm{o},i}$ $(i=1,\ldots,L)$ represent the incoming and the outgoing currents on the left-hand side, respectively, $\psi^{\mathrm{R}}_{\mathrm{i},i}$ and $\psi^{\mathrm{R}}_{\mathrm{o},i}$ $(i=1,\ldots,L)$ represent the amplitudes on the right-hand side of the sample.

$\{\psi^{\mathrm{R}}_{\mathrm{i},i}\}$ and $\{\psi^{\mathrm{R}}_{\mathrm{o},i}\}$, via the transfer matrix of the system of the lengths $M$ and the width $L$, $\mathbf{T}^M_L$,

$$\begin{pmatrix} \psi^{\mathrm{R}}_{\mathrm{o},1} \\ \psi^{\mathrm{R}}_{\mathrm{i},1} \\ \vdots \\ \psi^{\mathrm{R}}_{\mathrm{o},L} \\ \psi^{\mathrm{R}}_{\mathrm{i},L} \end{pmatrix} = \mathbf{T}^M_L \begin{pmatrix} \psi^{\mathrm{L}}_{\mathrm{i},1} \\ \psi^{\mathrm{L}}_{\mathrm{o},1} \\ \vdots \\ \psi^{\mathrm{L}}_{\mathrm{i},L} \\ \psi^{\mathrm{L}}_{\mathrm{o},L} \end{pmatrix} . \tag{144}$$

By introducing an operator $\mathbf{U}$ which changes the order of the components,

$$\begin{pmatrix} \psi^{\mathrm{L}}_{\mathrm{i},1} \\ \psi^{\mathrm{L}}_{\mathrm{o},1} \\ \vdots \\ \vdots \\ \psi^{\mathrm{L}}_{\mathrm{i},L} \\ \psi^{\mathrm{L}}_{\mathrm{o},L} \end{pmatrix} = \mathbf{U} \begin{pmatrix} \psi^{\mathrm{L}}_{\mathrm{i},1} \\ \vdots \\ \psi^{\mathrm{L}}_{\mathrm{i},L} \\ \psi^{\mathrm{L}}_{\mathrm{o},1} \\ \vdots \\ \psi^{\mathrm{L}}_{\mathrm{o},L} \end{pmatrix}, \quad \begin{pmatrix} \psi^{\mathrm{R}}_{\mathrm{o},1} \\ \psi^{\mathrm{R}}_{\mathrm{i},1} \\ \vdots \\ \vdots \\ \psi^{\mathrm{R}}_{\mathrm{o},L} \\ \psi^{\mathrm{R}}_{\mathrm{i},L} \end{pmatrix} = \mathbf{U} \begin{pmatrix} \psi^{\mathrm{R}}_{\mathrm{o},1} \\ \vdots \\ \psi^{\mathrm{R}}_{\mathrm{o},L} \\ \psi^{\mathrm{R}}_{\mathrm{i},1} \\ \vdots \\ \psi^{\mathrm{R}}_{\mathrm{i},L} \end{pmatrix}, \tag{145}$$

one can write

$$\begin{pmatrix} \psi_{\mathrm{o}}^{\mathrm{R}} \\ \psi_{\mathrm{i}}^{\mathrm{R}} \end{pmatrix} = \mathbf{U}^{\dagger}\mathbf{T}\mathbf{U} \begin{pmatrix} \psi_{\mathrm{i}}^{\mathrm{L}} \\ \psi_{\mathrm{o}}^{\mathrm{L}} \end{pmatrix} , \tag{146}$$

where $\psi_{\mathrm{o}}^{i}(i = \mathrm{R}, \mathrm{L})$ denotes the vector of amplitudes $(\psi_{\mathrm{o},1}^{i}, \psi_{\mathrm{o},2}^{i}, \ldots, \psi_{\mathrm{o},L}^{i})^{\mathrm{T}}$ and $\psi_{\mathrm{i}}^{i}$ $(i = \mathrm{R}, \mathrm{L})$ is $(\psi_{\mathrm{i},1}^{i}, \psi_{\mathrm{i},2}^{i}, \ldots, \psi_{\mathrm{i},L}^{i})^{\mathrm{T}}$ ($^{\mathrm{T}}$ denotes the transposed vector).

The linear zero-temperature conductance $G$ is given by the quantum transmission probability through the system [156,157,159].

$$G = \frac{e^2}{h} \mathrm{Tr}\, \mathbf{t}\mathbf{t}^{\dagger} . \tag{147}$$

Thus, a relation between the transfer matrix and the transmission matrix $t_{ij}$ $(i, j = 1 \ldots L)$ is required. In the following paragraph this relation will be established by writing the wave function on the left- and right-hand sides of the scatterer in terms of $L \times L$ transmission and reflection matrices $\mathbf{t}$ and $\mathbf{r}$ [160,161].

When a flux of probability amplitude is injected into the $i$th scattering channels from the left and from the right, represented by $\psi_{\mathrm{i},i}^{\mathrm{L}}$ and $\psi_{\mathrm{i},i}^{\mathrm{R}}$, respectively, the total scattering wave function in the $i$th channels is a superposition of the incident wave and the reflected and transmitted waves from all of the channels. This is described by the scattering matrix $\mathbf{S}$

$$\begin{pmatrix} \psi_{\mathrm{o}}^{\mathrm{L}} \\ \psi_{\mathrm{o}}^{\mathrm{R}} \end{pmatrix} = \mathbf{S} \begin{pmatrix} \psi_{\mathrm{i}}^{\mathrm{L}} \\ \psi_{\mathrm{i}}^{\mathrm{R}} \end{pmatrix} \tag{148}$$

with

$$\mathbf{S} = \begin{pmatrix} \mathbf{r} & \mathbf{t}' \\ \mathbf{t} & \mathbf{r}' \end{pmatrix} . \tag{149}$$

By solving Eq. (148) for $\psi_{\mathrm{o}}^{\mathrm{R}}$ and $\psi_{\mathrm{i}}^{\mathrm{R}}$ and inserting into Eq. (146) one obtains straightforwardly

$$\widetilde{\mathbf{T}} = \mathbf{U}^{\dagger}\mathbf{T}\mathbf{U} = \begin{pmatrix} \mathbf{t} - \mathbf{r}'\mathbf{t}'^{-1}\mathbf{r} & \mathbf{r}'\mathbf{t}'^{-1} \\ -\mathbf{t}'^{-1}\mathbf{r} & \mathbf{t}'^{-1} \end{pmatrix} := \begin{pmatrix} \widetilde{\mathbf{T}}_{11} & \widetilde{\mathbf{T}}_{12} \\ \widetilde{\mathbf{T}}_{21} & \widetilde{\mathbf{T}}_{22} \end{pmatrix} . \tag{150}$$

In order to determine the $(L \times L)$-matrix $\mathbf{t}'$ that one can use equivalently for the conductance instead of $\mathbf{t}$, it is sufficient to generate $\widetilde{\mathbf{T}}_{12}$ and $\widetilde{\mathbf{T}}_{22}$ by multiplying $\widetilde{\mathbf{T}}$ to the $2L \times L$ matrix which consists of the zero-matrix $\mathbf{0}_L$ in the upper half and the unit matrix $\mathbf{1}_L$ in the lower part,

$$\begin{pmatrix} \widetilde{\mathbf{T}}_{12} \\ \widetilde{\mathbf{T}}_{22} \end{pmatrix} = \widetilde{\mathbf{T}} \begin{pmatrix} \mathbf{0}_L \\ \mathbf{1}_L \end{pmatrix} . \tag{151}$$

Multiplying iteratively $\mathbf{T}^{(k)}$ $(k = 0, 1, 2, 3, \ldots, M)$ is numerically unstable. Thus, after each $m$ steps one must perform a $QR$ decomposition,

$$\mathbf{T}^{(i\times m+m)}\mathbf{T}^{(i\times m+m-1)} \cdots \mathbf{T}^{(i\times m+1)}\mathbf{V}^{i} = \mathbf{V}^{i+1}\omega^{i} , \tag{152}$$

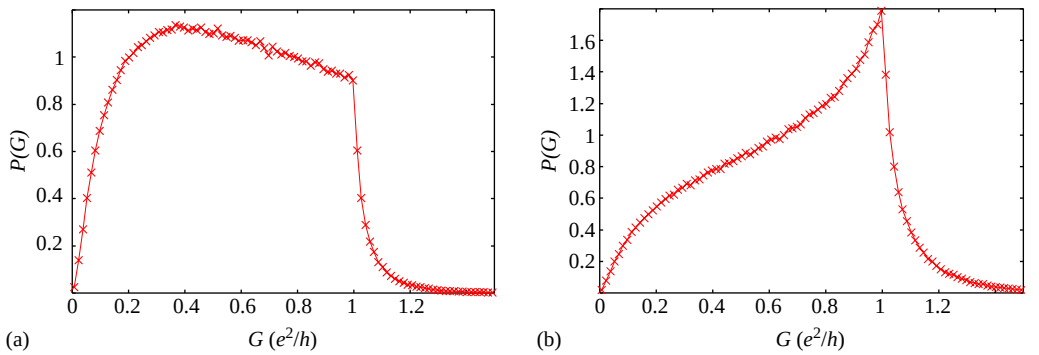


Fig. 15. Conductance distribution at the critical point. The number of incoming links is 128. The geometrical shape of the system is a square. Left: for periodic boundary conditions; right: for fixed boundary conditions. See also [158].

where $\mathbf{V}^i$ are $(2L \times L)$ orthonormalized matrices and $\omega^i$ are $(L \times L)$ upper triangular matrices. This eventually yields

$$\begin{pmatrix} \widetilde{\mathbf{T}}_{12} \\ \widetilde{\mathbf{T}}_{22} \end{pmatrix} = \begin{pmatrix} \mathbf{A} \\ \mathbf{B} \end{pmatrix} \omega^k \cdots \omega^2 \omega^1 \ , \tag{153}$$

with matrices $\omega^i$ generated during the iteration and $(L \times L)$-matrices $\mathbf{A}$ and $\mathbf{B}$ the upper and lower blocks of $V^{M/m}$.

Using this result, one finds for the transmission and reflection matrices from Eq. (150). Details and generalization can be found in [162].

$$\mathbf{t}' = (\omega^1)^{-1}(\omega^2)^{-1} \cdots (\omega^k)^{-1}\mathbf{B}^{-1}, \quad \mathbf{r}' = \mathbf{A}\mathbf{B}^{-1} \ . \tag{154}$$

### *5.2. The critical conductance and its statistics*

The conductance $G$ is a strongly fluctuating quantity with a broad distribution function. Therefore, not the conductance but its distribution function $P(G)$ has to be considered.

In the metallic regime, the conductance is described by a normal distribution with its variance independent of the details of the system as well as of the system size. This is known as the phenomenon of reproducible universal conductance fluctuations (UCF [163,164]). In the insulating regime, the distribution function has a log-normal shape, reflecting the exponential localization of wave functions. At the critical point of the localization–delocalization transition not only the variance but the whole distribution function becomes size independent. This reflects again the scale invariance of the quantum critical point [111,165,166,110,167,168]. Remarkably, however, the critical distribution depends on the boundary conditions [112].

In the case of the quantum Hall transition, all the states except those at the band center are localized, so that the conductance distribution is log-normal. As expected, at the band center the conductance distribution function becomes size independent. However, it has the peculiar form shown in Fig. 15. It neither is consistent with the log-normal distribution expected in the localized regime nor reproduces the non-universal behavior of the moments predicted for the metallic region [169]. It also depends strongly

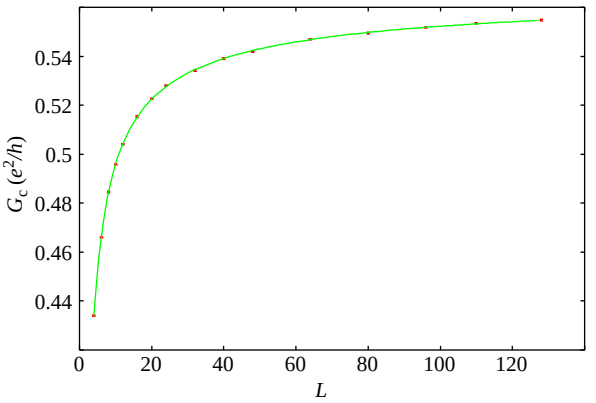


Fig. 16. The system size dependence of the "bulk conductance" at the critical point. Solid line: fit to the scaling law Eq. (155), $G_c = 0.5702 - 0.2150L^{-0.5587} - \frac{0.1486}{L}$.

on the boundary conditions. This is consistent with earlier results obtained for the level statistics at the Anderson transition [170,171].

From the distribution, one can calculate a configurationally averaged conductance $\langle G\rangle$ and its moments [172]. We consider here as an example only the two terminal conductance for periodic boundary conditions. We expect, in addition to corrections to scaling, effects of the contacts [173] and of the boundary conditions [112]. Both of them can be expected to give rise to contributions proportional to $L^{-1}$. Therefore, we attempted to fit the average conductance to the scaling Ansatz

$$\langle G\rangle = G_c + aL^y + \frac{b}{L}\ . \tag{155}$$

This fit yields the bulk ($L \to \infty$) conductance

$$G_c = (0.570 \pm 0.02)\frac{e^2}{h}, \quad y = -0.56 \pm 0.05\ . \tag{156}$$

The form of the distribution of the critical conductance is similar to that obtained from simulating the conductance of the tight-binding model in magnetic fields [174]. However, there are quantitative discrepancies. For example, the two terminal conductance in units of $e^2/h$ is 0.506 for the tight-binding model [169], but 0.57 for the Chalker–Coddington model. This might be due to the inter-band coupling present in the tight-binding model.

In Fig. 16, we observe a continuous increase of $P(G)$ from 0 near $G = 0$, and a kink near $G = e^2/h$. The kink is expected in one dimension [175,176], in the two-dimensional symplectic ensemble [167,177] and in three-dimensional disordered systems [168]. It is related to the fact that for one transport channel, one can achieve at best unit transmission. Fluctuations of the conductance to values larger than $e^2/h$ are related to the contributions from the exponentially smaller contributions of the other transport channels.

For better understanding the kinks in the distribution functions, the transmission eigenvalues $\{\tau_i\}$ obtained by diagonalizing $\mathbf{tt}^\dagger$ have been analyzed in more detail [172]. It has been found that for the quantum Hall transition the critical conductance distribution is well approximated by taking into account only the largest transmission eigenvalue as demonstrated in Fig. 17. This result suggests that the knowledge

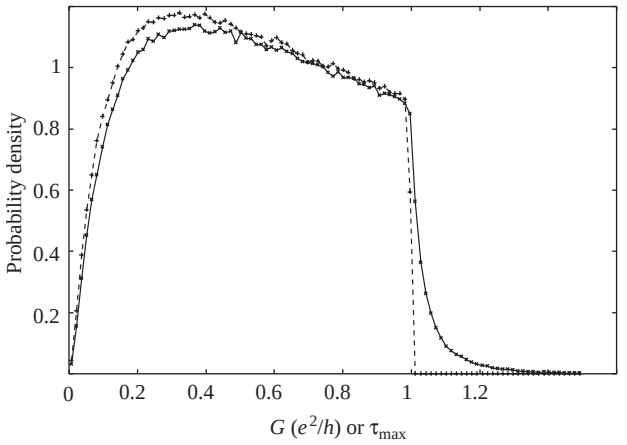


Fig. 17. The distribution of the critical conductance (×) compared with the distribution of the largest transmission eigenvalue $\tau_{\max}(+)$ at the critical point (after [172]).

of the distribution of $\tau_{\max}$ would enable us to approximately predict the transport coefficients at the quantum Hall transition.

In order to further investigate $P(\tau_{\max})$, we transform to a new variable $v_{\min}$ according to

$$\tau_{\max} = \frac{2}{\cosh v_{\min} + 1} \ . \tag{157}$$

It has been suggested in [178] that $v_{\min}^2$ is Poissonian distributed,

$$P(v_{\min}^2) = \beta N \Omega \mathrm{e}^{-\beta N \Omega v_{\min}^2} \tag{158}$$

or equivalently,

$$P(v_{\min}) = 2\beta N \Omega v_{\min} \mathrm{e}^{-\beta N \Omega v_{\min}^2} \ . \tag{159}$$

In Fig. 18, we show $P_c(v_{\min})$ and fitted the data to Eq. (159) by assuming $\beta N \Omega = 0.233$.

From the very good agreement between $P(v_{\min})$ and the Slevin–Nagao form [178] one might conclude that the distribution of $\{v_i\}$ is given by

$$P(v_1, v_2, \ldots, v_N) = C \prod_i \mathrm{e}^{-\beta\Omega\sum_i v_i^2} \prod_{i<j} |v_i^2 - v_j^2|^2 \ , \tag{160}$$

which defines the Laguerre ensemble [178,179]. However, the distribution of second and higher values, i.e. $v_i$ $(i = 2, 3, \ldots)$ as calculated from the Laguerre ensemble [180] deviate from the result of the present numerical simulation. This is not unexpected since the Laguerre ensemble has been proposed to be a good approximation for the statistics of the metallic diffusive regime. At the quantum Hall transition, the so-called eigenvalue "interaction" term may be modified,

$$P(v_1, v_2, \ldots, v_N) = C \prod_i \mathrm{e}^{-\beta\Omega\sum_i v_i^2} \prod_{i<j} f(|v_i^2 - v_j^2|) \ . \tag{161}$$

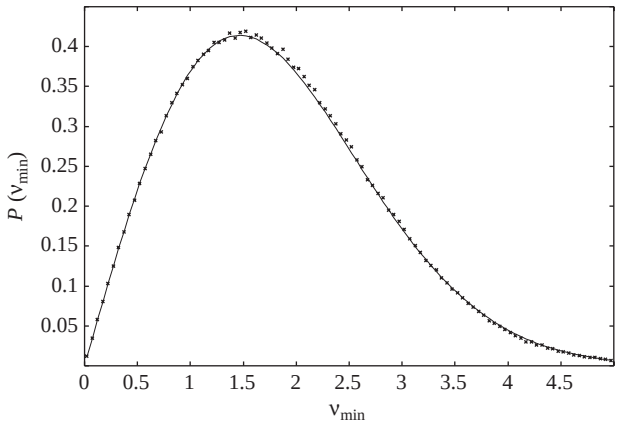


Fig. 18. The distribution of $v_{\min}$ compared with the Poissonian distribution $P(v_{\min}) = 2av_{\min}\exp(-av_{\min}^2)$ with $a = 0.233$ (after [172]).

This form leads to the same distribution for $v_{\min}$ but different distributions for higher $v_i$ $(i = 2, 3, \ldots)$ [172].

Before concluding this section, we mention that the energy correlation function of the two terminal conductance has been analyzed in detail by Jovanovic and Wang [103].

### 5.3. Conformal invariance at the critical point

We have presented above strong numerical evidence for the scale invariance of the wave functions, energy level statistics and the conductance distribution at the critical point. Under a scale transformation, the length scale is rescaled globally by some factor $b$ such that the coordinates of a given point transform according to

$$\boldsymbol{r}' = b^{-1}\boldsymbol{r}\ . \tag{162}$$

Scale invariance at a critical point means that correlation functions of scaling variables $\phi_j(\boldsymbol{r})$ $(j = 1, 2, 3\ldots)$ are invariant under such a transformation which generally can include also a rotation and a translation

$$\langle\phi_1(\boldsymbol{r}_1)\phi_2(\boldsymbol{r}_2)\ldots\rangle = \prod_j b^{-h_j}\langle\phi_1(\boldsymbol{r}_1')\phi_2(\boldsymbol{r}_2')\ldots\rangle\ . \tag{163}$$

The exponents $h_j$ are called scaling dimensions.

In analogy to classical phase transitions, one can expect not only that global scale invariance holds but also that the more general concept of conformal invariance [139,104] applies to the quantum Hall transition [181,31]. Generally, a conformal transformation corresponds to *local* translations, rotations and dilatations of the coordinates which preserve angles.

In order to explain this in more detail, we consider the above general correlation function in two dimensions, $\langle\phi_1(z_1, z_1^*)\phi_2(z_2, z_2^*)\cdots\rangle$, with the scaling variables $\phi_j$ $(j = 1, 2, 3\ldots)$ and the spatial

variables represented as $z_j = x_j + \mathrm{i}y_j$ and its complex conjugate $z_j^*$. Now let us consider an arbitrary analytic mapping

$$z' = w(z) \ . \tag{164}$$

Locally, close to some point $z_0$, which is equivalent to the infinitesimal map

$$z' - z_0' = w'(z_0)(z - z_0) \ , \tag{165}$$

with $w'(z_0) = \mathrm{d}w(z_0)/\mathrm{d}z_0$. Comparing with Eq. (162) one notes that the global scale factor $b^{-1}$ of the scaling transformation corresponds to $w'(z_0)$.

In analogy to Eq. (163), conformal invariance of the correlation functions can be defined by

$$\begin{aligned}&\langle\phi_1(z_1, z_1^*)\phi_2(z_2, z_2^*)\ldots\rangle \\ &\quad = \prod_i w'(z_i)^{h_i}(w'(z_i)^*)^{h_i'}\langle\phi_1(z_1', z_1'^*)\phi_2(z_2', z_2'^*)\ldots\rangle \ .\end{aligned} \tag{166}$$

The exponents $h_i$ and $h_i'$ are real-valued conformal scaling dimensions [104].

In order to show how powerful the concept of conformal invariance is for extracting properties of the correlation functions we consider the two-point correlation function of only one scaling variable. Conformal invariance requires

$$\langle\phi(z_1, z_1^*)\phi(z_2, z_2^*)\rangle = |w'(z_1)|^\eta |w'(z_2)^*|^\eta \langle\phi(z_1', z_1'^*)\phi(z_2', z_2'^*)\rangle \ . \tag{167}$$

It is a straightforward exercise to show that this implies a power-law decay of the correlation function [104],

$$\langle\phi(z_1, z_1^*)\phi(z_2, z_2^*)\rangle \sim |z_1 - z_2|^{-2\eta} \ . \tag{168}$$

As a second example, we consider the mapping between the infinite two-dimensional plane and the surface of cylinder with circumference $L$,

$$z' = \frac{L}{2\pi}\ln z \ . \tag{169}$$

This is motivated by our above numerical studies in which we have used systems of finite width $L$ and length $M \to \infty$. It is easy to get convinced that variation of $x$, $y$ in the complete two-dimensional plane implies $-\infty < x' < \infty$ and $0 < y' < L$. This corresponds to an infinitely long strip of width $L$ with periodic boundary conditions in the direction of $L$ which is equivalent to a cylinder. The correlation function on the cylinder reads

$$\begin{aligned}&\langle\phi(z_1', z_1'^*)\phi(z_2', z_2'^*)\rangle \\ &\quad \sim \frac{(2\pi/L)^{2\eta}}{\{2\cosh[2\pi(x_1' - x_2')/L] - 2\cos[2\pi(y_1' - y_2')/L]\}^\eta} \ .\end{aligned} \tag{170}$$

Therefore, the quasi-one-dimensional exponential decay length $\xi_{\mathrm{cyl}}$ and $\eta$ are related via

$$\xi_{\mathrm{cyl}} = \frac{L}{2\pi\eta} \ . \tag{171}$$

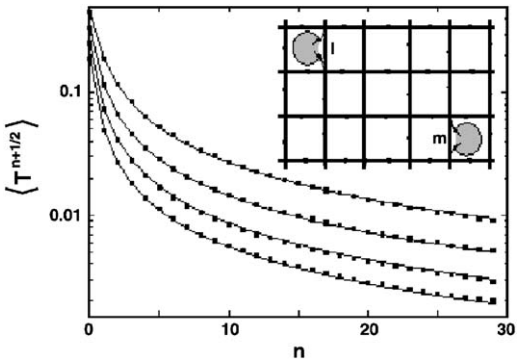


Fig. 19. Average half-integer moments $\langle T^{n+1/2} \rangle$ of the two-point contact conductance of the Chalker–Coddington model at the critical point as a function of $n$. Data sets (top to bottom) correspond to distances 5,10,15,20 (in units of the lattice constant) in a cylinder geometry with total length $M = 100$ and circumference $L = 10$. Solid lines are analytical results obtained by conformal invariance. For best fit an exponent $X_t = 0.54 \pm 0.01$ was found. Inset: schematic view for the model. Two links, $l$ and $m$, are cut and connected to reservoirs $l$ and $m$ (after [183]).

If we assume $\phi(z)$ to be the typical density of states defined via the square amplitude of the wave function,

$$\rho^{\mathrm{typ}} = \frac{(|\Psi|^2)^{\mathrm{typ}}}{\Delta E} \ , \tag{172}$$

where $\Delta E \sim L^{-2}$ is the mean level spacing, we obtain from Eq. (135)

$$\eta = \alpha_0 - 2 \ . \tag{173}$$

The transfer matrix estimates the exponential decay length by averaging $\log|\psi(0)\psi(z)|$. Therefore, it is the typical amplitude of the wave function which is related to the decay length. Combining Eqs. (171) and (135)

$$\xi_{\mathrm{cyl}} = \frac{L}{2\pi(\alpha_0 - 2)} \ , \tag{174}$$

which is the same as Eq. (137) since $\Lambda_c = 2\xi_{\mathrm{cyl}}/L$. This example illustrates how powerful the requirement of the conformal invariance is. Therefore, whether or not this symmetry holds for a phase transition is very important and can provide useful information about the properties near the critical point.

An important transport coefficient which can be used to clarify whether or not the conformal invariance applies is the point-contact conductance [182,183]. Consider a network with two links $l$ and $m$ cut from the interior, and connected to two reservoirs (Fig. 19). Then we can define a $2 \times 2$ **S** matrix

$$\mathbf{S} = \begin{pmatrix} S_{ll} & S_{lm} \\ S_{ml} & S_{mm} \end{pmatrix} \tag{175}$$

and the point-contact conductance is given by (in units of $e^2/h$) $T = |S_{lm}|^2$. The **S** matrix is calculated by

$$S_{ij} = \langle i|(1 - \mathbf{U}\mathbf{P}_l\mathbf{P}_m)^{-1}\mathbf{U}|j\rangle \quad (i, j = l, m) \ , \tag{176}$$

where $\mathbf{U}$ is the time evolution operator introduced by Eq. (121) and $\mathbf{P}_l = 1 - |l\rangle\langle l|$ and $\mathbf{P}_m = 1 - |m\rangle\langle m|$ the projection operators which describe the nature of reservoirs (Fig. 19).

The point-contact conductance $T$ is related to the wave function intensity at $l$ and $m$, $|\Psi_l|^2$ and $|\Psi_m|^2$ via [183]

$$2\pi\rho(E)\langle|\Psi_m|^2 f(|\Psi_m|^2/|\Psi_l|^2)\rangle = \langle F(T)\rangle \ , \tag{177}$$

where

$$F(T) := \int_0^{2\pi} \frac{\mathrm{d}\phi}{2\pi} f(T^{-1}|1 - \mathrm{e}^{\mathrm{i}\phi}\sqrt{1-T}|^2) \ , \tag{178}$$

Here $\rho(E)$ is the density of states and $\langle\cdots\rangle$ means the average over randomness. Assuming $f(x) = -\ln x$, we have

$$\langle \ln T\rangle = 2\pi\rho(E)\langle|\Psi_m|^2 \ln(|\Psi_l|^2/|\Psi_m|^2)\rangle \ . \tag{179}$$

Thus one can evaluate the typical conductance $T^{\mathrm{typ}} = \exp(\langle \ln T\rangle)$ very efficiently using only the information of the wave functions in an isolated system.

At the critical point, in the infinite two-dimensional plane $T^{\mathrm{typ}}$ is expected to decay as

$$T^{\mathrm{typ}} \sim r^{-X_{\mathrm{t}}} \ , \tag{180}$$

where $r$ is the distance between the links $l$ and $m$ and $X_{\mathrm{t}}$ a critical exponent related to $\tau(q)$ (cf. Eq. (128)) via $\tau'(0) - \tau'(1)$ [184].

From Eqs. (171) and (180), the decay of the typical conductance on a long cylinder surface becomes [183]

$$T^{\mathrm{typ}}_{\mathrm{cyl}}(x) = \left|\frac{L}{2\pi}\sinh\left(\frac{\pi x}{L}\right)\right|^{-X_{\mathrm{t}}} \ , \tag{181}$$

where $x$ is the distance between the links $l$ and $m$ along the cylinder axis.

Numerical results for the moments of $T(x)$, $\langle T(x)^{n+1/2}\rangle$ (Fig. 19) and the typical conductance $T^{\mathrm{typ}}_{\mathrm{cyl}}(x)$ (Fig. 20) coincide with the behavior expected from the conformal invariance [182,183]. This strongly supports the conjecture that the wave function at the quantum Hall transition is conformally invariant [181].

## 6. The renormalization group approach

In this section, we discuss the application of the real-space renormalization group approach that is widely used in classical percolation and spin systems [104,62] to the random network model. A closed set of renormalization group equations is derived which describes the universal distribution of the conductance. The numerical solution is used to estimate the critical exponent of the localization length and the behavior of the moments of the distribution function [33,185–187]. Amazingly enough, by adopting a slightly different point of view, eventually one can interpret the approach as providing an additional, independent precision determination of the critical exponent. The agreement of this critical exponent

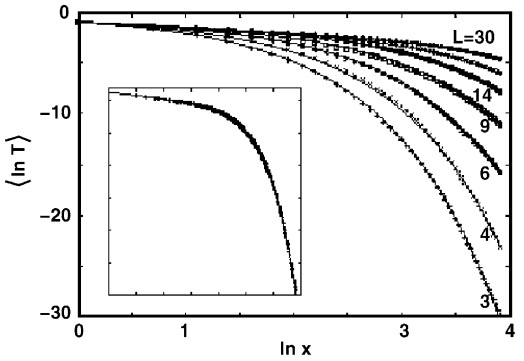


Fig. 20. Logarithm of the typical two-point conductance $\langle \ln T \rangle$ of the Chalker–Coddington network model at the critical point as a function of the logarithm of the distance $\ln|x|$ for system widths $L = 3, 4, 6, 9, 14, 20, 30$ (bottom to top). Solid lines: analytical result obtained using conformal invariance, Eq. (181). Inset: rescaled curves $\langle \ln T \rangle + X_t \ln L$ versus $\ln|x/L|$ with $X_t = 0.57$ (after [183]).

with the earlier results obtained for completely different models confirms that the quantum Hall phase transition is indeed a universal critical phenomenon.

The general idea is that near the quantum critical point all microscopic details of the system eventually must become irrelevant since the correlation length diverges with a universal exponent which, however, still can depend on the fundamental global symmetries. In order to detect such universal behavior one must perform a well-controlled thermodynamic limit. An example how to do this in a controlled way has been given above when applying the transfer matrix method and using the numerical scaling method. This procedure is basically exact and suffers only from technical numerical errors, but it does in general not provide analytical insight.

In classical phase transition theory, the renormalization group transformation is a well-established procedure to approach the critical point. Generally, this method consists of a sequence of unitary and subsequent scale transformations. The former are used to diagonalize relatively small systems. The latter scale the system back to the original length scale. From the behavior of the coupling parameters under this repeatedly applied transformation conclusions can be drawn on the critical behavior. In principle, this method would also be exact, apart from the fact that in each renormalization step couplings to states that are energetically far away from the critical point are neglected. While this seems not to be crucial for showing the very existence of a critical point, one needs quite substantial numerical efforts in order to correctly obtain the critical behavior quantitatively.

There are many alternative possibilities for constructing the renormalization group transformation which are all similar in spirit but may be different in the details. We will discuss here two of them. The random network model of Chalker and Coddington is an example in which the renormalization group transformation can most advantageously be used.

### *6.1. An illustrative example: the tile lattice*

A particularly instructive example which resembles the procedure invented originally by Migdal and Kadanoff is shown in Fig. 22 [186]. For a better understanding of this procedure, we first introduce different graphical representations of the scattering matrices of the saddle points which are more convenient for

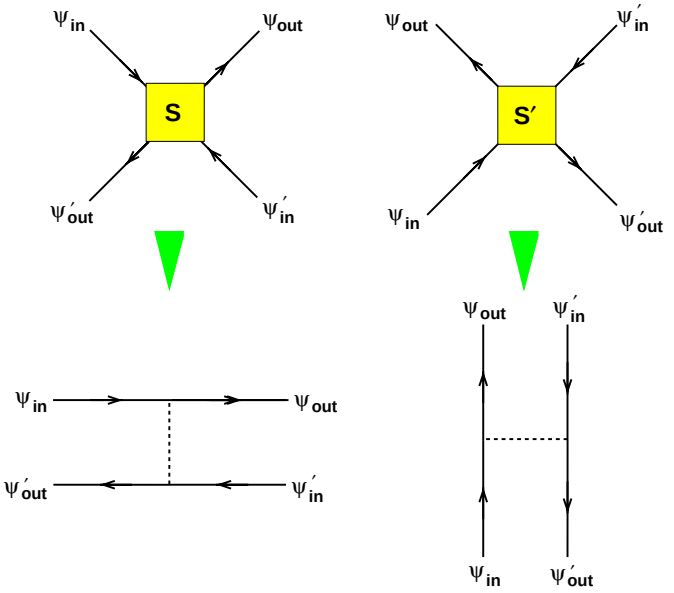


Fig. 21. Representations of saddle point scattering. The scattering matrices **S** and **S**′ relate outgoing with incoming flux amplitudes (top). The same information can be expressed by transfer matrices that relate top and bottom amplitudes (left) and left and right amplitudes (right).

the present purpose (Fig. 21). The original scattering matrices **S** and **S**′ relate outgoing and incoming amplitudes, $\psi_{\text{out}}$, $\psi'_{\text{out}}$ and $\psi_{\text{in}}$, $\psi'_{\text{in}}$, respectively. This is represented as in the top part of Fig. 21. Rewriting the equations such that the amplitudes on the right-hand side of the saddle point are obtained as functions of the amplitudes on the left, $\psi'_{\text{in}}$, $\psi'_{\text{out}}$ and $\psi_{\text{in}}$, $\psi_{\text{out}}$, respectively, one obtains the usual transfer matrix representation which we have used so far (Fig. 21, right). The saddle point vertex is now represented by a horizontal dashed line. For **S**, the corresponding representation is shown in the left part of Fig. 21. With this, the original random network of Fig. 8 can be graphically represented as shown in Fig. 22a. For simplicity, the system is assumed to consist of independent saddle points with randomly varying saddle point energies. The phases associated with the links between them are assumed to be completely random and independent.

Starting from this a renormalization group transformation may be constructed by removing every other saddle point line in a each row and column, and replacing the remaining single saddle point lines by two. Thereby, one reaches the situation shown in Fig. 22b. One observes that every other closed loop of amplitudes now is completely disconnected from the rest of the system and can be removed. On the other hand, each of the remaining saddle points is replaced by two saddle points in series. By combining these to new scattering centers as indicated in Fig. 22c one arrives at exactly the same lattice structure as in Fig. 22a but with renormalized saddle point scattering centers (Fig. 22d).

By iteratively applying this procedure, more and more of the network is incorporated into the scattering properties of the scattering centers until eventually one of the latter in corporates the whole system. If the energy is lower than the saddle point energy $E^*$, the transmission probability will eventually renormalize exponentially to zero. The system becomes completely localized since the closed loops labeled with

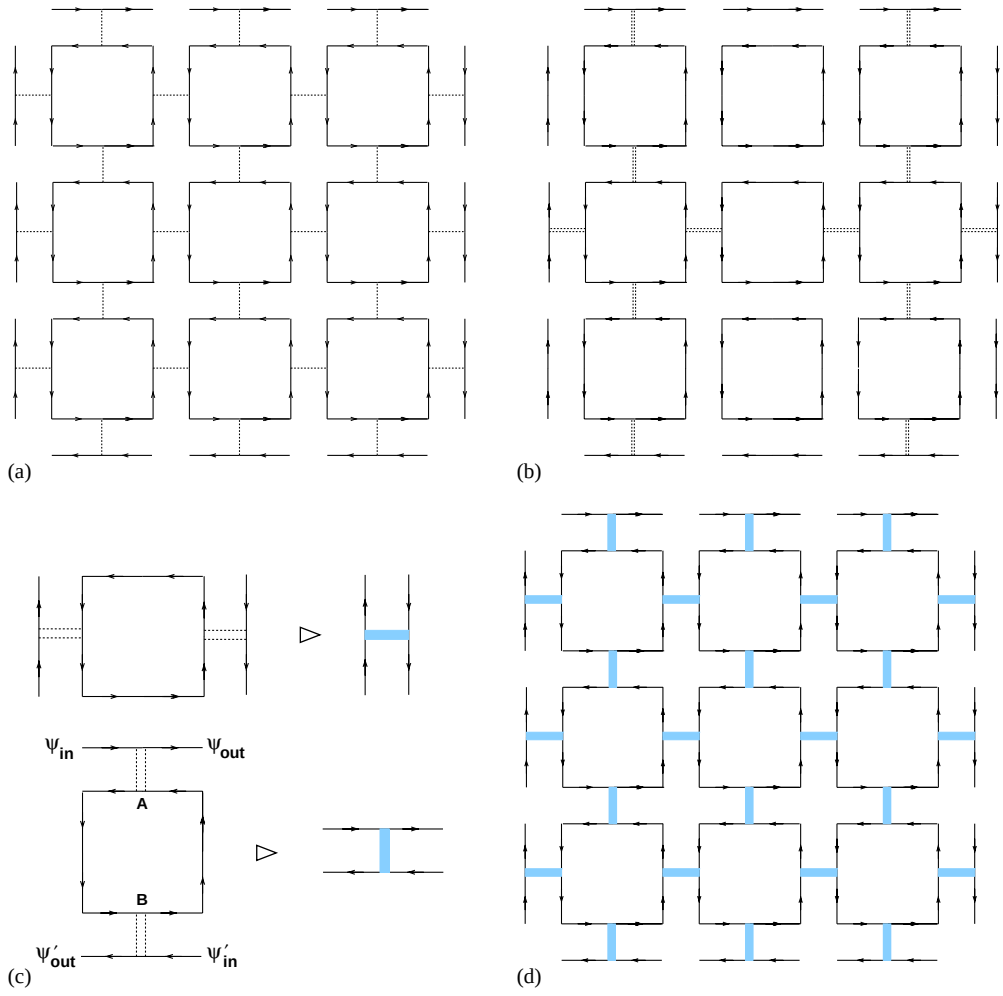


Fig. 22. Illustration of the renormalization procedure on a tile lattice. (a) Lattice of original saddle points. (b) Second-generation saddle point lattice where every other saddle point in the rows and columns are removed and the remaining saddle points are doubled. Isolated rings of amplitudes can be removed. (c) By renormalizing the saddle point as indicated one arrives (d) at a lattice that, apart from a scale transformation, is structurally identical to the original one (after [186]).

$E < E^*$ (Fig. 23) will be completely disconnected. If on the other hand the energy is higher than the saddle point energy, the transmission probability will renormalize to one. The states are again localized since now the loops labeled with $E > E^*$ in Fig. 23 become disconnected. Thus, the transmission probability has two stable fixed points $T = 0$ and 1) which correspond to the localized phases. The transmission probability becomes independent of the "size" of the scatterer exactly at the critical point $E^*$. Here, we have an *unstable* non-trivial fixed point $T^* \neq 0$. Even an infinitesimally small deviation of the energy from the critical point localizes the system completely.

For the tile lattice, the calculation of the scattering properties of a new scattering center by combining two original ones is an easy but nevertheless instructive exercise. The transmission matrix of the new

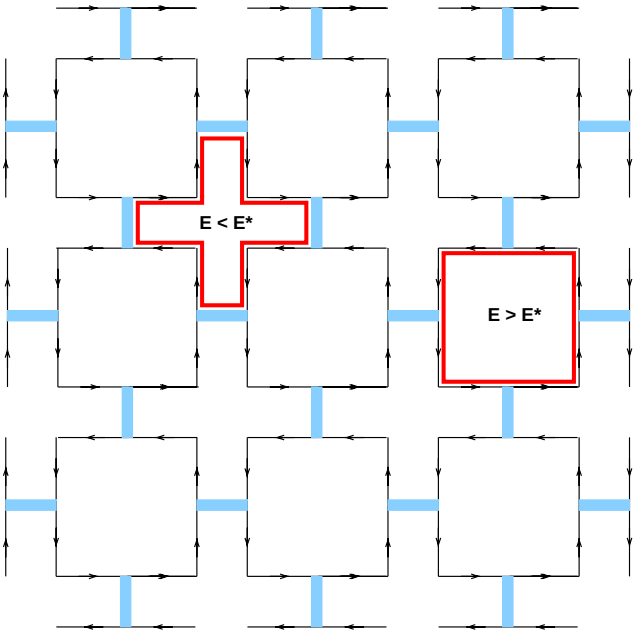


Fig. 23. Illustration of localization in the renormalized network for energies below the critical point, $E < E^*$, where the transmission renormalizes to zero, and above the critical point, $E > E^*$, where the transmission renormalizes to one. Extended states can exist only at $E = E^*$ where the transmission has a non-trivial fixed point $T^* \neq 0$.

scattering center (Fig. 22c) can be determined in terms of the transmission matrices of the original scattering centers by performing simple matrix multiplications. Consider, for example, the diagram at the bottom of Fig. 22c. First, one calculates the transmission of the two pairs of saddle points in series at the top (A) and the bottom (B) of the graph. Second, the two resulting effective scatterers are combined "in parallel" in order to obtain the transfer of amplitudes between channels ($\psi_{\text{in}}$, $\psi_{\text{out}}$) and ($\psi'_{\text{in}}$, $\psi'_{\text{out}}$). Eventually, one finds for the *typical* total transmission probability $T := \exp\langle \ln T \rangle$ (with $T = t^2$ and $\langle \ldots \rangle$ the ensemble average) the renormalization relation [186]

$$T' = 2T^2 - T^4 := f(T; 2) \ , \tag{182}$$

where $T'$ is the typical transmission probability of the renormalized scattering center.

This scaling relation has three fixed points defined by $T^* = 2T^{*2} - T^{*4}$, two stable ones at $T^* = 0$ and 1 and an unstable one at $T^* = (\sqrt{5} - 1)/2 = 0.618$. The stable fixed points correspond to the localized states at energies away from the saddle point energy. The unstable fixed point corresponds to the quantum critical point. The localization length exponent is found by linearizing around the unstable fixed point

$$\nu = \frac{\ln 2}{\ln \lambda} \tag{183}$$

with $\lambda = [\partial f/\partial T]_{T^*} = 6 - 2\sqrt{5}$. One gets $\nu \approx 1.635$.

In the general case, where one saddle point vertex is replaced by $b$ original vertices, the result is

$$T' = 1 - (1 - T^b)^b := f(T; b) \ . \tag{184}$$

Assuming $b = 1 + \epsilon$ one obtains the infinitesimal Migdal–Kadanoff transformation which has a fixed point at $T^* = 1/2$ and an eigenvalue $\lambda = 1 + 2(1 - \ln 2)\epsilon$. This gives an exponent

$$\nu = \frac{\ln b}{\ln \lambda} = \frac{1}{2(1 - \ln 2)} \approx 1.629 \tag{185}$$

and the beta function

$$\beta(T) := \left.\frac{\mathrm{d}}{\mathrm{d}\epsilon}\right|_{\epsilon=0} f(T; 1 + \epsilon) = T \ln T - (1 - T) \ln(1 - T) \ . \tag{186}$$

Although the result for the critical behavior is far from being satisfactory, it is nevertheless remarkable that the very existence of a non-trivial quantum critical point is correctly predicted by the model even in the crudest approximation for the renormalization group transformation. It is therefore worthwhile to investigate whether one can obtain more reliable quantitative results by refining the approximations.

### *6.2. State-of-the-art results for the hierarchical lattice*

A different procedure is outlined pictorially in Fig. 24. This is the model of a hierarchical lattice. In the first generation, the system consists again of the original, statistically independent saddle points. In a first step, a certain number of these original saddle points (five in the example of Fig. 24) are combined to form a new scattering center. The corresponding scattering matrix is calculated approximately as a function of the original ones. This is repeated: the new scattering centers are combined again into new units (Fig. 24c). Their scattering properties are calculated as functions of the previous ones, and so on and so forth.

The crucial approximation of the procedure is that in each step only two incoming and outgoing channels are taken into account (Fig. 24b) such that the new unit can be considered as a new, second-generation saddle point. The exact scattering matrix of the units in each generation would of course contain much more channels, and when repeating the construction, the number of channels would explode. Neglecting all of these channels apart from four is in fact the most severe approximation of the method—as also made in the previous procedure—since it cannot be very well controlled.

However, instead of viewing the hierarchical lattice as an approximation to the random network model one may also consider it as a model in its own right for which the critical behavior may be determined exactly. This would yield only an approximation to the critical behavior of the network model, but if the critical behavior was universal—independent of the microscopic details—the exponent of this model should be the same as for any other model in the same universality class. We will come back to this point below in more detail.

For the derivation of the renormalization group equations of the hierarchical lattice, we closely follow [33]. We consider the five saddle points in Fig. 25. The amplitudes must satisfy the five relations

$$\begin{pmatrix} \psi_{\mathrm{o},i} \\ \psi'_{\mathrm{o},i} \end{pmatrix} = \begin{pmatrix} -r_i & t_i \\ t_i & r_i \end{pmatrix} \begin{pmatrix} \psi_{\mathrm{i},i} \\ \psi'_{\mathrm{i},i} \end{pmatrix} \quad (i = 1, 2, \ldots, 5) \ , \tag{187}$$

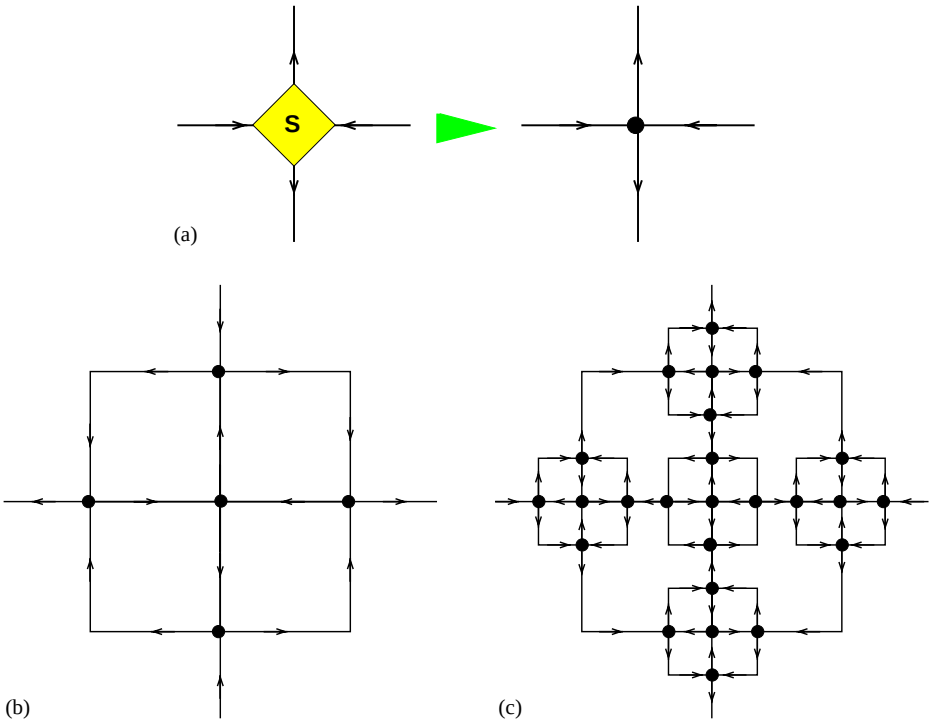


Fig. 24. Illustration of the renormalization procedure on a hierarchical lattice constructed iteratively. (a) Saddle point represented by a dot with two incoming and outgoing channels. (b) Second-generation saddle point consisting of five original (first-generation) saddle points. A total of eight incoming and outgoing channels are here neglected. (c) Second level of iteration where five second-generation saddle points are combined to form a third-generation saddle point consisting of 25 first-generation saddle points. In contrast to the original network (Fig 8), the hierarchical network contains considerably fewer saddle points and links (after Ref. [186]).

where i and o denote the input and output channels, respectively, and $r_i$ and $t_i$, $(=\sqrt{1-r_i^2})$ $(i=1,\ldots,5)$ are real quantities. The first goal is to replace the five saddle points by one.

Some of the amplitudes differ only by a phase factor. For example,

$$\psi_{2,\mathrm{i}} = \mathrm{e}^{\mathrm{i}\theta_{2,1}}\psi_{1,\mathrm{o}}\ , \tag{188}$$

where $\theta_{2,1}$ is the random phase factor gained when traveling from the saddle point 1 to 2. The phase factors are related to the Aharonov–Bohm fluxes $\phi_i$, $(i=1,2,3,4)$ obtained when traveling around a closed loop via

$$\begin{aligned}
&\theta_{5,1}+\theta_{3,5}+\theta_{1,3}=\phi_1\ ,\\
&\theta_{3,2}+\theta_{4,3}+\theta_{2,4}=\phi_2\ ,\\
&\theta_{2,1}+\theta_{3,2}+\theta_{1,3}=\phi_3\ ,\\
&\theta_{3,4}+\theta_{5,3}+\theta_{4,5}=\phi_4\ .
\end{aligned} \tag{189}$$

Since the phases $\theta$ are assumed to be randomly and uniformly distributed between $[0,2\pi)$, so are the fluxes $\phi_i$.

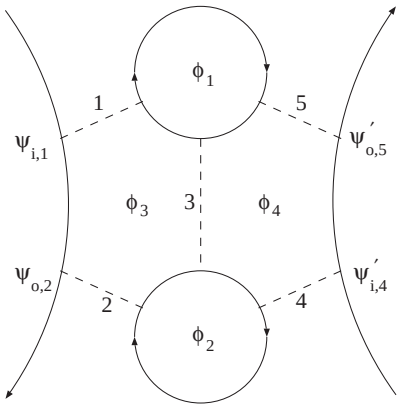


Fig. 25. Illustration of a transformation that can be used in a renormalization group transformation. Five original (first-generation) saddle points indicated here by dashed lines (right) are renormalized into one single second-generation saddle point. This relates $(\psi_{o,2}, \psi'_{o,5})$ to $(\psi_{i,1}, \psi'_{i,4})$. The quantities $\phi_1 \ldots \phi_4$ are random independent Aharonov–Bohm-fluxes that penetrate closed loops as indicated.

From relations (187), one can derive that the total outgoing amplitudes $(\psi_{o,2}, \psi'_{o,5})$ are related to the incoming amplitudes $(\psi_{i,1}, \psi'_{i,4})$ according to formally the same relation as Eq. (187)

$$\begin{pmatrix} \psi_{o,2} \\ \psi'_{o,5} \end{pmatrix} = \begin{pmatrix} -\tilde{r} & \tilde{t} \\ \tilde{t} & \tilde{r} \end{pmatrix} \begin{pmatrix} \psi_{i,1} \\ \psi'_{i,4} \end{pmatrix} . \tag{190}$$

The new reflection and transmission coefficients, $\tilde{r}, \tilde{t}$, characterize the scattering properties of the renormalized "super" saddle point. The new transmission and reflection amplitudes can be obtained straightforwardly by solving Eq. (187). One obtains after some tedious algebra

$$\tilde{t} = \left| \frac{t_1 t_5 + t_2 t_4 e^{i(\phi_3+\phi_4)} - t_2 t_3 t_5 e^{i\phi_3} - t_1 t_3 t_4 e^{i\phi_4}}{D} + \frac{t_1 r_2 r_3 r_4 t_5 e^{i\phi_2} - r_1 t_2 r_3 t_4 r_5 e^{i(\phi_3+\phi_4-\phi_1)}}{D} \right| . \tag{191}$$

The corresponding reflection amplitude is obtained from $\tilde{r} = \sqrt{1-\tilde{t}^2}$

$$\tilde{r} = \left| \frac{r_4 r_5 - r_1 r_2 e^{i(\phi_1+\phi_2)} - r_1 r_3 r_4 e^{i\phi_1} + r_2 r_3 r_5 e^{i\phi_2}}{D} - \frac{t_1 t_2 t_3 r_4 r_5 e^{i\phi_3} + r_1 r_2 t_3 t_4 t_5 e^{i(\phi_1+\phi_2-\phi_4)}}{D} \right| , \tag{192}$$

where $D$ is the abbreviation for

$$D = 1 - r_1 r_3 r_5 \mathrm{e}^{\mathrm{i}\phi_1} - t_1 t_2 t_3 \mathrm{e}^{\mathrm{i}\phi_3} - t_3 t_4 t_5 \mathrm{e}^{\mathrm{i}\phi_4} + r_2 r_3 r_4 \mathrm{e}^{\mathrm{i}\phi_2} + t_1 t_2 t_4 t_5 \mathrm{e}^{\mathrm{i}(\phi_3+\phi_4)} - r_1 r_2 r_4 r_5 \mathrm{e}^{\mathrm{i}(\phi_1+\phi_2)} \ . \tag{193}$$

Transformation (191) allows one to generate the new probability distribution of the transmission coefficient $P(\tilde{t})$ from the distribution $P(t)$. A certain distribution is unchanged by this transformation, which corresponds to the fixed point distribution. Slight deviations from the fixed point distribution increase after the renormalization transformation. This can be used to define the critical exponent $\nu$.

The renormalization group transformation of the distribution of the transmission amplitudes has been determined numerically by using this approach [34,188]. From $P(t)$ the distribution of the conductance $G = t^2$ can be determined,

$$P(G) = \frac{1}{2t} P(t) \ . \tag{194}$$

This may be transformed to the distribution $Q(z)$ of the heights of the saddle points $z$ measured relative to the critical energy $\epsilon = 0$ (cf. Eqs. (75), (84)). This can be obtained from Eq. (194) by using the relation

$$G = \frac{1}{\mathrm{e}^z + 1} \ . \tag{195}$$

The result is

$$Q(z) = P(G) \left| \frac{\mathrm{d}G}{\mathrm{d}z} \right| = \frac{1}{4\cosh^2(z/2)} P\left( \frac{1}{\mathrm{e}^z + 1} \right) \ . \tag{196}$$

The distributions $P(G)$ and $Q(z)$ are shown in Fig. 26.

The scaling properties of the distribution $Q(z)$ may be used to determine the critical exponent with very high accuracy. The idea is that an initial shift of the distribution by an amount $z_0$ will be amplified during the renormalization procedure since the quantum Hall fixed point is unstable. After $n$ steps, the maximum of the distribution will be shifted by an amount $z_{\max,n} = \lambda^n z_0$. After a certain number of steps, $n_L$, the saddle point will be no longer transparent. This limit can be defined by

$$z_{\max,n_L} = \lambda^{n_L} z_0 \approx 1 \ . \tag{197}$$

By defining the localization length $\xi$ with the length $2^{n_L} a$ ($a$ lattice constant of the original lattice) one finds that $\xi$ diverges for $z_0 \to 0$,

$$\xi \propto a z_0^{-\nu} \tag{198}$$

with the exponent $\nu = \ln 2 / \ln \lambda$ (cf. Eq. (183)). The critical exponent can then be determined from

$$\nu = \frac{\ln 2^n}{\ln(z_{\max,n})/z_0} \ , \tag{199}$$

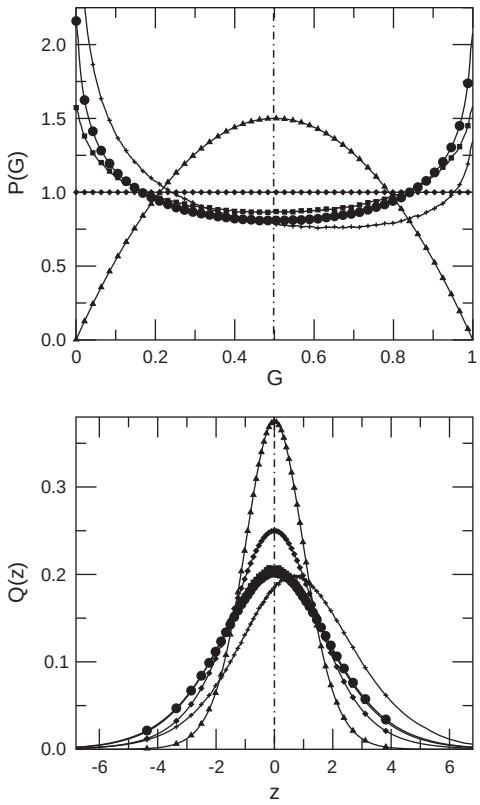


Fig. 26. Top: the fixed point distribution (∘) of the conductance, $P(G)$, at the quantum Hall transition obtained by starting from different initial distributions denoted by squares, diamonds, triangles, and the distribution after the 16th renormalization step (+). Bottom: the corresponding distributions of the heights of the saddle points, $Q(z)$ (From [188]).

with $z_{\max,n}/z_0 = \lambda^n$. Fig. 27 shows results of the numerical calculation [34,188]. The numerical analysis of the data yields the result $\nu = 2.39 \pm 0.01$, in excellent agreement with previous direct numerical simulations for the localization length [34,188]. As mentioned above, by assuming the model as an independent realization of the fixed point ensemble, one can interpret this result as an independent corroboration of the universality hypothesis for the quantum Hall phase transition.

Though the value of the critical exponent is extremely precise, the form of the critical distribution of the two terminal conductance is qualitatively different from the one of the Chalker–Coddington random network. Instead of $P(G) \to 0$ in the limit $G \to 0$ (Fig. 15), the renormalization group approach indicates divergence $P(G) \to \infty$. Also near $G = 1$, the present approach suggests $P(G) \to \infty$, while the actual $P(G)$ is constant. For $G > 1$, $P(G) = 0$ in the case of renormalization group, but in the simulation for the original model $P(G)$ shows a tail in this region. This indicates that the renormalization group approach in fact does *not* approximate the Chalker–Coddington network model although the underlying truncated-network model belongs to the same universality class.

This renormalization group has recently been extended to the calculation of the energy level statistics [35]. The finite-size scaling analysis of the energy level spacing, Eq. (139), has been applied to estimate $\nu$ to be $2.37 \pm 0.02$.

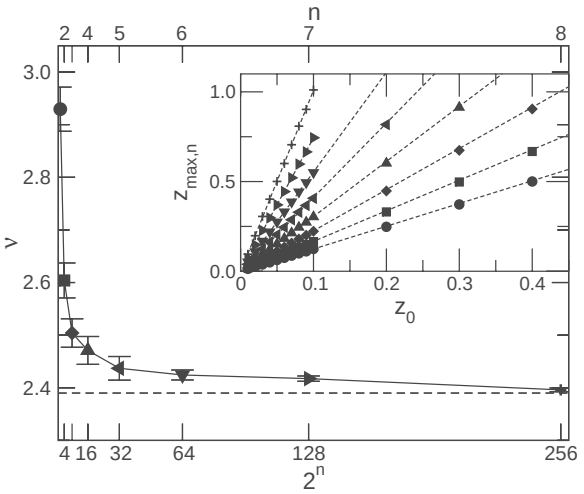


Fig. 27. The critical exponent $\nu$ determined from the scaling behavior of the distribution of the heights of the saddle points $Q(z)$ with the effective system size $2^n$ in the $n$th renormalization step. Dashed line: $\nu = 2.39$. Inset: maximum $z_{\max,n}$ as a function of $z_0$. The slopes yield $\lambda^n$ and thereby the critical exponents $\nu(n)$ (From [34]).

## 7. Hamiltonians related to the network model

The model defined above is not only suitable for quantitative studies of the critical behavior. By constructing effective Hamiltonians starting from the transfer matrix, one can recognize that it is of much more general importance. In the present section we will achieve such a construction. We first introduce an equivalent tight-binding Hamiltonian. In effective mass approximation, this will be shown to be equivalent to a Dirac Hamiltonian. For the latter, some analytical results are summarized which put the quantum Hall phenomenon in a new perspective.

In this and in the subsequent sections, we will use units such that $\hbar = 1$, $m^* = 1$, and $e = 1$, in order to simplify notation. However, in results for the conductivity tensors, the correct unit $e^2/h$ is reintroduced since it is of physical importance.

The above network system has been completely specified in terms of its transmission or scattering properties at *a given energy* of the original model of an electron moving in a strong magnetic field and a slowly varying random potential. By using this as a starting point for defining a Hamiltonian, we fix *an entire spectrum of* (*quasi-*)*energies* which contains as a parameter the original energy value. It is not obvious whether or not there is some arbitrariness in such a procedure [189].

### *7.1. A tight-binding Hamiltonian*

We first want to establish a connection with a nearest neighbor tight-binding Hamiltonian. We start from the unitary matrices **S** that describe the scattering at the individual saddle points, Eq. (87). We first rewrite **S** by redefining phases, $\phi_1 \to \phi_1 + \pi$ and $\phi_4 \to \phi_4 + \pi$, again in order to avoid unnecessary notation. This does not change the physics, as it will be seen below that one of the relevant system parameters is the total phase accumulated around a unit cell of the lattice, $\phi = \sum_j \phi_j$, which is the number of flux quanta

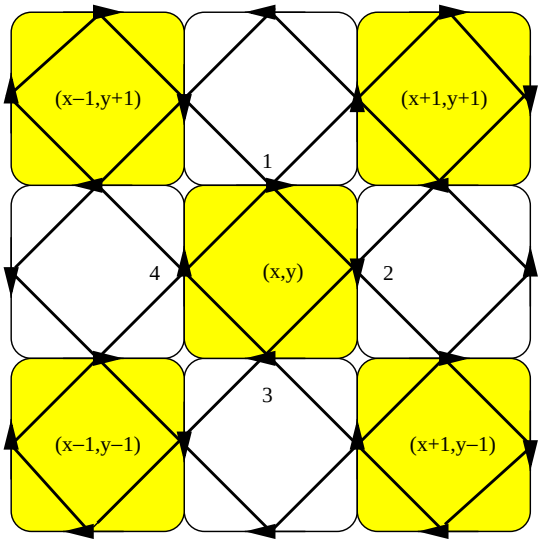


Fig. 28. The network model rearranged as a tight-binding model on a two-dimensional square lattice with four states per site. The links between saddle points are associated with the four directed site states (arrowheads) in the unit cell. These site states are connected by tunneling through the saddle points represented by ◇.

in the unit cell multiplied by $2\pi$.

$$\begin{aligned}\mathbf{S} &= \begin{pmatrix} \mathrm{e}^{-\mathrm{i}\phi_2} & 0 \\ 0 & -\mathrm{e}^{\mathrm{i}\phi_4} \end{pmatrix} \begin{pmatrix} -r & t \\ t & r \end{pmatrix} \begin{pmatrix} -\mathrm{e}^{\mathrm{i}\phi_1} & 0 \\ 0 & \mathrm{e}^{-\mathrm{i}\phi_3} \end{pmatrix} \\ &= \begin{pmatrix} \mathrm{e}^{-\mathrm{i}\phi_2} & 0 \\ 0 & -\mathrm{e}^{\mathrm{i}\phi_4} \end{pmatrix} \mathbf{S}_0 \begin{pmatrix} -\mathrm{e}^{\mathrm{i}\phi_1} & 0 \\ 0 & \mathrm{e}^{-\mathrm{i}\phi_3} \end{pmatrix}. \end{aligned} \tag{200}$$

Then, we rearrange the network in the way shown in Fig. 28. The loops that are connected by the saddle points, described by their scattering matrix $\mathbf{S}_0$, are arranged in the form of a two-dimensional square lattice such that the centers of the loops are associated with the lattice points

$$\boldsymbol{R}_{xy} = x\boldsymbol{e}_x + y\boldsymbol{e}_y \tag{201}$$

with $x$, $y$ integer numbers. This notation might appear unconventional, but is convenient for emphasizing the connection with the real space. The $x$- and $y$-directions are assumed to point into the directions of the links that connect $\mathbf{S}$ and $\mathbf{S}'$. The four links between adjacent saddle points within each of the loops (denoted by arrowheads labeled with 1,2,3,4 in Fig. 28 [189]) are now associated with four site states within a unit cell of the lattice. The site states are characterized by a lattice vector and a quantum number $\lambda$ in the lattice cell, and they are assumed to form a complete set,

$$\sum_{x,y,\lambda=1}^{4} |x, y, \lambda\rangle\langle x, y, \lambda| = \mathbf{1}\ . \tag{202}$$

These site states are connected via the tunneling and reflection matrix elements through the saddle points within a given unit cell, and between nearest neighbor cells.

In order to determine the matrix elements of the effective Hamiltonian, we adopt the method used in [121,189]. We write for the vector of the amplitudes in the lattice cell at $\boldsymbol{R} = x\boldsymbol{e}_x + y\boldsymbol{e}_y$ after $M+1$ iteration steps

$$\psi_{\boldsymbol{R}\lambda}(M+1) = \sum_{\boldsymbol{R}'\lambda'=1}^{4} U_{\boldsymbol{R}\lambda,\boldsymbol{R}'\lambda'}\psi_{\boldsymbol{R}'\lambda'}(M) \ . \tag{203}$$

The unitary operator $\mathbf{U}$ can be interpreted as describing the evolution of the wave function between steps $M$ and $M+1$. The eigenstates of the $4L$-dimensional matrix $\mathbf{U}$ ($L$ number of sites)

$$\mathbf{U}\,|\,\psi_\alpha\rangle = \mathrm{e}^{\mathrm{i}\omega_\alpha(E)}|\psi_\alpha\rangle \quad (\alpha = 1 \ldots\ldots 4L) \tag{204}$$

with eigenvalues 1 ($\omega_\alpha(E) = 0$) are the stationary states of the network with an energy parameterized by the energy-dependent reflection parameter of the saddle points, $r := r(E) = \sqrt{1 - t^2(E)}$.

Formally, one can interpret the above Eq. (203) as a "time-dependent" Schrödinger equation by writing

$$\psi_{\boldsymbol{R}\lambda}(M+1) - \psi_{\boldsymbol{R}\lambda}(M) = \sum_{\boldsymbol{R}',\lambda'=1}^{4} (\mathbf{U}-\mathbf{1})_{\boldsymbol{R}\lambda,\boldsymbol{R}'\lambda'}\,\psi_{\boldsymbol{R}'\lambda'}(M) \ . \tag{205}$$

This suggests

$$\mathbf{U} = \mathbf{1} - \frac{1}{\mathrm{i}}\mathbf{H} \ . \tag{206}$$

As the Hamiltonian $\mathbf{H}$ must be self adjoint we define

$$\mathbf{H} = \frac{1}{2\mathrm{i}}\left(\mathbf{U} - \mathbf{U}^\dagger\right) \ . \tag{207}$$

Note that the Hamiltonian is here dimensionless, since it contains a factor $\Delta t/\hbar$, with $\Delta t = 1$ the width of the time step in Eq. (205).

The Hamiltonian has quasi-energy eigenvalues

$$\varepsilon_\alpha = \sin\,\omega_\alpha \ . \tag{208}$$

Since each lattice cell is connected via four saddle points to its nearest neighbors, $\mathbf{U}$ must have a $4\times 4$ block structure. The midpoints of the links form a bipartite lattice. This means that each of the $4\times 4$ blocks can consist only of two non-zero $2\times 2$ blocks. By arranging the amplitudes according to the sequence $(\psi_{\boldsymbol{R}1}, \psi_{\boldsymbol{R}3}, \psi_{\boldsymbol{R}2}, \psi_{\boldsymbol{R}4})^{\mathrm{T}}$ one gets for the $4\times 4$ block connecting with each other the site states within a given lattice cell at $\boldsymbol{R}$, and with the states in the nearest-neighbor cells,

$$\mathbf{U} = \begin{pmatrix} 0 & \mathbf{M} \\ \mathbf{N} & 0 \end{pmatrix} \ , \tag{209}$$

such that the $2\times 2$ block $\mathbf{M}$ connects the states $\psi_{\boldsymbol{R}1}, \psi_{\boldsymbol{R}3}$ with $\psi_{\boldsymbol{R}2}, \psi_{\boldsymbol{R}4}$ and the block $\mathbf{N}$ links the states $\psi_{\boldsymbol{R}2}, \psi_{\boldsymbol{R}4}$ with $\psi_{\boldsymbol{R}1}, \psi_{\boldsymbol{R}3}$.

This gives for the $4 \times 4$ block of the effective Hamiltonian

$$\mathbf{H} = -\frac{1}{2\mathrm{i}} \begin{pmatrix} 0 & \mathbf{N}^\dagger - \mathbf{M} \\ \mathbf{M}^\dagger - \mathbf{N} & 0 \end{pmatrix} = \begin{pmatrix} 0 & \mathbf{H}_2 \\ \mathbf{H}_2^\dagger & 0 \end{pmatrix} . \tag{210}$$

The matrices

$$\mathbf{M} = \begin{pmatrix} t\mathrm{e}^{\mathrm{i}\phi_1}\tau_-^x\tau_+^y & r\mathrm{e}^{\mathrm{i}\phi_1} \\ r\mathrm{e}^{\mathrm{i}\phi_3} & -t\mathrm{e}^{\mathrm{i}\phi_3}\tau_+^x\tau_-^y \end{pmatrix} , \tag{211}$$

$$\mathbf{N} = \begin{pmatrix} r\mathrm{e}^{\mathrm{i}\phi_2} & t\mathrm{e}^{\mathrm{i}\phi_2}\tau_+^x\tau_+^y \\ t\mathrm{e}^{\mathrm{i}\phi_4}\tau_-^x\tau_-^y & -r\mathrm{e}^{\mathrm{i}\phi_4} \end{pmatrix} \tag{212}$$

contain the translation operators $\tau_\pm$ that connect nearest-neighbor cells,

$$\tau_\pm^x \psi_{\boldsymbol{R}\lambda} = \psi_{\boldsymbol{R}\pm\mathbf{e}_x\lambda} \quad \tau_\pm^y \psi_{\boldsymbol{R}\lambda} = \psi_{\boldsymbol{R}\pm\mathbf{e}_y\lambda} . \tag{213}$$

The Hamiltonian is then given by

$$\mathbf{H}_2 = -\frac{1}{2\mathrm{i}} \begin{pmatrix} r\mathrm{e}^{-\mathrm{i}\phi_2} - t\mathrm{e}^{\mathrm{i}\phi_1}\tau_-^x\tau_+^y & t\mathrm{e}^{-\mathrm{i}\phi_4}\tau_+^x\tau_+^y - r\mathrm{e}^{\mathrm{i}\phi_1} \\ t\mathrm{e}^{-\mathrm{i}\phi_2}\tau_-^x\tau_-^y - r\mathrm{e}^{\mathrm{i}\phi_3} & -r\mathrm{e}^{-\mathrm{i}\phi_4} + t\mathrm{e}^{\mathrm{i}\phi_3}\tau_+^x\tau_-^y \end{pmatrix} . \tag{214}$$

This means that within a given cell, say at $\boldsymbol{R}$, the tunneling matrix elements are proportional to the reflection amplitudes of the saddle points $r$

$$h_{\boldsymbol{R}1,\boldsymbol{R}4} = \frac{r}{2\mathrm{i}}\mathrm{e}^{\mathrm{i}\phi_1} , \tag{215}$$

$$h_{\boldsymbol{R}2,\boldsymbol{R}1} = \frac{r}{2\mathrm{i}}\mathrm{e}^{\mathrm{i}\phi_2} , \tag{216}$$

$$h_{\boldsymbol{R}3,\boldsymbol{R}2} = \frac{r}{2\mathrm{i}}\mathrm{e}^{\mathrm{i}\phi_3} , \tag{217}$$

$$h_{\boldsymbol{R}4,\boldsymbol{R}3} = -\frac{r}{2\mathrm{i}}\mathrm{e}^{\mathrm{i}\phi_4} . \tag{218}$$

On the other hand, the eight coupling matrix elements to the nearest neighbor cells are proportional to the transmission amplitude $t$. They are

$$h_{\boldsymbol{R}2,[\boldsymbol{R}+(1,1)]3} = \frac{t}{2\mathrm{i}}\mathrm{e}^{\mathrm{i}\phi_2} , \tag{219}$$

$$h_{\boldsymbol{R}3,[\boldsymbol{R}+(1,-1)]4} = -\frac{t}{2\mathrm{i}}\mathrm{e}^{\mathrm{i}\phi_3} , \tag{220}$$

$$h_{\boldsymbol{R}4,[\boldsymbol{R}+(-1,-1)]1} = \frac{t}{2\mathrm{i}}\mathrm{e}^{\mathrm{i}\phi_4} , \tag{221}$$

$$h_{\boldsymbol{R}1,[\boldsymbol{R}+(-1,1)]2} = \frac{t}{2\mathrm{i}}\mathrm{e}^{\mathrm{i}\phi_1} \tag{222}$$

and the four remaining matrix elements are the conjugates of these.

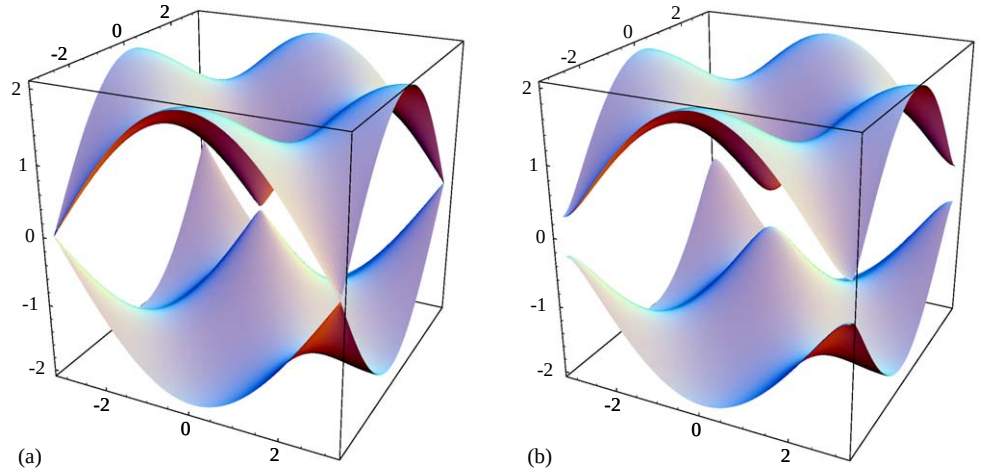


Fig. 29. The band structure of quasi-energies $\epsilon_j(\boldsymbol{q}-\boldsymbol{A})$ of the Hamiltonian representing a network with identical saddle points and equal phases in all of the cells of the tight-binding lattice such that there is half of a flux quantum in each unit cell ($\phi=\pi$). In this case, the four bands (Eq. (224)) are degenerated with respect to $\pm$. (a) The spectrum exactly at the saddle point energy, $r=t=1/\sqrt{2}$, (b) for $r=0.5$.

It is useful to consider as a starting point for the discussion of the properties of this Hamiltonian the periodic limit. This will also yield the Dirac Hamiltonian in the limit of small wave number, i.e. in effective mass approximation.

The periodic case is achieved by assuming the phases in each of the unit cells and all of the saddle points as identical. The Hamiltonian can be diagonalized exactly with the Bloch Ansatz

$$\psi_\lambda(\boldsymbol{R}) = \mathrm{e}^{\mathrm{i}\boldsymbol{q}\cdot\boldsymbol{R}} u_\lambda(\boldsymbol{q}) \ . \tag{223}$$

The resulting band structure is (Fig. 29)

$$\epsilon_j(\boldsymbol{q}) = (-1)^j\sqrt{2}\Big[1-2rt\cos\phi\cos(q_x-A_x)\cos(q_y-A_y) \pm \sin\phi\sqrt{1-4r^2t^2\cos^2(q_x-A_x)\cos^2(q_y-A_y)}\Big]^{1/2} \tag{224}$$

with $j=1,2$, $A_x=(\phi_1-\phi_3)/2$, $A_y=(\phi_4-\phi_2)/2$ and $\phi=\sum_{\lambda=1}^{4}\phi_\lambda$ the flux through the cell multiplied by $e/\hbar$. Exactly at the energy of the saddle points, $r=t=1/\sqrt{2}$, there is no gap between the bands. For $r\neq t$ a gap $\Delta=\epsilon_1-\epsilon_2$ is opened. For $\phi=0$ it is

$$\Delta = 2\sqrt{2}\sqrt{(1-2rt)} \approx m \tag{225}$$

for $r=1/\sqrt{2}+m/4$ ($m\ll 1$).

The formation of the gap can be discussed in better detail by expanding the band structure near $\boldsymbol{q}-\boldsymbol{A} \approx 0$. On finds for small $m$

$$\epsilon^2(\boldsymbol{q}) = m^2 + (\boldsymbol{q}-\boldsymbol{A})^2 \ . \tag{226}$$

Thus, the existence of the gap is closely related to the deviation from the saddle point.

In the following, we discuss briefly the disordered version of the network.

If the reflection amplitude is unity ($r = 1$, $t = 0$), i.e. if the energy $E$ is well below the saddle point energy, the unit cells decouple. The system consists then of independent wave functions localized within the grey unit cells in Fig. 28. On the other hand, if $t = 1$ ($r = 0$), i.e. for an energy well above the saddle point, the independent cell states are localized in the complementary lattice of the white unit cells. The quasi-energy eigenvalues in these decoupled limits are

$$\epsilon_j^{\pm}(\boldsymbol{R}, \phi) = (-1)^j \sqrt{2}\left[1 \mp \frac{1}{\sqrt{2}}(1-\cos\phi)^{1/2}\right]^{1/2} \quad (j = 1, 2) \tag{227}$$

and $\phi = \phi(\boldsymbol{R})$ is the flux through the loop at $\boldsymbol{R}$. For completely independent and random phases, the fluxes in the individual cells, and thus the quasi-energies $\epsilon_\alpha$ are statistically independent and random. When varying the energy $E$, i.e. varying $r(E)$ close to the value of 1, the quasi-energies $\epsilon(E)$ will perform random walks in the $(E, \epsilon)$-space. The energies of the original problem, $E_\beta(\epsilon_\alpha = 0)$, will then be statistically independent and random. They correspond to the localized states associated with the valleys and hills in the potential landscape.

If we assume that all saddle points have the same parameter $r$ and the phases are independently and randomly distributed one can see that the localization lengths of the eigenstates of $H$ are finite and independent of $\epsilon_\alpha$. As $r \to r_c = t_c = 1/\sqrt{2}$, the localization length diverges uniformly throughout the spectrum [189]. This reflects the singularity of the localization length as a function of the energy $E$ of the original problem.

We note that with disorder, i.e. assuming the phases to be independently and randomly distributed, the matrix elements of the Hamiltonian remain nevertheless strongly correlated. These correlations introduce peculiar features into the localization behavior of the corresponding eigenstates. In particular, they are responsible for the localization–delocalization transitions occurring in the sub-bands induced by the magnetic field. A very similar observation has been made earlier for the random matrix model where the matrix elements of the banded matrix are also strongly correlated [190].

### *7.2. The Dirac Hamiltonian*

One can also relate the network model with the two-dimensional Dirac equation. This can be done most straightforwardly by considering the effective mass approximation of the tight-binding Hamiltonian. Alternatively, one can consider the two-step unitary operator [190]

$$\mathbf{U}^2 = \begin{pmatrix} \mathbf{MN} & 0 \\ 0 & \mathbf{NM} \end{pmatrix} = \begin{pmatrix} \mathbf{V} & 0 \\ 0 & \mathbf{W} \end{pmatrix}. \tag{228}$$

The system of four equations decouples into pairs, and one can deal with, say, only the upper block $\mathbf{V}$.

Furthermore, by assuming that the displacement operators act on smooth functions one can replace

$$\tau_\pm^x = 1 \pm \partial_x, \quad \tau_\pm^y = 1 \pm \partial_y \ . \tag{229}$$

Table 2
Symmetry breaking by disorder in the various parameters of the Dirac model

| Symmetry | $\sigma \cdot \boldsymbol{p}$ | $m\sigma_z$ | $\phi$ | $\sigma \cdot \boldsymbol{A}$ |
|---|---|---|---|---|
| Parity | Yes | No | No | No |
| Time reversal | Yes | No | Yes | No |
| Particle–hole | Yes | No | No | Yes |

($\mathbf{p}$—momentum operator; $m$—Dirac mass parameter; $\boldsymbol{\sigma}$—vector of the Pauli matrices $\sigma_x$, $\sigma_y$; $\phi$ scalar potential; $\boldsymbol{A}$—vector potential).

For small phases and with the definition $r = r_c + m/4$ ($t \approx t_c - m/4$) one can expand

$$\mathbf{V} = \mathrm{e}^{-\mathrm{i}\tilde{H}} \approx \mathbf{1} - \mathrm{i}\tilde{\mathbf{H}} \tag{230}$$

with the unit matrix $\mathbf{1}$. This is justified for small $\tilde{\mathbf{H}}$. From the matrix elements of $\mathbf{M}$ and $\mathbf{N}$, Eqs. (211) and (212), one finds

$$\mathbf{V} \approx \mathbf{1} + \begin{pmatrix} -\partial_x + \mathrm{i}A_x & \partial_y - \mathrm{i}A_y + m \\ \partial_y - \mathrm{i}A_y - m & \partial_x - \mathrm{i}A_x \end{pmatrix} - \mathrm{i}\phi\mathbf{1} = \mathbf{1} - \mathrm{i}\tilde{\mathbf{H}} \ . \tag{231}$$

With the unitary transformation

$$\mathbf{R} = \frac{1}{\sqrt{2}} \begin{pmatrix} \mathrm{i} & -1 \\ \mathrm{i} & 1 \end{pmatrix} \tag{232}$$

one can transform

$$\mathbf{H} = \mathbf{R}\tilde{\mathbf{H}}\mathbf{R}^{-1} \tag{233}$$

such that one obtains finally the two-dimensional Dirac Hamiltonian

$$\mathbf{H} = (p_x - A_x)\sigma_x + (p_y - A_y)\sigma_y + m\sigma_z + \phi\mathbf{1} \ . \tag{234}$$

Here, $p_j = -\mathrm{i}\partial_j$ ($j = x, y$) are the components of the momentum operator and

$$\sigma_x = \begin{pmatrix} 0 & 1 \\ 1 & 0 \end{pmatrix}, \quad \sigma_y = \begin{pmatrix} 0 & -\mathrm{i} \\ \mathrm{i} & 0 \end{pmatrix}, \quad \sigma_z = \begin{pmatrix} 1 & 0 \\ 0 & -1 \end{pmatrix} \tag{235}$$

are the Pauli matrices. In this Hamiltonian, randomness can be introduced in different ways. Via randomness in the individual phases one can make the components of the vector potential random. Randomizing the total Aharonov–Bohm phases in the loops produces randomness in the scalar potential $\phi$. Finally, assuming the tunneling parameters of the saddle points to be random gives fluctuations in the mass parameter $m$.

Introducing disorder in the various parameters of the model leads to breaking of symmetries, as noted in [120] and indicated in Table 2. The first term in the Hamiltonian, $\mathbf{H}_0 = \boldsymbol{\sigma} \cdot \boldsymbol{p}$ [$\boldsymbol{\sigma} = (\sigma_x, \sigma_y)$, $\boldsymbol{p} = -\mathrm{i}\nabla = -\mathrm{i}(\partial_x, \partial_y)$], is invariant under an effective *time reversal* operation

$$\mathbf{H}_0 = \sigma_z \mathbf{H}_0^* \sigma_z \ . \tag{236}$$

This means that there is a Kramers degeneracy, $\psi$ and $\sigma_z\psi^*$ are degenerate eigenstates as is easily seen. Similarly, it is easy to see that $\psi$ and $\sigma_z\psi$ are eigenstates to energies $E$ and $-E$, respectively. This is equivalent to *particle–hole* symmetry

$$-\mathbf{H}_0 = \sigma_z \mathbf{H}_0 \sigma_z \ . \tag{237}$$

Finally, $\mathbf{H}_0$ is *parity* invariant under $x$- and $y$-reflections $P_j\, j\, P_j = -j,\ (j = x, y)$, for instance

$$\mathbf{H}_0 = P_y \sigma_x \mathbf{H}_0 \sigma_x P_y \ . \tag{238}$$

The Dirac mass term $\mathbf{H}_m = m\sigma_z$ possesses none of these symmetries, as is easily seen. The vector potential term $\mathbf{H}_{\boldsymbol{A}} = -\boldsymbol{A}\cdot\boldsymbol{\sigma}$ preserves only particle–hole symmetry, and the random scalar potential $\mathbf{H}_\phi = \phi\mathbf{1}$ only time reversal symmetry. These symmetries are very important for understanding the quantum phases of the system as will be seen below in more detail.

### *7.3. Some results for the two-dimensional Dirac model*

In this section we discuss briefly some instructive analytical results obtained for the Dirac Hamiltonian.

The correspondences between the quantum Hall problem, certain tight-binding models and the two-dimensional Dirac model have been noticed by several authors [120,191–193]. Fisher and Fradkin [191] have obtained the Dirac model by starting from a two-dimensional tight-binding model with diagonal on-site disorder in a perpendicular magnetic field with half a magnetic flux quantum in the unit cell. They constructed a field theory for the diffusive modes which was shown to be in the same universality class as the orthogonal $O(2n, 2n)/O(2n) \times O(2n)(n \to 0)$ non-linear $\sigma$-model. This implies that all states are localized as in the absence of a magnetic field. It suggests that if delocalization occurs with magnetic field, it must be a direct consequence of breaking time-reversal symmetry instead of some other properties of the field. Generalizations to the several-channel scattering problem have also been discussed [194].

Ludwig and collaborators [120] have used a tight-binding model on a square lattice with nearest and next-nearest neighbor coupling, half a flux quantum per unit cell and a staggered potential energy $\mu(-1)^{x+y}$ as a starting point. At low energies, the model was shown to be equivalent to a Dirac model with two Dirac fields. They found that without disorder this model exhibits an integer quantum Hall phase transition as a function of some control parameter which is essentially the mass $m$ of the lighter Dirac field. This is similar to the transitions of the Hall conductance between integer multiples of $e^2/h$ obtained in the original clean Landau model as a function of the *Fermi energy*, and does not mean that a plateau exists when the electron density is varied. The transition of the Dirac model has been shown to belong to the two-dimensional Ising universality class. The associated exponents and the critical transport properties were determined.

The density of states,

$$\rho(E) = \frac{|E|}{2\pi}\Theta(|E| - m) \ , \tag{239}$$

vanishes at $E = 0$. It can readily be obtained from Eq. (226) with $\boldsymbol{A} = 0$ using

$$\rho(E) = \frac{1}{(2\pi)^2}\int \mathrm{d}^2\boldsymbol{q}\left[\delta\left(E - \sqrt{q^2 + m^2}\right) + \delta\left(E + \sqrt{q^2 + m^2}\right)\right] \ . \tag{240}$$

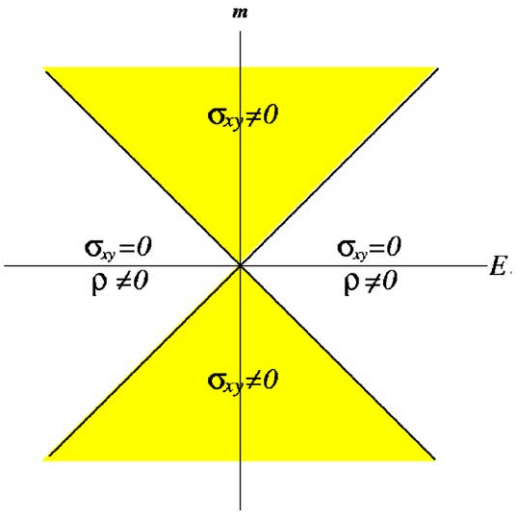


Fig. 30. The phase diagram of the ordered Dirac model [120] showing regions of non-zero density of states $\rho$ ($|E| > |m|$) and non-zero Hall conductance $\sigma_{xy} = \pm e^2/2h$ ($|E| < |m|$).

Applying linear response theory to the Dirac system one can determine the Hall conductivity by calculating the ratio of, say, the current density in the $x$-direction, $j_x$ and the electric field, $E_y$, in the $y$-direction

$$\sigma_{xy} = \frac{j_x}{E_y} = \frac{e^2}{h}\frac{m}{2\pi^2}\int \frac{\mathrm{d}^2\boldsymbol{q}\,\mathrm{d}\omega}{[(\mathrm{i}\omega - E)^2 - q^2 - m^2]^2}\ . \tag{241}$$

It is found that at zero energy, where the above density of states vanishes, the Hall conductance jumps by $e^2/h$ at $m = 0$ (Fig. 30)

$$\sigma_{xy}(m) = \frac{\mathrm{sgn}(m)}{2}\,\frac{e^2}{h}\ . \tag{242}$$

The heavier Dirac field contributes towards the Hall conductance with $e^2/2h$ such that the total Hall conductance jumps from 0 to $e^2/h$. Simultaneously, the magneto-conductivity $\sigma_{xx}$ is non-zero only at this critical point,

$$\sigma_{xx} = \sigma_0\frac{e^2}{h}\delta_{m,0}\ , \tag{243}$$

with the Kronecker-symbol $\delta_{m,0}$ equal 1 for $m = 0$ and 0 for $m \neq 0$, and the constant $\sigma_0$ is $\pi/8$. The critical point shows time-reversal, particle–hole and parity invariance. Thus, the clean two-dimensional Dirac model exhibits a quantum Hall transition at $E = m = 0$, i.e. a step in the Hall conductivity.

According to our above derivation of the Hamiltonian, introducing spatial randomness in the Dirac mass, $m = m(x, y)$, is equivalent to introducing randomness in the saddle point energies. This breaks all of the above symmetries (cf. Table 2). However, this kind of randomness alone, if it is sufficiently weak, does not introduce a non-vanishing density of states at zero energy. This means that it cannot place the system into the quantum Hall universality class, in contrast to what one might suspect. For

sufficiently slowly varying mass, the zero-energy wave functions are argued to be confined along the contours $m(x, y) = 0$ since for any region with a non-vanishing Dirac mass the energy must be non-zero. When the mass varies slowly in space, the transition can be interpreted in terms of the percolation of these states. In the absence of randomness of the phases (i.e. the vector potential), the corresponding critical exponent of the correlation length is that of the classical percolation model. The analysis in Ref. [120] for weak randomness using the replica trick and perturbative renormalization group analysis strongly suggests that the random Dirac mass term is always marginal for the critical properties of the quantum Hall transition. The system scales to vanishing disorder, and the transition is described by the free Dirac theory. The replicated effective action is formally equivalent to that of the random-bond Ising model (cf. next section) with the randomness in the Dirac mass corresponding to the randomness in the Ising bonds.

Randomness in the scalar potential is equivalent to assuming random fluxes piercing the plaquettes of the network. For small random scalar potential one can use the perturbative results obtained for the random Dirac mass. This can be suspected from the form of the Hamiltonian

$$H = \boldsymbol{\sigma} \cdot \boldsymbol{p} + m\sigma_z + \phi \mathbf{1} \ . \tag{244}$$

Specifically, it can be shown that the problem with real disorder in the Dirac mass is formally equivalent to a problem with a purely imaginary random scalar field which corresponds to a negative disorder strength, $\langle \phi^2 \rangle < 0$. Equivalently, a positive scalar disorder strength maps onto a *negative* disorder strength for the Dirac mass. Since randomness in the Dirac mass was found to be marginal, the opposite is true for the scalar randomness, and the renormalization flow of the scalar disorder will now be *away* from the fixed point instead of towards it. Thus, the scalar randomness drives the system to some strong coupling regime. Eventually, one then expects the generation of a non-vanishing density of states. It is further argued by considering two-particle properties that the transition very probably has to be described by a symplectic non-linear sigma model due to the time reversal invariance of every member of the ensemble [120].

The case of only a random vector potential was found to be particularly interesting since it can be treated to a large extent analytically [120,195–200]. This limit has several remarkable properties. The Hamiltonian is

$$H_A = \boldsymbol{\sigma} \cdot \boldsymbol{p} + \boldsymbol{\sigma} \cdot \boldsymbol{A} \tag{245}$$

and according to what has been said before, the random vector potential is due to to the random phases along the links of the network. We assume that $\boldsymbol{A}$ satisfies a Gaussian white noise distribution with zero mean and variance $\Delta_A$. The corresponding random magnetic field, $\boldsymbol{B} = \nabla \times \boldsymbol{A}$, is then also Gaussian distributed with the variance

$$\langle B(k) B(k') \rangle = (2\pi)^2 k^2 \Delta_A \delta(k + k') \tag{246}$$

with the Fourier transform $B(k)$ of the magnetic field (perpendicular to the $(x, y)$-plane). As the Dirac mass is assumed to vanish, this Hamiltonian is expected to implement a critical theory. In fact, the model exhibits a fixed line corresponding to multi-fractal wave functions at $E = 0$ [120].

For non-vanishing uniform Dirac mass the squared of the Hamiltonian is

$$H^2 = H_A^2 + m^2 \tag{247}$$

for each realization of the random vector potential. Thus, the energy eigenvalues satisfy $E^2 > m^2$. The gap in the pure Dirac model with $m \neq 0$ is thus not closed by the randomness in the vector potential, at least as long as the disorder is small.

For this model, several single particle and two-particle properties can be determined exactly. As an example, we consider the zero-energy wave function. It is useful to use the Coulomb gauge, $\nabla \cdot \boldsymbol{A} = 0$. This implies that $\boldsymbol{A}$ can be written in terms of a scalar field $\Phi(x, y)$

$$A_x = \partial_y \Phi \,, \tag{248}$$

$$A_y = -\partial_x \Phi \,. \tag{249}$$

By inserting the real Ansatz wave functions

$$\Psi_\pm \propto (\mathbf{1} \pm \sigma_z) \begin{pmatrix} \mathrm{e}^{\Phi} \\ \mathrm{e}^{-\Phi} \end{pmatrix} \tag{250}$$

into the Schrödinger equation of the Hamiltonian equation (245) one easily verifies that they are exact nodeless eigenfunctions corresponding to $E = 0$. Furthermore, it follows from the symmetry properties of the Hamiltonian and the assumption of zero fluxes in the plaquettes that these are *all* of the zero-energy eigenfunctions.

These random wave functions are *not* localized, and *not* normalizable in the thermodynamic limit. In order to quantify their statistical nature it is useful to introduce their counterparts normalized to a square of the size $L^2$.

$$\psi(x, y) = \frac{1}{C} \mathrm{e}^{\Phi(x,y)} \tag{251}$$

with

$$C^2 = \int_{L^2} \mathrm{e}^{2\Phi(x,y)} \mathrm{d}x \, \mathrm{d}y \,, \tag{252}$$

where the integration is over the square $L^2$ and to consider the moments of the corresponding density, the average inverse participation numbers introduced in Section 4.3

$$p_q(L) = \langle |\psi|^{2q} \rangle_{L^2} \tag{253}$$

with $\langle \ldots \rangle_{L^2}$ denoting the configurational average in $L^2$.

For the above-normalized zero energy wave function, Eq. (251), with Gaussian distributed $\Phi$, the average inverse participation numbers can be determined [120,201–204]. One finds for $q_\mathrm{c} = \sqrt{2\pi/\Delta_A} > 1$

$$\tau(q) = \begin{cases} 2(q-1)(1 - q/q_\mathrm{c}^2), & |q| \leqslant q_\mathrm{c} \,, \\ 2q(1 - \operatorname{sgn} q/q_\mathrm{c})^2, & |q| > q_\mathrm{c} \,. \end{cases} \tag{254}$$

For $q_\mathrm{c} \leqslant 1$ one gets

$$\tau(q) = \begin{cases} -2(1 - q/q_\mathrm{c})^2, & |q| \leqslant q_\mathrm{c} \,, \\ 4(q - |q|)q_\mathrm{c}^{-1}, & |q| > q_\mathrm{c} \,. \end{cases} \tag{255}$$

The non-linearity in $q$ indicates multi-fractal scaling of the *extended* wave function. The resulting $f(\alpha)$-spectrum is parabolic with

$$\alpha_0 = \begin{cases} 2(1 + q_\mathrm{c}^{-2}), & q_\mathrm{c} > 1 \,, \\ 4/q_\mathrm{c}, & q_\mathrm{c} \leqslant 1 \,. \end{cases} \tag{256}$$

depending on the variance of the random vector potential $\Delta_A$, Eq. (246) (see Section 4.3).

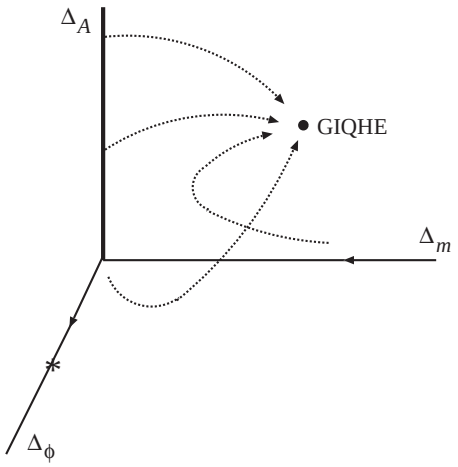


Fig. 31. The global phase diagram of the Dirac model including randomness in the vector potential, $\Delta_A$, the Dirac mass, $\Delta_m$, and the scalar potential, $\Delta_\phi$ (after [120]). The generic fixed point of the Integer Quantum Hall Effect corresponds to all of the three different kinds of disorder nonvanishing, and seems to be inaccessible analytically.

The density of states was found to show a power-law dependence of the energy near $|E| \approx 0$ with the exponent varying continuously upon moving along the fixed line [205],

$$\rho(E) \propto E^{(2-z)/z} \ , \tag{257}$$

with

$$z = \begin{cases} 1 + 2/q_c^2, & q_c > 1 \ , \\ 4/q_c - 1, & q_c \leqslant 1 \ . \end{cases} \tag{258}$$

For small disorder, the density of states vanishes. For $\Delta_A = \pi$, $\rho(E \to 0) = \text{const}$, and it diverges for $\Delta_A > \pi$.

The diagonal conductance was found to be $e^2/\pi h$ along the fixed line.

The Dirac model with only randomness in the vector potential belongs to the AIII symmetry class to be discussed in Section 9 (see also Table 5). The critical wave functions at $E = 0$ for random $\pi$ phase gauge field [206–208] as well as for arbitrary random gauge field [209] have been investigated in detail.

If the phases along the links of the network are assumed to be independent and random, the equivalent Dirac model has randomness both in the vector potential *and* in the fluxes through the plaquettes. Such a system has none of the above symmetries (cf. Table 2) and obviously belongs to the original Chalker–Coddington class with a fixed point that corresponds to the quantum Hall phase transition.

The scaling picture of the Dirac model with all of the three different kinds of disorder—random Dirac mass (parameter $\Delta_m$, random saddle point energies), random scalar potential (parameter $\Delta_\phi$, random fluxes through the plaquettes of the network) and random vector potential (parameter $\Delta_A$, random link phases)—has been qualitatively sketched by Ludwig and collaborators on the basis of their analytical results [120] (Fig. 31). The phase diagram consists of a critical line ($\Delta_m = \Delta_\phi = 0, \Delta_A \neq 0$) which is unstable with respect to both $\Delta_m$ and $\Delta_\phi$, a two-dimensional Ising fixed point at $\Delta_m = \Delta_\phi = \Delta_A = 0$ which is only stable for $\Delta_m \neq 0$, and a fixed point at some $\Delta_\phi \neq 0$ which was argued to belong to the

universality class of the symplectic non-linear sigma model. According to this scenario, the fixed point of the genuine integer quantum Hall transition is in a strong coupling regime with all of the three different kinds of disorder present. Until now, this has not yet been accessible analytically. It will be the subject of subsequent section to review the approaches to extract nevertheless analytical information on the GIQHE, and to shed some light on the obstacles which have still prevented an analytical derivation of its critical parameters.

## 8. Relation to the two-dimensional random bond Ising model

In the last section we have seen how mapping to different Hamiltonians can help to provide new insights into the properties of the quantum Hall phase transition. In this section we will address in addition the opposite question: given we know the network model and know how to use it for understanding the quantum Hall critical scenario, can we use this knowledge for understanding better the nature of phase transitions in two dimensions? As the random two-dimensional Ising model for a system of interacting spins is a fundamental prototype for phase transitions in two dimensions, for answering this question it is useful first to establish a relation between the random network and the Ising model. Such a mapping has been performed by various authors [209a,210,211]. We describe here the elementary route that has been worked out in the seminal paper by Merz and Chalker [212].

### 8.1. The Ising model

The Ising model in two dimensions is defined by the Hamiltonian [213]

$$H = -\sum_{ij} J_{ij} S_i S_j \ . \tag{259}$$

The exchange integrals $J_{ij}$ connect the sites $i$ and $j$ of a regular square lattice. The variables $S_i$ are the $z$-components of the spin operators associated with the lattice sites.

We consider the simplest case, where $J_{ij}$ connect nearest neighbors only, and spin $1/2$. In the ordered limit all of the exchange integrals are the same. This has been solved exactly by Onsager in classical paper using Lie algebras [214]. A comprehensive treatment using the transfer matrix method is described in [215]. The basic reason for the Ising model to be an exactly solvable many-body problem is that eventually it amounts to nothing else but the diagonalization of a quadratic form.

However, in the disordered case, when the exchange parameters are chosen at random, the model cannot be treated exactly, in spite of being quadratic. We consider $J_{ij}$ as independent random variables with a distribution $P(J_{ij})$. Specifically one can assume a two-component distribution,

$$P(J_{ij}) = p\delta(J_{ij} + J) + (1 - p)\delta(J_{ij} - J) \ . \tag{260}$$

This is the random bond Ising Model. For $J > 0$, it corresponds to a lattice containing $p$ antiferromagnetic and $(1 - p)$ ferromagnetic bonds. In this simple case, the model shows a phase transition between an ordered ferromagnetic phase at low temperatures and a paramagnetic high-temperature phase for small $p$. At larger $p$ the ferromagnetic phase is destroyed in favor of a spin glass phase in high dimensions, $d \geqslant 3$, with a multi-critical point, also called Nishimori point [216–218], where the three phases coexist (Fig. 32) [219–224]. In two dimensions the spin glass phase becomes unstable for $T \neq 0$. However, the

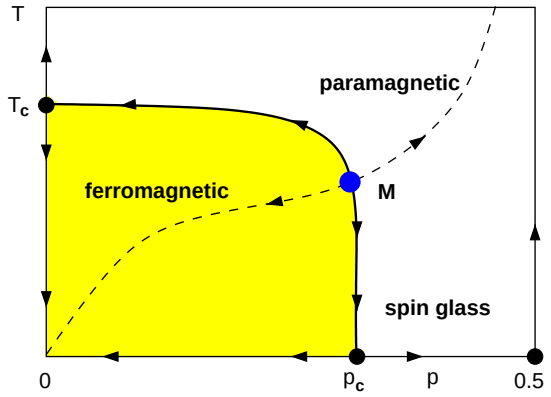


Fig. 32. Schematic phase diagram of the random bond Ising Model. For small fraction of antiferromagnetic bonds one observes a transition from a ferromagnetic to a paramagnetic phase with increasing temperature. For larger fraction of antiferromagnetic bonds, the ferromagnetic phase is changed to a spin glass. At the multicritical point $M$ the three phases coexist (dashed: Nishimori line; arrows: renormalization flow).

multi-critical point survives. Along the Nishimori line which crosses the phase boundary at the Nishimori point, the internal energy can be calculated exactly.

The disordered Ising system has been studied using Monte Carlo simulations and the transfer matrix method in the spin basis [222–230]. Mapping the random Ising model to fermionic models can have technical advantages: one can avoid the random-sampling errors of the Monte Carlo technique and it is possible to avoid the exponential growth of the transfer matrix. Pioneering work in this direction has been done by starting from the solution of the two-dimensional Ising model using a Pfaffian [231–237]. In this approach the statistical properties of the system are written in terms of the spectral properties of the corresponding matrix. The latter is essentially a tight-binding Hamiltonian on the underlying Ising lattice with random hopping matrix elements. Thus, a link between the random bond Ising system and the non-interacting localization problem is established. Alternative approaches have been formulated by using Dirac fermions which eventually have been condensed into a random network model with a special symmetry [120,158,210–212,238].

The mapping of the Ising model to a random network model is done in three steps. First, one introduces the conventional description of the partition function in terms of transfer matrices [215]. In the second step, the transfer matrices are written in terms of fermion operators instead of spinors. Finally, the network model is introduced by using the equivalence of second- and first-quantized forms of linear transformations. In the next sections, we establish the random network version of the Ising model following [212].

### *8.2. Transfer matrix formulation of the Ising model*

We consider the two-dimensional Ising model on a square lattice of length $L$ and width $M$ with random nearest-neighbor exchange couplings $J_\delta(l, m)$ (Fig. 33). The pair of integers $(l, m)$ denotes the coordinates of a lattice point in $L$- and $M$-directions, respectively. The index $\delta = \lambda, \mu$ indicates whether $J_\delta(l, m)$ couples to a nearest neighbor in the directions along $L$ or $M$, respectively.

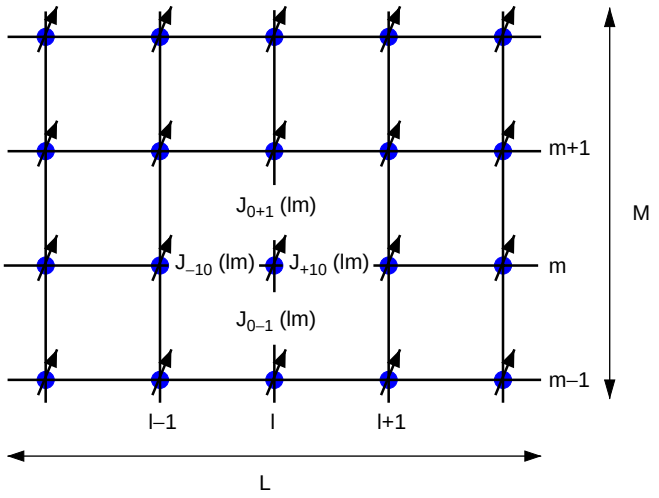


Fig. 33. The two-dimensional Ising model on a square lattice of length $L$ and width $M$ with exchange matrix elements $J_\delta(n, m)$ between nearest neighbors.

In order to introduce the transfer matrix description we start by considering the one-dimensional case $M = 1$ [215]. The Hamiltonian in suitable units is

$$H(\sigma_1 \dots \sigma_L) = -\sum_{l=1}^{L-1} J_\lambda(l)\sigma_l\sigma_{l+1} \ , \tag{261}$$

with independent random $J_\lambda(l)$. The partition function is

$$Z = \mathrm{Tr}\, \mathrm{e}^{-\beta H(\sigma_1 \dots \sigma_L)} = \mathrm{Tr}\, \exp \sum_l \kappa_\lambda(l)\sigma_l\sigma_{l+1} = \mathrm{Tr} \prod_l T_l \ , \tag{262}$$

with the "bond strength" $\kappa_\lambda(l) = \beta J_\lambda(l)$ ($\beta$ inverse temperature) and the transfer matrices

$$T_l = \mathrm{e}^{\kappa_\lambda(l)\sigma_l\sigma_{l+1}} \ . \tag{263}$$

Since the spin can take only values $\pm 1$ on the lattice sites the transfer matrices can be rewritten as $2 \times 2$ matrices with the matrix elements given by $\langle \pm, l+1 \mid T \mid \pm, l \rangle$,

$$T_l = \mathrm{e}^{\kappa_\lambda(l)}\boldsymbol{\sigma_0} + \mathrm{e}^{-\kappa_\lambda(l)}\boldsymbol{\sigma_1} \ . \tag{264}$$

With the definition of the Kramers–Wannier dual $\kappa^*$ of the bond strength $\kappa$

$$\kappa^* = -\frac{1}{2} \ln \tanh \kappa \tag{265}$$

the transfer matrices may be written in the diagonal form

$$T_l = \left[\frac{2}{\sinh 2\kappa^*_\lambda(l)}\right]^{1/2} \mathrm{e}^{-\kappa^*_\lambda(l)\boldsymbol{\sigma_3}} \ . \tag{266}$$

Here, $\boldsymbol{\sigma_j}$ ($j = 0, 1, 2, 3$) are the complete set of Pauli matrices denoted earlier as $\mathbf{1}_2$, $\sigma_x$, $\sigma_y$, and $\sigma_z$ ($\mathbf{1}_2$ two-dimensional unit matrix).

In the two-dimensional case the Hamiltonian is

$$H(\{\sigma_{l,m}\}) = -\sum_{l=1}^{L-1}\sum_{m=1}^{M} J_\lambda(l)\sigma_{l,m}\sigma_{l+1,m} - \sum_{l=1}^{L-1}\sum_{m=1}^{M} J_\mu(l)\sigma_{l,m}\sigma_{l,m+1} \tag{267}$$

and we assume periodic boundary conditions in the direction of $M$ such that $M+1 \to 1$. Also in this case one can write the partition function as a product of transfer matrices, Eq. (262), but now these consist of two factors

$$T_l = V_l W_l \ . \tag{268}$$

The matrix $W_l$ is the obvious generalization of Eq. (266),

$$W_l = \prod_{m=1}^{M}\left[\frac{2}{\sinh 2\kappa^*_\lambda(l,m)}\right]^{1/2} \exp\left[-\sum_{m=1}^{M}\kappa^*_\lambda(l,m)\boldsymbol{\sigma}^m_{\mathbf{3}}\right] \ , \tag{269}$$

but with the $2M \times 2M$ matrix

$$\boldsymbol{\sigma}^m_{\mathbf{3}} = \boldsymbol{\sigma_0}\otimes\boldsymbol{\sigma_0}\otimes\cdots\otimes\boldsymbol{\sigma_3}\otimes\cdots\otimes\boldsymbol{\sigma_0} \ , \tag{270}$$

which is the direct product of $M-1$ unit matrices and $\boldsymbol{\sigma_3}$ at position $m$. The $2M \times 2M$ matrix $V_l$ contains the Hamiltonian of the $l$th column of the system

$$V_l = \exp\left[\sum_{m=1}^{M-1}\kappa_\delta(l,m)\boldsymbol{\sigma}^m_{\mathbf{1}}\boldsymbol{\sigma}^{m+1}_{\mathbf{1}}\right] \ . \tag{271}$$

The formulation in terms of transfer matrices has two implications which are of immense importance for practical purposes. First, one can show that it is the largest eigenvalue of the total transfer matrix that determines for $L \to \infty$ the partition function and thus the physical properties of the system [215]. Second, one can write the transfer matrix of a system of length $L+1$ as a function of the transfer matrix of the system of the length $L$. We will see below, that these two properties are essential for numerical evaluation of the phase diagram and critical properties.

### *8.3. Transforming to fermions*

The above transfer matrices involve linear and quadratic forms of the spin operators. The raising and lowering operators fulfill mixed commutation and anticommutation relations

$$\begin{aligned}
&[\sigma^m_\pm, \sigma^l_\pm] = 0 \quad (m \neq l) \ , \\
&\{\sigma^m_+, \sigma^l_-\} = 1 \ , \\
&(\sigma^m_+)^2 = (\sigma^m_-)^2 = 0 \ .
\end{aligned} \tag{272}$$

In one dimension, it is well known how to transform these operators to ones obeying fermion anticommutation relations. This is done by the Jordan–Wigner transformation [239–242]. Annihilation and creation

operators are introduced by

$$c_m = \left[\exp\left(\mathrm{i}\pi \sum_{j=1}^{m-1} \sigma_+^j \sigma_-^j\right)\right] \sigma_-^m \ ,$$

$$c_m^\dagger = \left[\exp\left(\mathrm{i}\pi \sum_{j=1}^{m-1} \sigma_+^j \sigma_-^j\right)\right] \sigma_+^m \ . \tag{273}$$

It is easy to show that these operators obey fermion statistics and

$$c_m^\dagger c_m = \sigma_+^m \sigma_-^m \ . \tag{274}$$

The inverse transformation is

$$\sigma_-^m = \left[\exp\left(\mathrm{i}\pi \sum_{j=1}^{m-1} c_j^\dagger c_j\right)\right] c_m \ ,$$

$$\sigma_+^m = \left[\exp\left(\mathrm{i}\pi \sum_{j=1}^{m-1} c_j^\dagger c_j\right)\right] c_m^\dagger \ . \tag{275}$$

This gives

$$\sigma_1^m = \left[\exp\left(\mathrm{i}\pi \sum_{j=1}^{m-1} c_j^\dagger c_j\right)\right] (c_m^\dagger + c_m), \quad \sigma_3^m = 2c_m^\dagger c_m - 1 \ . \tag{276}$$

The fermion representation of the above transfer matrices is

$$W_l = \prod_{m=1}^{M} \left[\frac{2}{\sinh\ 2\kappa_\lambda^*(l,m)}\right]^{1/2} \exp\left[-2 \sum_{m=1}^{M} \kappa_\lambda^*(l,m) \left(c_m^\dagger c_m - \frac{1}{2}\right)\right] \ ,$$

$$V_l = \exp\left[\sum_{m=1}^{M-1} \kappa_\delta(l,m)(c_m^\dagger - c_m)(c_{m+1}^\dagger + c_{m+1}) \right.$$

$$\left. - \kappa_\mu(l,M)\mathrm{e}^{\mathrm{i}\pi N_\mathrm{c}}(c_M^\dagger - c_M)(c_1^\dagger + c_1)\right] \ , \tag{277}$$

with the number operator $N_\mathrm{c} = \sum_{m=1}^{M} c_m^\dagger c_m$. The last term in (277) represents the periodic boundary condition in the direction of $M$.

The matrix $V_l$ is biquadratic in the fermion operators. It does not conserve the number of fermions since it contains terms that create and annihilate fermions in pairs. Thus, diagonalization of the transfer matrix in principle should be possible via a unitary Bogoliubov–de-Gennes transformation.

It is illustrative for the disordered case to consider first the ordered limit in which $\kappa_\lambda^*(l,m)=\kappa_\lambda^*$ and $\kappa_\mu(l,m)=\kappa_\mu$. First one notes that evenness and oddness of $N_c$ commute with $W$ and $V$ [215] since the latter contains only quadratic forms of the fermion operators,

$$[(-1)^{N_c}, W]=[(-1)^{N_c}, V]=0\ . \tag{278}$$

Therefore one can classify the eigenstates of $WV$ according to whether they contain even and odd numbers of fermions. One can then write

$$V^{\pm}=\exp\left[\kappa_\mu\sum_{m=1}^{M}(c_m^\dagger-c_m)(c_{m+1}^\dagger+c_{m+1})\right]\ , \tag{279}$$

with $c_{M+1}=\mp c_1$ and $c_{M+1}^\dagger=\mp c_1^\dagger$ where $\pm$ denote the operators acting on the even (with anticyclic boundary condition) and odd states (with cyclic boundary condition), respectively. The task is then to find the eigenvalues and eigenvectors of the transfer operators

$$\begin{aligned}T^{\pm}=V^{\pm}W=&\left[\frac{2}{\sinh\,2\kappa_\lambda^*}\right]^{M/2}\exp\left[\frac{1}{2}\,\kappa_\mu\sum_{m=1}^{M}(c_m^\dagger-c_m)(c_{m+1}^\dagger+c_{m+1})\right]\\&\times\exp\left[-2\kappa_\lambda^*\sum_{m=1}^{M}\left(c_m^\dagger c_m-\frac{1}{2}\right)\right]\\&\times\exp\left[\frac{1}{2}\,\kappa_\mu\sum_{m=1}^{M}(c_m^\dagger-c_m)(c_{m+1}^\dagger+c_{m+1})\right]\ .\end{aligned} \tag{280}$$

The diagonalization can be straightforwardly performed by introducing plane wave operators via the canonical transformation

$$c_m=\frac{1}{\sqrt{M}}\sum_q \mathrm{e}^{\mathrm{i}qm}\eta_q\ , \tag{281}$$

where $q\leqslant\pi$ is given by the odd and even multiples of $\pi/M$ for anticyclic and cyclic boundary conditions, respectively ($M$ is assumed to be even). The resulting quadratic forms in the transfer operator which has four eigenstates is very reminiscent of the pair Hamiltonian in the BCS theory of superconductivity. It can be diagonalized by transforming to new variables

$$\xi_{\pm q}=\cos\phi_q\eta_{\pm q}\pm\sin\phi_q\eta_{\mp q}^\dagger\ , \tag{282}$$

with $\tan 2\phi_q=2C_q/(B_q-A_q)$ containing

$$\begin{aligned}A_q&=\mathrm{e}^{-2\kappa_\lambda^*}(\cosh\,\kappa_\mu+\sinh\,\kappa_\mu\cos q)^2+\mathrm{e}^{2\kappa_\lambda^*}(\sinh\,\kappa_\mu\sin q)^2\ ,\\B_q&=\mathrm{e}^{-2\kappa_\lambda^*}(\sinh\,\kappa_\mu\sin q)^2+\mathrm{e}^{2\kappa_\lambda^*}(\cosh\,\kappa_\mu-\sinh\,\kappa_\mu\cos q)^2\ ,\\C_q&=(2\sinh\,\kappa_\mu\sin q)(\cosh\,2\kappa_\lambda^*\,\cosh\,\kappa_\mu-\sinh\,2\kappa_\lambda^*\,\sinh\,\kappa_\mu\cos q)\ .\end{aligned}$$

With these operators one obtains the diagonal form of the transfer operators

$$T^{\pm} = \left[\frac{2}{\sinh\, 2\kappa_\lambda^*}\right]^{M/2} \exp\left[-\sum_q \epsilon_q \left(\xi_q^\dagger \xi_q - \frac{1}{2}\right)\right] . \tag{283}$$

The energy dispersion is given implicitly by the solution of

$$\cosh\, \epsilon_q = \cosh\, 2\kappa_\mu \cosh\, 2\kappa_\lambda^* - \sinh\, 2\kappa_\mu \sinh\, 2\kappa_\lambda^* \cos q\ . \tag{284}$$

The four eigenstates in terms of the $\xi$-operators are the vacuum $\psi_0$, $\psi_{\pm q} = \xi_{\pm q}^\dagger \psi_0$ and the pair state $\psi_{-qq} = \xi_{-q}^\dagger \xi_q^\dagger \psi_0$.

The partition function is given by the $L$th power of the largest eigenvalue of $T^{\pm}$. The critical temperature $T_c$ is defined by $\kappa_\lambda^* = \kappa_\mu$. We do not want to discuss here how to use the results for obtaining the critical properties. The important lesson to keep in mind at this stage is the importance of the parity of the fermion number for the structure of the eigenvalue problem.

### *8.4. Mapping to a localization problem for non-interacting particles*

In the case of a disordered Ising system, the unitary transformation for achieving the diagonalization of the transfer matrix depends on the disorder, and the different transfer steps are not independent. Therefore, a different approach must be used. This consists of mapping the Ising problem to a localization problem for non-interacting particles.

Starting point is the rewriting of the transfer matrix in terms of Dirac fermions fulfilling particle conservation [158,211]. In order to achieve this, an identical copy of the Ising model is introduced. The corresponding fermions are denoted as $d_m^\dagger$, $d_m$. New Dirac fermions are then defined by (suppressing the indices for the sake of simplicity)

$$c = \frac{1}{2}(f + f^\dagger + g - g^\dagger), \quad d = \frac{\mathrm{i}}{2}(f^\dagger - f - g - g^\dagger) \tag{285}$$

and the inverse of these,

$$f = \tfrac{1}{2}[c + c^\dagger + \mathrm{i}(d + d^\dagger)], \quad g = \tfrac{1}{2}[c - c^\dagger + \mathrm{i}(d - d^\dagger)]\ . \tag{286}$$

The Hamiltonian of the doubled system is the sum of the two Hamiltonians, $H = (H^c + H^d)/2$. This implies that one deals eventually with products of the corresponding transfer matrices. In terms of the new fermion operators they are given by

$$\begin{aligned} W_l^c W_l^d &= \exp\left[-2\sum_{m=1}^{M} \kappa_\lambda^*(l,m)(g_m^\dagger f_m + f_m^\dagger g_m)\right] , \\ V_l^c V_l^d &= \exp\left[2\sum_{m=1}^{M-1} \kappa_\mu(l,m)(g_m^\dagger f_{m+1} + f_{m+1}^\dagger g_m) + b\right] \end{aligned} \tag{287}$$

and they are particle conserving. The term

$$b = -\kappa_\mu(l, M)[(e^{i\pi N_c} + e^{i\pi N_d})(g_M^\dagger f_1 + f_1^\dagger g_M) + (e^{i\pi N_c} - e^{i\pi N_d})(g_M^\dagger f_1^\dagger + f_1 g_M)] \tag{288}$$

is due to the boundary conditions in the direction of $M$. This contains the two boundary operators

$$B^\pm = e^{i\pi N_c} \pm e^{i\pi N_d} . \tag{289}$$

In order to perform the mapping to the network model it is required that the transfer operator conserves the number of fermions. This implies that the Hilbert space for first quantization of the transfer matrix must be constructed from the Hilbert space of the two copies of the Ising model in such a way that the term involving $B^-$ in Eq. (288) vanishes [212].

In particular, one may consider the parity operators $R$ defined by

$$R = \prod_{m=1}^{M} \sigma_m^3 \tag{290}$$

which change the sign of a complete column of the spins,

$$R\sigma_\mu^1 R = -\sigma_\mu^1 , \quad R^2 = \mathbf{1} . \tag{291}$$

These obviously commute with the transfer operators and have eigenvalues $\pm 1$. The transfer matrix of the two copies of the Ising system written in the basis corresponding to the product space of $R_c + R_d$ can then be cast into a block-diagonal form where the four block matrices describe the transfer of amplitudes in the subspaces corresponding to eigenvalues of the parity operators operating in the Hilbert spaces of the two copies of the system, $(1_c, 1_d)$, $(1_c, -1_d)$, $(-1_c, 1_d)$, and $(-1_c, -1_d)$. Since the eigenvalues of $\exp(i\pi N)$ are $\pm 1$ depending on whether $M$ is even or odd, the boundary operators can be written as $B^\pm = R_c \pm R_d$. Then, in the subspaces corresponding to the same eigenvalues, $B^- = 0$. The number of fermions is conserved.

### 8.5. The equivalent network model

In order to construct the first quantized form of the transfer matrix, we start by comparing first and second quantized forms of an operator in a Hilbert space, say of the dimension $N = 2M$ with a basis $\{|j\rangle\}$. Assume that the operator can be written in the second quantized form as $\exp[\alpha_j^\dagger \langle j|G|k\rangle \alpha_k]$ with the creation and annihilation operators $\alpha_j^\dagger$, and $\alpha_k$, respectively. The first quantized form of this operator is the $(2M \times 2M)$-matrix $\langle j| \exp G|k\rangle$.

By identifying $\{\alpha_1, \ldots, \alpha_{2M}\} = \{f_1, \ldots, f_M, g_1, \ldots, g_M\}$ one finds that the first quantization equivalent of the second quantization transfer operator corresponding to the $\lambda$-bonds, $\exp[-2\kappa_\lambda^*(l, m)](g_m^\dagger f_m + f_m^\dagger g_m)$, is given by (Fig. 34)

$$W_{lm} = \exp[-2\kappa_\lambda^*(l, m)\sigma_1] = \cosh[2\kappa_\lambda^*(l, m)] - \sigma_1 \sinh[2\kappa_\lambda^*(L, M)] . \tag{292}$$

By analogy, the first quantized form of the $\mu$-bonds in the transfer matrix is

$$V_{lm} = \exp[2\kappa_\mu(l, m)\sigma_1] = \cosh[2\kappa_\mu(l, m)] + \sigma_1 \sinh[2\kappa_\mu(l, m)] . \tag{293}$$

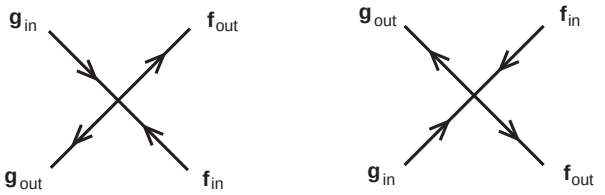


Fig. 34. Graphical representation of the scattering nodes of the first quantized form of the transfer matrix of the Ising model. Left: $\lambda$-bond; right: $\mu$-bond.

In terms of right- and left-moving amplitudes $\tilde{f}_j$ and $\tilde{g}_j$, respectively, the transfer operators of the lattice sites can be written as

$$\begin{pmatrix} \tilde{f}_{\rm out} \\ \tilde{f}_{\rm in} \end{pmatrix} = \begin{pmatrix} \cosh\, 2\kappa_\lambda^* & -\sinh\, 2\kappa_\lambda^* \\ -\sinh\, 2\kappa_\lambda^* & \cosh\, 2\kappa_\lambda^* \end{pmatrix} \begin{pmatrix} \tilde{g}_{\rm in} \\ \tilde{g}_{\rm out} \end{pmatrix} \tag{294}$$

and

$$\begin{pmatrix} \tilde{f}_{\rm in} \\ \tilde{f}_{\rm out} \end{pmatrix} = \begin{pmatrix} \cosh\, 2\kappa_\mu & \sinh\, 2\kappa_\mu \\ \sinh\, 2\kappa_\mu & \cosh\, 2\kappa_\mu \end{pmatrix} \begin{pmatrix} \tilde{g}_{\rm out} \\ \tilde{g}_{\rm in} \end{pmatrix} . \tag{295}$$

The relations

$$\sigma_3 \mathbf{W}^\dagger \sigma_3 = \mathbf{W}^{-1} , \quad \sigma_3 \mathbf{V}^\dagger \sigma_3 = \mathbf{V}^{-1} \tag{296}$$

ensure flux conservation (Fig. 35).

The network model constructed in this way is completely analogous to the U(1) network of saddle point scatterings used in the previous section for describing the critical localization behavior of the quantum Hall system, with plaquettes of definite senses of circulation of the fluxes which can be clockwise and counterclockwise. Disorder can be introduced in the former network by random quenched phases and random saddle point energies. In the present case, randomness enters only via the randomness of the exchange integrals represented in the Ising model by the bonds. The latter have been mapped to the nodes of the network represented by the parameters $\kappa$ and $\kappa^*$. An antiferromagnetic $\mu$-bond leads to $\kappa < 0$. An antiferromagnetic $\lambda$-bond, however, leads to a complex $\kappa^*$, where $^*$ denotes the Kramers–Wannier dual defined by the function, Eq. (265). It implies the relation

$$(-|\kappa|)^* = |\kappa|^* + \mathrm{i}\,\frac{\pi}{2} . \tag{297}$$

This gives a minus sign in the matrices $W$ representing the scattering at the nodes. Starting from an Ising system with ferro- and antiferromagnetic bonds distributed randomly, one arrives at an equivalent network model with nodes $W$ that have random signs. In the node matrices $V$, the off-diagonal matrix elements $\sinh(2\kappa)$ acquire random signs. Thus, scattering at the nodes only causes real phase factors $\pm 1$. Taking into account the topology of the network (Fig. 35), this means that a single antiferromagnetic node introduces phases $\pi$ in both of the anticlockwise plaquettes that are linked at this node.

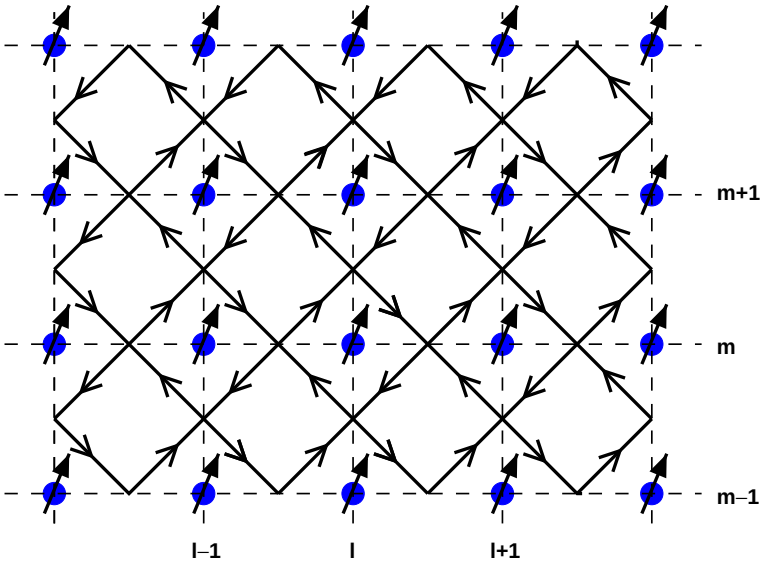


Fig. 35. The network model equivalent to the random bond Ising model. Arrows indicate the propagation of flux. The transfer matrix relates flux amplitudes from the left to the right. The Ising lattice of spins (arrows) with the exchange matrix elements (dashed) are also shown.

This specific property of the disorder determines the symmetry class of the model. In the classification scheme introduced recently by Altland and Zirnbauer [243,244] this network model belongs to the class D (see below, Table 4 in Section 9). Hamiltonian matrices of this class are purely imaginary, $H^* = -H$. The corresponding time evolution operator $\exp(-\mathrm{i}Ht)$ is represented by a matrix with real elements and can introduce only scattering phase factors $\pm 1$, in accordance with the above network model of the random bond Ising model.

The total transfer matrix of the doubled Ising system is then obtained by combining the node matrices $W$ and $V$. It is a $2M \times 2M$ matrix which can be arranged in such a way that propagation in one direction is described by the first $M$ rows and propagation in the other direction is contained in the $M$ last rows. In the former case of the U(1) network the transfer matrix was unitary. In the present case it is real and orthogonal. For a random network, it has the form $\exp \gamma L$ with a real diagonal matrix $\gamma$. The fluctuations are $\propto \sqrt{L}$. It can be calculated numerically recursively for very long strips [17,88,89], $L \to \infty$, and converges according to the theorem by Oseledec [106] to a diagonal matrix with diagonal elements $\gamma_1, \ldots, \gamma_M, -\gamma_1, \ldots, -\gamma_M$ with the Lyapunov exponents $\gamma_j$.

The above random-bond Ising network model has been analyzed exhaustively numerically in [212] for systems containing as many as $M \times L = 256 \times 5 \cdot 10^5$ lattice sites including scaling analysis along the phase boundary where systems of size up to $M \times L = 32 \times 2 \cdot 10^8$ lattice sites were used. From the scaling behavior of the data a critical index of $\nu = 1.50 \pm 0.03$ has been extracted along the Nishimori line at the multicritical point. On the other hand, along the phase boundary, the scaling analysis gives a critical exponent $\nu_T = 4.0 \pm 0.5$.

Also other network models, but belonging to the same symmetry class D, have been studied [209a,210,238]. Most strikingly, these different choices seem to yield different localization properties. This will be reviewed in the following section.

## 9. Symmetry classes

Having established above a network model belonging to a certain symmetry class corresponding to the quantum Hall transition, one may ask the question if one can generalize the model to cover *all* existing symmetry classes.

Conventionally, random electron systems are classified into three universality classes [144] according to their symmetry with respect to reversal of time and rotation of spin. Systems belonging to the orthogonal class have both time reversal and spin rotation invariance. Models belonging to the unitary class are not invariant under time reversal. The symplectic class contains models that have time reversal symmetry but the spin rotation symmetry is broken. This is realized in random electron systems with spin–orbit interaction. The notation originates from the fact that a distribution of random matrices $\mathbf{H}$ of the orthogonal, unitary, and symplectic classes is invariant under transformations, $\mathbf{H} \rightarrow \mathbf{U}^{-1}\mathbf{H}\mathbf{U}$, $\mathbf{O}^{\mathrm{T}}\mathbf{H}\mathbf{O}$, $\mathbf{W}^{\mathrm{R}}\mathbf{H}\mathbf{W}$ with unitary, orthogonal, and symplectic (commuting with the antisymmetric Pauli matrix $\sigma_y$) matrices, $\mathbf{U}$, $\mathbf{O}$, $\mathbf{W}$, respectively. Here, $\mathbf{O}^{\mathrm{T}}$ is the transpose of $\mathbf{O}$, and $\mathbf{W}^{\mathrm{R}}$, the time reverse of $\mathbf{W}$ [144], as defined by $\mathbf{W}^{\mathrm{R}} = \mathbf{K}\mathbf{W}^{\mathrm{T}}\mathbf{K}^{-1}$, with the unitary matrix $\mathbf{K}$ which can be symmetric or antisymmetric, $\mathbf{K}\mathbf{K}^{*} = \pm 1$, corresponding to integer spin and half-integer spin, respectively. Any random matrix in each of the classes can be diagonalized by a unitary, orthogonal, and symplectic matrix, respectively.

The symmetry properties of a random Hamiltonian have strong impact on the distribution and statistical correlations between its eigenvalues and the distribution of moments of local eigenfunction amplitudes. The level repulsion of extended states increases as the symmetry is changed from the orthogonal to unitary to the symplectic class. At the same time the tendency to localization decreases, accompanied by an according decrease of local wave function fluctuations [144,245]. As reviewed in Section 4, these properties have been studied in detail for the Chalker–Coddington network model. By construction, the model belongs to the unitary symmetry class, since the links are directed, and correspond to scattering paths which have a well-defined chirality (handedness). This breaks the time reversal symmetry. The question arises, whether or not the integer quantum Hall transition as modeled by the Chalker–Coddington network model is uniquely characterized by being identified as belonging to the unitary symmetry class. This would lead one to the conclusion that all quantum Hall-type transitions had the same critical exponents.

Since there can be a strong overlap between spin split Landau bands [246], the question is of great experimental importance [247] whether or not the delocalization transition is sensitive to the spin rotation symmetry. When the time reversal symmetry is broken, the conventional unitary class makes no distinction whether or not the spin symmetry is broken. However, for a modified Chalker–Coddington model with two spin channels, fixing the scattering phases and introducing random SU(2) mixing between the spin channels—which corresponds to spin flip scattering by spin–orbit interaction—the critical exponent has been found to be $\nu \approx 1.1$ [248,249]. This is close to the one of classical percolation, $\nu = \nu_{\mathrm{p}} = 4/3$, see Section 2.4. On the other hand, one recovers the critical exponent $\nu = 2.4(2)$ close to that of the quantum Hall phase transition [97,98,248] (Table 3) by choosing in addition the scattering phases at random. In the latter case, the unitary matrices mixing the two spin channels are randomly chosen from the group $\mathrm{U}(2) = \mathrm{U}(1) \times \mathrm{SU}(2)$ where $\mathrm{U}(n)$ denotes the group of complex unitary $(n \times n)$-matrices $\mathbf{A}$, and S stands for the special condition that its determinant is one, $\det A = 1$.

Recently, it has been realized that there can be two additional discrete symmetries in Hamiltonians of disordered electrons. These symmetries have been found to give rise to four distinct transitions of the

Table 3
Classification of network models (NM) according to their symmetry: the Wigner–Dyson class with no discrete symmetry

| Wigner–Dyson class | | | | |
|---|---|---|---|---|
| Property | Orthogonal | Unitary | Unitary | Symplectic |
| TRS | Yes | No | No | Yes |
| SRS | Yes | Yes | No | No |
| Cartan class | AI | A | A | AII |
| $\beta$ | 1 | 2 | 2 | 4 |
| $m_l$ | 1 | 1 | 1 | 1 |
| $s$ | 1 | 1 | 2 | 1 |
| NDNM | Insulator | Insulator[a] | Insulator | MIT [76] |
| DOS ($E \to 0$) | Constant | Constant | Constant | Constant |
| Phase factor in DNM | | U(1) | U(2)[b] | |
| PT in DNM | — | IQHT | IQHT[c] | — |
| $\nu$ | — | 2.5(5) [31] | 2.4(2) [97,98] [20][c] | 2.8(1) (Section 9.2) |
| $\alpha_0$ | — | 2.261(3) [137] | | 2.174(3) [260] |
| $\Lambda_c$ | — | $1/\pi(\alpha_0 - 2)$ | $2/\pi(\alpha_0 - 2)$ | 1.83(1) (Section 9.2) |
| Equivalent models | | RSVDM | RSVDM | |

Abbreviations: TRS time reversal symmetry, SRS, spin rotation symmetry, $\beta$ level repulsion exponent, $m_l$ multiplicity of long root on symmetric space [256], $s$ spin factor, IQHT Integer Quantum Hall Transition, MIT metal–insulator transition, DOS density of states, (N)DNM (non-)directed network model, PT phase transition, $\nu$ critical exponent, $\alpha_0$ position of maximum of $f(\alpha)$, $\Lambda_c$ MacKinnon–Kramer parameter, RSVDM Dirac model with both, random scalar and vector potentials.

[a] Electrons in a random magnetic field belong to this unitary class. The U(2) network model proposed by Chalker and Lee [97] describes electrons in random magnetic field with large correlation length, and does not show a delocalization transition.

[b] Spin degenerate levels with spin–orbit interaction [97].

[c] Two IQHTs at two distinct energies [97].

quantum Hall type with different critical exponents and different behavior of the quasi-particle density of states. In the next section, we introduce these symmetry classes before we review the present knowledge about the properties of the corresponding random models. In particular, we will concentrate on the nature of the quantum Hall-type transitions.

### 9.1. The additional discrete symmetries

In addition to the invariance under time reversal and spin rotation, there can be at least two more discrete symmetry operations in condensed matter systems. One is realized in two-sublattice models [250–253]. It corresponds to an interchange of the two sublattices together with a sign change of the Hamiltonian. A physical realization is a tight-binding lattice Hamiltonian with randomness only in the hopping amplitude. Disordered systems with such a symmetry belong to the *chiral class*.

The other one is the electron–hole symmetry [254] arising from Andreev scattering in normal metal wires attached to a superconductor [244] or in superconductors with a gapless quasi-particle density of

Table 4
Classification of network models according to their symmetry: the Bogoliubov–de-Gennes–Oppermann class with particle–hole discrete symmetry

| Bogoliubov–de-Gennes–Oppermann class | | | | |
|---|---|---|---|---|
| Property | Orthogonal | Unitary | Unitary | Symplectic |
| TRS | Yes | No | No | Yes |
| SRS | Yes | Yes | No | No |
| Cartan class | CI | C | D | DIII |
| $\beta$ | 2 | 4 | 1 | 2 [261] |
| $m_l$ | 2 | 3 | 0 | 0 [261] |
| $s$ | 1 | 1 | 4 | 2 |
| Transport | SI | SI | TM | TM[a] |
| DOS ($E \to 0$) | $\|E\|$ [244,262] | $\|E\|^2$ [244] | $\|E\|$[b] $\sqrt{\ln(1/\|E\|)}$ [c][263] | $\|E\|$[244] |
| Phase factor | | SU(2) | $Z_2$ | |
| PT in DNM | — | SQHT | TQHT | — |
| DOS at CP | | $\|E\|^{1/7}$ [264,265] | | |
| $\nu$ | — | 4/3 [264] | —[d] | ? |
| $\alpha_0$ | — | 2.137(3) [184] | —[d] | ? |
| $\Lambda_c$ | — | $1/\pi(\alpha_0 - 2)$ | —[d] | ? |
| Equivalent models | | CP | RBIM | |

SQHT spin quantum Hall transition, TQHT thermal quantum Hall transition, CP classical percolation model, RBIM random bond Ising model [158].

Abbreviations: SI spin insulator, TM thermal metal.

[a]Critical metal for uncorrelated disorder of arbitrary strength, MIT for correlated disorder.

[b]DOS in the localized phase.

[c]DOS in the metallic phase.

[d]Line of critical points, on the Nishimori line $\nu = \nu_p = 4/3$ [158].

states [254]. Disordered systems with such a particle–hole symmetry are in the Bogoliubov–de-Gennes-Oppermann (BdGO) class.

Both of the discrete symmetries share the property that the eigenenergies of the corresponding Hamiltonians come in pairs $(-E_n, E_n)$, where $E = 0$ is the center of the band of eigenvalues for the chiral models, and the Fermi energy for the BdGO-models. Random Hamiltonians with either of these two discrete symmetries show very different behavior in their density of states and transport properties. Their properties are presently the subject of intensive ongoing research. In Tables 3–5, and we have attempted to summarize what is presently known about the properties of the non-directed and directed network models for all of the existing symmetry classes.

There are strong arguments, based on a classification of Lie Algebras by Cartan [255,256], that these symmetries make the classification of possible random systems complete. In a perturbative renormalization group study in $2 + \epsilon$ dimensions, the corrections to the conductance in the bosonic and the fermionic replica formulations have been obtained to 3-loop order for all of the symmetric spaces [257].

Table 5
Classification of network models according to their symmetry: the chiral class with bipartite discrete symmetry (two sublattices)

| Chiral class | | | |
|---|---|---|---|
| Property | Orthogonal | Unitary | Symplectic |
| TRS | Yes | No | Yes |
| SRS | Yes | Yes(no) | No |
| Cartan class | BDI | AIII | CII |
| $\beta$ | 1 | 2 | 4 |
| $m_l$ | 1 | 1 | 1 |
| $s$ | 1 | 1(2) | 1 |
| Transport ($E=0$) | Metal | Metal | ? |
| DOS ($E\to 0$) | $\rho(E)$ | $\rho(E)$ | ? |
| Phase factor | $2\times Z_2$ | $2\times$ U(1) | $2\times$ SU(2) |
| PT in DNM | — | Yes (a) | — |
| $\nu$ | — | | |
| $\alpha_0$ | — | | |
| $\Lambda_c$ | — | | |
| Equivalent models | RXY [266] | RVDM | |

Abbreviations: $\rho(E)=\exp(-c|\ln E|^{1/x})/|E|$ [252] ($x=3/2$ for BDI [204,205] and possibly also for AIII, CII [205]), RXY random XY model, RVDM Dirac model with random vector potentials.
(a) The phase diagram is shown in Fig. 46.

There is an ongoing debate whether or not this symmetry classification is sufficient to characterize the quantum critical properties of random systems [210,258,204,259]. As we will review below, there are some results which do not seem to fit into this scheme, since the critical properties sensitively do depend on the spatial correlation of the disorder. As discussed above, the conventional quantum Hall transition is insensitive to the correlation length of the disorder potential, unless the disorder has an extremely long-range correlation length [84].

In the following, we first discuss the properties of quasi-one-dimensional disordered wires, and how their transport properties depend on the symmetry properties. Then, we consider the critical properties in two dimensions. We present an overview of the network models studied for the various symmetry classes.

For a quasi-one-dimensional wire, where the localization length $\xi$ is larger than the wire width $L_y$, a beautiful formula, valid for all of the 10 symmetry classes has been derived recently by solving the Fokker–Planck equation [261,267]

$$\xi = l\left[s\,\frac{\beta}{m_l}(N-1)+1+\frac{1}{m_l}\right]. \tag{298}$$

Here, $m_l$ is the multiplicity of the root on the symmetric space (see below), $\beta$ the level repulsion coefficient, $N$ the number of channels proportional to the width, and $s$ the spin factor. This formula displays explicitly the importance of the symmetry properties of the disordered Hamiltonian for the localization. We have seen already that the transfer matrix $\mathbf{T}$ of the Chalker–Coddington model fulfills the commutation relation equation (91), which is a result of current conservation. Thereby, transfer matrices form a group.

Since they are parameterized by continuous variables, such groups are called Lie groups. For the Chalker–Coddington transfer matrix this group is $G = U(N, N)$, the group of non-compact $2N \times 2N$ matrices, which fulfill Eq. (91). For the other ensembles additional conditions are imposed, restricting the corresponding transfer matrices to be in different Lie groups. Now, all the powerful tools of representation theory of Lie groups [268] can be used to analyze these transfer matrices systematically. There is a further simplification, that a transport property like the conductance equation (147) does depend only on products $\mathbf{TT}^+$ and $\mathbf{T}^+\mathbf{T}$ [160,162]. As a result, there is a subgroup K of matrices $\mathbf{k}$ by which $\mathbf{T}$ can be multiplied from right $\mathbf{T} \to \mathbf{kT}$ or left $\mathbf{T} \to \mathbf{Tk}$, without changing the conductance through the system. For the Chalker–Coddington model this subgroup is found to be $K = U(N) \times U(N)$, the group of $2N$ times $2N$ matrices which consist of two blocks of unitary $N \times N$ matrices. Thus, this subgroup is not relevant for a physical property like the conductance, and can be divided from the group G. The resulting group G/K is for the Chalker–Coddington model $G/K = U(N, N)/(U(N) \times U(N))$. This is a so-called simple Lie group and is also called a symmetric space. There is a full classification of all symmetric spaces by Cartan. The way to characterize a symmetric space is to consider the corresponding Lie algebra, that is the properties of matrices $\mathbf{A}$, defined by $\mathbf{T} = \exp(\mathbf{A})$. Now, one defines eigenvectors $X$ of $A$, by the commutation relation $[\mathbf{A}, \mathbf{X}] = a\mathbf{X}$. The degeneracy of the eigenvalue $a = 0$ defines the rank $r$ of the Lie algebra. The set of eigenvectors $\mathbf{H}_i$, $i = 1, \ldots, r$ witheigenvalue $a = 0$ forms an Abelian subalgebra, the so called Cartan Algebra, since $[\mathbf{H}_i, \mathbf{H}_j] = 0$ for all $i = 1, \ldots, r$. Since every matrix $\mathbf{A}$ commutes with itself, $[\mathbf{A}, \mathbf{A}] = 0$, it can be written as a linear superposition $\mathbf{A} = \sum_{i=1}^{r} \lambda_i \mathbf{H}_i$. There are $N - r$ eigenvectors $\mathbf{E}_i$, $i = r + 1, \ldots, N$ of $\mathbf{H}_i$, $i = 1, \ldots, r$ with non-zero eigenvalues $\alpha_1, \ldots, \alpha_r$. The vector of non-zero eigenvalues $\boldsymbol{\alpha} = (\alpha_1, \ldots, \alpha_r)$ is called the root of the algebra. These roots can be characterized by their length, and their degeneracy, the so-called multiplicity. If there is only one eigenvector to a root $\alpha$ it is called a simple root. Now, it can be shown that the parameters entering in the above formula for the quasi-one-dimensional localization length, Eq. (298), $\beta$ and $m_l$ are the multiplicities of roots on the respective symmetric space G/K [255,256].

We have listed their values in Tables 3–5. The factor $s$ accounts for the fact that spin flip scattering from magnetic impurities mixes the two spin channels, and thereby can double the effective number of channels. Thus, $s = 1$, without spin scattering, and $s = 2$ with spin scattering. The integer $N$ is the number of transverse channels in the quantum wire, and $l$ the elastic mean free path. This formula, Eq. (298) coincides for the ordinary symmetry classes with the well-known result derived independently by Efetov and Larkin, and by Dorokhov, namely that the localization length is proportional to the symmetry parameter $\beta$ [87,269–274]. For the ordinary and the chiral classes $\beta$ takes the well-known conventional values $\beta = 1, 2, 4$, $m_l = 1$ for the orthogonal, unitary and symplectic class, respectively.

For the Bogoliubov–de-Gennes–Oppermann class, however, $\beta$ and $s$ have quite unexpected values. Moreover, in the classes D and DIII, the multiplicity $m_l$ vanishes. This implies a diverging localization length. For weak Gaussian disorder the conductance in classes D and DIII has the broad distribution typical for a critical state [261]. Accordingly, in a gapless superconductor with broken spin symmetry the quasi-particles are delocalized for weak disorder. Since both, the charge and the spin, are not good quantum numbers in such a system, the metallic character of the quasi-particles can only be measured due to their finite contribution to transport of heat which can be measured via the thermal conductance [263].

In order to understand this better, it is enlightening to generalize briefly the concept of the quantization of the electrical—charge—conductance to the thermal and the spin conductance.

The defining relations of charge, spin and heat conductivities are

$$\boldsymbol{j}^{\mathbf{c}} = \left(\frac{\sigma^{\mathrm{c}}}{e}\right) \nabla(eV) \ , \tag{299}$$

$$\boldsymbol{j}^{\mathbf{s}} = \left(\frac{\sigma^{\mathrm{s}}}{\mu_{\mathrm{B}}\hbar/2}\right) \ , \nabla\left(\frac{\mu_{\mathrm{B}}\hbar}{2}B\right) \ , \tag{300}$$

$$\boldsymbol{j}^{\mathbf{q}} = \left(\frac{\kappa}{k_{\mathrm{B}}}\right) \nabla(k_{\mathrm{B}}T) \ , \tag{301}$$

with electron charge $-e$, voltage $V$, Bohr magneton $\mu_{\mathrm{B}}$, Boltzmann constant $k_{\mathrm{B}}$, and temperature $T$. The charge, spin and heat conductivities are denoted as $\sigma^{\mathrm{c}}$, $\sigma^{\mathrm{s}}$ and $\kappa$, respectively. One can easily verify that these are consistent with the usual linear response definition apart from rewriting the current densities as the responses to gradients of energies instead of fields. We also recall that thermal and electrical currents are related via the Wiedemann–Franz law

$$\frac{\kappa}{\sigma^{\mathrm{c}}T} = \frac{\pi^2}{3}\frac{k_{\mathrm{B}}^2}{e^2} \ . \tag{302}$$

The quantization of the charge conductance in terms of $\sigma_0 = e^2/h$ implies that the conductance per charge is given by the ratio of the elementary charge and the Planck constant, $\sigma_0^{\mathrm{c}}/e = e/h$. Analogously, the quantum of the spin conductance will then be given by the ratio between elementary spin and the Planck constant, $\sigma_0^{\mathrm{s}}/(\mu_{\mathrm{B}}\hbar/2) = (\hbar/2)/h$. This implies

$$\sigma_0^{\mathrm{s}} = \mu_{\mathrm{B}}\frac{(\hbar/2)^2}{h} \ . \tag{303}$$

The quantum of the heat conductance should be given by the ratio between the heat per free particle $Q_0$ and the Planck constant. The heat per charge carrier can be deduced from the thermopower $S$

$$eST = \frac{\pi^2}{3}k_{\mathrm{B}}T\left(\frac{k_{\mathrm{B}}T}{2E_{\mathrm{F}}}\right) \ , \tag{304}$$

where the last factor accounts for the fact that only electrons in a temperature window $k_{\mathrm{B}}T$ near the surface of the Fermi sea contribute. Note that the factor $\pi^2/3$ is the first Sommerfeld expansion parameter in the expansion of the energy integral around the Fermi surface, which does not depend on dimensionality. From this one concludes

$$Q_0 = \frac{\pi^2}{3}k_{\mathrm{B}}T \tag{305}$$

and from

$$\frac{\kappa_0}{k_{\mathrm{B}}} = \frac{Q_0}{h} \tag{306}$$

follows that

$$\kappa_0 = \frac{\pi^2}{3}\frac{k_{\mathrm{B}}^2 T}{h} \ . \tag{307}$$

In the following, we apply this to the case of a quantum Hall system. We use units such that $\mu_{\mathrm{B}} = 1$.

When a temperature difference smaller than the Landau gap is applied to two opposite edges of a quantum Hall bar, there is no thermal transport between the edges, if the Fermi energy is pinned to localized bulk states. Still, the total heat current perpendicular to the temperature gradient is non-vanishing, since the quasi-particles on the hot edge of the sample carry more heat in one direction than the quasi-particles on the cooler edge in the opposite direction. This results in a finite thermal Hall conductance $\kappa_{xy}$ defined by

$$I_x^Q = \kappa_{xy} \Delta_H T \ , \tag{308}$$

where $\Delta_H T$ is the temperature difference between the edges and $I_x^Q$ the total heat current. One finds that one edge channel contributes towards the thermal Hall conductance with the quantized amount given in Eq. (307) [275],

$$\kappa_{xy} = \frac{\pi^2}{3} \frac{k_B^2 T}{h} \ . \tag{309}$$

As the *charge* Hall conductance, the *thermal* Hall conductance is non-zero only for broken time reversal symmetry and broken parity. Non-vanishing values can thus only be obtained in *directed* network models.

There has been some debate [238,263,276,277] if this critical metal phase of classes D and DIII persists due to the particular symmetry even at strong disorder as argued in [267], or if there could be a regime of localized phases characterized by a quantized thermal Hall conductance parameter, in units of the thermal conductance quantum $\kappa_0$,

$$\sigma_{xy}^T = \frac{3h\kappa_{xy}}{\pi^2 k_B^2 T} \ , \tag{310}$$

with quantum Hall-type transitions between phases with $\sigma_{xy}^T = 0$ and $\sigma_{xy}^T = 1$ [275]. One could refer to this transition, accordingly, as the thermal quantum Hall transition.

Recently, several investigations have concluded that the phase diagram of models belonging to class D critically depends on the spatial correlations of the disorder potential and that the metal phase persists to strong disorder only for uncorrelated, white noise disorder [210,258,261,278]. If there is at strong disorder a transition to a localized phase, and the time reversal symmetry is broken, as it is the case in class D, there can be a finite thermal Hall conductance $\kappa_{xy}$. Fig. 36 shows schematically the suggested two-parameter flow diagram for correlated disorder [238,263,277] as a function of the thermal conductance parameter

$$\sigma_{xx}^T = \frac{3h\kappa_{xx}}{\pi^2 k_B^2 T} \tag{311}$$

and the thermal Hall conductance parameter $\sigma_{xy}^T$. Such a thermal metal insulator transition and the corresponding thermal quantum Hall transition are expected to have very different critical properties from the integer quantum Hall transition (Table 4).

When the time reversal symmetry is broken but global SU(2) spin rotation symmetry is not, then the quasi-particles in a superconductor can be studied both by their contribution to thermal and to spin transport. In two dimensions this class, denoted as C in Table 4, can be studied in d-wave superconductors. Here, the order parameter vanishes at four nodal points on the Fermi surface. This allows to study the peculiar properties of the quasi-particles which occur close to the Fermi energy due to the particle–hole

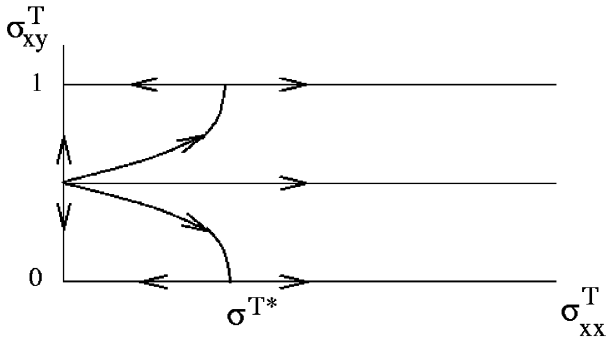


Fig. 36. Scheme of the quantum Hall flow diagram of class D systems in the plane of the local thermal conductance and thermal Hall conductance parameters, $\sigma^{\mathrm{T}}_{xx}$ and $\sigma^{\mathrm{T}}_{xy}$, respectively, for correlated disorder where an insulating and a quantum Hall phase can exist [238,263,277]. For weak disorder (large $\sigma^{\mathrm{T}}_{xx}$), the critical metal phase is stable for all values of the Hall conductance. For uncorrelated disorder, this is the only possible phase for any value of $\sigma^{\mathrm{T}}_{xx}$. Correspondingly, $\sigma^{T*}=0$ for uncorrelated disorder. For strong correlated disorder there is a flow towards an insulating phase for $\sigma^{\mathrm{T}}_{xy}<1/2$, and a flow to a phase with quantized Hall thermal conductance for $\sigma^{\mathrm{T}}_{xy}>1/2$, respectively.

symmetry in class C. As seen from Eq. (298), the quasi-particles in a quasi-one-dimensional wire belonging to class C are localized. From results of perturbative renormalization group studies, one can conclude that they stay localized in two dimensions [279].

However, in close analogy to the quantum Hall transition, a localization–delocalization transition is possible in which the quantized Hall conductance for the *spin*, $\sigma^{\mathrm{s}}_{xy}$, is quantized.

The spin transport is caused by a gradient in the perpendicular magnetic field which results in a gradient in the Zeeman energy. In linear response the spin current is [280] (Eq. (300)),

$$\boldsymbol{j}^{\mathrm{s}} = \sigma^{\mathrm{s}} \nabla B \ , \tag{312}$$

where $\sigma^{\mathrm{s}}$ is now a $2\times 2$-matrix with components $\sigma^{\mathrm{s}}_{xx}$ and $\sigma^{\mathrm{s}}_{xy}$. When the Fermi energy is pinned to localized bulk states, the edge states carry a finite spin current perpendicular to the gradient of the magnetic field,

$$j^{\mathrm{s}}_x = \sigma^{\mathrm{s}}_{xy} \nabla_y B \ . \tag{313}$$

When the quasi-particles carry the spin $1/2$, the spin Hall conductance, $\sigma^{\mathrm{s}}_{xy}$ turns out to be quantized in two dimensions in multiples of the quantum of the spin conductance $\sigma_0$ (Eq. (303)),

$$\sigma^{\mathrm{s}}_{xy} = m\mu_{\mathrm{B}} \frac{(\hbar/2)^2}{h} \ , \tag{314}$$

where $m$ is found to take only values $0, \pm 2$ [277], very similar to the quantization of the charge Hall conductance in units of $e^2/h$. The spin angular momentum $\hbar/2$ is substituted for the electron charge $e$. Changing the Fermi energy one finds spin quantum Hall plateau transitions where the spin Hall conductance changes by two units. This transition is in a new universality class, and called the *spin quantum Hall transition* (SQHT). When a strong Zeeman term is introduced which reduces the SU(2) symmetry of the spin to U(1), this transition splits into two, each of them being in the usual universality class of the integer quantum Hall transition [264,265,279–281]. The spin quantum Hall transition can also be probed

by the thermal conductance, which in a metal phase is related to the spin conductance by the analogue of the above Wiedemann–Franz law

$$\frac{\kappa}{\sigma^{\mathrm{s}} T} = \frac{\pi^2}{3} \frac{k_{\mathrm{B}}^2}{(\hbar/2)^2} \ . \tag{315}$$

Recently, a model belonging to class C has been mapped on the classical percolation model [264,282]. This made it possible to determine the exact critical exponents of the spin quantum Hall transition, like the exponent of the divergent localization length, $\nu = \nu_{\mathrm{p}} = 4/3$. The mapping is reviewed below, when the Class C network model is introduced in more detail. We note that disordered d-wave superconductors also have been argued to be in the chiral class AIII, yielding delocalized quasi-particles close to the Fermi energy [262]. This situation arises for a slowly varying disorder which has negligibly small Fourier components for scattering between the four nodal points where the gap in the quasi-particle density of states is vanishing. For each node, the quasi-particles independently can be modeled by Dirac fermions. In a magnetic field, which breaks the time reversal invariance, this leads to the sub-lattice class AIII [262].

Sub-lattice models exhibit some similarity to a quantum Hall transition, since they have one extended state in the middle of a band of localized states. Their Hamiltonian is given by a tight-binding model on a two-dimensional bipartite lattice. There are no on-site potentials, and the hopping matrix elements are random. Thus, they have perfect particle–hole symmetry. In contrast to the models for the integer Quantum Hall Effect, two-sub-lattice models have a divergent density of states in the center of the band where the extended states appear. For the unitary (AIII) and the orthogonal (BDI) chiral classes, the density of states diverges,

$$\rho(E) \propto \frac{1}{|E|} \mathrm{e}^{-c|\ln E|^{1/x}} \ , \tag{316}$$

with constant $c$. By using field theory, Gade obtained $x = 2$ for both classes, AIII and BDI [251,252]. By considering random Gaussian surfaces, and numerically, the value $x = 3/2$ was obtained for class BDI [204]. This result for BDI was also derived with the supersymmetry method [205] and was argued to be a direct consequence of the freezing transition of the dynamical exponent $z$ [204,205,283–285], which is related to the fact that the multi-fractal spectrum is bounded [285]. While it has been suggested that this freezing transition is not sensitive to time reversal and spin symmetry and therefore the value $x = 3/2$ could be valid for the chiral classes, AIII and CII, as well [205], a derivation is pending.

The model of Dirac fermions in a random vector potential (Section 7.2) is another member of the symmetry class AIII. Although a divergence of the density of states has been found here as well, the corresponding exponent is varying continuously with the disorder strength [120]. When moving away from the band center, the sub-lattice models acquire the properties of the ordinary models, and the states are localized for the orthogonal and unitary models. Sub-lattice models with directed bonds have recently been established [259]. Their critical properties still have to be studied in detail. So far, the symplectic sub-lattice class has been studied only briefly [286].

According to the above description, the delocalization transition of the Chalker–Coddington network model without particle–hole symmetry should be insensitive to the spin rotation symmetry, since the conventional unitary class makes no distinction whether or not that symmetry is broken. This argument does not take into account that the lifting of the spin degeneracy can result in a change of the statistically relevant density of states and thereby also a change in the localization behavior. This has been first noted for localization in quasi-one-dimensional disordered wires without time reversal symmetry, where the

localization length is doubled when the spin degeneracy is broken, Eq. (298) [269,274]. Recently, it has been argued within a semi-classical percolation model [287], that spin–orbit scattering can change the universality class from the one of the conventional quantum Hall transition to the one of classical percolation. In short, the argument is that the Hamiltonian with spin–orbit scattering and random scalar potential reduces—in an adiabatic approximation—to the Hamiltonian of electrons with opposite spins moving in the effective potential which is the sum of the scalar potential and the positive/negative locally varying random Zeeman fields for the electrons with spin up and spin down, respectively. Thus, the electrons with opposite spins do see different randomness. Close to saddle points in the effective potential, the electrons have the choice of either to tunnel while keeping their spin or to flip their spin using the non-adiabatic part of the spin–orbit interaction, and then continue to propagate in the potential landscape corresponding to the opposite spin. For a potential with a sufficiently short correlation length, the potential landscapes for the electrons with spin up and spin down should be sufficiently different that this argument applies. This argument suggests that the critical exponent of the localization length in that situation is close to the one of classical percolation, $\nu = \nu_{\mathrm{p}} = 4/3$ [287]. The obvious similarity of this model to models of the Bogoliubov–de-Gennes–Oppermann class, when identifying the spin flip scattering with the anomalous pairing amplitude $\Delta$, coupling electrons with holes may be used as a heuristic explanation for the change of the universality class to the one of the classical percolation transition, in class C models. Indeed, the network model of class C with SU(2)-scattering phases at the links has been first studied as a model of spin degenerate Landau levels with negligible random potential and strong spin–orbit scattering [248]. Another realization would be Landau levels with strong magnetic impurities [253]. This was found to have a single quantum critical point with $\nu \approx 1.1$ [248].

In order to study quantitatively the localization properties of the metal–insulator transitions and the quantum Hall transitions it is necessary to formulate specific network models for the various symmetry classes. In the next section, we introduce non-directed network models for the three ordinary symmetry classes, of which only the symplectic one is expected to have a metal–insulator transition. Next, we review unitary network models with two spin channels that describe the transition of quantum Hall systems with mixing between spin split Landau levels. Then, we review the network models for transitions of the quantum Hall type belonging to the Bogoliubov–de-Gennes–Oppermann class. Finally, we provide an overview on the network models for sub-lattice systems.

### *9.2. Non-directed network models*

In order to construct network models belonging to the orthogonal and symplectic classes, one should assume links that are not directed. Following early work on the scattering matrix formulation of the scaling theory of Anderson localization [288], an example of such a model has been established and studied by using the real space renormalization group method by Shapiro in 1982 [289]. Recently, such network models have been explored numerically for all of the three conventional symmetry classes [260,290]. The results of the scaling theory of localization have been reproduced: a localized phase exists for the unitary and orthogonal classes, and a metal–insulator transition occurs in the symplectic class. The corresponding **S** matrices are unitary, symmetric, and symplectic [87].

The fact that the links are not directed, but nevertheless the time reversal symmetry is broken for non-directed unitary network models, makes these models equivalent to two-dimensional random fermions in a weak magnetic field that does not affect the classical motion of the electrons. Accordingly, extended states are not expected to exist. This has been confirmed by extensive numerical studies [290].

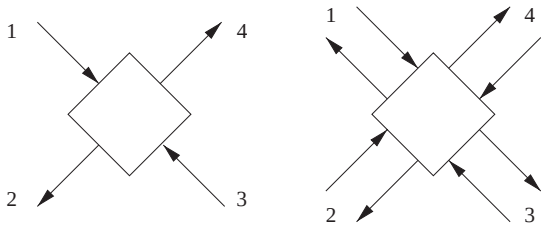


Fig. 37. Comparison of the nodes of a directed (left) and a non-directed network model (right).

In non-directed networks, the scattering matrices representing the nodes relate four incoming to four outgoing currents (Fig. 37),

$$\begin{pmatrix} \psi_1^{\mathrm{o}} \\ \psi_2^{\mathrm{o}} \\ \psi_3^{\mathrm{o}} \\ \psi_4^{\mathrm{o}} \end{pmatrix} = \mathbf{S}_{\mathrm{orth}} \begin{pmatrix} \psi_1^{\mathrm{i}} \\ \psi_2^{\mathrm{i}} \\ \psi_3^{\mathrm{i}} \\ \psi_4^{\mathrm{i}} \end{pmatrix} . \tag{317}$$

With time reversal invariance, the **S** matrix is symmetric [87]. By assuming isotropy of the scattering, it can be cast into the form [260]

$$\mathbf{S}_{\mathrm{orth}} = \begin{pmatrix} r & d & t & d \\ d & r & d & t \\ t & d & r & d \\ d & t & d & r \end{pmatrix} , \tag{318}$$

where $t$, $r$ and $d$ denote transmission, reflection and deflection amplitudes, respectively. It is assumed here that the deflection to the left and to the right are equal, as it should be for a network without chirality. The scattering parameters are complex and satisfy the conditions

$$\begin{aligned} &|r|^2 + |t|^2 + 2|d|^2 = 1 \ , \\ &d^* r + d r^* + d^* t + d t^* = 0 \ , \\ &2|d|^2 + r^* t + r t^* = 0 \ . \end{aligned} \tag{319}$$

From the 1st and the 3rd condition one finds the relations

$$|r|^2 + |t|^2 \leqslant 1 \ , \quad 1 \leqslant |r| + |t| \ . \tag{320}$$

The second inequality is violated when the time reversal symmetry is broken.

Due to random phases attached to links, we can always set $d$ to be a real positive number. Then, once $|r|$ and $|t|$ are given, $r$, $t$ and $d$ are uniquely determined by Eq. (320).

Though the transfer matrix, at first sight, seems to be complex, the calculation can be performed with only real (or quaternion-real) numbers after a proper unitary transformation [291].

In order to construct a model belonging to the symplectic class, we first establish a scatterer that rotates the direction of the spin [260]. The **S** matrix relates the currents with spin up (↑) and spin down (↓)

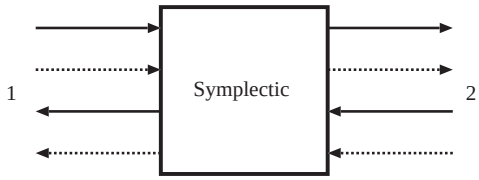


Fig. 38. Schematic view of a scatterer that provides spin rotation. Solid arrows correspond to spin-up currents. Broken arrows indicate spin-down currents.

according to Fig. 38

$$\begin{pmatrix} \psi^{\mathrm{o}}_{1,\uparrow} \\ \psi^{\mathrm{o}}_{1,\downarrow} \\ \psi^{\mathrm{o}}_{2,\uparrow} \\ \psi^{\mathrm{o}}_{2,\downarrow} \end{pmatrix} = \mathbf{S}_{\mathrm{symp}} \begin{pmatrix} \psi^{\mathrm{i}}_{1,\uparrow} \\ \psi^{\mathrm{i}}_{1,\downarrow} \\ \psi^{\mathrm{i}}_{2,\uparrow} \\ \psi^{\mathrm{i}}_{2,\downarrow} \end{pmatrix} \tag{321}$$

with

$$\mathbf{S}_{\mathrm{symp}} = \begin{pmatrix} 0 & q \\ \overline{q} & 0 \end{pmatrix} . \tag{322}$$

This choice of symplectic scattering matrices mixes only different spin channels moving in the same direction, but does not have backscattering matrix elements. Backscattering occurs thus in this model at the orthogonal nodes only. Here, $q$ is a quaternion-real number,

$$q = \sum_{k=0}^{3} q_k \tau_k \ , \quad \tau_k = \mathrm{i}\sigma_k \ (k = 1, 2, 3) \quad \tau_0 = \mathbf{1} \ . \tag{323}$$

The coefficients $q_k$ are real numbers that satisfy

$$\sum_{k=0}^{3} q_k^2 = 1 \tag{324}$$

and the $2 \times 2$-matrices $\sigma_k$ are the Pauli spin matrices. The quaternion conjugate is denoted by $\overline{q}$.

$$\overline{q} = q_0 \mathbf{1} - \sum_{i=1}^{3} q_i \tau_i \ . \tag{325}$$

The strength of the spin–orbit scattering is characterized by the distribution of $q_i$. When $q_0 = 1$, $q_1 = q_2 = q_3 = 0$ there is no spin–orbit scattering. The spin rotation is most random when

$$\begin{aligned} q_0 + \mathrm{i}q_3 &= \mathrm{e}^{\mathrm{i}\alpha} \cos\beta \ , \\ q_1 + \mathrm{i}q_2 &= \mathrm{e}^{\mathrm{i}\gamma} \sin\beta \end{aligned} \tag{326}$$

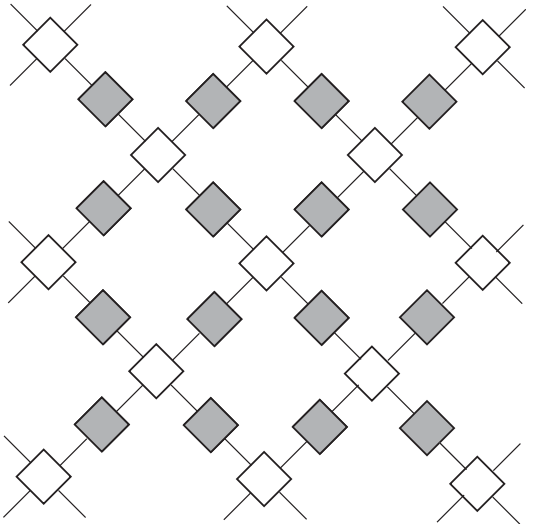

Fig. 39. Network of nodes realizing the symplectic class. White boxes describe scattering with orthogonal symmetry. Shaded boxes rotate spin, thus breaking spin rotation invariance.

with $\alpha$ and $\gamma$ distributed uniformly between $[0, 2\pi)$, and $\beta$ distributed according to the probability density,

$$P(\beta) = \begin{cases} \sin(2\beta) & 0 \leqslant \beta \leqslant \pi/2 \ , \\ 0 & \text{otherwise} \ . \end{cases} \tag{327}$$

As before, one attaches random phases between the nodes described by the **S** matrix

$$\mathbf{S}_{\text{link}} = \begin{pmatrix} 0 & \mathrm{e}^{\mathrm{i}\phi} \\ \mathrm{e}^{\mathrm{i}\phi} & 0 \end{pmatrix} \ . \tag{328}$$

The resulting network is shown in Fig. 39. This model is similar in spirit but different in the details as the tight-binding Hamiltonian on a square lattice including spin–orbit scattering proposed in [292,293,114]. A similar model also has been proposed in [294].

Fig. 40 shows some results for the localization length $\lambda(L)$ in a two-dimensional strip of the width $L$. The renormalized localization length $\Lambda = \lambda(L)/L$ as a function of $|r|$ is plotted for different $L$. When $|r|$ is smaller than 0.61, $\Lambda$ increases with increasing $L$. It is decreasing function of $L$ for $|r| > 0.63$. This behavior indicates a delocalization–localization transition [17]. For the symplectic symmetry there occurs a metal–insulator transition in two dimensions as has been conjectured before [295]. By analyzing the data using the finite-size scaling method the critical exponent can be extracted (cf. Table 3). The estimates with 95% confidence interval, $\nu = 2.81 \pm 0.05$, $\Lambda_{\mathrm{c}} = 1.836 \pm 0.027$, agree within the uncertainty with the result of numerical studies done for the tight-binding Hamiltonian, $\nu = 2.746 \pm 0.009$, $\Lambda_{\mathrm{c}} = 1.843 \pm 0.001$ [114,115].

To construct orthogonal and a unitary nondirected network models, we assume in $\mathbf{S}_{\text{symp}}$ $q = 1$. In the unitary case, $\mathbf{S}_{\text{link}}$ is no longer symmetric,

$$\mathbf{S}_{\text{link}}^{\text{unitary}} = \begin{pmatrix} 0 & \mathrm{e}^{\mathrm{i}\phi} \\ \mathrm{e}^{\mathrm{i}\phi'} & 0 \end{pmatrix} \ . \tag{329}$$

In both cases, we have spin degeneracy, and the dimension of the transfer matrix is halved.

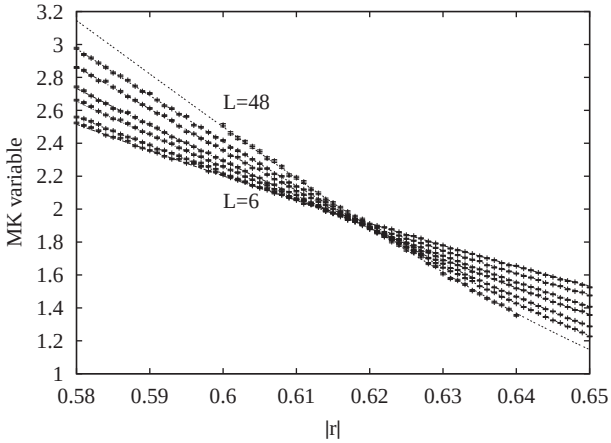


Fig. 40. MacKinnon–Kramer variable $\Lambda$ as a function of $|r|$ for $|t| = 0.6$; $|d|$ is determined according to Eq. (320); $L = 6,8,12,16,24,32$ and 48; precision of the data is 0.2% except for $L = 48$ where it is 0.4%. Curves intersect approximately at $|r| = 0.62$, which indicates the presence of an Anderson metal–insulator transition in two dimensions.

### *9.3. Network models of the Bogoliubov–de-Gennes–Oppermann class*

#### *9.3.1. Class C*

As mentioned above, systems belonging to the Bogoliubov–de-Gennes–Oppermann class have a particle–hole symmetry, and the spectrum of eigenvalues consist of pairs, $(-E_n, E_n)$. The zero of energy, $E = 0$, is the chemical potential in the superconductor. Class C describes quasi-particles in a spin-singlet superconductor in which time-reversal symmetry is broken, but spin rotation symmetry is conserved. This corresponds to systems with negligibly small Zeeman splitting [244]. Far away from the Fermi energy, the transport properties show a crossover to the conventional unitary class A. Therefore, class C behavior can only be studied in gapless superconductors or in metals closely attached to superconductors, where quasi-particles close to the Fermi energy exist. As summarized in Table 4, the quantum states of quasi-particles in non-directed models of the class C are localized. This phase is named spin insulator, because the insulating behavior reveals itself only as a vanishing spin or thermal conductance, since the charge is not conserved in a superconductor. When parity symmetry is broken, as in directed network models, there can be a quantum Hall-type transition to a phase with a critical state and an integer-quantized spin Hall conductance $\sigma^{\mathrm{s}}_{xy}$. This is called the SQHT.

Thus, we are now looking for a generalization of the Chalker–Coddington model which satisfies the particular symmetries of class C [264,265,281]. In the simplest case, one has two-component wave functions, which propagate on directed links through the lattice, and which scatter at nodes between adjacent links. All the nodes in the lattice have two incoming and two outgoing links. It turns out [264], that the SQHT can be determined from the properties of the perimeters, or hulls, of classical percolation clusters on a two-dimensional lattice constructed of such nodes and links. This classical problem is much simpler than the original quantum problem, and can be solved exactly, for example by mapping it on an integrable super-spin chain [264] which will be introduced below in Section 10.

In the following, we review the models for class C, as introduced by Beamond et al. [265]. A similar network model with SU(2) scattering phases at the links has been studied before in the context of the

Quantum Hall Effect of spin degenerate Landau levels [248]. We consider a set of nodes $n$ connected by links $l$. Each node is assumed to be of the degree four, such that at each node two directed links enter and two leave. A two-component wave function is assumed to propagate along each link. This propagation may be described by a unitary evolution operator $\mathbf{U}$, which describes the evolution of the wave function one unit forward in "time", as the particle moves from a given link to a neighboring one. The evolution operator plays a similar role in defining the network model as the time evolution operator corresponding to a Hamiltonian, for example, of a tight-binding model. This procedure has been discussed in detail before for the U(1) network model in [121,189] (Section 7).

The model can be constructed by associating each link $l$ with a unitary $2 \times 2$-matrix $\mathbf{U}_l$. This matrix specifies the phase accumulated when traversing the link. Each node $n$ is assumed to be represented by a scattering matrix (Section 3.2)

$$\mathbf{S}_n = \mathbf{1}_2 \otimes \begin{pmatrix} \cos\theta_n & \sin\theta_n \\ -\sin\theta_n & \cos\theta_n \end{pmatrix} , \tag{330}$$

where $\mathbf{1}_2$ is the $2 \times 2$ unit matrix. The $\mathbf{S}$ matrix describes scattering at the node from the incoming links to the outgoing ones. If the network has $M$ links (and therefore $M/2$ nodes), then $\mathbf{U}$ is an $N \times N$ matrix, with $N = 2M$. It consists of $M/2$ blocks, each associated with a particular node and of size $4 \times 4$. The block at the node $n$ has the form

$$\begin{pmatrix} \mathbf{U}_3^{1/2} & 0 \\ 0 & \mathbf{U}_4^{1/2} \end{pmatrix} \mathbf{S}_n \begin{pmatrix} \mathbf{U}_1^{1/2} & 0 \\ 0 & \mathbf{U}_2^{1/2} \end{pmatrix} , \tag{331}$$

where $(1, 2)$ and $(3, 4)$ label the links which are incoming and outgoing at the given node.

So far, we only have assumed the links to be directed, so that time reversal symmetry is broken. To identify a network model to belong to class C, one can start [281] from the defining property of a Hamiltonian $\mathbf{H}$ with this symmetry [244]

$$\mathbf{H}^* = -\sigma_y \mathbf{H} \sigma_y , \tag{332}$$

with the Pauli matrix $\sigma_y$ acting on the spin variables. The operator $H^*$ is the complex conjugate of $\mathbf{H}$. With this Hamiltonian, and using that $\mathbf{U}$ can be written as

$$\mathbf{U} = \mathrm{e}^{-\mathrm{i}\mathbf{H}} , \tag{333}$$

Eq. (332) implies

$$\mathbf{U} = \sigma_y \mathbf{U}^* \sigma_y . \tag{334}$$

From this, an equivalent restriction follows for the phases of the links,

$$\mathbf{U}_l = \sigma_y \mathbf{U}_l^* \sigma_y \tag{335}$$

which are therefore unitary Sp(2)-matrices equivalent to SU(2)-matrices, where $Sp(2N)$ is defined to be the symplectic group of $2N \times 2N$ matrices $\mathbf{A}$ which fulfill the condition $\mathbf{A}^{\mathrm{T}} \sigma_y \mathbf{A} = \sigma_y$ [265]. The wave function consists of two components in each link. The space of states on each link may be viewed as consisting of a two-dimensional subspace, within which $\sigma_y$ operates.

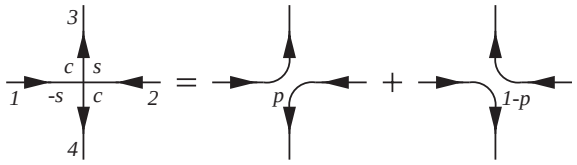


Fig. 41. Decomposition of the scattering at a given node: **S** matrix elements $\cos\theta_n$ and $\pm\sin\theta_n$ are associated with the transitions $(1,2)\to(3,4)$ as indicated on the left. The two decompositions are weighted with factors $p_n=\cos^2\theta_n$ and $1-p_n=\sin^2\theta_n$ (figure taken from [265]).

One possibility to introduce randomness into the model consists of assuming the link phases to be random variables drawn independently from a distribution which is uniform on the invariant (Haar-)measure of Sp(2). The ensemble average of a physical quantity in the network model, denoted by $\langle\ldots\rangle$, is the mean with respect to this measure.

As reviewed in Section 5.1, the conductance of an open network of a finite length can be expressed by the multi-channel Landauer formula in terms of the transmission probability. Specifically, the spin conductance measured between two contacts in units of $(\hbar/2)^2/h$ is given by Eq. (147),

$$g=\mathrm{Tr}\,\mathbf{t}\mathbf{t}^\dagger\ . \tag{336}$$

Here, $\mathbf{t}$ is the rectangular $N\times N$ transmission matrix containing the matrix elements for $z=1$ of the propagation operator

$$\mathbf{G}(z)=\frac{1}{1-z\mathbf{U}} \tag{337}$$

between the incoming and outgoing link states $l_\mathrm{i}$ and $l_\mathrm{o}$.

One can now show that the disorder average $\mathrm{Tr}\,\langle\mathbf{G}(z)\rangle$ taken over the Sp(2)-phase factors of the Green function

$$G(z;l,l')=\langle l|(1-z\mathbf{U})^{-1}|l'\rangle \tag{338}$$

can be expressed in terms of classical paths [264,265].

To illustrate this, we define for the same network a *classical* scattering problem as follows. The scattering at each node may be decomposed into disconnected processes in two different ways, $(1\to3,2\to4)$ and $(1\to4,2\to3)$ (Fig. 41).

A two-dimensional model exhibiting the spin Quantum Hall Effect is obtained by taking the network to be the so-called L-lattice shown in Fig. 42. The two possible classical decompositions of a node may be associated with the presence or absence of a bond, with probabilities $p$ and $1-p$ between neighboring sites on an associated square lattice [264]. The latter is rotated by 45° relative to the L-lattice, and has a lattice spacing increased by a factor $\sqrt{2}$. In this model, closed loops of the classical problem form interior or exterior hulls of bond percolation clusters on the larger lattice. It is known that such loops are finite with characteristic size $\xi(p)<\infty$ except at the critical point, $p=p_c$, which for bond percolation on the square lattice occurs at $p_c=1/2$. When approaching the critical point, $\xi$ diverges as $\xi\sim|p-p_c|^{-\nu}$ with $\nu=\nu_\mathrm{p}=4/3$ (Section 2), while at the critical point the distribution of the hull lengths is $P(L)\sim L^{-y}$ at large $L$, with $y=8/7$.

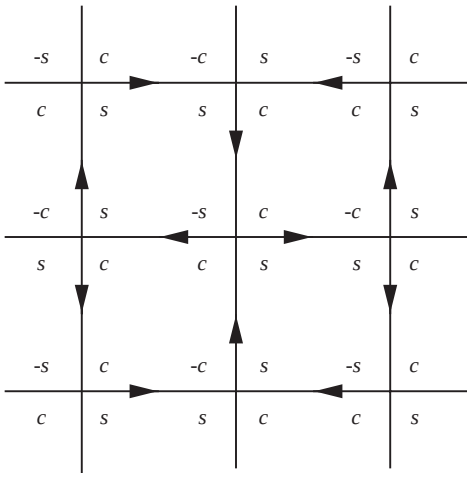


Fig. 42. The network model for the spin Quantum Hall Effect. Scattering amplitudes $\pm\cos\theta_n$ and $\pm\sin\theta_n$ are indicated by $\pm c$ and $\pm s$ (figure taken from [265]).

The quantum localization length in this class C model diverges with the same value of the exponent, $\nu = \nu_{\mathrm{p}} = 4/3$, as the plateau transition is approached. The density of states

$$\rho(E) = -\frac{1}{\pi}\,\mathcal{I}m\,\mathrm{Tr}\langle \mathbf{G}(E)\rangle \tag{339}$$

varies for small $E$ as

$$\rho(E) \sim E^2 \tag{340}$$

in the localized phase, and as

$$\rho(E) \sim |E|^{1/7} \tag{341}$$

near the critical point (Table 4).

### 9.3.2. Class D

As described in the introduction to this section (Table 4 and Fig. 36), models in class D have particularly rich phase diagrams in two dimensions. The symmetry is realized in superconductors with broken time reversal invariance, and either broken spin rotation invariance, as in d-wave superconductors with spin–orbit scattering, or spin-less or spin-polarized fermions, as in certain p-wave states. Since the spin rotation symmetry is broken, and the charge is not conserved, the quasi-particles can only be measured by their contribution to thermal transport. Eq. (298) shows that quasi-particles are delocalized in quasi-one-dimensional quantum wires belonging to class D. In the two-dimensional case, the flow under the renormalization group is towards larger thermal conductance [263,276,277,296]. Thus, there is a phase in which there is a diverging density of extended eigenstates at zero excitation energy (Table 4 [263]). A superconductor described by this model is in a thermal-metal phase. A phase with localized quasi-particles is a natural possibility, although it has only been found so far for models with correlated disorder [238] which gives rise to a phase with a quantized Hall conductance (Fig. 36).

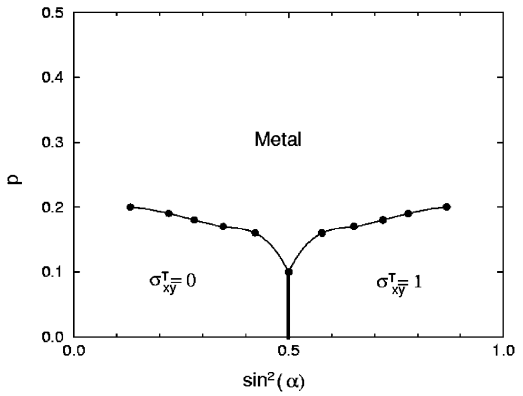


Fig. 43. The phase diagram in the $(p, \alpha)$-plane of the model of Cho and Fisher [209a] obtained by numerical calculations [238]. Here, $\sigma^{\mathrm{T}}_{xy}$ is the thermal Hall conductance parameter defined in Eq. (310), $p$ the disorder parameter, and $\sin^2(\alpha)$ is the tunneling probability (figure taken from [238]).

In analogy with the network models belonging to class C introduced in the previous section, one can formulate a directed network model with the symmetries of class D [238]. Disorder appears in the network model in the form of random scattering phases, and the symmetries of the class D restrict scattering phases to the values 0 and $\pi$, multiplying the wave function at each node at random with phase factors $\pm 1$. Remarkably, within this framework, different particular forms of disorder result in quite different physical behaviors. Depending on the level of correlations between the random phases three cases have been found so far [238,258,297].

The first of these was introduced by Cho and Fisher [209a] with the intention of modeling the two-dimensional random bond Ising model (RBIM) (Section 8) which possesses a fermion representation with the symmetries of class D. Subsequently, it has been noted [210,298] that a precise mapping of the Ising model leads to a second version of the model which accordingly is denoted as random bond Ising model. In both of the models, scattering phases $\pi$ appear in correlated pairs. A third model [238,276] denoted by O(1), can be established if one assumes the scattering phases to be independent random variables. Each model has two parameters: the disorder concentration, $p$ $(0 \leqslant p \leqslant 1)$, and a tunneling amplitude $\sin\alpha$ $(0 \leqslant \alpha \leqslant \pi/2)$ which controls the value of the thermal Hall conductance at short distances.

A phase diagram for the Cho–Fisher model in the $(p, \alpha)$-plane is shown in Fig. 43. It contains three regions: a metallic phase, a localized phase, and a thermal quantum Hall phase. While the random bond Ising model has been shown to have no metallic phase [210] the O(1) model has been argued to have no insulating and thus no quantum Hall phase [267]. Only the Cho–Fisher model has all three phases. It features three potentially different critical points: a quantum Hall-type transition, an insulator-to-metal transition, and a multi-critical point at which all three phases meet. This phase diagram has the form proposed generically for class D [263]. The phase diagram is very complex. The corresponding critical parameters remain to be determined quantitatively. The network model reviewed here [238] will certainly be central in achieving a better understanding of this phase diagram in future investigations. An attempt of understanding the implications of the all-orders beta functions has been made in [299].

### 9.4. Chiral network models

In the following, we shortly summarize the network models of the chiral symmetry classes introduced recently [259]. The network models presented here are connected in two distinct ways to the models without chiral symmetry introduced in the previous sections. Class AIII is connected with the U(1) network model, while CII and BDI belong to the SU(2) and O(1) network models, respectively. They describe the plateau transitions in dirty superconductors, as briefly explained above. In each case, the model with chiral symmetry is constructed by coupling two copies of the partner model. After a transformation, this coupling is equivalent to introducing absorption and coherent amplification in the original models. This equivalence parallels the established link [300] between the chiral symmetry classes and non-Hermitian random operators.

We formulate the network models for each of the chiral symmetry classes by treating in some detail the chiral unitary class (AIII), and outlining the equivalent steps for the chiral orthogonal (BDI) and chiral symplectic (CII) classes [259]. The strategy is to construct the two-dimensional internal space associated with chiral symmetry using two related copies of a network model without that symmetry.

The symmetry may be discussed in terms of a Hamiltonian $\mathbf{H}$, a scattering matrix $\mathbf{S}$, or a transfer matrix $\mathbf{T}$. We consider systems which conserve probability density. The Hamiltonian is Hermitian and the scattering matrix is unitary. The equivalent condition for the transfer matrix involves the operator of the current $J$, and is imposed by current conservation as in Eq. (91),

$$\mathbf{H}^\dagger = \mathbf{H}, \quad \mathbf{S}^\dagger = \mathbf{S}^{-1}, \quad \mathbf{T}^{-1} = \mathbf{J}\mathbf{T}^\dagger\mathbf{J} \ . \tag{342}$$

Chiral symmetry is implemented on a two-dimensional internal space in which the Pauli operator $\sigma_x$ operates. For the Hamiltonian this is equivalent to

$$\sigma_x \mathbf{H} \sigma_x = -\mathbf{H} \ . \tag{343}$$

By assuming the scattering matrix to have the symmetry of $\mathrm{e}^{-\mathrm{i}\mathbf{H}}$, one has

$$\sigma_x \mathbf{S} \sigma_x = \mathbf{S}^{-1} \ . \tag{344}$$

Systems in class AIII have no other relevant discrete symmetry. Those in classes BDI and CII are also invariant under time-reversal, in the presence and absence of spin rotation symmetry, respectively.

#### 9.4.1. Class AIII

We recall first the essential features of the U(1) network model for the integer quantum Hall plateau transition (Section 3), and put them into the present context. The forms of the transfer matrix and of the evolution operator follow from the properties of the elementary building units, sketched in Fig. 44. A wave function in this model takes complex values $\psi_l$ on the links $l$ of the lattice illustrated by the full lines of Fig. 45. A particle acquires a phase $\phi_l$ on traversing link $l$, so that in a stationary state amplitudes at either end are related by

$$\psi' = \mathrm{e}^{\mathrm{i}\phi}\,\psi \ . \tag{345}$$

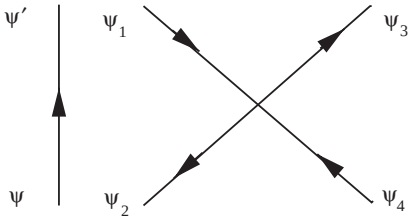


Fig. 44. The elements of the network model: a link (left) and a node (right) (figure taken from [259]).

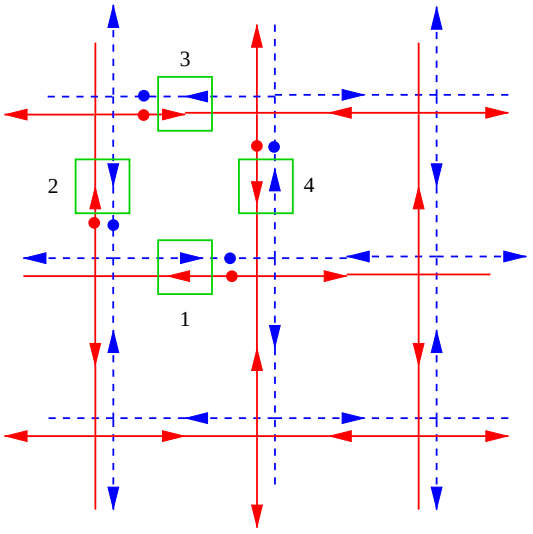


Fig. 45. The structure of the AIII network model. Full and dashed lines indicate the two U(1) models from which the system is constructed, with nodes located at the vertices of the two lattices. Scattering that couples the sub-systems is represented schematically by boxes (upper left plaquette), as parameterized by $\mathbf{T}_{\text{link}}$, Eq. (350). In one step of time evolution, flux propagates between successive points marked with filled circles, in the directions indicated by the arrows (figure taken from [259]).

In a similar way, stationary state amplitudes on the four links which meet at a node are related by a $2 \times 2$ transfer matrix

$$\begin{pmatrix} \psi_1 \\ \psi_2 \end{pmatrix} = \begin{pmatrix} \cosh a & \sinh a \\ \sinh a & \cosh a \end{pmatrix} \begin{pmatrix} \psi_3 \\ \psi_4 \end{pmatrix} , \tag{346}$$

where $a$ is real and all phase factors are associated with links. This equation may be rewritten in terms of a scattering matrix as

$$\begin{pmatrix} \psi_3 \\ \psi_2 \end{pmatrix} = \begin{pmatrix} \cos\alpha & -\sin\alpha \\ \sin\alpha & \cos\alpha \end{pmatrix} \begin{pmatrix} \psi_1 \\ \psi_4 \end{pmatrix} , \tag{347}$$

with $\sin\alpha = \tanh a$. The transfer matrix that results from assembling these units is described in detail in [31], and the time evolution operator in [121,189] (cf. Section 3).

Introducing a two-dimensional internal space associated with the chiral symmetry results in a doubling of the number of wave function components. Thus, starting from two copies of the U(1) model the link amplitudes become two-component complex numbers $\psi_l$. Instead of Eq. (345), the scattering properties of a link now are characterized by a $2 \times 2$ transfer matrix $\mathbf{T}_{\text{link}}$, with

$$\boldsymbol{\psi}' = \mathbf{T}_{\text{link}} \boldsymbol{\psi} \ . \tag{348}$$

Requiring

$$\sigma_x \mathbf{T}_{\text{link}} \sigma_x = \mathbf{T}_{\text{link}} \ , \tag{349}$$

the transfer matrix must have the form

$$\mathbf{T}_{\text{link}} = \mathrm{e}^{\mathrm{i}\phi} \begin{pmatrix} \cosh\, b & \sinh\, b \\ \sinh\, b & \cosh\, b \end{pmatrix} \ , \tag{350}$$

where $\phi$ is a real phase and $b$ is a real hyperbolic angle. It remains to discuss scattering at nodes of the doubled system. We replace Eq. (346) by

$$\begin{pmatrix} \psi_1 \\ \psi_2 \end{pmatrix} = \mathbf{1}_2 \otimes \begin{pmatrix} \cosh\, a & \sinh\, a \\ \sinh\, a & \cosh\, a \end{pmatrix} \begin{pmatrix} \psi_3 \\ \psi_4 \end{pmatrix} \ , \tag{351}$$

where $\mathbf{1}_2$ is here the unit matrix in the two-component space introduced on links. This choice is the most general one which is compatible with chiral symmetry, since scattering within the two-component space may be included in the link transfer matrices $\mathbf{T}_{\text{link}}$.

By combining these elements into a two-dimensional system, we arrive at the model schematically shown in Fig. 45. The transfer matrix for the system as a whole acts in the [1, 1] (or [1, $\bar{1}$]) direction and may be written as a product of factors relating amplitudes on successive slices of the system. Alternate factors in the product represent links and nodes, and consist, respectively, of repeated versions of the $2 \times 2$ and $4 \times 4$ blocks appearing in Eqs. (350) and (351). Disorder is introduced by assuming the phase $\phi$ in Eq. (350) to be independently and uniformly distributed on the links. The parameter $a$, characterizing scattering at nodes, is assumed to be non-random (Section 3).

Two possibilities have been considered for setting the value of the coupling between the chiral subspaces. They are parameterized in terms of either the hyperbolic angle in Eq. (350) or the compact angle $\beta$ related to $b$ by $\sin\beta = -\tanh\, b$. Either $\beta$ is assumed to be uniformly distributed, or $b$ is assumed to be normally distributed with a variance $g$. A disorder parameter $\gamma$ can be defined by

$$\sin\gamma = \tanh\, \sqrt{g} \ . \tag{352}$$

It is guaranteed that the system is statistically invariant under $\pi/2$ rotations of the lattice. This constrains the node parameter $a$, exactly as in the U(1) model: nodes lie on two distinct sub-lattices, and the node parameter $a$ on one sub-lattice is related to the parameter $a'$ on the other sub-lattice by the duality relation (cf. Eq. (95))

$$\sinh\, a\, \sinh\, a' = 1 \ . \tag{353}$$

As before (Section 4.3), the system can alternatively be described using a time evolution operator instead of a transfer matrix. In order to specify this unitary operator, which has the symmetry of a scattering matrix, it is convenient first to consider the limit $b = 0$. Then, the two copies of the network model are

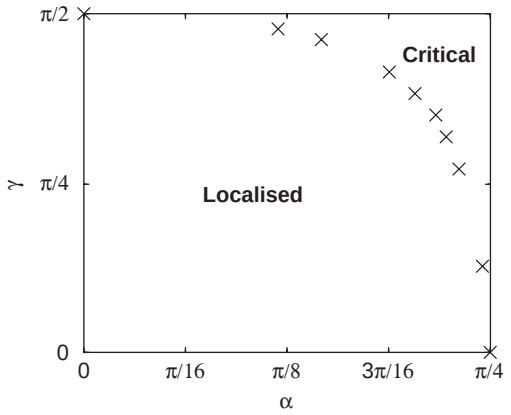


Fig. 46. Phase diagram of the AIII network model in the $(\alpha, \gamma)$-plane (figure taken from [259]).

uncoupled. One denotes the time evolution operator for one copy by $\mathbf{U}$. Since from Eq. (350) link phases are the same in both copies but propagation directions are opposite, the evolution operator for the other copy is $\mathbf{U}^\dagger$. The dimension of $\mathbf{U}$ is equal to the number of links in the system. It is useful to define a diagonal matrix of the same dimension, with angles $\beta_l$ for each link $l$ as diagonal entries: we use $\beta$ to denote this matrix. The time evolution operator for the system with chiral symmetry can then be written

$$\mathbf{U}_\mathrm{T} = \begin{pmatrix} \mathbf{U}\cos\beta & -\mathbf{U}\sin\beta\,\mathbf{U}^\dagger \\ \sin\beta & \cos\beta\mathbf{U}^\dagger \end{pmatrix}. \tag{354}$$

One can straightforwardly verify that $\sigma_x \mathbf{U}_\mathrm{T}\sigma_x = \mathbf{U}_\mathrm{T}^{-1}$ and that $\mathbf{U}_\mathrm{T}^\dagger = \mathbf{U}_\mathrm{T}^{-1}$.

For this model, two regimes of behaviors have been identified [259]. For small $\gamma$, there is a localized phase. For $\gamma$ close to $\pi/2$, one finds a critical phase. By identifying the value of $\gamma$ which divides the two regimes and studying its dependence on $\alpha$, one arrives at the phase diagram shown in Fig. 46. The line $\alpha = \pi/4$ corresponds to the critical-metal states studied by Gade and Wegner [252]. On the line without hopping between the sub-lattices, $\gamma$ has a single critical point at $\alpha = \pi/4$ which is in the universality class of the Integer Quantum Hall Transition.

### *9.4.2. Classes BDI and CII*

A model in class BDI can be obtained from one in class AIII simply by imposing time reversal invariance as an additional symmetry. This condition is conventionally written in the form $\mathbf{H}^* = \mathbf{H}$, but for a discussion based on scattering matrices it is more convenient to transform

$$\mathbf{H} \to \mathbf{Q}\mathbf{H}\mathbf{Q}^{-1} \quad \text{with } \mathbf{Q} = \mathrm{e}^{\mathrm{i}\pi\sigma_x/4}\,. \tag{355}$$

This transformation leaves the chiral symmetry relation $\sigma_x \mathbf{H}\sigma_x = -\mathbf{H}$ intact. In the transformed basis one has

$$\mathbf{H}^* = -\mathbf{H}, \quad \mathbf{S} = \mathbf{S}^*, \quad \mathbf{T}^* = \mathbf{T}\,. \tag{356}$$

To ensure a real time evolution operator, we restrict the link phases $\phi$ to the values 0 and $\pi$. Choosing these values randomly, the BDI model consists of two coupled copies of the class D models reviewed in

the previous section. Alternatively, one could assume $\phi = 0$ on all links, and introduce disorder only via the chiral couplings $\beta$.

For class CII, Kramers degeneracy is a defining feature of the class and requires the introduction of an additional two-dimensional space arising from the spin. The time reversal operation includes reversal of spin direction. Defining $\mathscr{C} = \mathrm{i}\sigma_y$, where $\sigma_y$ is a Pauli matrix acting in the additional space, it is conventionally written in the form

$$\mathscr{C}\mathbf{H}^*\mathscr{C}^{-1} = \mathbf{H} \ . \tag{357}$$

As for the class BDI, it is again convenient to transform according to Eq. (355). This gives

$$\mathscr{C}\mathbf{H}^*\mathscr{C}^{-1} = -\mathbf{H}, \quad \mathscr{C}\mathbf{S}^*\mathscr{C}^{-1} = \mathbf{S}, \quad \mathscr{C}\mathbf{T}^*\mathscr{C}^{-1} = \mathbf{T} \tag{358}$$

as equivalent expressions of time reversal invariance. Applying these ideas to a network model, four channels propagate along a single link which, generalizing Eq. (350), is transferred according to a $4 \times 4$ transfer matrix $\mathbf{T}_{\mathrm{link}}$ with the generic form

$$\mathbf{T}_{\mathrm{link}} = v \otimes \begin{pmatrix} \cosh b & \sinh b \\ \sinh b & \cosh b \end{pmatrix} \ , \tag{359}$$

where $v$ is an SU(2) matrix and $b$ a real hyperbolic angle. Adopting this form, the time evolution operator for class CII has the structure given in Eq. (354), but with $\mathbf{U}$ representing a network model of class C, as reviewed in the preceding section. The links of a such a model of class C carry two co-propagating channels, coming from two spin components, and the evolution operator satisfies

$$\mathscr{C}\mathbf{U}^*\mathscr{C}^{-1} = \mathbf{U} \ . \tag{360}$$

## 10. Supersymmetry and localization

In the present section, we comment on recent developments which open new perspectives for better understanding of the field theoretical models that have been developed during the past two decades for describing the quantum Hall phase transition. This development is closely related to a mapping to a chain of superspins starting from the random network model.

While the numerical and experimental evidences for the universality of the quantum Hall transition appear to be striking, the quantum Hall critical point has so far successfully escaped any attempts to be placed into a classification of two-dimensional phase transitions, based on the conformal invariance at the critical point. Recently, it has been suggested that the quantum Hall critical point may belong to a new class of critical points being described by a supersymmetric conformal field theory [60,61]. Much progress has been achieved towards the analytical derivation and characterization of the quantum Hall transition. Nevertheless, an analytical calculation of its critical exponents is still missing.

Soon after the discovery of the Quantum Hall Effect a field theory has been derived from the microscopic Hamiltonian of the random Landau model with short-range disorder, the correlation length of the disorder potential, $\ell_{\mathrm{c}}$, being much smaller than the magnetic length $\ell_B$ [301–304]. It has been shown to have two coupling parameters $\sigma_{xx}^0$ and $\sigma_{xy}^0$, the longitudinal and Hall conductance as defined on small length scales of the order of the elastic mean free path $l$. This field theory is based on the theory of localization of electrons in weakly disordered systems.

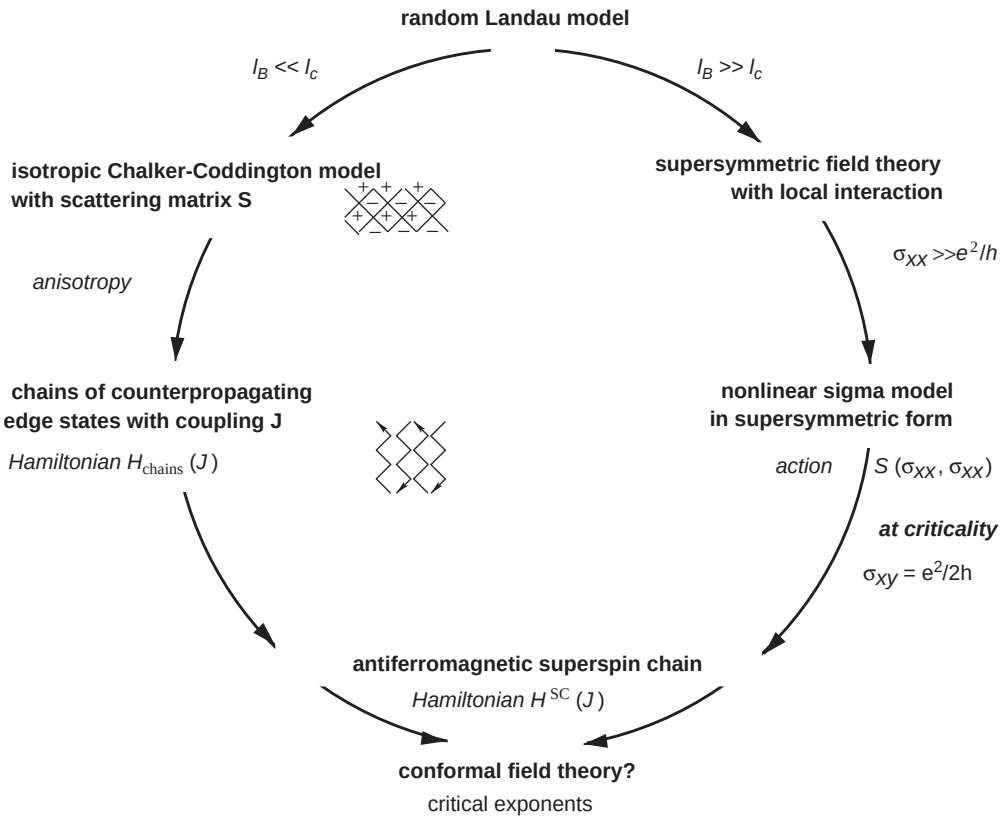


Fig. 47. Sketch of the development of the analytical proofs for the equivalence of the critical theory for the random Landau model and the Chalker–Coddington network model.

Subsequently, it has been shown rigorously that this field theory is indeed critical at half integer Hall conductance parameters $\sigma^0_{xy}$ [301,305,306], and that it has a spectral gap to fluctuations at other values of $\sigma^0_{xy}$. This indicates the localization of the electron eigenstates of the random Landau model in the tails of the Landau bands [307]. Since the longitudinal conductance at the critical point $\sigma^*$ is known to be smaller than 1 (in units of $e^2/h$), the critical point is located, quite unfortunately, in the strong coupling limit of the field theory. Thus, it is outside of the validity of the available analytical methods which can be used to extract quantitative information on the critical exponents.

Recently, an anisotropic version of the Chalker–Coddington model has been mapped directly onto the Hamiltonian of a chain of antiferromagnetically interacting superspins [37,192,308,309]. It had been shown before that the non-linear sigma model for short-range disorder at the critical point, $\sigma_{xy} = e^2/2h$, and in the strong coupling limit, can also be mapped onto the Hamiltonian of a chain of antiferromagnetically interacting superspins [310]. This provides strong analytical support for the notion of universality of the quantum Hall transition as sketched schematically in Fig. 47. Thereby, the problem of the quantum Hall transition has been transformed to the task of finding the ground state and the dispersion of the excitations of the chain of antiferromagnetic superspins [37,309,311].

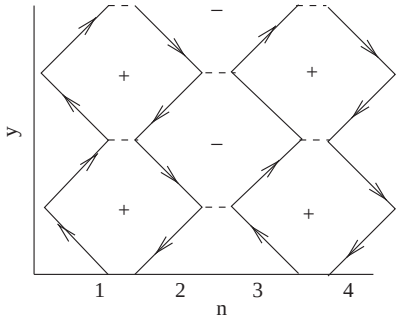


Fig. 48. The network model with counter-propagating chiral fermions with random on-site potential $w_{n,y}$ describing the propagation along edge states around Hall droplets with random tunneling amplitudes $t_{n,y}$ between them (dashed).

The model of antiferromagnetically interacting superspins has been shown to be critical [309]. Numerically, the critical exponent $\nu$ has been obtained from a finite length scaling of superspin chains, by means of the density matrix renormalization group method, and found to be $\nu = 2.4(4)$ [37].

So far, no analytical information could be directly obtained on the critical parameters, the localization exponent $\nu$, the MacKinnon–Kramer parameter $\Lambda_c$ of the scaling function, and the multi-critical exponents $D(q)$. However, starting from the model of a superspin chain, a class of supersymmetric conformal field theories has been suggested to be relevant for the quantum Hall transition, which ultimately should yield the critical parameters of the quantum Hall transition [60,61]. In yet another development, the Bethe–Ansatz method has been applied to the Hamiltonian of superspin chains. Still, it is not yet clear if that model is integrable and a closed solution for its ground state and its excitations can be obtained in this way [312,313].

In the next section we will provide a derivation of the Hamiltonian of an antiferromagnetic superspin chain starting from an anisotropic version of the Chalker–Coddington model, following closely the original derivations by Lee [192], Zirnbauer [308], and by Kondev and Marston [37]. In the second section, the derivation of Pruisken's non-linear sigma model in supersymmetric form is summarized [301–304]. Finally, the connection between that model and the superspin chain is discussed following the work of Zirnbauer [60,308,310].

### *10.1. From the network model to the antiferromagnetic superspin chain*

We start from a modification of the network model, recently proposed by Lee [192], where the random scattering matrices are replaced by a Hamiltonian which describes a quasi-one-dimensional array of counter-propagating edge states in the presence of disorder (Fig. 48). The $x$-coordinate is discretized, the integer index $n$ enumerates the discrete vertices of the network model. The fact that the direction of propagation alternates between sites $n$ will be shown in the following to result in an antiferromagnetic interaction between superspins. A one-dimensional array of edge states, which propagate all in the same direction, has accordingly been mapped to a ferromagnetic super spin chain [311]. This is an effective model of the surface states of a layered quantum Hall system, a so-called chiral metal (Section 11).

In terms of electron creation $\hat{\psi}^\dagger$ and annihilation $\hat{\psi}$ operators the Hamiltonian may be written as

$$H[\hat{\psi}^\dagger, \hat{\psi}] = \sum_{n,y} [\hat{\psi}^\dagger_{n,y}((-1)^n \mathrm{i} v_\mathrm{F} \partial_y + w_{n,y})\hat{\psi}_{n,y} - (t_{n,y}\hat{\psi}^\dagger_{n,y}\hat{\psi}_{n+1,y} + t^*_{n,y}\hat{\psi}^\dagger_{n+1,y}\hat{\psi}_{n,y})] \ , \tag{361}$$

where the sum is over the discrete vertices of the network model. This Hamiltonian reflects the chiral nature and the linear dispersion of the edge states, with alternating propagation forward and backward in the $y$-direction with Fermi velocities $\pm v_\mathrm{F}$. The complex tunneling amplitudes $t_{n,y}$ between the edge states are assumed to have random phases. These represent the random Anaronov–Bohm phases of the electrons, accounting for the fact that in a network of edge states, closed orbits vary randomly in size and thereby encircle randomly varying magnetic fluxes. There are also random on-site potentials $w_{n,y}$. These random terms are assumed to be Gaussian distributed with zero means, and the variances

$$\begin{aligned} \langle w_{n,y}\, w_{n',y'}\rangle &= 2U\delta_{n,n'}\,\delta(y-y') \ , \\ \langle t^*_{n,y}\, t_{n',y'}\rangle &= 2J_n\delta_{n,n'}\,\delta(y-y') \ , \end{aligned} \tag{362}$$

with $J_n = J[1+(-1)^n R]$. The staggered modulation in the parameter $J_n$ allows to trace the differences in tunneling between counter-propagating electrons in adjacent columns of plaquettes as depicted in Fig. 48. At $R=-1$, there are disconnected pairs of counter-propagating edge states, such that electrons circulate only clockwise around the (+)-plaquettes. In the opposite case, $R$=1, electrons circulate counterclockwise only around the (−)-plaquettes. At $R=0$, there is tunneling between all sites, and critical quantum percolation is expected, corresponding to the transition between the quantum Hall plateaus.

Critical behavior consistent with this scenario was found from the disorder averaged two-particle Green function describing transport corresponding to the Hamiltonian equation (361) by Wang and Lee [38]. From a Monte-Carlo treatment of the replicated Hamiltonian they obtained a correlation length exponent $\nu = 2.33(3)$, in good agreement with other numerical simulations and experiments. It can furthermore be shown that the Hamiltonian equation (361) can be identified in the continuum limit with the Hamiltonian of two-dimensional Dirac fermions with random mass and random vector fields [192], which is in the universality class of the integer quantum Hall transition, as discussed previously in Section 7.

It is well known [75–79], that in weakly disordered systems, $k_\mathrm{F} l \gg 1$, one needs to go beyond lowest order perturbation theory in the disorder potential in order to describe quantum localization. One also has to take full advantage of the symmetries occurring in the calculation of correlation functions of disordered systems. This can be traced back to the fact that the disorder averaged electron wave function amplitude $\langle\psi(\boldsymbol{r},t)\rangle$ decays on length scales of the order of $l$, since the random scattering phase shifts associated with the scattering at the impurities are averaged out. This destroys the information on quantum coherent multiple scattering, and thus on quantum localization. In order to describe quantum localization, one needs to consider higher moments of the wave function amplitudes such as the impurity averaged evolution of the electron density $n(\boldsymbol{r},t) = \langle|\psi(\boldsymbol{r},t)|^2\rangle$.

The time evolution of the electron amplitudes can be written in terms of the retarded propagator $G^\mathrm{R}$,

$$\psi(\boldsymbol{r},t) = \int \mathrm{d}\boldsymbol{r}' G^\mathrm{R}(\boldsymbol{r},t;\boldsymbol{r}',t')\psi(\boldsymbol{r}',t') \ , \tag{363}$$

with $t > t'$. The electron density becomes

$$\langle n(\mathbf{r}, t)\rangle = \int \mathrm{d}\mathbf{r}' \int \mathrm{d}\mathbf{r}'' \Gamma(\mathbf{r}, t; \mathbf{r}', \mathbf{r}'', t')\psi(\mathbf{r}', t')\psi^*(\mathbf{r}'', t') \ , \tag{364}$$

where the quantum diffusion propagator is given by

$$\Gamma(\mathbf{r}, t; \mathbf{r}', \mathbf{r}'', t') = \langle G^{\mathrm{R}}(\mathbf{r}, t; \mathbf{r}', t')G^{\mathrm{A}}(\mathbf{r}'', t'; \mathbf{r}, t)\rangle \ . \tag{365}$$

After performing a Fourier transformation from time $t - t'$ to energy $E$, a non-perturbative averaging of products of retarded and advanced propagators, $\langle G^{\mathrm{R}}(E)G^{\mathrm{A}}(E')\rangle$ is needed in order to obtain information on quantum localization.

In a useful analogy to the study of spin systems, the field theoretical approach contracts the information on localization into a theory of Goldstone modes $Q$, arising from the global symmetry of rotations between the functional integral representation of the retarded propagator $G^{\mathrm{R}}$ ("spin up") and the advanced propagator $G^{\mathrm{A}}$ ("spin down"). The field theory can either be formulated by means of the replica trick, where the $N$ replicas are represented either by $N$ fermionic or $N$ bosonic fields, yielding a bounded or unbounded symmetric space, respectively, on which the modes $Q$ are defined [301].

Because of the necessity and the difficulty to perform the delicate limit $N \to 0$ at the end of the calculation in the replica formulation, a more rigorous supersymmetric field theory has been formulated. This technique represents the product of Green functions $G^{\mathrm{R}}(E)G^{\mathrm{A}}(E')$ by functional integrals over two fermionic and bosonic field components, composing a supersymmetric field vector $\psi$. The supersymmetric representation enables one to perform the averaging over the disorder potential as a simple Gaussian integral [302–304].

Thus, in order to study the localization–delocalization transition in the network model as described by the random Hamiltonian, Eq. (361), we consider the average of the quantum diffusion propagator

$$K(1, 2) = \langle G^{\mathrm{R}}_E(1, 2)G^{\mathrm{A}}_{E'}(2, 1)\rangle \ , \tag{366}$$

where

$$G^{\mathrm{R,A}}_E(1, 2) = \langle 1|\frac{1}{E - H \pm \mathrm{i}\eta}|2\rangle \ , \tag{367}$$

are the retarded and advanced Green functions. The parameter $\eta$ is a positive infinitesimal number. We have introduced here the usual shorthand notation for the coordinates with $1 := (n_1, y_1)$ and $2 := (n_2, y_2)$. For non-zero disorder parameter $R$ we expect the quantum diffusion propagator to decay exponentially

$$K(1, 2) \sim \mathrm{e}^{-2r_{12}/\xi} \ , \tag{368}$$

where $r_{12}$ is the distance between points 1 and 2. This defines the localization length $\xi \gg l$, reflecting the finite extent of the electron wave functions near energy $E$. At the critical point $R = 0$, the localization length is expected to diverge like

$$\xi \sim R^{-\nu} \ . \tag{369}$$

By introducing a pair of complex scalar fields

$$\phi(n, y) = \begin{pmatrix} \phi_+(n, y) \\ \phi_-(n, y) \end{pmatrix} \ , \tag{370}$$

with + and − denoting the retarded and the advanced sector, respectively, the advanced and retarded Green functions, Eq. (366), can be rewritten. One obtains for the two-particle propagator

$$\langle K(1,2)\rangle = \frac{1}{Z}\int \mathrm{D}[\phi]\mathrm{D}[\phi^*]\,\phi_+(1)\phi_+^*(2)\phi_-(2)\phi_-^*(1)\,\mathrm{e}^{-S[\phi,\phi^*]}\,, \tag{371}$$

with the action

$$\begin{aligned} S[\phi,\phi^*] = \sum_{n,y}\sum_{\alpha=\pm}[\mathrm{i}\alpha\{&\phi_\alpha^*(n,y)(-E_\alpha + (-1)^n \mathrm{i}v_\mathrm{F}\partial_y + w_{n,y})\phi_\alpha(n,y) \\ &- [t_{n,y}\phi_\alpha^*(n,y)\phi_\alpha(n+1,y) + t_{n,y}^*\phi_\alpha^*(n+1,y)\phi_\alpha(n,y)]\} \\ &+ \eta\phi_\alpha(n,y)\phi_\alpha^*(n,y)]\,. \end{aligned} \tag{372}$$

Here, we have defined $E_{\alpha=+,-} = E, E'$. The choice of the signs guarantees that the Gaussian integrals are convergent for $\eta > 0$. The normalization factor

$$Z = \int \mathrm{D}[\phi]\mathrm{D}[\phi^*]\,\mathrm{e}^{-S[\phi,\phi^*]}\,, \tag{373}$$

is an inverse spectral determinant. Therefore, its inverse can be lifted to the numerator by introducing another Gaussian integral, this time over *Grassmann fields* [314]

$$\frac{1}{Z} = \int \mathrm{D}[\chi]\mathrm{D}[\bar{\chi}],\,\mathrm{e}^{-S[\chi,\bar{\chi}]}\,, \tag{374}$$

with the anticommuting fields

$$\chi(n,y) = \begin{pmatrix}\chi_+(n,y)\\ \chi_-(n,y)\end{pmatrix}\,, \tag{375}$$

that are the supersymmetric partners of the scalar bosonic fields. Using Eqs. (374) and (371) the correlation function, Eq. (366), can be written as a combined Gaussian integral over scalar and Grassmann fields

$$\langle K(1,2)\rangle = \int \mathrm{D}[\phi]\mathrm{D}[\phi^*]\mathrm{D}[\chi]\mathrm{D}[\bar{\chi}]\,\phi_+(1)\phi_+^*(2)\phi_-(2)\phi_-^*(1)\mathrm{e}^{-(S[\phi,\phi^*]+S[\chi,\bar{\chi}])}\,. \tag{376}$$

Now the average over the disorder can be performed as a simple Gaussian integral.

Before considering the full Hamiltonian, let us look first at the correlation function of a single chiral edge state $n$, which is expected to behave metallic for any disorder strength $U$ since its Hamiltonian contains no backscattering, $J = 0$.

Performing the ensemble averaging as the Gaussian integral over the random potential $w(n,y)$ leads to the functional integral

$$Z = \int \mathrm{D}[\psi,\bar{\psi}]\exp\int \mathrm{d}x[\bar{\psi}(\Lambda v_\mathrm{F}\partial_x - \eta + \mathrm{i}\omega)\psi - U(\bar{\psi}\Lambda\psi)^2]\,, \tag{377}$$

We have here introduced a four-component superspinor $\psi(x)$ with components $\psi_X$ where $X = R\mathrm{B}$ (retarded Boson), $X = R\mathrm{F}$ (retarded fermion), $X = A\mathrm{B}$ (advanced Boson), and $X = A\mathrm{F}$ (advanced fermion).

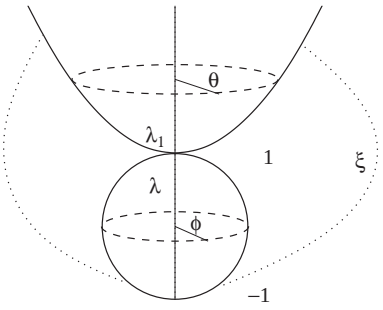


Fig. 49. Schematic view of the supersymmetric space $\mathrm{U}(1,1|2)/(\mathrm{U}(1|1)\times\mathrm{U}(1|1))$ on which the Hamiltonian of supersymmetric operators $Q$ is defined. The point at which the compact sphere (corresponding to that part of $Q$ which arises from decoupling the fermionic $\psi_{\mathrm{F}}^4$-term) and the hyperbolic (arising from the decoupling of the bosonic $\psi_{\mathrm{B}}^4$-term) meet, is the classical point which yields the classical correlation function. Diagrammatic expansion around that point would miss the curvature, and the non-perturbative integral over the whole supersymmetric space is needed to describe quantum localization. The compact sphere is parameterized by $\Phi\in[0,2\pi)$ and $\lambda\in[-1,1]$, and the non-compact hyperbolic is parameterized by $\lambda_1\in[-1,\infty]$ and $\theta\in[0,2\pi)$. The unitary rotations between the sphere and the hyperbolic are parameterized by Grassmann variables $\xi$ as indicated by dotted lines.

The $4\times4$ supersymmetric $\Lambda$ is defined by

$$\bar\psi\Lambda\psi=\sum_{\sigma=\mathrm{B,F}}(\bar\psi_{R\sigma}\psi_{R\sigma}-\bar\psi_{A\sigma}\psi_{A\sigma})\ . \tag{378}$$

Since the energies in the retarded and advanced sectors are different, we have defined $\omega=E-E'\neq0$.

One can decouple the interaction term $(\bar\psi\Lambda\psi)^2$ by introducing a Hubbard–Stratonovitch field $Q$ coupling to $\bar\psi\psi\Lambda$ and then integrate out $\psi$ and $\bar\psi$. The resulting effective action for $Q$ is

$$S[Q]=\int \mathrm{d}x\ \mathrm{STr}\left[-\frac{U}{4v_{\mathrm{F}}^2}\,Q^2+\ln\left(\partial_x+\frac{\mathrm{i}\omega-\eta}{v_{\mathrm{F}}}\Lambda+\frac{U}{v_{\mathrm{F}}^2}\,Q\right)\right]\ . \tag{379}$$

The next step is to simplify the $Q$-field functional integral by means of the saddle-point approximation. As a result, $Q$ gets restricted to the non-linear space $Q=g\Lambda g^{-1}$. It belongs to the supersymmetric space $\mathrm{U}(1,1|2)/(\mathrm{U}(1|1)\times\mathrm{U}(1|1))$ which is sketched schematically in Fig. 49. Here the notation is reminiscent of the notation for a two-dimensional hyperbolic space $\mathrm{U}(1,1)$ and the group of $2\times2$ unitary matrices $\mathrm{U}(2)$. Accordingly, the supermatrices $A\in\mathrm{U}(1,1\mid2)$ have the form

$$\mathbf{A}=\begin{pmatrix}\mathbf{A}^{BB} & \mathbf{A}^{BF}\\ \mathbf{A}^{FB} & \mathbf{A}^{FF}\end{pmatrix}\ , \tag{380}$$

where $\mathbf{A}^{BB}\in\mathrm{U}(1,1)$ and $\mathbf{A}^{FF}\in\mathrm{U}(2)$ and $\mathbf{A}^{FB}$, $\mathbf{A}^{BF}$ are parameterized by Grassmann variables, and transform between $\mathrm{U}(1,1)$ and $\mathrm{U}(2)$.

This step, being in general only an approximation, here becomes *exact* in the limit $U\to\infty$. By expanding $\ln[\Lambda g^{-1}(\partial_x+A)g+U/v_{\mathrm{F}}^2]$ to linear order in $g^{-1}(\partial_x+A)g$, one obtains the action of the

Wess–Zumino functional $Z_{\rm WZ}[A]$,

$$Z_{\rm WZ}[\omega] = \int {\rm D}Q \exp\left\{ \int {\rm d}x\, {\rm STr}\left[ \frac{\Lambda}{2} g^{-1}(v_{\rm F}\partial_x + {\rm i}\omega\Lambda) g \right] \right\} . \tag{381}$$

Higher orders are suppressed by powers of $v_{\rm F}^2/L_x U$, with $L_x$ the system size.

By interpreting the integral over $x$ as an integral over time, one can rewrite this in terms of a Hamiltonian

$$Z_{\rm WZ}[\omega] = {\rm STr}\, {\rm e}^{-L_y H_g(\omega)} , \tag{382}$$

where

$$H_g(\omega) = {\rm i}\omega\, {\rm STr}\, \frac{\Lambda}{2} \frac{1}{g} \Lambda g . \tag{383}$$

This is identical to the super Hamiltonian which one obtains from the unitary ensemble of random matrices [302], typical for a random metallic system with extended states. Thus, as expected, we recover the result that a single disordered chiral line supports only metallic states.

Let us next discuss the case of many counter-propagating chiral modes that are coupled by hopping matrix elements between neighboring modes, with variance $J$. This corresponds to the anisotropic Chalker–Coddington model. The Gaussian random hopping matrix elements give rise to an additional term in the Lagrangian,

$$\begin{aligned} \mathscr{L} &\mapsto \mathscr{L} + 2J \sum_n (\bar\psi_n \Lambda \psi_{n+1})(\bar\psi_{n+1}\Lambda\psi_n) \\ &= \mathscr{L} + 2J \sum_n {\rm STr}(\psi_n \bar\psi_n \Lambda)(\psi_{n+1}\bar\psi_{n+1}\Lambda) . \end{aligned} \tag{384}$$

This is obtained by averaging Eq. (376) with Eq. (372) over $t$ using Eq. (362). By using the bosonization rule $v_{\rm F}\psi\bar\psi\Lambda \to Q/2$ for $U \to \infty$, the additional term can be cast into $(J/2v_{\rm F}^2)\sum_n {\rm STr}(Q_n Q_{n+1})$. The condition for the validity of this step is $U \gg J$. As a result one obtains the $Q$-field action

$$S[Q] = \int {\rm d}x \sum_n {\rm STr}\left[ (-1)^n \frac{\Lambda}{2} g_n^{-1}\partial_x g_n + \frac{J}{2v_{\rm F}^2} Q_n Q_{n+1} \right] . \tag{385}$$

This is the action [311,315] of the coherent-state path integral for a quantum superspin Hamiltonian. The resulting effective supersymmetric (SUSY) Hamiltonian describes interacting spin-up and spin-down fermions $c_\sigma$ and bosons $b_\sigma$. The two spin species formally correspond to the retarded and advanced Green functions introduced above [37,309,316],

$$\begin{aligned} H = &\sum_{j=0}^{L-2} J_j \left[ \lambda_H \sum_{a=1}^{4} g_a S_j^a S_{j+1}^a + \sum_{a=5}^{8} g_a S_j^a S_{j+1}^a + \lambda_H (-1)^j \sum_{a=9}^{16} g_a S_j^a S_{j+1}^a \right] \\ &+ \eta \sum_{j=0}^{L-1} [S_j^1 + S_j^2 + S_j^5 + S_j^6] . \end{aligned} \tag{386}$$

The signs $g_a$ are given by

$$g_a = \begin{cases} 1 & \text{for } a = 1, 2, 10, 12, 14, 16 \ , \\ -1 & \text{for } a = 3, \ldots, 9, 11, 13, 15 \ . \end{cases} \tag{387}$$

Eq. (386) contains 16 spin operators, the components of a $4 \times 4$ superspin matrix,

$$\begin{aligned} S^1 &:= b_\uparrow^\dagger b_\uparrow + 1/2, & S^5 &:= c_\uparrow^\dagger c_\uparrow - 1/2, & S^9 &:= c_\downarrow^\dagger b_\downarrow, & S^{13} &:= b_\downarrow c_\uparrow \ , \\ S^2 &:= b_\downarrow^\dagger b_\downarrow + 1/2, & S^6 &:= c_\downarrow^\dagger c_\downarrow - 1/2, & S^{10} &:= c_\uparrow^\dagger b_\uparrow, & S^{14} &:= b_\uparrow c_\downarrow \ , \\ S^3 &:= b_\uparrow^\dagger b_\downarrow^\dagger, & S^7 &:= c_\uparrow^\dagger c_\downarrow^\dagger, & S^{11} &:= b_\downarrow^\dagger c_\downarrow, & S^{15} &:= b_\downarrow^\dagger c_\uparrow^\dagger \ , \\ S^4 &:= b_\downarrow b_\uparrow, & S^8 &:= c_\downarrow c_\uparrow & S^{12} &:= b_\uparrow^\dagger c_\uparrow, & S^{16} &:= b_\uparrow^\dagger c_\downarrow^\dagger \ . \end{aligned} \tag{388}$$

The boson-valued operators $S^1, \ldots, S^8$ constitute the symmetric sector of the Hamiltonian. The fermion-valued operators $S^9, \ldots, S^{16}$ form the anti-symmetric sector. Despite that $H$ is non-Hermitian, it only has real-valued eigenvalues. For $\lambda_H = 0$ one has only fermionic spin operators. One does arrive at this Fermion model directly from the Chalker–Coddington network model when calculating the disorder averaged auto correlation function of spectral determinants [60,306]. Another derivation via the Landauer conductance formula was recently reported in Ref. [316a]. This yields the antiferromagnetic spin-1/2 Heisenberg chain, which is critical [317]. The crossover to the integrable superspin chain of the spin Quantum Hall Effect [264,280], which is critical in the universality class of the classical percolation model, can be studied by freezing out 8 of the 16 spin components [318]. This raises the question whether or not the critical parameters vary continuously, as for the crossover from the antiferromagnetic Heisenberg spin chain to the XY model [319,317].

The Hamiltonian commutes with four fermion-valued supersymmetry generators,

$$[H, Q_{1\sigma}] = [H, Q_{2\sigma}] = 0 \tag{389}$$

with the supersymmetric charges

$$\begin{aligned} Q_{1\sigma} &:= \sum_j [b_{j\sigma}^\dagger c_{j\sigma} - (-1)^j c_{j\sigma}^\dagger b_{j\sigma}] \ , \\ Q_{2\sigma} &:= \sum_j [(-1)^j b_{j\sigma}^\dagger c_{j\sigma} + c_{j\sigma}^\dagger b_{j\sigma}] \ . \end{aligned} \tag{390}$$

One can see that the supersymmetric Hamiltonian must have a unique, zero-energy ground state. All excited states appear in quartets or larger multiples of 4, half with odd total fermion content. These cancel out in the partition function by virtue of the super-trace, yielding the correct value of 1 that we have encountered above when introducing the functional integral over Grassmann variables to cancel the normalization factor of the bosonic integral

$$Z = \mathrm{STr}\, \mathrm{e}^{-\beta H} := \mathrm{Tr}(-1)^{N_\mathrm{c}} \mathrm{e}^{-\beta H} = 1 \ . \tag{391}$$

Here, $N_\mathrm{c}$ is the total number of fermions. The ground state of this supersymmetric non-Hermitian antiferromagnetic Hamiltonian is very complicated. The ground state of the *Hermitian* supersymmetric ferromagnet that describes a chiral metal with all edge states propagating in the same direction is simply the vacuum state [311].

The Lieb–Schultz–Mattis theorem proves that for half-odd-integer spin antiferromagnets on a periodic chain of length $L$ sites ($\vec{S}_L := \vec{S}_0$) either the ground state is degenerate or there are gapless spin excitations in the thermodynamic limit $L \to \infty$ [240]. In the supersymmetric problem, Marston and Tsai were able to make even a stronger statement [309,316], because its ground state is unique by supersymmetry. For $\eta > 0$ they showed that low-energy excitations are gapless in the thermodynamic limit. This proves that the antiferromagnetic superspin chain is critical.

In the following section the field theory of the quantum Hall critical point is approached starting from a model of electrons in uncorrelated disorder in a strong magnetic field. The resulting supersymmetric field theory, with the action of a non-linear sigma model was used as a basis of the two parameter scaling of the Quantum Hall Effect. It has recently been shown that it can in a long wave length limit be mapped onto the Hamiltonian of the superspin chain, Eq. (386). This, together with the derivation of the spin chain from the opposite limit of a model with long-range potential as sketched above, provides very strong support to the surmise that the Chalker–Coddington model is a good model for the universal quantum Hall transition [308].

### *10.2. From the Landau model to Pruisken's non-linear sigma model*

The Hamiltonian of non-interacting electrons in a magnetic field in the presence of uncorrelated disorder is (Section 1)

$$H = \frac{1}{2m}(\boldsymbol{p} + e\boldsymbol{A})^2 + V(\boldsymbol{r}) + V_0(\boldsymbol{r}) \ . \tag{392}$$

Here, $V(\boldsymbol{r})$ is assumed to be a Gaussian distributed random function with a distribution

$$P([V]) = \exp\left[ -\int \frac{\mathrm{d}\boldsymbol{r}}{\Omega}\frac{\mathrm{d}\boldsymbol{r}'}{\Omega} J(\boldsymbol{r}-\boldsymbol{r}')V(\boldsymbol{r})V(\boldsymbol{r}') \right] , \tag{393}$$

where $\Omega$ is the volume of the system. Impurity averaging is thus given by $\langle \dots \rangle_V = \int \prod_{\mathbf{r}} \mathrm{d}[V] P([V]) \dots$ . We assume

$$J(\boldsymbol{r}-\boldsymbol{r}') = \Omega\Delta \frac{\hbar}{\tau}\delta(\boldsymbol{r}-\boldsymbol{r}') \tag{394}$$

for uncorrelated impurities, where $1/\tau$ is the elastic scattering rate and $\Delta = 1/(\rho\Omega)$ the mean level spacing of the mesoscopic sample with volume $\Omega$. It is related to the variance of the disorder potential $V(\boldsymbol{r})$ according to $W^2 = \Delta\hbar/2\pi\tau$. The function $V_0(\boldsymbol{r})$ is the electrostatic confinement potential defining the width of the wire $L$.

In order to describe localization, we consider again the correlation function $K(1,2)$ studied in the previous section for the Chalker–Coddington model, but using this time the Hamiltonian equation (392). Formulating the supersymmetric field theory by representing the product of Green functions $G^{\mathrm{R}}(E)G^{\mathrm{A}}(E')$ by functional integrals over two fermionic and bosonic field components, composing a supersymmetric field vector $\psi$, as in the previous section, the averaging over the disorder potential can again be performed as a simple Gaussian integral [302–304]. As a result of the averaging one obtains a locally interacting theory of the fields $\psi$ containing an interaction term $\propto \psi^4$, where the *interaction strength* is proportional to the variance of the disorder potential $W^2$. This term is next decoupled by introducing another Gaussian integral over $Q$-matrices. Clearly, the field $Q$ should not be a scalar, otherwise we would simply reintroduce the Gaussian integral over the random potential $V$. Rather, in order to be able to describe the physics

of localization, the field $Q$ should capture the full symmetry of the functional integral representation of the correlation function. Therefore, the Gaussian integral is chosen to be over a $4\times4$ matrix $Q$ which itself is an element of the symmetric space defined by the matrices $\mathbf{A}$ that leave the functional integral invariant under the transformation $\psi \to \mathbf{A}\psi$. In the supersymmetric formulation, this matrix consists of two blocks of $2\times2$ matrices whose parameter space consists of a compact (bounded) and a non-compact (unbounded) sector, Eq. (380) (Fig. 49). The off-diagonal blocks, so to say the rotations between the compact and the non-compact sector, are then found to be parameterized by Grassmann (fermionic) variables. Now, the spatial variations of $Q$ are governed by the action

$$S[Q] = \frac{\pi\hbar}{4\Delta\tau}\int \frac{\mathrm{d}\boldsymbol{r}}{L^2}\,\mathrm{Tr}\; Q^2(\boldsymbol{r}) + \frac{1}{2}\int \mathrm{d}\boldsymbol{r}\,\langle \boldsymbol{r}|\mathrm{Tr}\;\ln G(\hat{\boldsymbol{r}},\hat{\boldsymbol{p}})|\boldsymbol{r}\rangle\ , \tag{395}$$

where

$$G^{-1}(\hat{\boldsymbol{r}},\hat{\boldsymbol{p}}) = \frac{(\omega+\mathrm{i}\eta)\Lambda_3}{2} - \frac{(\hat{\boldsymbol{p}}+e\,\boldsymbol{A})^2}{2m^*} - V_0(\hat{\boldsymbol{r}}) + \frac{\mathrm{i}\hbar}{2\tau}\,Q(\hat{\boldsymbol{r}})\ . \tag{396}$$

The $4\times4$ matrix $\Lambda_3$ is the diagonal Pauli matrix in the sub-basis of the retarded and advanced propagators, $\eta > 0$ and $\omega = E - E'$ break the symmetry between the retarded and advanced sector.

It turns out that the physics of diffusion and localization, which arises on length scales much larger than the elastic mean free path $l$, is governed by the action of the long wavelength modes of $Q$. Thus, one can simplify and proceed with the analysis by expanding around a homogeneous solution of the saddle point equation, $\delta S = 0$. For $\omega = 0$, this is

$$Q = \frac{\mathrm{i}}{\pi\rho}\,\langle \boldsymbol{r}|\left[E - H_0 - V_0(\boldsymbol{r}) + \frac{\mathrm{i}}{2\tau}\,Q\right]^{-1}|\boldsymbol{r}\rangle\ . \tag{397}$$

This is solved by $Q_0 = \Lambda_3\mathbf{P}$, which corresponds to the self-consistent Born approximation for the self-energy of the impurity averaged Green function. At $\omega = 0$, rotations $\mathbf{U}$ which leave the action invariant yield the complete manifold of saddle point solutions as $Q = \bar{\mathbf{U}}\Lambda_3\mathbf{P}\mathbf{U}$, where $\mathbf{U}\bar{\mathbf{U}} = 1$ where $\bar{\mathbf{U}}$ is the supersymmetric Hermitian conjugate.

The modes which leave $\Lambda_3$ invariant can be factorized out, leaving the saddle point solutions in this supersymmetric theory to be elements of the semi-simple supersymmetric space $\mathrm{Gl}(2|2)/(\mathrm{Gl}(1|1)\times\mathrm{Gl}(1|1))$ [303,304]. Here the notation is chosen in analogy to $\mathrm{Gl}(n)$, denoting invertible $n\times n$ matrices, that is $\det A \neq 0$ for all $A \in \mathrm{Gl}(n)$. Thus, $\mathrm{Gl}(n\mid n)$ denote invertible $2n\times 2n$ supermatrices

$$\mathbf{A} = \begin{pmatrix} \mathbf{A}^{FF} & \mathbf{A}^{FB} \\ \mathbf{A}^{BF} & \mathbf{A}^{BB} \end{pmatrix}\ , \tag{398}$$

with

$$\mathrm{Sdet}\,\mathbf{A} = \det(\mathbf{A}^{FF} - \mathbf{A}^{FB}\mathbf{A}^{BB-1}\mathbf{A}^{BF})\,\det\mathbf{A}^{BB-1} \neq 0\ , \tag{399}$$

where Sdet is the superdeterminant. See [243] for a more detailed definition. In the semi-simple space the subgroup $\mathrm{Gl}(1|1)\times\mathrm{Gl}(1|1)$ consisting of matrices

$$\mathbf{h} = \begin{pmatrix} \mathbf{h}^{11} & 0 \\ 0 & \mathbf{h}^{22} \end{pmatrix}\ , \tag{400}$$

with $\mathbf{h}^{11}, \mathbf{h}^{22} \in \mathrm{Gl}(1|1)$, are factorized out.

In addition to these gapless modes there are massive longitudinal modes with $Q^2 \neq 1$ which only change the short-distance physics, and not the physics of localization. They can be integrated out [301,302]. Thus, the partition function reduces to a functional integral over the transverse modes **U**.

The action at finite frequency $\omega$ and slow spatial fluctuations of $Q$ around the saddle point solution can be found by an expansion of the action $S$. Inserting $Q = \tilde{\mathbf{U}}\Lambda_3\mathbf{P}\mathbf{U}$ into Eq. (395) and performing the cyclic permutation of **U** under the trace Tr allows a simple expansion to first order in the energy difference $\omega$ and to second order in the commutator $\mathbf{U}[H_0, \tilde{\mathbf{U}}]$ [301]. The first-order term in $\mathbf{U}[H_0, \tilde{\mathbf{U}}]$ is proportional to the local current. It is found to be finite only at the edge of the wire in a strong magnetic field, due to the chiral edge currents. It can be rewritten as

$$S_{xy\mathrm{II}} = -\frac{1}{8}\int \mathrm{d}x\,\mathrm{d}y\,\frac{\sigma_{xy}^{0\mathrm{II}}(\boldsymbol{r})}{e^2/h}\,\mathrm{STr}(Q\partial_x Q\partial_y Q)\ , \tag{401}$$

where the pre-factor is the non-dissipative term in the Hall conductivity in self-consistent Born approximation [302]

$$\sigma_{xy}^{0\mathrm{II}}(\boldsymbol{r}) = -\frac{1}{\pi}\frac{\hbar e^2}{m}\,\langle \boldsymbol{r}|(x\pi_y - y\pi_x)\,\mathrm{Im}\,G^{\mathrm{R}}(E)|\boldsymbol{r}\rangle\ , \tag{402}$$

where $\pi = (\hbar/\mathrm{i})\boldsymbol{\nabla} + \mathrm{e}\boldsymbol{A}$. This field theory has now the advantage that one can treat the physics on different length scales separately: the physics of diffusion and localization is governed by the action of spatial variations of **U** on length scales larger than the mean free path $l$. That is why this field theory is often called diffusive non-linear sigma model.

The physics on smaller length scales is included in the coupling parameters of the theory, which is identified in the above derivation as correlation functions of Green functions in self consistent Born approximation, being related to the conductivity by the Kubo–Greenwood formula,

$$\sigma_{\alpha\beta}^{0}(\omega, \boldsymbol{r}) = \frac{\hbar e^2}{\pi m^2}\,\langle \boldsymbol{r}|\pi_\alpha G_0^{\mathrm{R}}(E)\pi_\beta G_0^{\mathrm{A}}(E+\omega)|\boldsymbol{r}\rangle\ . \tag{403}$$

The remaining averaged correlators, involve products $G_0^{\mathrm{R}}(E)G_0^{\mathrm{R}}(E+\omega)$ and $G_0^{\mathrm{A}}(E)G_0^{\mathrm{A}}(E+\omega)$ and are therefore by a factor $\hbar/\tau E$ smaller than the conductivity, and can be disregarded for small disorder. Using the Kubo formula (403), the action of $Q$ simplifies to

$$\begin{aligned} S = {} & \frac{h}{16e^2}\int \mathrm{d}\boldsymbol{r}\sum_{i=x,y}\sigma_{ii}^{0}(\omega=0,\boldsymbol{r})\,\mathrm{Tr}[(\nabla_i Q(\boldsymbol{r}))^2] \\ & -\frac{h}{8e^2}\int \mathrm{d}\boldsymbol{r}\sigma_{xy}^{0}(\omega=0,\boldsymbol{r})\,\mathrm{Tr}[Q\partial_x Q\partial_y Q]\ , \end{aligned} \tag{404}$$

where $\sigma_{xy}^{0}(\omega=0,\boldsymbol{r}) = \sigma_{xy}^{\mathrm{I}}(\omega=0,\boldsymbol{r}) + \sigma_{xy}^{\mathrm{II}}(\omega=0,\boldsymbol{r})$ and $\sigma_{xy}^{\mathrm{I}}(\omega=0)$ is the dissipative part of the Hall conductivity in self-consistent Born approximation equation (403).

The first term in this action yields localization in two-dimensional electron systems, signaled by the presence of a gap in the field theory. The second term could not be obtained by any order in perturbation theory. It is of topological nature.

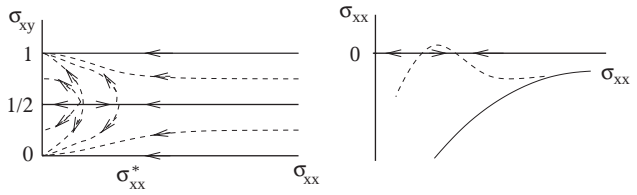


Fig. 50. The conjectured two parameter flow diagram of the integer Quantum Hall Effect (left), and the corresponding beta function, $\beta_{xx} = \mathrm{d}\ \ln\ \sigma_{xx}/\mathrm{d}\ \ln\ L$ (right) at $\sigma_{yx} = -\sigma_{xy} = 1/2$ (dashed line) and at $\sigma_{xy} = 0$ (full line, units of conductivities $e^2/h$).

In two dimensions, and for a homogeneous Hall conductance it can be shown that this term can take only discrete purely imaginary values,

$$S_{\mathrm{Top}} = 2\pi \mathrm{i}\, \frac{h}{e^2}\, \sigma^0_{xy} n\ , \tag{405}$$

where the integers $n$count how often the field $Q(\boldsymbol{r})$ is winding around its symmetric space as it varies spatially in two dimensions. Thus, disregarding the spatial variation of the coupling functions $\sigma_{ij}(\boldsymbol{r})$ in Eq. (405), and assuming isotropy, one finds in the two-dimensional limit that there are instantons with non-zero topological charge $q$, which are identical to the skyrmions of the compact $O(3)$ non-linear sigma model, as obtained form the compact part of the supersymmetric non-linear sigma model [301,302]. Their action is given by

$$F_q = 2\pi|q|\sigma_{xx} + 2\pi \mathrm{i} q \sigma_{xy}\ , \tag{406}$$

where $\sigma_{xx} = \sigma_{yy}$ and $\sigma_{xy}$ are the spatially averaged conductivities.

Now, we can repeat the derivation of the scaling function, by integrating out Gaussian fluctuations around these instantons. It is clear, however that the contribution from instantons with $q \neq 0$ is negligible, as long as $\sigma_{xx} > e^2/h$. Within the validity of the $1/g$-expansion one does not find a sizable influence of the topological term on the scaling function $\Lambda = \xi/L_y$. Still, the tendency is seen that at $\sigma_{xy} = -e^2/2h$ the renormalization of the longitudinal conductance is slowed down and one may conclude from this observation the two parameter scaling diagram with a critical state of finite conductance $0 < \sigma^*_{xx} < e^2/h$, which is an attractive fixed point for $\sigma_{xy} = -e^2/2h$ as shown in Fig. 50 [301,320]. Considering the beta function of the $N$th fermionic replica one notes [301,305] that only the last one $N = 1$, becomes critical and touches 0 like $\beta \sim -(\sigma_{xx} - \sigma^*_{xx})^2$, which is the beta function of the antiferromagnetic Heisenberg chain [306]. From that, one can conjecture that for $N \to 0$ the maximum of the beta function moves to positive values, which yields the form drawn in Fig. 50 with another, repulsive fixed point at smaller values of the conductance $\sigma_{xx}$, below which there is a flow to an insulating phase for all values of $\sigma_{xy}$. One can also come to that conclusion noting that, when freezing out the bosonic degrees of freedom from the supersymmetric non-linear sigma model at $\sigma_{xy} = -1/2$, one arrives again at the beta function of the antiferromagnetic Heisenberg chain, given above. It remains still to be shown explicitly that the beta function evolves indeed continuously from that beta function, as one adds the bosonic degrees of freedom, and to see if it results in the beta function drawn in Fig. 50.

Subsequently, it has been argued by other means that this field theory is indeed critical at half integer Hall conductance parameters $\sigma^0_{xy}$ [301,305,306], and that it has a spectral gap to fluctuations

at other values of $\sigma_{xy}^{0}$. This indicates the localization of the electron eigenstates of the random Landau model in the tails of the Landau bands [307]. Since the longitudinal conductance at the critical point $\sigma_{xx}^{*}$ is known to be smaller than 1, the critical point is located in the strong coupling limit of the field theory. Thus, it is outside of the validity of available analytical methods which can be used to extract quantitative information on the critical exponents. Furthermore, it is seen explicitly that in order that the instanton solutions with non-zero topological charge do exist the system must exceed the non-critical localization length $\xi_{\mathrm{2Dunit}} \sim \exp(\pi^2 g^2)$, where $g = h\sigma_{xx}/e^2$, when the assumption of uniform coupling parameters $\sigma_{ij}$ is made. Accordingly, it has been shown that the Hamiltonian of a chain of antiferromagnetically interacting superspins can be derived from the non-linear sigma model for short-ranged disorder at the critical point $\sigma_{xy} = -e^2/2h$ on length scales larger than $\xi_{\mathrm{2Dunit}}$ [310]. At criticality, $\sigma_{xy} = -e^2/2h$, and at strong coupling, $\sigma_{xx} < e^2/h$, Zirnbauer [310] showed by discretization, following Shankar and Read [321], that the supersymmetric non-linear sigma model can be mapped on the chain of antiferromagnetic superspin chains in the low energy, long wavelength limit, meaning that the lattice spacing of the super spin chain is on the order of the non-critical localization length $\xi_{\mathrm{2Dunit}}$.

So far, no analytical information has been obtained for the critical parameters, such as the localization exponent, $\nu$ and the critical value $\Lambda_{\mathrm{c}}$. However, building on the model of a superspin chain, supersymmetric conformal field theories have been suggested, which ultimately are supposed to yield the critical parameters of the quantum Hall transition [60,61,183].

Restricting this theory to quasi-one dimension, by assuming a finite width $L_y$ of the quantum Hall bar, of the order of the unitary non-critical localization length $\xi_{\mathrm{2Dunit}} = l \exp(\pi^2 \sigma_{xx}^2)$, which serves as the ultraviolet cutoff of the conformal field theory, one finds that the critical value of the scaling function $\Lambda_{\mathrm{c}} \approx 1.2$, the ratio of the localization length in a quantum Hall wire and its finite width $L_y$ when the energy is in the center of the Landau band, see Section 2.3, is fixed by the eigenvalues of the Laplace–Beltrami operator of this supersymmetric conformal field theory [182,183,61]. This is a characteristic invariant of the theory, arising from the conformal symmetry, just as the quantization of angular momentum arises from the rotational symmetry of a Hamiltonian. Furthermore, based on the properties of this constrained class of supersymmetric conformal field theories, it has been predicted that the distribution function of local wave function amplitudes is very broadly, namely log-normally, distributed. This prediction has recently been confirmed by high-accuracy numerical calculations [137].

The quest to derive the critical exponent of the localization length at the quantum Hall transition from a critical supersymmetric theory has thus recently gained much progress, by mapping both the Chalker–Coddington model and the random Landau model on the Hamiltonian of the superspin chain, Eq. (386), which has been shown to be critical at $R = 0$ [37,309,316] as defined in Eq. (362). Thus, it has been proven to be a good starting point to continue in the quest for an analytical derivation of the critical exponent $\nu$ and the multi-critical exponents at the quantum Hall critical point.

## 11. Extension to higher dimensions

A natural extension of the two-dimensional quantum Hall system is to consider layers stacked in parallel, where electrons can tunnel from one layer to another. Such layered systems can be fabricated in experiments and the magneto-transport properties have been investigated [322–325].

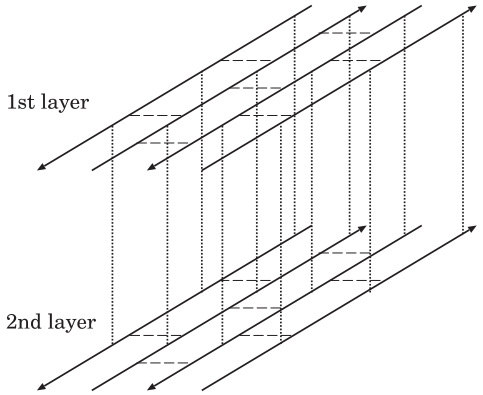


Fig. 51. Schematic view of a double layer network model. The dashed lines indicate intra-layer saddle points. Dotted lines represent tunneling between the layers.

### 11.1. Double layer network model

The simplest case is a double layer system. In this case, there appear two energies where electron states are delocalized [29,326,327], instead of a single energy for delocalized states in case of a single layer system. If the tunneling integral $t'$ between layers is vanishing, the positions of the delocalized states are both at the Landau band center, while if the random potential is the same for both layers, delocalized states appear at $E = \pm t'$. The really interesting situation, however, is none of the above, i.e., uncorrelated disorder and finite tunneling. The position of the delocalized states is analyzed in detail in [327], while the critical behavior has been discussed numerically in [29].

To incorporate interlayer tunneling in the network model, we introduce scattering between links in different layers. In Fig. 51, a schematic view for double layer system is presented. The dashed lines are the saddle points that describe intra-layer scattering described by the **S** matrix, Eq. (87), and dotted lines represent tunnelings between the layer. Detailed expressions are presented in Section 11.3. Note that the situation is similar to the class AIII discussed in Section 9.4, but the discrete symmetry (Eq. (349)) is not present in this double layer system.

The density of states of such a system is sketched in Fig. 52. The Landau band splits due to inter-layer tunneling. Whether or not the localization length exhibits two singularities with the same critical exponent as a single layer is under debate, but it is likely to be so.

The application of the renormalization group process (Section 6) to two-channel network model has been discussed in detail [328,329], where the limitation of the hierarchy model is clarified.

### 11.2. Localization–delocalization transition

With the increase of the number of layers, the positions of energies where delocalized states appear increase. The number of positions coincides with the number of layers. In the limit of infinite number of layers, the delocalized states form a band of energies [330] (Fig. 53).

As long as the number of layers is finite, the critical behavior of the localization–delocalization transition is conjectured to be the same as for a single layer. In the limit of infinite number of layers, the

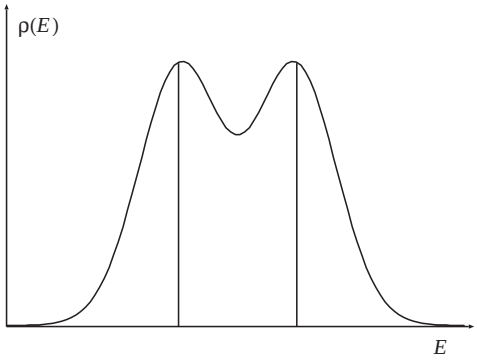


Fig. 52. Schematic view of the density of states $\rho(E)$ and the positions of delocalized states for a double layer quantum Hall system. Delocalized states are indicated by solid lines.

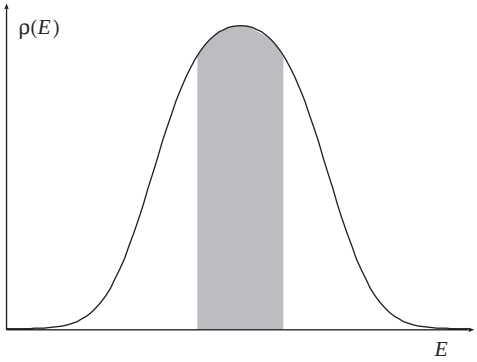


Fig. 53. Schematic view of the density of states $\rho(E)$ and the positions of delocalized states for a multi-layer system. Delocalized states are indicated by the shaded region.

localization–delocalization transition should become that of the three-dimensional unitary system. For this limit, the localization length exponent has been estimated numerically in the multi-layer Landau model [330] and the anisotropic tight-binding model [331]. In all cases, it has been found to be consistent with the value of the three-dimensional unitary class [111,332], $\nu = 1.43 \pm 0.03$. This value is not far from 4/3 obtained by mapping the three-dimensional layered system onto a spin Hamiltonian [333].

The numerical estimate of the exponent $\nu$ in the multi-layer network model via finite-size scaling analysis of the MacKinnon–Kramer scaling variable gives $\nu = 1.45 \pm 0.2$ [100], which is again consistent with the result for three-dimensional unitary class. The quasi-energy spectral properties of the multi-layer network model [132,334] as well as wave packet dynamics [124] have been studied numerically, which are also consistent with that for three-dimensional unitary class [130,170]. These results suggest that the bulk localization–delocalization properties of three dimensional layered Chalker–Coddington model (Chalker–Dohmen model) can be described within the conventional three-dimensional unitary class.

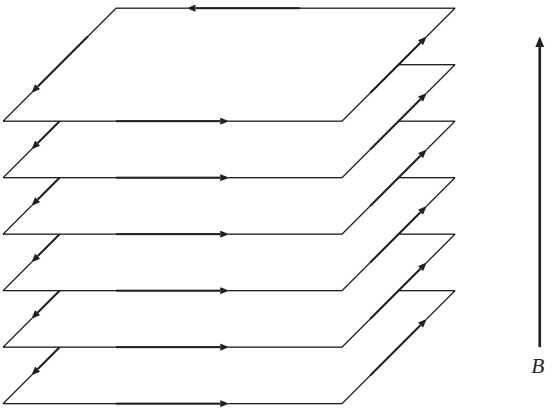


Fig. 54. The electrons circulate about the two-dimensional plane in the case of fbc. They can hop from one layer to another, and form an "edge sheath".

### 11.3. Chiral metal

Most of the discussions so far have assumed the periodic boundary condition in the transverse direction, Eq. (106). If we impose the fixed boundary condition, Eq. (107), the electrons travel along the boundary of the systems and form edge states.

If we consider a multi-layer system where each layer has edge states circulating around the plane, the edge states are connected due to tunneling. When the Fermi energy is set between the center of the Landau band, bulk states are localized and the edge states are decoupled. In this situation, they form a sheath [100,335–337] in which the motion of electrons is directed (Fig. 54). The transport properties along the magnetic field ($z$-direction) is determined by this sheath, since the bulk states are all localized. We therefore can consider as independent the electron states in this two-dimensional sheath which can be modeled by a two-dimensional directed network model, Fig. 55.

In this directed network model, at a saddle point, the incoming and outgoing waves are related via an **S** matrix as

$$\begin{pmatrix} \psi_1' \\ \psi_2' \end{pmatrix} = \begin{pmatrix} -r' & t' \\ t' & r' \end{pmatrix} \begin{pmatrix} \psi_1 \\ \psi_2 \end{pmatrix} . \tag{407}$$

In terms of the transfer matrix along $z$-direction, the wave functions are related via

$$\begin{pmatrix} \psi_1 \\ \psi_1' \end{pmatrix} = \begin{pmatrix} -r'/t' & 1/t' \\ 1/t' & -r'/t' \end{pmatrix} \begin{pmatrix} \psi_2 \\ \psi_2' \end{pmatrix} . \tag{408}$$

The resulting two-dimensional network model is described in Fig. 56. It is similar to Fig. 8, but in this case the arrows are always rightward and $\mathbf{S} = \mathbf{S}'$.

An interesting property of the transport in this edge sheath is that one can estimate the sheet conductivity along the $z$-axis exactly [100,337]. In the limit of large circumference $C$, the path connecting the bottom edge to the top cannot circulate along the system. This and the chiral nature of edge states lead to the fact that the interference between the paths with different wrapping is absent, i.e., a path does not self-intersect, and we can estimate the conductivity classically. Let $T = |t'|^2$ be the single layer transmission

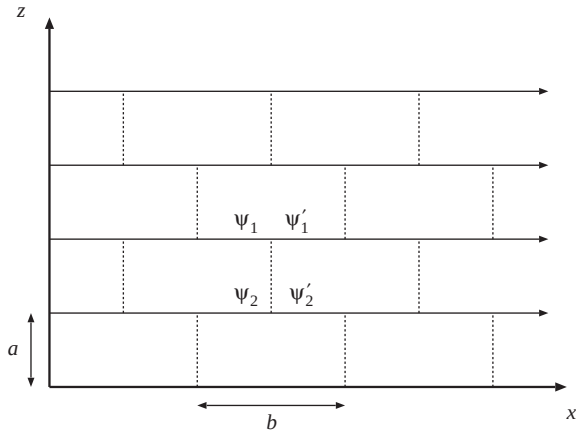


Fig. 55. Schematic view of electron motion in the two-dimensional sheath. The arrows indicate the edge states circulating around the two-dimensional plane. It tunnels to that in a different layer through interlayer coupling indicated by dotted lines.

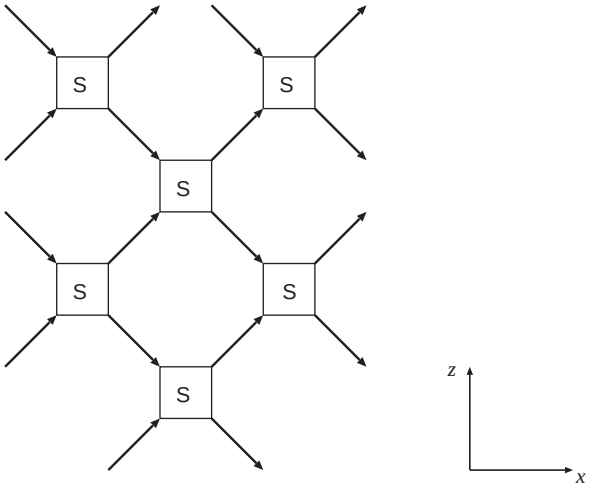


Fig. 56. The directed network model. It is similar to Fig. 8, but different in that the arrows are always towards the right in the $x$-direction, and only one type of the **S** matrix appear, not **S** and **S**′ as before.

probability, and let $T_N$ the transmission probability for $N$ layers ($T_1 = T$). Then the following recurrence equation holds:

$$T_{N+1} = T_N \frac{1}{1 - RR_N} T, \quad R = 1 - T, \quad R_N = 1 - T_N \tag{409}$$

or

$$\frac{1}{T_{N+1}} = \frac{1}{T_N} + \frac{1-T}{T} = N\,\frac{1-T}{T} + \frac{1}{T}\ . \tag{410}$$

This gives

$$T_N = \frac{1}{N}\,\frac{T}{1-T(1-1/N)}\ . \tag{411}$$

The conductance along the $z$-axis, $G_z$, is given by

$$G_z = \frac{e^2}{h}\,N_{\rm c}T_N = \frac{e^2}{h}\,\frac{N_{\rm c}}{N}\,\frac{T}{1-T(1-1/N)}\ , \tag{412}$$

where $N_{\rm c}$ is the number of channels. Setting the distance of the saddle point along the $x$-direction to be $b$ and the layer distance to be $a$, the expression for the conductivity $\sigma_{zz}$ becomes

$$\sigma_{zz} = \frac{L}{C}\,G_z = \frac{e^2}{h}\,\frac{a}{b}\,\frac{T}{1-T(1-1/N)}\ , \tag{413}$$

where $L$ is the length of the system along $z$-axis. For a sufficiently large system, one finds

$$\sigma_{zz} = \frac{e^2}{h}\,\frac{a}{b}\,\frac{T}{1-T} \tag{414}$$

and for perfectly transmitting channels, $T \to 1$, $\sigma_{zz} = (e^2/h)L/b$. Eq. (412) almost completely describes the numerical data for $z$-axis conductance [337].

The results indicate than $\sigma_{zz}$ can be much smaller than $e^2/h$, but the system is still metallic. This is in contrast to the conventional two-dimensional metal–insulator [338] or two-dimensional superconductor–insulator transitions [339], where the transition occurs near $e^2/h$. This peculiar property is due to the chiral nature of the states in the surface, so that the system is called chiral metal.

The conductivity is related to the localization length along the $z$-axis. By parameterizing the transmission eigenvalues, i.e., the eigenvalues of $tt^\dagger$, $\tau_n$ via the Lyapunov exponent $\nu_n$ as (cf. Eq. (157))

$$\tau_n = \frac{1}{\cosh^2(\nu_n N/N_{\rm c})} \tag{415}$$

we have

$$\sigma_{zz} = \lim_{L\to\infty}\lim_{C\to\infty}\,\frac{L}{C}\,\frac{e^2}{h}\sum_{n=1}\frac{N_{\rm c}}{\cosh^2(\nu_n N/N_{\rm c})}\ . \tag{416}$$

By noting that $\nu_n \approx n\nu_1$ due to spectral rigidity, the expression of the conductivity becomes

$$\begin{aligned}\sigma_{zz} &= \lim_{N\to\infty}\lim_{N_{\rm c}\to\infty}\,\frac{Na}{N_{\rm c}b}\,\frac{e^2}{h}\sum_{n=1}\frac{N_{\rm c}}{\cosh^2(\nu_n N/N_{\rm c})}\\ &= \lim_{N\to\infty}\lim_{N_{\rm c}\to\infty}\,\frac{Na}{b}\,\frac{e^2}{h}\int_0^1 \cosh^{-2}(\nu_1 N x)\,{\rm d}x\\ &= \frac{e^2}{h}\,\frac{a}{b}\,\frac{1}{\nu_1}\ .\end{aligned} \tag{417}$$

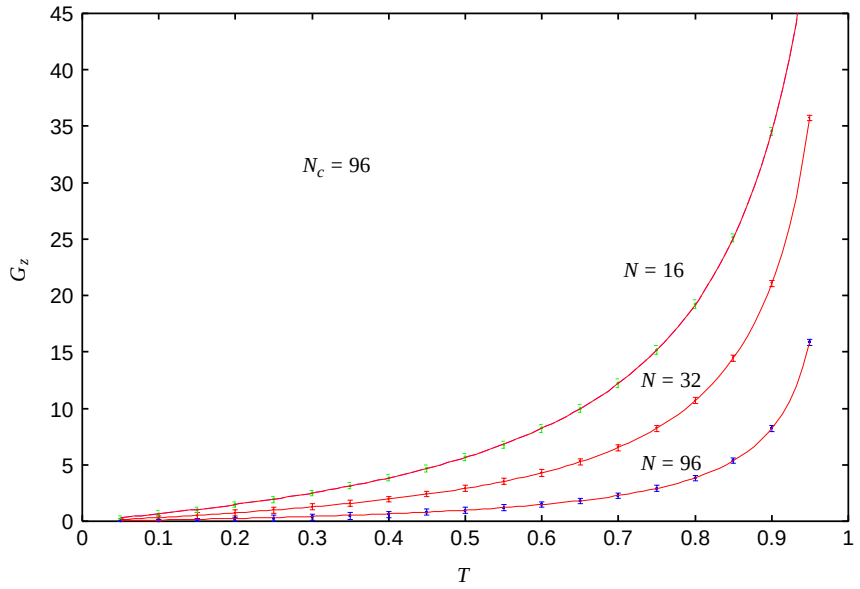


Fig. 57. Numerical transfer matrix calculation of conductance $G_z(e^2/h)$ as a function of the layer transmission probability $T$. $N_c = 96$ while $N = 16, 32$ and 96. Bars around the points indicate the conductance fluctuation. Solid lines correspond to Eq. (412).

Since the smallest Lyapunov exponent is related to the one-dimensional localization length $\xi_z$ via

$$\nu_1 \frac{N}{N_c} = \frac{L}{\xi_z}, \quad \xi_z = \frac{aN_c}{\nu_1}, \tag{418}$$

in terms of localization length the conductivity is expressed as

$$\sigma_{zz} = \frac{e^2}{h} \frac{\xi_z}{C}. \tag{419}$$

From Eqs. (414) and (419) the MacKinnon–Kramer parameter is obtained [100]

$$\Lambda_c = \frac{\xi_z}{C} = \frac{a}{b} \frac{T}{1-T}. \tag{420}$$

It is independent of the size of the system. This means that the wave function is critical.

With the increase of the system length $L$, the paths of electrons from the bottom to the top begin to self-intersect. In this case, the transport properties are conjectured to be metallic. On the basis of mapping onto a ferromagnetic super spin chain [340], this conjecture was quantitatively discussed in [341,342], and then numerically verified [343] (Fig. 57).

In Fig. 58, the qualitative phase diagram of a layered quantum Hall system is shown. The width of the metallic region $W$ is expected to increase with the tunneling amplitude like $W(t) \sim t^{1/\nu_{IQHT}}$, where $\nu_{IQHT}$ is the critical exponent of the two-dimensional quantum Hall transition. This behavior is obtained from the following argument for the delocalization [100]: When the level spacing in a localized region $\Delta_c \sim 1/\xi^2$ with localization length $\xi$ is smaller than the tunneling matrix elements between the localized wave

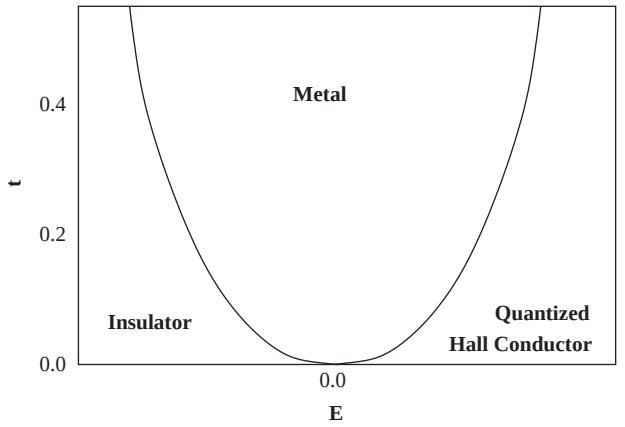


Fig. 58. Phase diagram of the layered network model, where $E = 0$ denotes the center of the lowest Landau band [100]. The width of the metallic region for small tunneling amplitude $t$ is expected to increase like $W(T) \sim t^{1/\nu_{\mathrm{IQHT}}}$.

functions in adjacent layers, the state becomes delocalized. This tunneling matrix elements is estimated to be $\sim t/\xi$, hence $t \sim 1/\xi$ should hold at the mobility edge. Since in the two-dimensional system the localization length diverges at $E = 0$ like $\xi \sim |E|^{-\nu_{\mathrm{IQHT}}}$, one obtains the above dependence of the width $W(t)$.

The chiral metal has been theoretically predicted in 1995 [100,335]. Soon, it has been verified experimentally in an organic conductor [344] and in semiconductor quantum well structures [345–349]. Magneto-conductance [350], conductance fluctuations and the effect of interactions [351–353] have been discussed in relation to the experiments.

Recently, layered network models have been considered for other symmetry classes as well. Since, as reviewed in the previous Section 9, classes C and D (disordered superconductor with broken time reversal symmetry, see Table 4) exhibit a rich phase diagram already in two dimensions, the corresponding phase diagram of the layered network can have additional phase boundaries to the one shown in Fig. 58 [354,355]. Still, the width of the metallic region is expected to be for small tunneling amplitudes $t$, $W(t) \sim t^{1/\nu}$, where $\nu$ is now the critical exponent of the corresponding quantum Hall transition at $t = 0$.

## 12. Conclusion

We have attempted to describe the development during the past decade of the random network model originally designed by Chalker and Coddington for the critical behavior of the quantum Hall phase transition. As the field is presently in a transient state with new ideas and developments appearing very rapidly, we cannot hope to have covered all of the different facettes completely. We can only hope that we have been successful in sketching at least the most important aspects such that a newcomer to the field can get an idea about what is going on.

Two distinct and characteristic features of the model have been very important during the development. The first is of great practical importance. Similar to the tight-binding Anderson model for localization, the network model is perfectly suited for numerical studies since the defining scattering operator is

represented by a *sparse* matrix. Thus, quantitative numerical studies of the fundamental quantum critical properties of the model have been the subject of uncountably many works. These include not only the critical exponents but also the quantum fluctuations of the multi-fractal wave functions and the statistics of the conductances.

The second property is perhaps of more fundamental nature. The network model can be mapped onto a great variety of Hamiltonians ranging from a bipartite tight-binding Hamiltonian—of which the Dirac model is a limiting case, the Ising model to an antiferromagnetic chain of superspins. The versatility of the model invented by Chalker and Coddington for combining results from different areas seems to be truly unique. Using this, and the already mentioned remarkable practical flexibility, reliable quantitative information about quantum phase transitions in very different kinds of disordered systems can be obtained which include all of the 10 presently known universality classes of disordered quantum systems in two dimensions.

Moreover, the mapping to the antiferromagnetic superspin chain and applying field theoretical methods has opened novel possibilities of putting the quantum Hall phase transition in a much wider context. Several new phenomena, such as the thermal Quantum Hall Effect, the spin Quantum Hall Effect, and the chiral metal, have been predicted and are waiting for more theoretical and experimental efforts. Eventually, this also may contribute to explaining the universality of the quantum Hall phenomena which forms the underlying basis for the exactness of the quantization of the Hall conductance.

Thus, the model can be considered as paradigmatic. It seems to us that the development has not yet come to an end. Many of the questions that have been raised during the development are still waiting for answers (Tables 3–5). These are especially the quantitative investigations of the critical properties at the boundaries of the various novel quantum phases that are predicted to occur in the models belonging to the different symmetry classes.

As a major challenge, it remains to be explored how the model can be generalized to include eventually interactions and correlation effects. There is evidence that electron–electron interaction is of great importance for understanding the properties of the two-dimensional electron system in the region of the integer Quantum Hall Effect [58,356,357]. Also, generalizations to the regime of the Fractional Quantum Hall Effect should be desirable [358]. Therefore, the generalization of the model towards including Coulomb interaction will eventually be crucial for getting insight into the physics behind the quantum critical phenomenon which seems to be of central importance in modern condensed matter physics.

## Acknowledgements

We thank Ferdinand Evers, Rochus Klesse and Philipp Cain for providing the originals of the figures 11 (F. E.), 12, (R. K.) and 26 (P. C.), 27 (P. C.). We are also grateful to Kai Dittmer for plotting Fig. 29. We want to thank all the colleagues who have been contributing with useful discussions and enlightening remarks, especially on those issues for which we do not feel to be the real experts. In particular, we would like to mention John Chalker, Ferdinand Evers, Bodo Huckestein, Rochus Klesse, Hidetoshi Nishimori, Shinsei Ryu, Keith Slevin, and Shan-Wen Tsai. We thank Hajo Leschke for providing mathematical references concerning the theorem of Oseledec. One of us (T.O.) wishes to thank Kosuke Yakubo and Tsuneyoshi Nakayama of Hokkaido University, the Sonderforschungsbereich 508 “Quantenmaterialien” and the Graduiertenkolleg “Nanostrukturierte Festkörper” of the Universität Hamburg for kind hospitality during this work. He also wishes to thank Yoshiyuki Ono and Jànos Hajdu

for guiding him to this interesting field of research. S. K. gratefully acknowledges the hospitality of the Max-Planck Institut für die Physik Komplexer Systeme in Dresden where several issues concerning especially Sections 9–11 have been discussed with visitors especially attending the workshops *Quantum Phase Transitions* and *Quantum Transport and Correlations in Mesoscopic Systems and QHE*. B. K. acknowledges gratefully financial support from the Japan Society for the Promotion of Science, and the hospitality of Sophia University, Tokyo, during a stay as a JSPS fellow, during which this work has been completed. Financial support of the Schwerpunktprogramm "Quantum Hall Effect" of the Deutsche Forschungsgemeinschaft is gratefully acknowledged. The work has been performed within the TMR and RTN programmes of the European Union (contracts FMRX-CT96-0044, FMRX CT98-0180, and HPRN-CT2000-00144).

## References

[1] K. von Klitzing, G. Dorda, M. Pepper, Phys. Rev. Lett. 45 (1980) 494.
[2] J. Bortfeldt, B. Kramer (Eds.), Units and Fundamental Constants in Physics and Chemistry. Landolt-Börnstein, Numerical Data and Functional Relationships in Science and Technology, New Series, Subvolume b, Springer, Berlin, 1992.
[3] H. Aoki, Rep. Prog. Phys. 50 (1987) 655.
[4] R.E. Prange, S.M. Girvin (Eds.), The Quantum Hall Effect, Springer, Berlin, 1990.
[5] M. Janssen, O. Viehweger, U. Fastenrath, J. Hajdu, Introduction to the Integer Quantum Hall Effect, VCH-Verlag, Weinheim, 1994.
[6] K. von Klitzing, Rev. Mod. Phys. 58 (1986) 519.
[7] D.C. Tsui, H.L. Störmer, A.C. Gossard, Phys. Rev. Lett. 48 (1982) 1559.
[8] D.C. Tsui, H.L. Störmer, A.C. Gossard, Rev. Mod. Phys. 71 (1999) S298.
[9] R.B. Laughlin, Phys. Rev. Lett. 50 (1983) 1395.
[10] T. Chakraborty, P. Pietiläinen, The Quantum Hall Effects: Fractional and Integral, second ed., Springer, Berlin, 1995.
[11] S. Das Sarma, A. Pinczuk (Eds.), Perspectives in Quantum Hall Effects, Wiley, New York, 1997.
[12] T. Dittrich, P. Hänggi, G.-L. Ingold, B. Kramer, G. Schön, W. Zwerger, Quantum Transport and Dissipation, Wiley-VCH Verlag, Weinheim, 1997.
[13] P.W. Anderson, Phys. Rev. 109 (1958) 1492.
[14] H. Aoki, T. Ando, Solid State Commun. 38 (1981) 1079.
[15] D.C. Tsui, S.J. Allen, Phys. Rev. B 24 (1981) 4082.
[16] P.A. Lee, T.V. Ramakrishnan, Rev. Mod. Phys. 57 (1985) 287.
[17] B. Kramer, A. MacKinnon, Rep. Prog. Phys. 56 (1993) 1469.
[18] A.H. MacDonald, in: B. Kramer (Ed.), Quantum Transport in Semiconductor Submicron Structures, Kluwer Academic Publishers, Dordrecht, 1996.
[19] B. Huckestein, B. Kramer, Phys. Rev. Lett. 64 (1990) 1437.
[20] B. Huckestein, Rev. Mod. Phys. 67 (1995) 357.
[21] Y. Ono, J. Phys. Soc. Japan 51 (1982) 2055.
[22] L. Schweitzer, B. Kramer, A. MacKinnon, J. Phys. C 17 (1984) 4111.
[23] H. Aoki, T. Ando, Phys. Rev. Lett. 54 (1985) 831.
[24] T. Ando, H. Aoki, J. Phys. Soc. Japan 54 (1985) 2238.
[25] B. Miek, Europhys. Lett. 13 (1990) 453.
[26] B. Huckestein, Europhys. Lett. 20 (1992) 451.
[27] Y. Huo, R. Bhatt, Phys. Rev. Lett. 68 (1992) 1375.
[28] C.B. Hanna, D.P. Arovas, K. Mullen, S.M. Girvin, Phys. Rev. B 52 (1995) 5221.
[29] E.S. Sørensen, A.H. MacDonald, Phys. Rev. B 54 (1996) 10675.
[30] Y. Ono, T. Ohtsuki, B. Kramer, J. Phys. Soc. Japan 65 (1996) 1734.
[31] J.T. Chalker, P.D. Coddington, J. Phys. C 21 (1988) 2665.
[32] D.-H. Lee, Z. Wang, S. Kivelson, Phys. Rev. Lett. 70 (1993) 4130.

[33] A.G. Galstyan, M.E. Raikh, Phys. Rev. B 56 (1997) 1422.
[34] P. Cain, R.A. Römer, M. Schreiber, M.E. Raikh, Phys. Rev. B 64 (2001) 235 326.
[35] P. Cain, R.A. Römer, M.E. Raikh, Phys. Rev. B 67 (2003) 075307.
[36] R.A. Römer, P. Cain, Adv. Solid State Phys. 43 (2003) 235.
[37] J. Kondev, J.B. Marston, Nucl. Phys. B 497 (FS) (1997) 639.
[38] D.-H. Lee, Z. Wang, Philos. Mag. Lett. 73 (1996) 145.
[39] H.P. Wei, D.C. Tsui, M.A. Paalanen, A.M.M. Pruisken, Phys. Rev. Lett. 61 (1988) 1294.
[40] S. Koch, R.J. Haug, K. von Klitzing, Phys. Rev. B 43 (1991) 6828.
[41] L.W. Engel, D. Shahar, C. Kurdak, D.C. Tsui, Phys. Rev. Lett. 71 (1993) 2638.
[42] B. Huckestein, B. Kramer, R. Meisels, K.Y. Lim, F. Kuchar, G. Weimann, W. Schlapp, in: E.M. Anastassakis, J.D. Joannopoulos (Eds.), The Physics of Semiconductors, World Scientific Publishers, Singapore, 1991, p. 849.
[43] F. Kuchar, R. Meisels, K. Dybko, B. Kramer, Europhys. Lett. 49 (2000) 480.
[44] F. Hohls, U. Zeitler, R.J. Haug, R. Meisels, K. Dybko, F. Kuchar, Phys. Rev. Lett. 89 (2002) 276801.
[45] R.B. Laughlin, Phys. Rev. B 23 (1981) 5632.
[46] B.I. Halperin, Phys. Rev. B 25 (1982) 2185.
[47] R.E. Prange, Phys. Rev. B 23 (1981) 4802.
[48] W. Brenig, Z. Phys. B 50 (1983) 305.
[49] J.T. Chalker, J. Phys. C 16 (1983) 4297.
[50] R. Joynt, R.E. Prange, Phys. Rev. B 29 (1984) 3303.
[51] R. Lassnig, E. Gornik, Solid State Commun. 47 (1983) 959.
[52] E. Gornik, R. Lassnig, G. Strasser, H.L. Störmer, A.C. Gossard, W. Wiegmann, Phys. Rev. Lett. 54 (1985) 1820.
[53] J.P. Eisenstein, H.L. Störmer, V. Narayanamurti, A.Y. Cho, A.C. Gossard, C.W. Tu, Phys. Rev. Lett. 55 (1985) 875.
[54] D. Heitmann, M. Ziesmann, L.L. Chang, Phys. Rev. B 34 (1986) 7463.
[55] V. Mosser, D. Weiss, K. von Klitzing, K. Ploog, G. Weimann, Solid State Commun. 58 (1986) 5.
[56] R.C. Ashoori, R.H. Silsbee, Solid State Commun. 81 (1992) 821.
[57] A. Potts, R. Shepherd, W.G. Herrenden-Harker, M. Elliott, C.L. Jones, A. Usher, G.A.C. Jones, D.A. Ritchie, E.H. Linfield, M. Grimshaw, J. Phys. Condens. Matter 8 (1996) 5189.
[58] L. Spies, W. Apel, B. Kramer, Phys. Rev. B 55 (1997) 4057.
[59] D.H. Cobden, C.H.W. Barnes, C.J.B. Ford, Phys. Rev. Lett. 82 (1999) 4695.
[60] M.R. Zirnbauer, hep-th (1999) 9905054.
[61] M.J. Bhaseen, I.I. Kogan, O.A. Soloviev, N. Taniguchi, A.M. Tsvelik, Nucl. Phys. B 580 (FS) (2000) 688.
[62] D. Stauffer, A. Aharony, Introduction to Percolation Theory, revised second ed., Taylor and Francis, London, 1994.
[63] M. Tsukada, J. Phys. Soc. Japan 41 (1976) 1466.
[64] R. Kubo, S.J. Miyake, N. Hashitsume, Sol. State Phys. 17 (1965) 269.
[65] L.D. Landau, E.M. Lifschitz, Course of Theoretical Physics, vol. III, third ed., Pergamon Press, New York, 1977.
[66] S.A. Trugman, Phys. Rev. B 27 (1983) 7539.
[67] R.E. Prange, R. Joynt, Phys. Rev. B 25 (1982) 2943.
[68] D. Stauffer, Phys. Rep. 54 (1979) 1.
[69] V. Gurarie, A. Zee, Int. J. Mod. Phys. B 15 (2001) 1225.
[70] J.E. Moore, Phys. Rev. B 65 (2002) 035307.
[71] R.F. Kazarinov, S. Luryi, Phys. Rev. B 25 (1982) 7626.
[72] A.V. Khaetskii, B.I. Shklovskii, Sov. Phys. JETP 85 (1983) 721.
[73] H. Saleur, B. Duplantier, Phys. Rev. Lett. 58 (1987) 2325.
[74] G.V. Mil'nikov, I.M. Sokolov, JETP Lett. 48 (1988) 536.
[75] E. Abrahams, P.W. Anderson, D.C. Licciardello, T.V. Ramakrishnan, Phys. Rev. Lett. 42 (1979) 673.
[76] S. Hikami, Prog. Theor. Phys. 64 (1980) 1466.
[77] F. Wegner, Z. Phys. B 36 (1979) 1209.
[78] F. Wegner, Nucl. Phys. B 316 (1989) 663.
[79] K.B. Efetov, A.I. Larkin, D.E. Khmel'nitskii, Sov. Phys. JETP 52 (1980) 568.
[80] H.A. Fertig, B.I. Halperin, Phys. Rev. B 36 (1987) 7969.
[81] S. Hikami, Prog. Theor. Phys. 76 (1986) 1210.
[82] B. Huckestein, Physica A 167 (1990) 175.

[83] B. Huckestein, Phys. Rev. Lett. 72 (1994) 1080.
[84] N. Sandler, H.R. Maei, J. Kondev, Phys. Rev. B 68 (2003) 205315.
[85] P.M. Morse, H. Feshbach, Methods of Theoretical Physics, McGraw-Hill, New York, 1953.
[86] P.A. Mello, P. Pereyra, N. Kumar, Ann. Phys. 181 (1988) 290.
[87] C.W.J. Beenakker, Rev. Mod. Phys. 69 (1997) 731.
[88] A. MacKinnon, B. Kramer, Phys. Rev. Lett. 47 (1981) 1546.
[89] A. MacKinnon, B. Kramer, Z. Phys. B 53 (1983) 1.
[90] L. Jaeger, J. Phys. Condens. Matter 3 (1991) 2441.
[91] K.I. Wysokiński, F. Evers, W. Brenig, Phys. Rev. B 54 (1996) 10720.
[92] M. Metzler, J. Phys. Soc. Japan 68 (1999) 144.
[93] M. Kohmoto, J. Phys. Soc. Japan 62 (1993) 4001.
[94] D.J. Thouless, M. Kohmoto, M.P. Nightingale, M. den Nijs, Phys. Rev. Lett. 49 (1982) 405.
[95] D.K.K. Lee, J.T. Chalker, D.Y.K. Ko, Phys. Rev. B 50 (1994) 5272.
[96] Y.B. Kim, A. Furusaki, D.K.K. Lee, Phys. Rev. B 52 (1995) 16646.
[97] D.K.K. Lee, J.T. Chalker, Phys. Rev. Lett. 72 (1994) 1510.
[98] Z. Wang, D.-H. Lee, X.G. Wen, Phys. Rev. Lett. 72 (1994) 2454.
[99] V. Kagalovsky, B. Horovitz, Y. Avishai, Phys. Rev. B 52 (1995) R17044.
[100] J.T. Chalker, A. Dohmen, Phys. Rev. Lett. 75 (1995) 4496.
[101] K. Slevin, T. Ohtsuki, Phys. Rev. Lett. 82 (1999) 382.
[102] F. Evers, W. Brenig, Phys. Rev. B 57 (1998) 1805.
[103] B. Jovanovic, Z. Wang, Phys. Rev. Lett. 81 (1998) 2767.
[104] J. Cardy, Scaling and Renormalization in Statistical Physics, Cambridge University Press, Cambridge, 1996.
[105] I.Kh. Zharekeshev, B. Kramer, Phys. Rev. Lett. 79 (1997) 717.
[106] V.I. Oseledec, Trans. Moscow Math. Soc. 19 (1968) 197.
[107] D. Ruelle, Ann. Math. 155 (1982) 243.
[108] U. Krengel, Ergodic Theorems, Verlag de Gruyter, Berlin, 1985.
[109] R. Carmona, J. Lacroix, Spectral Theory of Random Schrödinger Operators, Birkhauser Verlag, Boston, 1990.
[110] P. Markos, B. Kramer, Philos. Mag. B 68 (1993) 357.
[111] K. Slevin, T. Ohtsuki, Phys. Rev. Lett. 78 (1997) 4083.
[112] K. Slevin, T. Ohtsuki, T. Kawarabayashi, Phys. Rev. Lett. 84 (2000) 3915.
[113] K. Slevin, P. Markos, T. Ohtsuki, Phys. Rev. Lett. 86 (2001) 3594.
[114] Y. Asada, K. Slevin, T. Ohtsuki, Phys. Rev. Lett. 89 (2002) 256601.
[115] Y. Asada, K. Slevin, T. Ohtsuki, Phys. Rev. B 70 (2004) 035115.
[116] F. Evers, private communications.
[117] B. Huckestein, K. Slevin, private communications.
[118] H. Aoki, J. Phys. C 16 (1983) L205.
[119] C.M. Soukoulis, E.N. Economou, Phys. Rev. Lett. 52 (1984) 565.
[120] A.W.W. Ludwig, M.P.A. Fisher, R. Shankar, G. Grinstein, Phys. Rev. B 50 (1994) 7526.
[121] R. Klesse, M. Metzler, Europhys. Lett. 32 (1995) 229.
[122] I. Edrei, M. Kaveh, B. Shapiro, Phys. Rev. Lett. 62 (1989) 2120.
[123] H.A. Fertig, Phys. Rev. B 38 (1988) 996.
[124] B. Huckestein, R. Klesse, Phys. Rev. B 59 (1999) 9714.
[125] R. Ketzmerick, G. Petschel, T. Geisel, Phys. Rev. Lett. 69 (1992) 695.
[126] B. Huckestein, L. Schweitzer, Phys. Rev. Lett. 72 (1994) 713.
[127] T. Brandes, B. Huckestein, L. Schweitzer, Ann. Phys. (Leipzig) 5 (1996) 633.
[128] T. Kawarabayashi, T. Ohtsuki, Phys. Rev. B 51 (1995) 10897.
[129] T. Kawarabayashi, T. Ohtsuki, Phys. Rev. B 53 (1996) 6975.
[130] T. Ohtsuki, T. Kawarabayashi, J. Phys. Soc. Japan 66 (1997) 314.
[131] W. Pook, M. Janssen, Z. Phys. B 82 (1991) 295.
[132] B. Huckestein, R. Klesse, Phys. Rev. B 55 (1997) R7303.
[133] T. Nakayama, K. Yakubo, Fractal Concepts in Condensed Matter Physics, Springer, Berlin, 2003.
[134] T.C. Halsey, M.H. Jensen, L.P. Kadanoff, I. Procaccia, B.I. Shraiman, Phys. Rev. A 33 (1986) 1141.

[135] A.W.W. Ludwig, Nucl. Phys. B 330 (1990) 639.
[136] B. Duplantier, A.W.W. Ludwig, Phys. Rev. Lett. 66 (1991) 247.
[137] F. Evers, A. Mildenberger, A.D. Mirlin, Phys. Rev. B 64 (2001) 241303(R).
[138] R. Klesse, M. Metzler, Int. J. Mod. Phys. C 10 (1999) 577.
[139] J. Cardy, J. Phys. A 17 (1984) L385.
[140] M. Janssen, Int. J. Mod. Phys. B 8 (1994) 943.
[141] M. Janssen, Phys. Rep. 295 (1998) 1.
[142] M. Janssen, Fluctuations and Localization in Mesoscopic Electron Systems, World Scientific, Singapore, 2001.
[143] A. Dohmen, P. Freche, M. Janssen, Phys. Rev. Lett. 76 (1996) 4207.
[144] M.L. Mehta, Random Matrices, third ed., Elsevier, Amsterdam, 2004.
[145] F. Haake, Quantum Signature of Chaos, second ed., Springer, Berlin, 2001.
[146] B.I. Shklovskii, B. Shapiro, B.R. Sears, P. Lambrianides, H.B. Shores, Phys. Rev. B 47 (1993) 11487.
[147] B.L. Altshuler, I.Kh. Zharekeshev, S. Kotochigova, B. Shklovskii, Sov. Phys. JETP 67 (1988) 625.
[148] Y. Ono, T. Ohtsuki, J. Phys. Soc. Japan 62 (1993) 3813.
[149] S.N. Evangelou, Phys. Rev. B 49 (1994) 16805.
[150] T. Kawarabayashi, T. Ohtsuki, K. Slevin, Y. Ono, Phys. Rev. Lett. 77 (1996) 3593.
[151] R. Klesse, M. Metzler, Phys. Rev. Lett. 79 (1997) 721.
[152] T. Ohtsuki, Y. Ono, J. Phys. Soc. Japan 64 (1995) 4088.
[153] J.T. Chalker, V.E. Kravtsov, I.V. Lerner, JETP Lett. 64 (1996) 386.
[154] F. Evers, A.D. Mirlin, Phys. Rev. Lett. 84 (2000) 3690.
[155] F. Evers, A.D. Mirlin, Phys. Rev. B 62 (2000) 7920.
[156] R. Landauer, IBM J. Res. Dev. 1 (1957) 223.
[157] R. Landauer, Z. Phys. B 21 (1975) 247.
[158] S. Cho, M.P.A. Fisher, Phys. Rev. B 55 (1997) 1637.
[159] D.S. Fisher, P.A. Lee, Phys. Rev. B 23 (1981) 6851.
[160] J.-L. Pichard, Ph.D. Thesis, Université Paris-Sud, Orsay, 1984.
[161] J.-L. Pichard, G. André, Europhys. Lett. 2 (1986) 477.
[162] K. Slevin, T. Ohtsuki, Anderson Localisation: The Numerical Approach, unpublished.
[163] P.A. Lee, A.D. Stone, Phys. Rev. Lett. 55 (1985) 1622.
[164] P.A. Lee, A.D. Stone, H. Fukuyama, Phys. Rev. B 35 (1987) 1039.
[165] B. Shapiro, Philos. Mag. B 56 (1990) 1032.
[166] B. Shapiro, Phys. Rev. Lett. 65 (1990) 1510.
[167] P. Markos, Europhys. Lett. 26 (1994) 431.
[168] P. Markos, Phys. Rev. Lett. 83 (1999) 588.
[169] Z. Wang, B. Jovanovic, D.-H. Lee, Phys. Rev. Lett. 77 (1996) 4426.
[170] M. Batsch, L. Schweitzer, I.Kh. Zharekeshev, B. Kramer, Phys. Rev. Lett. 77 (1996) 1552.
[171] D. Braun, G. Montambaux, M. Pascaud, Phys. Rev. Lett. 81 (1998) 1062.
[172] T. Ohtsuki, K. Slevin, B. Kramer, Physica E 22 (2004) 248.
[173] D. Braun, E. Hofstetter, A. MacKinnon, G. Montambaux, Phys. Rev. B 55 (1997) 7557.
[174] X. Wang, Q. Li, C.M. Soukoulis, Phys. Rev. B 58 (1998) 3576.
[175] K.A. Muttalib, P. Wölfle, A. Garcia-Martin, V.A. Gopar, Europhys. Lett. 61 (2003) 95.
[176] K.A. Muttalib, P. Wölfle, V.A. Gopar, Ann. Phys. 308 (2003) 156.
[177] M. Rühländer, P. Markos, C.M. Soukoulis, Phys. Rev. B 64 (2001) 212202.
[178] K. Slevin, T. Nagao, Phys. Rev. Lett. 70 (1993) 635.
[179] K. Slevin, T. Nagao, Phys. Rev. B 50 (1994) 2380.
[180] P.H. Damgaard, S.M. Nishigaki, Phys. Rev. D 63 (2001) 045012.
[181] J.T. Chalker, J. Phys. C 21 (1988) L119.
[182] M. Janssen, M. Metzler, M.R. Zirnbauer, Phys. Rev. B 59 (1999) 15836.
[183] R. Klesse, M. Zirnbauer, Phys. Rev. Lett. 86 (2001) 2094.
[184] F. Evers, A. Mildenberger, A.D. Mirlin, Phys. Rev. B 67 (2003) 041303(R).
[185] T.V. Shahbazyan, M.E. Raikh, Phys. Rev. Lett. 75 (1995) 304.
[186] D.P. Arovas, M. Janssen, B. Shapiro, Phys. Rev. B 56 (1997) 4751.

[187] M. Janssen, R. Merkt, J. Meyer, A. Weymer, Physica B 256 (1998) 65.
[188] P. Cain, Ph.D. Thesis, TU Chemnitz, Chemnitz, 2004.
[189] C.-M. Ho, J.T. Chalker, Phys. Rev. B 54 (1996) 8708.
[190] B. Huckestein, B. Kramer, Solid State Commun. 71 (1989) 445.
[191] M.P.A. Fisher, E. Fradkin, Nucl. Phys. B 251 (FS13) (1985) 457.
[192] D.-H. Lee, Phys. Rev. B 50 (1994) 10788.
[193] K. Ziegler, Europhys. Lett. 31 (1995) 549.
[194] E. Fradkin, Phys. Rev. B 33 (1986) 3257, 3263.
[195] Y. Aharonov, A. Casher, Phys. Rev. A 19 (1979) 2461.
[196] A.A. Nersesyan, A.M. Tsvelik, F. Wenger, Phys. Rev. Lett. 72 (1994) 2628.
[197] A.A. Nersesyan, A.M. Tsvelik, F. Wenger, Nucl. Phys. B 438 (FS) (1995) 561.
[198] D. Bernard, Nucl. Phys. B 441 (FS) (1995) 471.
[199] J.-S. Caux, I.I. Kogan, A.M. Tsvelik, Nucl. Phys. B 466 (FS) (1996) 444.
[200] I.I. Kogan, C. Mudry, A.M. Tsvelik, Phys. Rev. Lett. 77 (1996) 707.
[201] C.deC. Chamon, C. Mudry, X.-G. Wen, Phys. Rev. Lett. 77 (1996) 4194.
[202] H.E. Castillo, C.deC. Chamon, E. Fradkin, P.M. Goldbart, C. Mudry, Phys. Rev. B 56 (1997) 10668.
[203] D. Carpentier, P. Le Dussal, Phys. Rev. E 63 (2001) 026110.
[204] O. Motrunich, K. Damle, D.A. Huse, Phys. Rev. B 65 (2002) 064206.
[205] C. Mudry, S. Ryu, A. Furusaki, Phys. Rev. B 67 (2003) 064202.
[206] Y. Hatsugai, X.-G. Wen, M. Kohmoto, Phys. Rev. B 56 (1997) 1061.
[207] Y. Morita, Y. Hatsugai, Phys. Rev. Lett. 79 (1997) 3728.
[208] Y. Morita, Y. Hatsugai, Phys. Rev. B 58 (1998) 6680.
[209] S. Ryu, Y. Hatsugai, Phys. Rev. B 63 (2001) 233307.
[209a] S. Cho, M.P.A. Fisher, Phys. Rev. B 55 (1997) 1025.
[210] N. Read, A.W.W. Ludwig, Phys. Rev. B 63 (2001) 024404.
[211] I.A. Gruzberg, N. Read, A.W.W. Ludwig, Phys. Rev. B 63 (2001) 104422.
[212] F. Merz, J.T. Chalker, Phys. Rev. B 65 (2002) 054425.
[213] E. Ising, Z. Phys. 31 (1925) 253.
[214] L. Onsager, Phys. Rev. 65 (1944) 117.
[215] T. Schultz, D. Mattis, E. Lieb, Rev. Mod. Phys. 36 (1964) 856.
[216] H. Nishimori, Prog. Theor. Phys. 66 (1981) 1169.
[217] H. Nishimori, J. Phys. Soc. Japan 55 (1986) 3305.
[218] P. Le Doussal, A.B. Harris, Phys. Rev. Lett. 61 (1988) 625.
[219] K. Binder, A.P. Young, Rev. Mod. Phys. 58 (1986) 801.
[220] B.W. Southern, A.P. Young, J. Phys. C 10 (1977) 2179.
[221] R. Maynard, R. Rammal, J. Phys. (Paris) Lett. 43 (1982) L347.
[222] W.L. McMillan, Phys. Rev. B 29 (1984) 4026.
[223] Y. Ozeki, H. Nishimori, J. Phys. Soc. Japan 56 (1987) 1568.
[224] Y. Ozeki, H. Nishimori, J. Phys. Soc. Japan 56 (1987) 3265.
[225] J. Houdayer, Eur. Phys. J. B 22 (2001) 479.
[226] I. Morgenstern, K. Binder, Phys. Rev. B 22 (1980) 288.
[227] Y. Ueno, Y. Ozeki, J. Stat. Phys. 64 (1991) 227.
[228] H. Kitatani, T. Oguchi, J. Phys. Soc. Japan 61 (1992) 1598.
[229] F.D.A.A. Reis, S.L.A. de Queiroz, R.R. dos Santos, Phys. Rev. B 60 (1999) 6740.
[230] A. Honecker, M. Picco, P. Pujol, Phys. Rev. Lett. 87 (2001) 047201.
[231] J.A. Blackman, Phys. Rev. B 26 (1982) 4987.
[232] J.A. Blackman, J. Poulter, Phys. Rev. B 44 (1991) 4374.
[233] J.A. Blackman, J.R. Gonzalves, J. Poulter, Phys. Rev. E 58 (1998) 1502.
[234] L. Saul, M. Kardar, Phys. Rev. E 48 (1993) R3221.
[235] L. Saul, M. Kardar, Nucl. Phys. B 432 (FS) (1994) 641.
[236] M. Inoue, J. Phys. Soc. Japan 64 (1995) 3699.
[237] E.S. Sørensen, cond-mat (2000) 0006233.

[238] J.T. Chalker, N. Read, V. Kagalovsky, B. Horovitz, Y.Avishai.A.W.W. Ludwig, Phys. Rev. B 65 (2002) 012506.
[239] P. Jordan, E. Wigner, Z. Phys. 47 (1928) 631.
[240] E. Lieb, T. Schultz, D. Mattis, Ann. Phys. 16 (1961) 407.
[241] E. Lieb, D. Mattis, Phys. Rev. 125 (1962) 164.
[242] T. Schultz, J. Math. Phys. 4 (1963) 666.
[243] M.R. Zirnbauer, J. Math. Phys. 37 (1996) 4986.
[244] A. Altland, M.R. Zirnbauer, Phys. Rev. B 55 (1997) 1142.
[245] A.D. Mirlin, Phys. Rep. 326 (2000) 259.
[246] D.G. Polyakov, M.E. Raikh, Phys. Rev. Lett. 75 (1995) 1368.
[247] F. Kuchar, R. Meisels, K. Dybko, B. Kramer, Europhys. Lett. 49 (2000) 480.
[248] V. Kagalovsky, B. Horovitz, Y. Avishai, Phys. Rev. B 55 (1997) 7761.
[249] V. Kagalovsky, B. Horovitz, Y. Avishai, Phys. Stat. Sol. (b) 205 (1998) 377.
[250] R. Oppermann, F. Wegner, Z. Phys. B 34 (1979) 327.
[251] R. Gade, Ph.D. Thesis, Heidelberg, 1990.
[252] R. Gade, Nucl. Phys. B 398 (1993) 499.
[253] S. Hikami, M. Shirai, F. Wegner, Nucl. Phys. B 408 (1993) 415.
[254] R. Oppermann, Physica A 167 (1990) 301.
[255] S. Helgason, Differential Geometry and Symmetric Spaces, Academic Press, New York, 1962.
[256] S. Helgason, Groups and Geometric Analysis, American Mathematical Society, Providence, 2000.
[257] S. Hikami, Phys. Lett. B 98 (1981) 208.
[258] P.W. Brouwer, A. Furusaki, C. Mudry, Phys. Rev. B 67 (2003) 014530.
[259] M. Bocquet, J.T. Chalker, Phys. Rev. B 67 (2003) 054204.
[260] R. Merkt, M. Janssen, B. Huckestein, Phys. Rev. B 58 (1998) 4394.
[261] I.A. Gruzberg, N. Read, S. Vishveshwara, Phys. Rev. B 71 (2005) 245124.
[262] A. Altland, Phys. Rev. B 65 (2002) 104525.
[263] T. Senthil, M.P.A. Fisher, Phys. Rev. B 61 (2000) 9690.
[264] I.A. Gruzberg, A.W.W. Ludwig, N. Read, Phys. Rev. Lett. 82 (1999) 4524.
[265] E.J. Beamond, J. Cardy, J.T. Chalker, Phys. Rev. B 65 (2002) 214301.
[266] S. Guruswamy, A. LeClair, A.W.W. Ludwig, Nucl. Phys. B 583 (2000) 475.
[267] P.W. Brouwer, A. Furusaki, I.A. Gruzberg, C. Mudry, Phys. Rev. Lett. 85 (2000) 1064.
[268] J.-Q. Chen (Ed.), Group Representation Theory for Physicists, World Scientific, Singapore, 1989.
[269] K.B. Efetov, A.I. Larkin, Sov. Phys. JETP 58 (1983) 444.
[270] O.N. Dorokhov, JETP Lett. 36 (1982) 318.
[271] O.N. Dorokhov, Sov. Phys. JETP 58 (1983) 606.
[272] O.N. Dorokhov, Solid State Commun. 51 (1984) 381.
[273] J.L. Pichard, in: B. Kramer (Ed.), Quantum Coherence in Mesoscopic Systems, NATO ASI Series B254, Plenum, New York, 1991, p. 369.
[274] S. Kettemann, Phys. Rev. B 62 (2000) R13282.
[275] C.L. Kane, M.P.A. Fisher, Phys. Rev. B 55 (1997) 15832.
[276] M. Bocquet, D. Serban, M.R. Zirnbauer, Nucl. Phys. B 578 (2000) 628.
[277] N. Read, D. Green, Phys. Rev. B 61 (2000) 10267.
[278] O. Motrunich, K. Damle, D.A. Huse, Phys. Rev. B 63 (2001) 224204.
[279] T. Senthil, M.P.A. Fisher, L. Balents, C. Nayak, Phys. Rev. Lett. 81 (1998) 4704.
[280] T. Senthil, J.B. Marston, M.P.A. Fisher, Phys. Rev. B 60 (1999) 4245.
[281] V. Kagalovsky, B. Horovitz, Y. Avishai, J.T. Chalker, Phys. Rev. Lett. 82 (1999) 3516.
[282] R.M. Gade, J. Phys. A 32 (1999) 7071.
[283] B. Horovitz, P. Le Doussal, Phys. Rev. B 65 (2002) 125323.
[284] T. Fukui, Phys. Rev. B 68 (2003) 153307.
[285] S. Ryu, C. Mudry, A. Furusaki, J. Phys. Soc. Japan A 72 (Suppl.) (2003) 219.
[286] Y. Asada, K. Slevin, T. Ohtsuki, J. Phys. Soc. Japan A 72 (Suppl.) (2003) 145.
[287] Y. Avishai, Y. Meir, Phys. Rev. Lett. 89 (2002) 076602.
[288] P.W. Anderson, D.J. Thouless, E. Abrahams, D.S. Fisher, Phys. Rev. B 22 (1980) 3519.

[289] B. Shapiro, Phys. Rev. Lett. 48 (1982) 823.
[290] P. Freche, M. Janssen, R. Merkt, Phys. Rev. Lett. 82 (1999) 149.
[291] Y. Asada, K. Slevin, private communications.
[292] S.N. Evangelou, T. Ziman, J. Phys. C 20 (1987) L235.
[293] T. Ando, Phys. Rev. B 40 (1989) 5325.
[294] K. Minakuchi, Phys. Rev. B 58 (1998) 9627.
[295] S. Hikami, A. Larkin, Y. Nagaoka, Prog. Theor. Phys. 63 (1980) 707.
[296] R. Bundschuh, C. Cassanello, D. Serban, M.R. Zirnbauer, Phys. Rev. B 59 (1999) 4382.
[297] M. Jeng, A.W.W. Ludwig, T. Senthil, C. Chamon, Bull. Am. Phys. Soc. 46 (2001) 231.
[298] S. Cho, Ph.D. Thesis, UCSB, Santa Barbara, 1997.
[299] A. LeClair, Phys. Rev. B 64 (2001) 045329.
[300] C. Mudry, B.D. Simons, A. Altland, Phys. Rev. Lett. 80 (1998) 4257.
[301] H. Levine, S.B. Libby, A.M.M. Pruisken, Phys. Rev. Lett. 51 (1983) 1915.
[302] K.B. Efetov, Adv. Phys. 32 (1983) 53.
[303] H.A. Weidenmüller, Nucl. Phys. B 290 (FS20) (1987) 87.
[304] H.A. Weidenmüller, M.R. Zirnbauer, Nucl. Phys. B 305 (FS23) (1988) 339.
[305] I. Affleck, Nucl. Phys. B 265 (FS15) (1986) 409.
[306] S. Kettemann, A. Tsvelik, Phys. Rev. Lett. 82 (1999) 3689.
[307] K.B. Efetov, V.G. Marikhin, Phys. Rev. B 40 (1989) 12126.
[308] M.R. Zirnbauer, J. Math. Phys. 38 (1997) 2007.
[309] J.B. Marston, S.-W. Tsai, Phys. Rev. Lett. 82 (1999) 4906.
[310] M.R. Zirnbauer, Ann. Phys. (Leipzig) 3 (1994) 513.
[311] L. Balents, M.P.A. Fisher, M.R. Zirnbauer, Nucl. Phys. B 483 (FS) (1997) 601.
[312] R.M. Gade, J. Phys. A 31 (1998) 4909.
[313] F.H.L. Essler, H. Frahm, H. Saleur, Nucl. Phys. B 712 (2005) 513.
[314] J.W. Negele, H. Orland, Quantum Many-Particle Systems, Addison-Wesley, Redwood City, 1988.
[315] E. Fradkin, Field Theories of Condensed Matter Systems, Addison-Wesley, Redwood City, 1991.
[316] S.-W. Tsai, J.B. Marston, in: M. Schreiber (Ed.), Ann. Phys. (Leipzig), Special Issue. Proceedings (poster contributions) of the International Conference on Localizaion 1999, Wiley-VCH Verlag, 1999, p. 261.
[316a] A. Sedrakyan, Phys. Rev. B 68 (2004) 235329.
[317] S.-W. Tsai, J.B. Marston, Phys. Rev. B 62 (2000) 5546.
[318] S.-W. Tsai, Ph.D. Thesis, Brown University, Providence, 2001.
[319] E. Brézin, J. Zinn-Justin (Ed.), I. Affleck in Fields, Strings and Critical Phenomena, Les Houches Summer School, North-Holland, Amsterdam, 1985.
[320] D.E. Khmel'nitskii, JETP Lett. 38 (1983) 552.
[321] R. Shankar, N. Read, Nucl. Phys. B 336 (1990) 457.
[322] H.L. Störmer, J.P. Eisenstein, A.C. Gossard, W. Wiegmann, K. Baldwin, Phys. Rev. Lett. 56 (1986) 85.
[323] H.L. Störmer, J.P. Eisenstein, A.C. Gossard, K. Baldwin, J.H. English, in: O. Engstrom (Ed.), 18th International Conference Physics of Semiconductions, World Scientific, Singapore, 1987, p. 385.
[324] S.S. Murzin, A.G.M. Jansen, P.v.d. Linden, Phys. Rev. Lett. 80 (1998) 2681.
[325] K. Kodera, A. Endo, K. Kobayashi, S. Katsumoto, Y. Iye, Physica E 22 (2004) 64.
[326] T. Ohtsuki, Y. Ono, B. Kramer, Surf. Sci. 263 (1992) 134.
[327] A. Gramada, M.E. Raikh, Phys. Rev. B 56 (1997) 3965.
[328] A. Manze, B. Huckestein, Presented at "Quantum Hall Systems and Quantum Materials" Hamburg, September 2004, unpublished.
[329] A. Manze, Ph.D. Thesis, Bochum.
[330] T. Ohtsuki, B. Kramer, Y. Ono, J. Phys. Soc. Japan 62 (1993) 224.
[331] X.R. Wang, C.Y. Wong, X.C. Xie, Phys. Rev. B 59 (1999) R5277.
[332] T. Kawarabayashi, B. Kramer, T. Ohtsuki, Phys. Rev. B 57 (1998) 11842.
[333] Y. Meir, Phys. Rev. B 58 (1998) R1762.
[334] M. Metzler, J. Phys. Soc. Japan 67 (1998) 4006.
[335] L. Balents, M.P.A. Fisher, Phys. Rev. Lett. 76 (1996) 2782.

[336] Y.B. Kim, Phys. Rev. B 53 (1996) 16420.
[337] S. Cho, L. Balents, M.P.A. Fisher, Phys. Rev. B 56 (1997) 15814.
[338] E. Abrahams, S.V. Kravchenko, M.P. Sarachik, Rev. Mod. Phys. 73 (2001) 251.
[339] A. Goldman, N. Markovic, Phys. Today 51 (1998) 39.
[340] L. Balents, M.P.A. Fisher, M.R. Zirnbauer, Nucl. Phys. B 483 (1997) 601.
[341] I.A. Gruzberg, N. Read, S. Sachdev, Phys. Rev. B 55 (1997) 10593.
[342] I.A. Gruzberg, N. Read, S. Sachdev, Phys. Rev. B 56 (1997) 13218.
[343] V. Plerou, Z. Wang, Phys. Rev. B 58 (1998) 1967.
[344] M.M. Honold, N. Harrison, J. Singleton, H. Yaguchi, C. Mielke, D. Rickel, I. Deckers, P.H.P. Reinders, F. Herlach, M. Kurmoo, P. Day, J. Phys. Condens. Matter 9 (1997) L533.
[345] D.P. Druist, P.J. Turley, K.D. Maranowski, E.G. Gwinn, A.C. Gossard, Phys. Rev. Lett. 80 (1998) 365.
[346] B. Zhang, J. Brooks, Z. Wang, J. Simmons, J. Reno, N. Lumpkin, J. O'Brien, R. Clark, Phys. Rev. B 60 (1999) 8743.
[347] M. Kawamura, A. Endo, S. Katsumoto, Y. Iye, J. Phys. Soc. Japan 68 (1999) 2186.
[348] D.P. Druist, E.G. Gwinn, K.D. Maranowski, A.C. Gossard, Phys. Rev. B 68 (2003) 075305.
[349] H.A. Walling, D.P. Dougherty, D.P. Druist, E.G. Gwinn, K.D. Maranowski, A.C. Gossard, Phys. Rev. B 70 (2004) 045312.
[350] J.T. Chalker, S.L. Sondhi, Phys. Rev. B 59 (1999) 4999.
[351] J.J. Betouras, J.T. Chalker, Phys. Rev. B 62 (2000) 10931.
[352] J.J. Betouras, Europhys. Lett. 53 (2001) 66.
[353] J.W. Tomlinson, J.S. Caux, J.T. Chalker, Phys. Rev. Lett. 94 (2005) 086804.
[354] V. Kagalovsky, B. Horovitz, Y. Avishai, Physica E 22 (2004) 753.
[355] V. Kagalovsky, B. Horovitz, Y. Avishai, Phys. Rev. Lett. 93 (2004) 246802.
[356] D.-H. Lee, Z. Wang, Phys. Rev. Lett. 76 (1996) 4014.
[357] S. Ilani, J. Martin, E. Teitelbaum, J.H. Smet, D. Mahalu, V. Umansky, A. Yacoby, Nature 427 (2004) 328.
[358] L.P. Pryadko, K. Chaltikian, Phys. Rev. Lett. 80 (1998) 584.